UNIVERSITA' DEGLI STUDI DELL'INSUBRIA

Dipartimento di Scienza e Alta Tecnologia (DISAT)
PhD in Chemical Sciences, XXXI cycle

Diketopiperazines as scaffold for the synthesis of new compounds modulating protein-protein interactions and functions

Sara Parente

727890

Tutor

Prof. Umberto Piarulli

A.Y. 2017/2018

To whom has believed in me.

The presented work was led by Prof. Umberto Piarulli, Università degli studi dell'Insubria

Doctoral Final Oral Examination: 22nd February 2019

Examination Committee: Prof. Laura Belvisi, Università degli studi di Milano

Prof. Gábor Mező, Eötvös Loránd University, Budapest

Prof. Tiziana Benincori, Università degli studi dell'Insubria

The work herein described was performed at University of Insubria (Como) in the period from October 2015 to September 2018 under the supervision of Prof. Umberto Piarulli and at the Department of Biochemistry, University of Cologne in the period from June 2017 to December 2017 in the research group of Prof. Ines Neundorf.

Three projects, based on the use of diketopiperazines (DKP) as scaffold for the synthesis of small molecules with peptidomimetic character, will be examined in this thesis.
Our efforts to investigate on the use of these small molecules for the synthesis of peptidomimetic ligands for integrins and cadherins to explore modulation of protein-protein interactions and functions are described in ***Part 1****.*
In particular, in Part 1 the integrin-targeting properties of c[DKP-RGD] were exploited for the synthesis of small molecule drug conjugates. The synthesis of two conjugates bearing Daunomycin and Paclitaxel as cytotoxic payloads, was planned and developed in collaboration with Professor Neundorf's group (University of Cologne).
Furthermore, synthesis of linear and cyclic DKP-based inhibitors for cadherin-mediated homophilic interactions has been described in this part of the thesis.
Finally, the drug delivery properties of the cell penetrating peptide sC18 were employed in the synthesis of drug delivery systems and are reported in* ***Part 2****. Two cyclic cell penetrating peptides, bearing DKP scaffolds with different stereochemistry, were synthesized in collaboration with Professor Neundorf's group.*

Table of contents

List of abbreviations

Ac	Acetil
ACN	Acetonitrile
aq.	Aqueous solution
Bn	Benzyl
Boc	*tert*-Butyloxycarbonyl
Boc_2O	di-*tert*-butyldicarbonate
Boc-ON	2-(Boc-oxymino)-2-phenylacetonitrile
Bu	Butyl
c	*cyclo*
Cbz	Carboxybenzyl
CD	Circular dicroism
COSY	Correlated Spectroscopy
CuAAC	Cu(I)-catalyzed Azide-Alkyne Click chemistry
DCC	N,N'-dicyclohexylcarbodiimide
Dde	N-(1-(4,4-dimethyl-2,6-dioxocyclohexylidene)ethyl)
DIAD	Diisopropyl azodicarboxylate
DIC	N,N'-diisopropylcarbodiimide
DIPEA	*N*-ethyldiisopropylamine
DKP	2,5-Diketopiperazine
DMAP	4-Dimethylaminopiridine
DMF	N,N-Dimethylformamide
DMSO	Dimethyl sulfoxide
ECD	Extracellular domain
ECM	Extracellular matrix
EDC HCl	1-Ethyl-3-(3-dimethylaminopropyl)carbodiimide
EDT	1,2-Ethanedithiol
EEDQ	N-Ethoxycarbonyl-2-ethoxy-1,2-dihydroquinoline
eq	Equivalents
ESI	Electrospray ionization
Et	Ethyl
EtOAc	Ethyl acetate
FA	Formic acid
FC	Flash Chromatography
Fmoc	9-Fluoroenylmethoxycarbonyl
HATU	O-(7-azabenzotriazol-1-yl)-tetramethyl-uronium hexafluorophosphate
HOAt	1-Hydroxy-7-azabenzotriazole
HPLC	High performance liquid chromatography
IC	Inhibitory capacity
*i*Pr	Isopropyl
J	Scalar coupling costant
Me	Methyl
Me_3P	trimethylphosphine
MIDAS	Methal ion-dependent adhesion site
MS	Mass spectroscopy
Mtr	4-Methoxy-2,3,6-trimethylbenzensulphonyl
NMR	Nuclear Magnetic Resonance
NHS	N-Hydroxysuccinimide
o.n.	overnight
PAB	4-aminobenzyl
Pbf	2,2,4,6,7-pentamethyldihydrobenzofuran-5-sulfonyl
PBS	Phosphate-buffered saline
PEG	Polyethylene glycol
PPh_3	triphenilphosphine
ppm	Part per million
PTX	Paclitaxel
quant.	Quantitative
Rf	Retention factor
r.t.	Room temperature
SMDC	Small molecule drug conjugate
SPPS	Solid-phase peptide synthesis
tBu	tert-Butyl
TFA	Trifluoroacetic acid
THF	tetrahydrofuraan
TLC	Thin-layer chromatography
TMS	tetramethylsilane
tR	Retention time
δ	Chemical shift

Amino acid name	Three letter code	One letter code
alanine	Ala	A
arginine	Arg	R
asparagine	Asn	N
aspartic acid	Asp	D
cysteine	Cys	C
glutamine	Gln	Q
glutamic acid	Glu	E
glycine	Gly	G
histidine	His	H
isoleucine	Ile	I
leucine	Leu	L
lysine	Lys	K
methionine	Met	M
phenylalanine	Phe	F
proline	Pro	P
serine	Ser	S
threonine	Thr	T
tryptophan	Trp	W
tyrosine	Tyr	Y
valine	Val	V

PART I

I.1 General aspects of PPIs modulation

Proteins involved in biological functions did not act alone and their functions tend to be regulated mostly through the formation of protein-protein complexes. Factors that influence the formation of different protein-protein complexes were studied since 1996.[1] Several complexes were compared and the diversity reflected their role in different biological functions. Up to date, several experimental methods, together with bioinformatic tools, were used to determine protein-protein interactions (PPIs).[1–4]

PPIs refers to physical contact, not accidental, established between protein interfaces as a result of non-generic biochemical events.[2] In this way cells can control numerous cellular processes such as chemotaxis, proliferation, differentiation, endocytosis and apoptosis; they are also involved in oncogenic signalling network leading to tumor progression as their misregulation can result in numerous tumor diseses.[5]

The design of structural mimetics of the active portions in the PPIs has proven an effective mean to modulate protein functions.[5,6] To date, PPI inhibition with small molecules (such as peptidomimetic ligands) is a novel and effective strategy towards drug development.[7,8] As a matter of fact, the number of pubblications on this field is growing and growing in the last few decades.

The mimetic approach involves the synthesis of molecules, with defined dimensions, to target protein surface, which includes specific amino acid residues. The space in which the targeting happens is also known as "hot spot". For example, α-helices are important recognition sites on protein surfaces for different interactions (protein-DNA, protein-protein…) which were found to be characterized by conserved structural features within the α-helical domain.[6]

More recently, structural conservation of the "hot-spots" was established.[9] In fact, hot spots are different from other regions of the protein surface due to their incurve topology and a mosaic-like pattern of hydrophobic and polar functionality. This combination of properties confers on the hot spots a tendency to bind organic compounds with different structures.[9]

Many recent success studies showed that small molecules, with drug-like potencies, bind to "hot spots" on the surfaces involved in protein–protein interactions.[10,11]

Structure-based design is therefore essential for developing PPI inhibitors, especially when peptide binding epitopes are the starting point in the design process.[12] Different strategies were used for the structure-based design of PPI inhibitors, which include mimicking or simply stabilizing β-sheets, helices and turns. For example, macrocyclization and β-hairpin inducers are useful to mimick or stabilize β-sheets,[13] while thiol-based and lactam cross-linkers can be used to stabilize α-helices.[12]

Cell adhesion molecules (CAMs)

Cell adhesion underlies tissue formation as it is one of the key processes in different cell activity as morphogenesis, cell division, apoptosis. Since cell adhesion molecules (CAMs) are essential in intercellular protein-protein interactions, they also play a key role in cell life and survival;[14] for example chemical synapses, through which neurons transfer electrical and chemical signals to other cells, are based on interactions of CAMs.[15] Cell adhesion molecules are mostly transmembrane proteins, including four protein classes: integrins, cadherins, immunoglobulins and selectins (**Figure 1**). Integrins are transmembrane heterodimeric glycoproteins which mediate events like cell proliferation and migration; cadherins are calcium-dependent adhesive transmembrane proteins, which promote cell-cell adhesion by forming homophilic interactions between the N-terminal domains of two proteins on adjacent cells. Immunoglobulins are produced by plasma cells and lymphocites and are essential for body's immune system. Selectins recognize and bind sugar moieties and act in leukocyte trafficking.

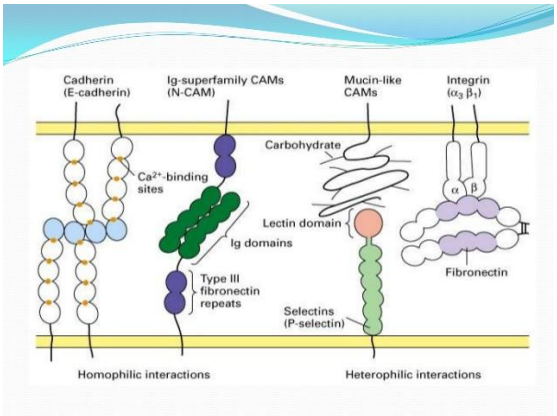

Figure 1. Families of Cell Adhesion Molecules.

1 Integrin ligand-based conjugates for targeted cancer therapy

1.1 Integrin receptors and ligands

Integrins are transmembrane receptors comprising non-covalent heterodimers, which mediate cell adhesion to extracellular matrix (ECM) proteins and other cells. They are involved in physiological and pathological situations such as angiogenesis, tumor growth, transmembrane connection to the cytoskeleton, activation of many intracellular signalling pathways, embryological development, hemostasis, thrombosis, wound healing, immune and nonimmune defence mechanisms, etc. They are also receptors for many viruses and bacteria. Since their identification as a receptor family,[16] they have become the best-understood cell adhesion receptors. Recently it was demonstrated that malignant cells' proliferation, migration, survival and aggressiveness, are triggered essentially by the ECM and so also by integrins. The importance of these integrins as potential therapeutic targets as well as in the regulation of breast cancer cells differentiation has been established.[17]

Integrins are bi-directional allosteric signalling molecules in the sense that they transfer information from the extracellular environment ("outside-in" causing adhesion, spreading, migration, growth and survival signalling, invasion) and from the cytoplasm ("inside-out") to modulate cell activity through long-range allosteric conformational changes.[18,19]

Integrins consist of α- and β-subunits; each subunit crosses the membrane once, with a large polypeptide in the extracellular space and a short cytoplasmic tail. **Figure 2** shows the subunits and their associations; 8 β-subunits pair together with 18 α-subunits in a non-covalent manner to form 24 distinct integrins. The α-subunit seems to be important in defining the ligand binding properties of integrins.[18,20]

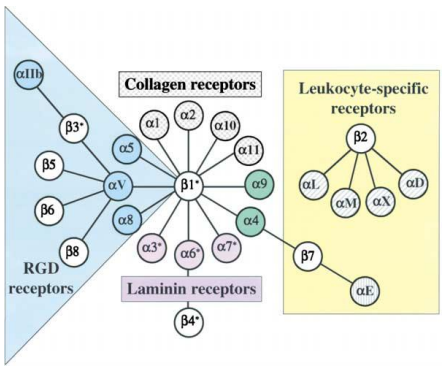

Figure 2. The integrin families and their ligands.[18]

Integrins exist in different conformational states in equilibrium between each other; in particular, the equilibrium between its inactive and active forms are showed in **Figure 3**. Conformational changes expose the external ligand-binding site (between the α- and β-subunit) to which ligands bind, allowing the transmission of signals from the outside to the inside. In particular, in the inside-out direction, activating signals induce conformational changes of the integrin extracellular domain and force integrin to pass from a resting to an active state.[21,22] In the outside-in direction, ligand binding to the extracellular domain of active integrin also induces long-range conformational

changes, which lead to association and activation of kinases and the transmission of signals in the cytosol.[22,23]

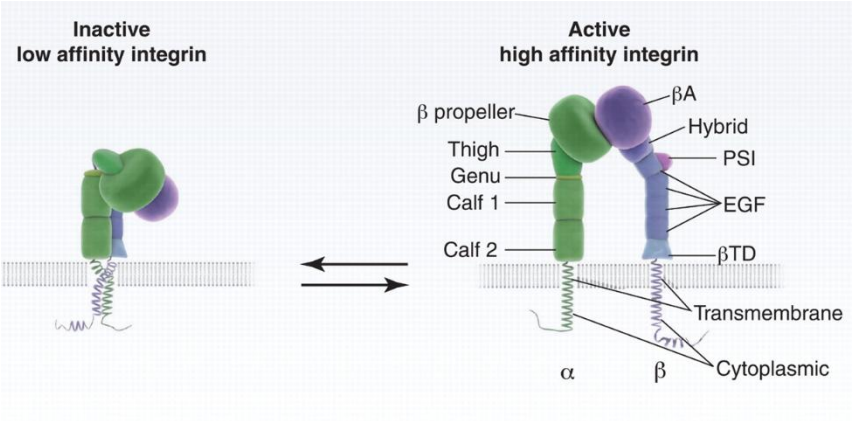

Figure 3. Representation of integrin states.[24]

Integrin binding with endogenous ligand is essential for their role; the great variety of integrin ligands includes ECM proteins (fibronectins, laminins, collagens, RGD receptors, etc), ICAMs and VICAMs receptors but also microorganisms (adenoviruses, echoviruses) can enter cells via integrins.[25] Actually, the classification of integrins showed in **Figure 2** is done considering that each integrin recognizes a specific type of endogenous ligand.

Integrins αvβ3, α5β1 and αvβ6 are usually expressed at low levels in healthy tissues and in the same time they were found to be abundant on membrane of cancer cells.[26]

Among the great variety of integrins, $\alpha_V\beta_3$ has been extensively studied and it has been found that it is mostly expressed in angiogenic vasculature. During angiogenesis, regulation of the matrix-metalloproteinase-2 (MMP-2) on the surface of angiogenic blood vessels is mediated by integrin $\alpha_V\beta_3$ resulting in collagen degradation and ECM reorganization to form new vessel for the cancer cells.[27] As a consequence, the integrin $\alpha_V\beta_3$ antagonism with either functional blocking antibodies or ligand-mimetic peptides have shown promising antiangiogenic and antitumor effects.[28]

Different approaches were studied to inhibit integrin function: impeding ligand binding, blocking downstream integrin signalling, but also modulating integrin expression. The most applied approach is to block the binding site with peptidomimetic ligands.

1.1.1 RGD-integrin ligands

Endogenous ligands bearing the tripeptide sequence RGD (**Figure 4**) have become very important in the therapeutic field, with implications in fibrosis, thrombosis, cancer, and other diseases.[20] The RGD sequence interacts with different integrin receptors related to tumor angiogenesis and cancer development such as $\alpha_V\beta_3$, $\alpha_V\beta_5$ and $\alpha_5\beta_1$.[29]

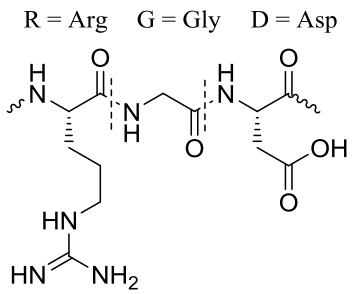

The importance of the RGD sequence was established in 1984 when Pierschbacher and Ruoslahti found that the ability of fibronectin to recognize its target receptors on cell membrane was accounted by this particular recognition motif (**Figure 4**).[29] Since then, different peptide and peptidomimetic libraries have been

Figure 4 RGD recognition motif.

developed. The presentation of the RGD sequence in the binding site is important and it is a common feature for all the RGD proteins. Higher rigidity of the backbone and low flexibility of flanking residues, needed to properly fold the RGD sequence, were obtained in different ways; blocking the RGD sequence in a cyclic structure was the most used. Among the great variety of RGD peptidomimetic ligands found in literature, Cilengitide (**Figure 5**) is the most famous. It was developed by the research group of Professor Kessler as a potent integrin ligand in 1991[30] with high binding affinity for $\alpha_v\beta_3$ (IC_{50} $\alpha_v\beta_3$ = 0.61 ± 0.06 nM) and $\alpha_v\beta_5$ (IC_{50} $\alpha_v\beta_5$ = 8.4 ± 2.1 nM) and sub-nanomolar antagonistic activity for the $\alpha_v\beta_3$ receptor.[31,32]
Cilengitide has been the first integrin ligand to be tested for antagonistic behaviour in clinical trials; it failed phase III clinical trial for treatment of patients with glioblastoma,[33] but it is currently undergoing phase II studies for the treatment of other tumors.[34–36] The interaction mechanism by which RGD ligands bind the integrin receptor was studied by Xiong *et al* through X-ray analysis.[37] The crystal structure of the isolated $\alpha_v\beta_3$ co-crystalized with Cilengitide was obtained and some key interactions were established. A distance of about 9 Å between the C_β atoms of the arginine and the aspartic acid was necessary in order to allow the following interactions shown in **Figure 6**: the guanidine group of arginine interacts with two aspartic acid residues (Asp 218 and Asp 150 of the α-subunit), whereas the aspartic acid binds to Mn^{2+} in the MIDAS (metal-ion dependent adhesion site) region of the β-subunit. These interactions, which were then addressed as "electrostatic clamp", proved to be essential to obtain ligand-protein interaction.

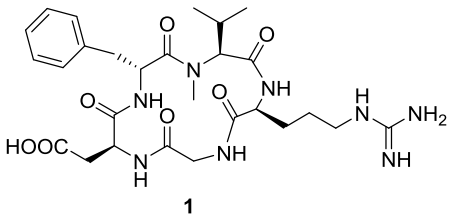

Figure 5 Cilengitide.

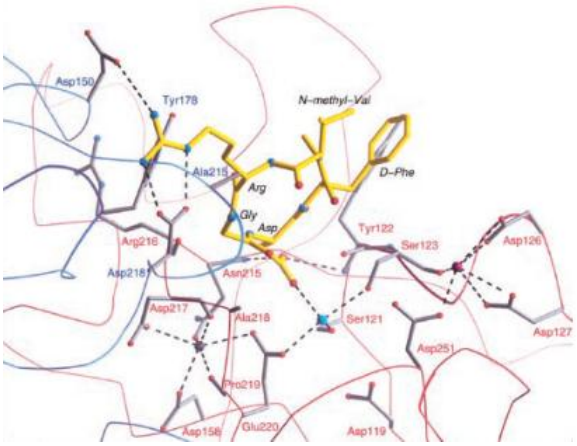

Figure 6 Crystal structure of the $\alpha_v\beta_3$ receptor complexed with Cilengitide (in yellow). Adapted from ref 37

In principle all the RGD ligands, presenting the RGD motif in the proper conformation, can interact with the integrin binding site. On these basis, a great variety of RGD ligands were designed in order to develop anti-angiogenic agents; some examples are reported in **Figure 7**, which is not an exhaustive list of these integrin ligands.

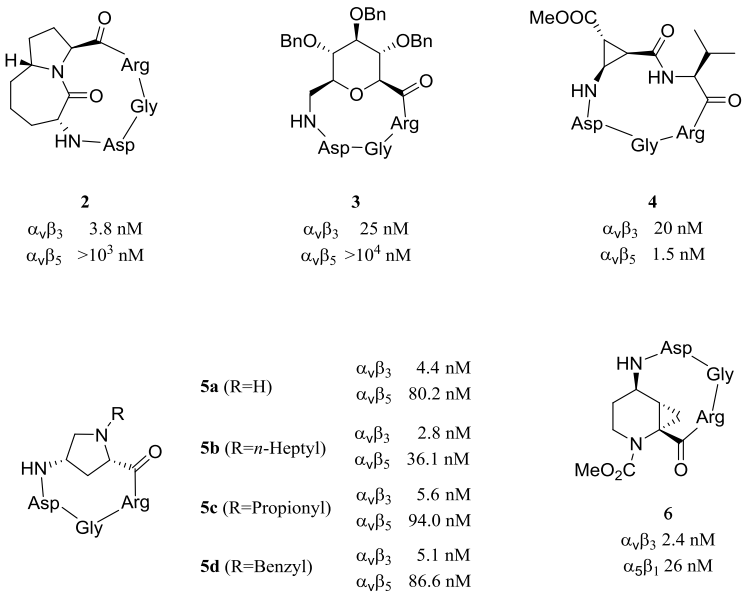

Figure 7 Few examples of integrin ligands (**2**[38], **3**[39], **4**[40], **5**[41], **6**[42]) and their relative integrin affinity (IC_{50} values).

Although the great activity of these and others integrin ligands versus angiogenesis, inconsistent observations were found regarding the enhanced tumor growth observed on integrin β_3-deficient mice.[43] Furthermore, low concentrations of RGD-mimetic integrin $\alpha_v\beta_3$ inhibitors stimulate tumor growth and angiogenesis in mice.[28,44] Cilengitide's question itself has turned to be controversial despite cilengitide is well tolerated and non toxic; it showed to act as agonist of angiogenesis in low concentrations, compromising its antiangiogenic effects.[45]

Anyway, a different way of use of these small molecules, exploiting the $\alpha_v\beta_3$ over expression on the membrane of tumor cells, has become attractive. As a matter of the fact, they can be seen as vectors to selectively deliver imaging agents[46,47] and also chemotherapeutics[48,49].

Starting from 2009, our research group together with the research group of Professor Gennari from University of Milan developed low nanomolar peptidomimetics RGD integrin ligands.

2,5-diketopiperazine (DKP) bifunctional scaffolds were used to display the RGD sequence in the proper conformation for targeting integrins. Among the great variety of conformationally constrained scaffolds which have been used to develop ligands for integrins, or in general for PPI's modulation, DKP have shown very promising properties. In fact, the structural similarity of DKP to peptides opens a new way for medicinal chemistry in designing molecules with similar characteristics. Reducing the susceptibility to metabolic amide bond cleavage and inducing conformational rigidity are the results of constraining the nitrogen atom of an α-amino amide into a DKP ring. Functional diversity and stereochemistry can be introduced at different positions. A DKP library was developed in our research group (**Figure 8**).[50,51] These DKPs differ for the stereochemistry at C3 and C6 and for the substitution on the endocyclic nitrogens.

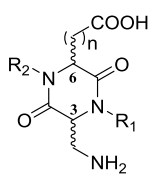

DKP1: (3S,6S), R_1 = Bn, R_2 = H, n = 1
DKP2: (3R,6S), R_1 = Bn, R_2= H, n = 1
DKP3: (3S,6R), R_1 = Bn, R_2= H, n = 1
DKP4: (3R,6S), R_1 = H, R_2= Bn, n = 1
DKP5: (3R,6S), R_1 = R_2 = Bn, n = 1
DKP6: (3S,6R), R_1= H, R_2= Bn, n = 1
DKP7: (3S,6R), R_1 = R_2 = Bn, n = 1
DKP8: (3S,6R), R_1 = Bn, R_2= H, n = 2

Figure 8 DKP1-DKP8 scaffold library[50,51]

Based on these DKP scaffolds, a small library of cyclic(DKP-RGD) integrin ligands were synthesized by our group exploiting the two carboxylic and amino functions (**Figure 9**).[52,53]

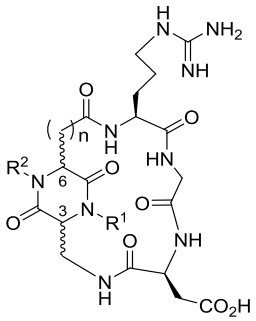

7 *c*[**DKP1**-RGD]: 3*S*, 6*S*, R^1 = Bn, R^2 = H, n = 1
8 *c*[**DKP2**-RGD]: 3*R*, 6*S*, R^1 = Bn, R^2 = H, n = 1
9 *c*[**DKP3**-RGD]: 3*S*, 6*R*, R^1 = Bn, R^2 = H, n = 1
10 *c*[**DKP4**-RGD]: 3*R*, 6*S*, R^1 = H, R^2 = Bn, n = 1
11 *c*[**DKP5**-RGD]: 3*R*, 6*S*, R^1 = Bn, R^2 = Bn, n = 1
12 *c*[**DKP6**-RGD]: 3*S*, 6*R*, R^1 = H, R^2 = Bn, n = 1
13 *c*[**DKP7**-RGD]: 3*S*, 6*R*, R^1 = Bn, R^2 = Bn, n = 1
14 *c*[**DKP8**-RGD]: 3*S*, 6*R*, R^1 = Bn, R^2 = H, n = 2

Figure 9 *c*[DKP-RGD] peptidomimetics (**7-14**).

All the ligands were tested *in vitro* for their ability to inhibit biotinylated vitronectin binding on the isolated $\alpha_v\beta_3$ and $\alpha_v\beta_5$ integrin receptors (see **Table 1**). Vitronectin is an endogenous integrin ligand. In particular, compounds **8-14**, bearing the *trans*-DKP scaffolds (DKP2-DKP7), were qualified as low nanomolar ligands for $\alpha_v\beta_3$. They also showed a higher $\alpha_v\beta_3/\alpha_v\beta_5$ selectivity with respect to the Cilengitide (**1**, **Figure 5**) taken as reference ligand.
The differences in the binding ability among the different compounds **8-14** were elucidated by NMR spectroscopy experiments and MC/SD (Monte Carlo/Stochastic Dynamics) simulations. The binding ability is essentially due to the intramolecular H-bonds formed and to the extended conformation of the RGD motif, as for Cilengitide. The ligands with the best pose of the RGD motif (particularly a distance of 9 Å between C_β(Arg) and C_β(Asp) was found) are the ones with the highest affinity values.

Compound	Structure	$\alpha_v\beta_3$ IC_{50} [nM]	$\alpha_v\beta_5$ IC_{50} [nM]
7	*c*[DKP1-RGD]	3898 ± 418	$>10^4$
8	*c*[DKP2-RGD]	3.2 ± 2.7	114 ± 99
9	*c*[DKP3-RGD]	4.5 ± 1.1	149 ± 25
10	*c*[DKP4-RGD]	7.6 ± 4.3	216 ± 5
11	*c*[DKP5-RGD]	12.2 ± 5.0	131 ± 29
12	*c*[DKP6-RGD]	2.1 ± 0.6	79 ± 3
13	*c*[DKP7-RGD]	0.2 ± 0.09	109 ± 15
14	*c*[DKP8-RGD]	7.5 ± 0.0	$>10^3$
Cilengitide	*c*(RGDfV)	3.2 ± 1.3	7.5 ± 4.8

Table 1 Binding affinity of compounds **7-14** on isolated receptor.

C[DKP3-RGD] **9** was further analyzed *in vitro* on HUVEC (Human umbilical vein endothelial cells) and it was found to efficiently inhibit angiogenesis also in the presence of pro-angiogenic growth factors without affecting other cellular aspects such as proliferation and cell viability.[54]

It was also found that compound **9** significantly inhibit the phosphorylation of Akt (protein kinase important in the regulation of vascular angiogenesis),[54] FAK/Akt integrin-activated transduction signalling pathway and integrin-mediated cell infiltration process in U373 (human glioblastoma) cell line.[55] This results increased the interest toward *c*[DKP3-RGD] **9** as true integrin $\alpha_v\beta_3$ antagonist. With the aim to use **9** as potential vehicle for delivery cytotoxic agents, the DKP3 scaffold was modified on the benzyl moiety, obtaining the *c*[DKP3-RGD]-CH_2-NH_2 functionalized ligand **15** named *c*[DKPf3-RGD] (**Figure 10**).[56]

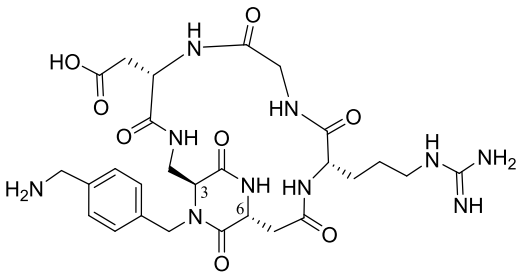

15

Figure 10 *c*[DKPf3-RGD] integrin ligand (**15**).

The amino group on the benzylic moiety has been used as linkage point for further functionalizations and in particular for developing SMDCs (small molecule drug conjugates) targeting the $\alpha_v\beta_3$ receptor.[48,57,58]

1.1.2 RGD-based integrin ligands as SMDCs

Small molecule drug conjugates are small vehicles for targeted drug delivery and they are composed by low-molecular weight targeting ligands covalently conjugated to a cytotoxic agent through a suitable linker (**Figure 11a**).[59]

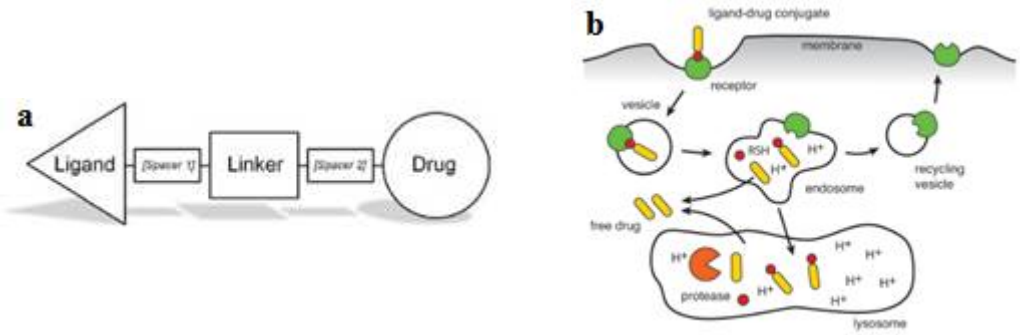

Figure 11 General structure of SMDCs (**a**). Adapted from ref 59. General mode of action for the SMDCs internalization (**b**). Adapted from ref 60.

In some cases, additional linker spacers can be added when there is the necessity to enhance solubility in aqueous media or to improve the drug release. The internalization mechanism has been described in 2013 (**Figure 11b**).[60] Generally, the ligand binds to the target on the cell membrane to form a complex which is then internalized in a vesicle. Its fusion with the early endosome may release the drug (if pH-dependent linker system is present), or it may proceed to the lysosome in which proteases hydrolize amide and ester specific bonds releasing the drug. The drug needs to be expelled outside the endosome or lysosome (normally by passive diffusion) in order to act on the target.[60]

The linker strategy as well as the choice of the drug and the targeting ligand are key factors for developing an effective drug delivery system. Different types of linkers can be used: acid sensitive (e.g. esters or hydrazones), enzimatically-cleavable linkers (e.g. Val-Ala, Val-Cit, GFLG), disulfide linkers (reduced by Glutathione), etc.

Many examples of RGD-drug conjugates can be cited,[61–66] including the work developed by our research group in the field.[52,56–58,67,68] Some of them are described in the following section.

- **RGD-Paclitaxel (PTX) conjugates**

Paclitaxel (PTX, **Figure 12**) is one of the most effective antineoplastic agents for treatment of many cancers. It is effective on both solid and disseminated tumors thanks to the particular mechanism of action. Its antitumor efficacy is due to the combination of antiproliferative and cytotoxic properties. In fact, it hampers tumor angiogenesis and also it binds selectively the tubulin proteins promoting their stabilization; the latter leads to disruption of microtubules, thus inducing mitotic arrest which

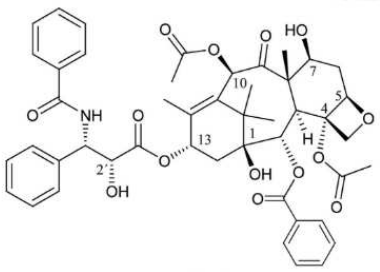

Figura 12 Structure of PTX.

eventually leads to cell death. The OH group in position 2' is essential for the biological activity and represents an ideal position for the insertion of functional groups to create prodrugs or conjugates.[69] Having synthesized peptidomimetic ligands targeting $\alpha_v\beta_3$ receptor with high affinity (**15**, **Figure 10**) Gennari and Piarulli's research group developed the *c*[DKPf3-RGD]-PTX conjugate (**Figure 13a**). Paclitaxel was linked to the DKPf3-RGD targeting moiety by an acid-labile ester bond through a succinate fragment. The conjugate retained a low nanomolar affinity and a high selectivity for $\alpha_v\beta_3$ receptor (IC_{50} $\alpha_v\beta_3$: 5.2 nM; IC_{50} $\alpha_v\beta_5$: 219 nM). Moreover, *in vivo* test on compound **a** in nude mice xenografted with IGROV-1/Pt1 cancer cells ($\alpha_v\beta_3$ over-expressing cells) showed that conjugate **a** (**Figure 13**) was more effective than free PTX.[56]

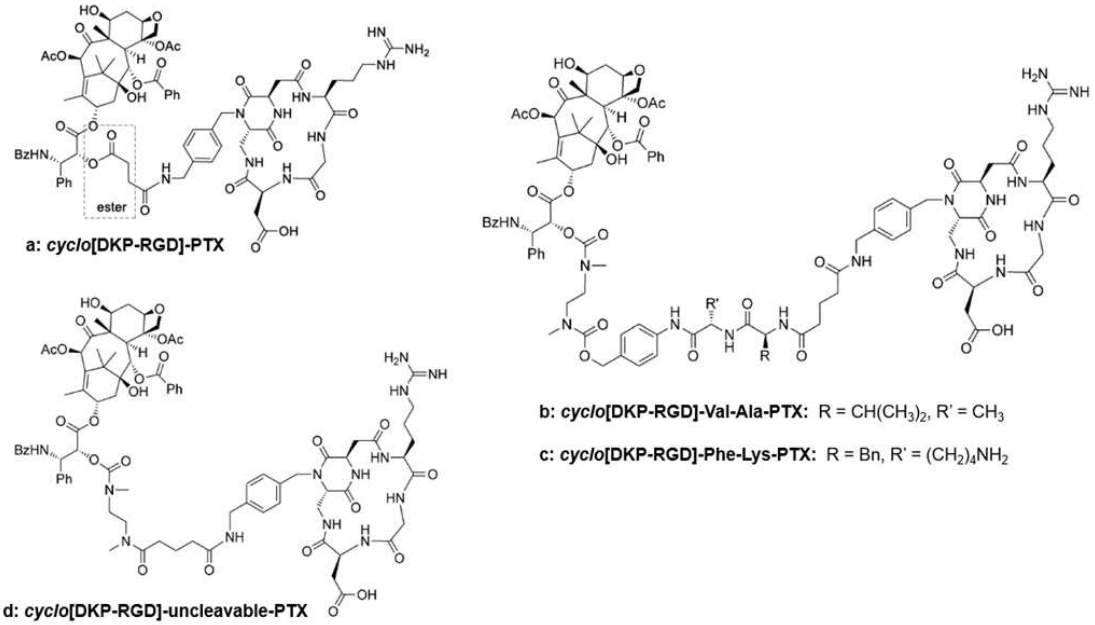

Figure 13. *c*[DKPf3-RGD]-PTX conjugates (**a**-**d**) developed in Gennari and Piarulli's research group.

PTX was also linked to *c*[DKPf3-RGD] through lysosomally cleavable linkers: Val-Ala and Phe-Lys (**Figure 13b-c**). The conjugates were stable at different pH conditions and showed an efficient linker cleavage and release of the drug after treatment with lysosomal extract. The integrin targeting affinity of the conjugates was suggested as their antiproliferative activity was similar to free PTX with an increased potency in CCRF-CEM ($\alpha_v\beta_3$+) compared to the negative cell line. The conjugate **d** in **Figure 13** contains an 'uncleavable' nonpeptide linker. It was synthetized as a negative control of the linker efficacy and showed no cytotoxicity. In the competitive binding assay, the three conjugates displayed slightly lower binding affinity than the unconjugated ligand **15**, remaining in the low nanomolar range and conserving the selectivity towards $\alpha_v\beta_3$ compared to $\alpha_v\beta_5$.[48]

To note the presence of a self-immolative linker between the PTX moiety and the peptide linker. It offers an elegant mechanism of releasing the free PTX inside the cells; once the conjugate reaches lysosomes, cathepsin B proteases hydrolize the C-terminus of the dipeptide linker (**Figure 14**). A fast electron cascade takes place in the aniline ring, releasing CO_2 and forming a stable free amine. Finally, a slow cyclization step liberates the free paclitaxel in the tumor cell.

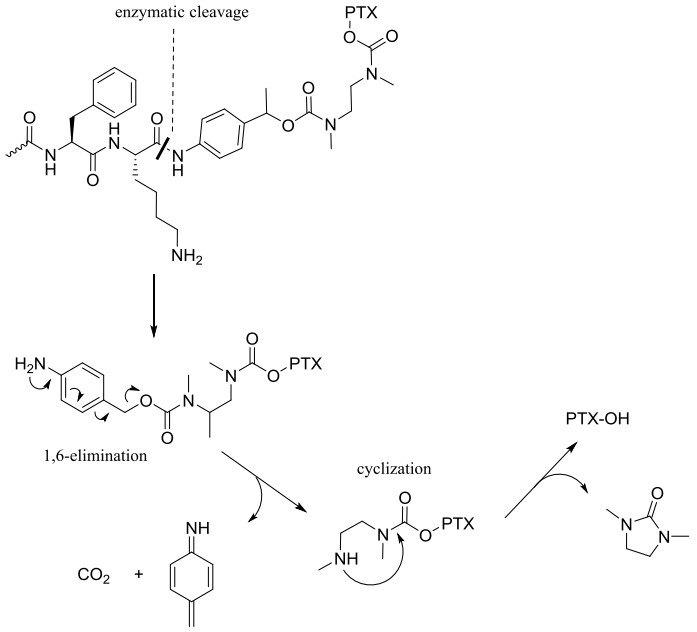

Figure 14. Enzymatic cleavage and drug release of PTX prodrug containing the peptide linker Phe–Lys.

- **RGD-Doxorubicin (DOX) conjugates**

In 2008, Ryppa and co-workers[70] reported the synthesis of two DOX-E[*c*(RGDfK)]$_2$ conjugates. DOX was attached to the ligand through an amide bond (**Figure 15a**) or a MMP2/MMP9 cleavable octapeptide linker was used (**Figure 15b**). The conjugate bearing the protease cleavable linker demonstrated to be more efficient in the HUVEC antiproliferative, but *in vivo* it displayed only a moderate antitumor activity compared to free DOX.

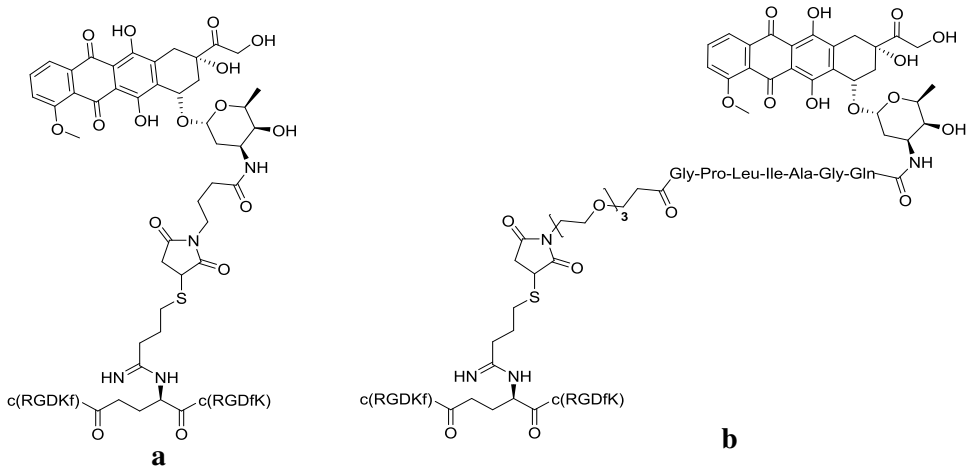

Figure 15. RGD-DOX conjugates (**a**, **b**) developed by Ryppa and co-workers.

- **RGD-Camptothecin (CPT) conjugates**

In 2017, the synthesis of the new *c*[DKP-RGD]-Naph-S-S-CPT conjugate[57] (**Figure 16b**) and its biological evaluation compared to the previously reported conjugate *c*[RGDyK]-Naph-S-S-CPT (**Figure16a**)[71] was reported by Gennari's research group. The two conjugates were able to bind the purified integrin $\alpha_v\beta_3$ at nanomolar concentrations. The internalization process was also investigated thanks to the fluorescent moiety present in the conjugates; U87 (human glioblastoma, $\alpha_v\beta_3$ +) cells and U87 clone non expressing $\alpha_v\beta_3$ were chosen. Internalization was found to be not dependent on the $\alpha_v\beta_3$ expression as it was detected for both cell lines. Moreover, due to the premature cleavage of the disulfide linker and the release of the free CPT, conjugates **a** and **b** were not stable in the cell media.[57]

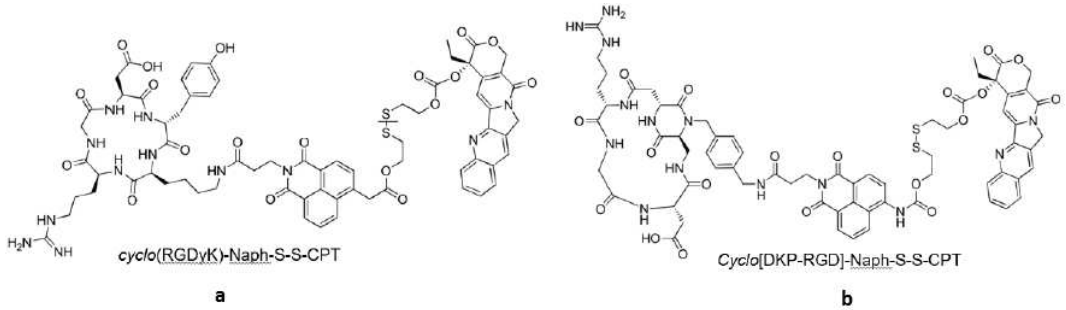

Figure 16. RGD-CPT conjugates (**a**, **b**).

Many other RGD-drug conjugates were developed bearing the previously reported drugs and new other drugs such as mono Monomethyl auristatin E and F.[49,72]

1.2 Aim of the project

Considering the great potential of *c*[DKPf3-RGD] **15** (**Figure 10**) as targeting integrin ligand, we decided to use it and develop novel drug-conjugates exploring different linker strategies and two different cytotoxic payloads, Daunomycin and Paclitaxel.

Daunomycin (or Daunorubicin, Dau, **Figure 17**) is an anthracycline anticancer drug which intercalates between the base pair of the DNA interfering with its functions and replication.[73] Despite its high efficiency, daunomycin has numerous side effects, in particular cardiotoxic effects.[74] Anyway, daunomycin's cardiotoxicity is lower than the one of doxorubicin.[75] It was demonstrated that coupling the drug to peptide carrier could improve solubility, decreases side effects and offers the possibility to enhance selectivity by targeting tumor cells.[76,77] Following this approach, we planned to link Dau to our *c*[DKPf3-RGD] (**15**) previously reported by our group. Considering that modification of the amino group on the sugar moiety of the Dau might lead to loss of bioavailability of the compound[78], the oxo group at the C-13 position was used as conjugation site. Two conjugates (**16** and **17**, **Figure 18)** were synthesized and in both cases Dau was linked to the targeting moiety *via* oxyme linkage through two aminooxyacetylated peptides. In the case of the conjugate **16**, the targeting moiety is directly linked to Dau, without any cleavable linker through the dipeptide PropargylGly-Aoa which corresponds to the minimum peptide sequence necessary to link Dau and the targeting moiety. On the other hand, compound **17** displays the *c*[DKPf3-RGD] linked to Dau through the Aoa-GFLG cleavable linker, with the aim to investigate whether the presence of a cleavable linker is required for the antitumor activity of the conjugates. The GFLG linker is degraded by lysosomal enzymes ensuring the release of the Dau=Aoa-Gly-OH as the smallest bioactive metabolite in lysosomes.[79] In fact, previous studies demonstrated that not only the free Dau but also Dau containing metabolites, such as Dau=Aoa-Gly-OH, bind to DNA efficiently, thus presenting antitumor activity.[79,80]

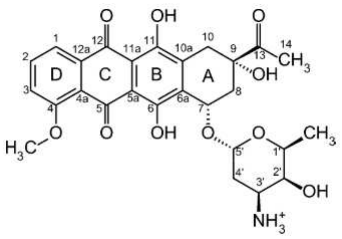

Figure 17. Daunomycin structure

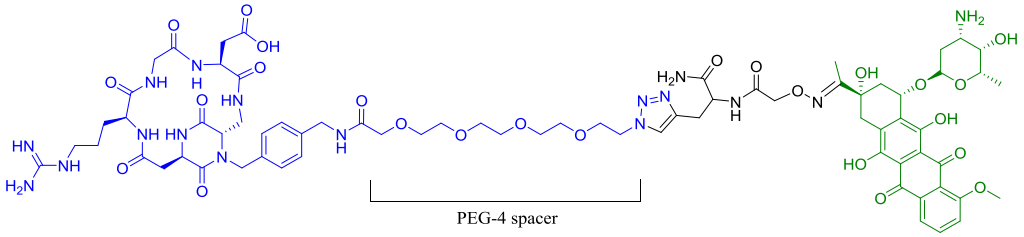

16 *c*[DKPf3-RGD]-PEG$_4$-PropargylGly-Aoa=DAU)

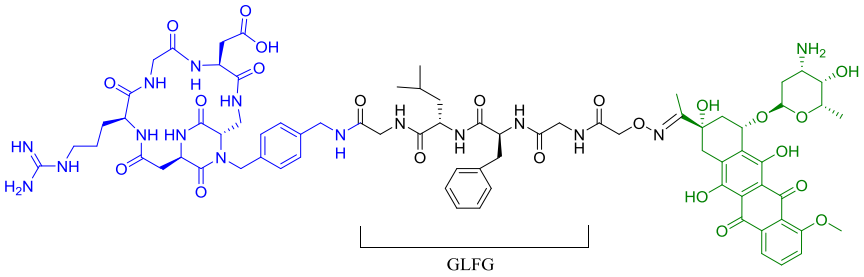

17 *c*[DKPf3-RGD]-GLFG-Aoa=DAU)

Figure 18 Conjugates *c*[DKPf3-RGD]-PEG-4-PropargylGly-Aoa-DAU **16** and *c*[DKPf3-RGD]-PEG-4-GLFG-Aoa-DAU **17**; in blue the targeting moiety, in green the Dau.

For what concern the Paclitaxel conjugate, different strategies were previously adopted in Gennari and Piarulli's group in order to improve the cytotoxicity of *c*[DKPf3-RGD]-Paclitaxel conjugates; an acid-labile ester bond through a succinate fragment was initially used to link PTX to the targeting moiety[56], as previously described in **Paragraph 1.1**. Because of the poor stability of this ester in circulation, the insertion of lysosomally cleavable linkers (Val-Ala or Phe-Lys), was employed as they show high plasma stability and they are rapidly cleaved upon endocytosis by tumor-associated extracellular or lysosomal cysteine proteases.[48] As a further step, multivalency was considered to improve binding affinity of RGD ligand to integrin $\alpha_v\beta_3$.[68] In fact, through linking PTX to two to four *c*[DKPf3-RGD] ligands was demonstrated to be an effective strategy to enhance targeting and thus cytotoxicity.

Among these strategies, we decided to use the well known cell penetrating properties of the peptide sC18 to develop a *c*[DKPf3-RGD]-PTX conjugate with the aim to improve the CPP-mediate internalization and in consequence cytotoxicity. Conjugate **18** is represented in **Figure 19**; it was designed to release PTX intra-cellularly by means of a self-immolative spacer (PABC-N,N'-di-methylethylene diamine) and a lysosomally cleavable dipeptide linker (Val-Ala), which connects PTX to an heterobifunctional cross linker, N-(-2-aminoethyl) maleimide. As sC18 was equipped with a β-alanine-cysteine dipeptide on Lys_{13}, the maleimide group can react with the thiol group of the cysteine, thus connecting the *c*[DKPf3-RGD] **15** which is, in turn, linked to the sC18 through a PEG-4 N_3 spacer.

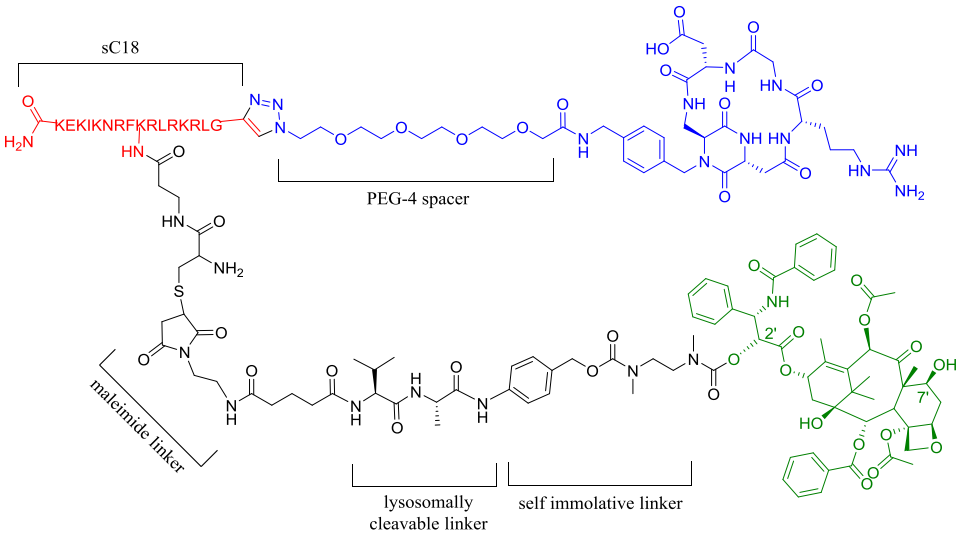

Figure 19 conjugate *c*[DKPf3-RGD]-Ptx (**18**) bearing sC18 and a self immolative linker.

1.2.1 Synthesis of the functionalized *c*[DKP-RGD] integrin ligand 15

- Synthesis of DKPf3 scaffold (28)

Synthesis of the DKP-f3 scaffold is presented in **Scheme 1**, starting from commercially available D-aspartic acid **19** and L-serine methyl ester **21**.[56] Side chain of the aspartic acid was protected with the allyl group before *N*-Boc protection, giving compound **20**. Aldehyde **22** underwent a reductive amination with L-serine methyl ester using sodium triacetoxyborohydride to obtain the functionalized serine **23**. Intermediates **20** and **23** reacted under direct coupling conditions (HATU, HOAt, DIPEA) to afford the isopeptide **24** in high yield (80%). The selective acylation of the unprotected β-hydroxy group of the functionalized serine occurs instead of the expected peptide bond formation, as reported also in the synthesis of DKP1-3.[52,81] Once Boc protecting group of **24** was cleaved, O,N-acyl migration and subsequent ring closure were prompted by treatment with DIPEA in a protic solvent (isopropyl alcohol)[81], giving the DKP-f3-OH **25** (84% over two steps). The hydroxyl group of **25** was substituted by an azide group via a Mitsunobu reaction using HN_3 as nucleophile, affording compound **26** in satisfactory yield (60%). The reaction was carried out at low temperature (-20°C) to avoid the formation of the elimination by-product. An one-pot Staudinger reduction-Boc protection allowed to reduce the azide under mild conditions and directly attack the 2-(*t*-butoxy-carbonyl-oxyimino)-2-phenylacetonitrile (Boc-ON) present in the medium, affording the DKP-f3-NHBoc **27** in good yield (88%). Finally, allyl deprotection yielded the *trans* DKPf3 scaffold **28** in 85% yield.

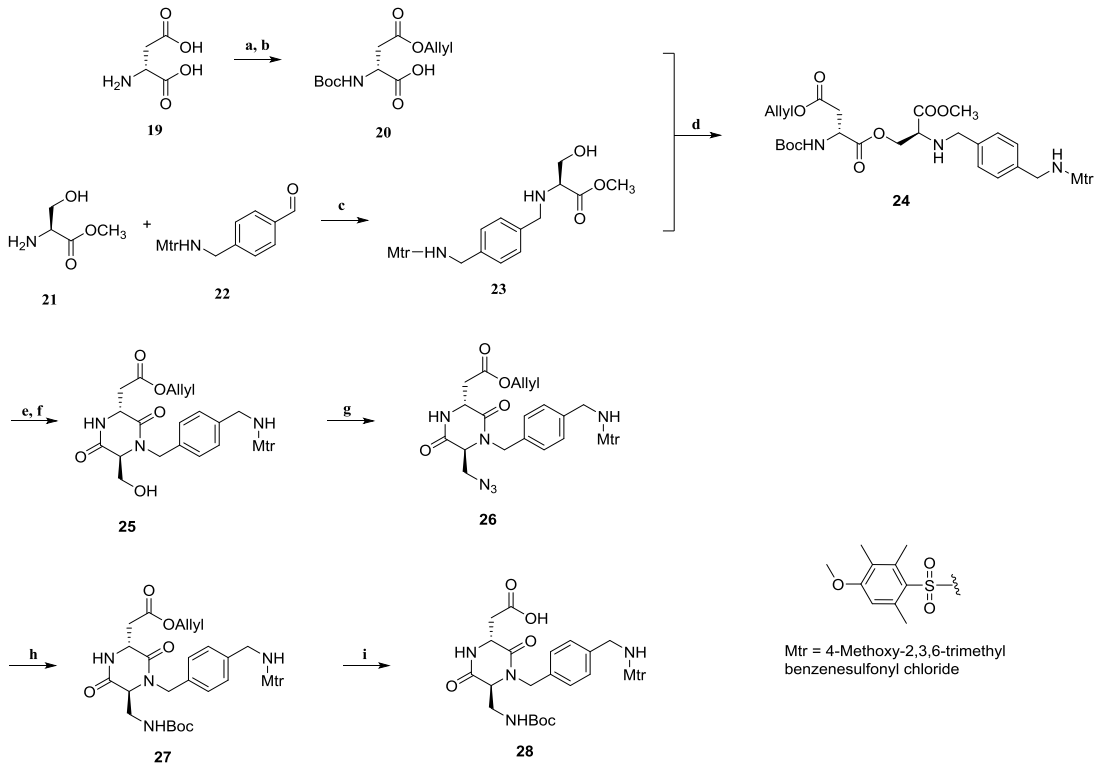

Scheme 1. Synthesis of DKPf3 scaffold (**28**): a) Allyl alcohol, acetyl chloride; b) Boc_2O, TEA, dioxane, water, 95% over two steps; c) aldehyde **22**, $NaBH(OAc)_3$, THF, 3 h, r.t., quant.; d) HATU, HOAT, DIPEA, DMF, 3 h, 0 °C to r.t. 80%; e) TFA/DCM 1:2, 3 h, 0 °C to r.t.; f) DIPEA, *i*PrOH, overnight, r.t., 84% over two steps; g) HN_3·in Tol, DIAD, Ph_3P, DCM/Toluene 1:2, 4 h, -20 °C, 60%; h) Me_3P, BOC-ON, THF, 3 h, -20 °C to r.t., 88%; i) pyrrolidine, PPh_3, $[Pd(PPh_3)_4]$, DCM, 4h, 0 °C to r.t., 85%.

- Synthesis of *c*[DKPf3-RGD] (15)

Diketopiperazine DKPf3 was used as scaffold for the synthesis of functionalized *c*[DKPf3-RGD] integrin ligand **15** (**Figure 10**), following a solution phase strategy (**Scheme 2**). Dipeptide Boc-Arg(Mtr)-Gly-OBn, prepared following a reported procedure[52], was Boc-deprotected and coupled to **28** to give compound **29** in good yield (85%). The Boc protecting group of compound **29** was then removed and the resulting free amine was coupled to Cbz-Asp(O*t*Bu)-OH to obtain the linear peptidomimetic ligand **30** in high yields (89%). After carboxybenzyl and benzyl groups simultaneous deprotection by catalytic hydrogenolysis to give compound **31** quantitatively, the 17-membered macrolactamization in highly diluted DMF solution (1.4 mM) using HATU, HOAt and DIPEA (4:4:6) yielded the protected cyclo **32** in good yield (68%). The final step was the removal of the side chain protecting groups using TFA/TMSBr/thioanisol/EDT/phenol 70:14:10:5:1, obtaining **15** in satisfactory yield (70%).

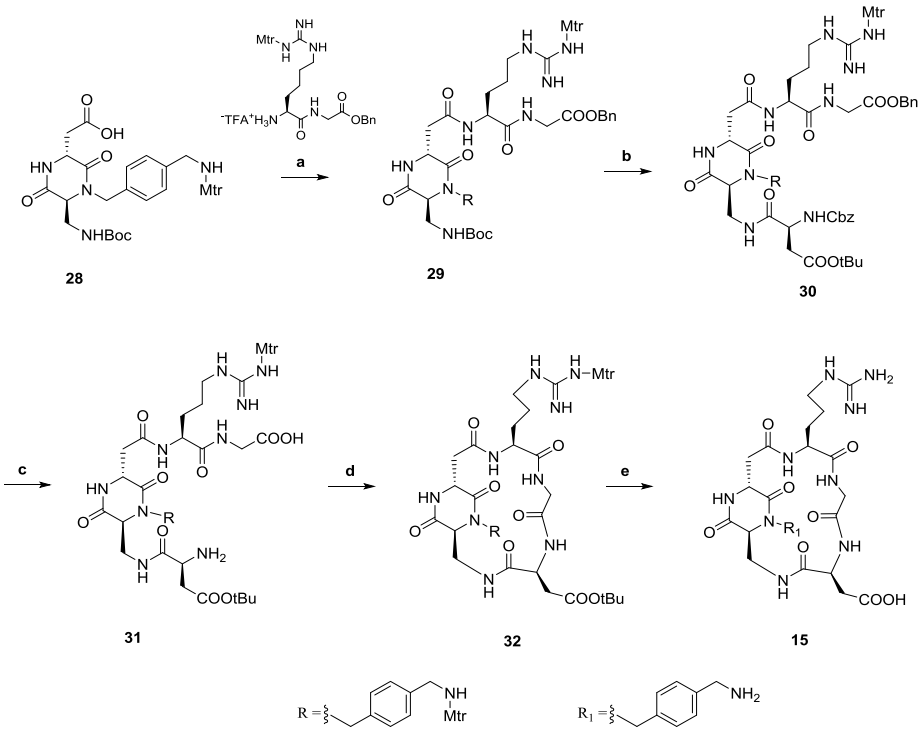

Scheme 2. Synthesis of *c*[DKPf3-RGD] (**15**): a) Boc-Arg(Mtr)-Gly-OBn, HATU, HOAT, DIPEA, DMF, o.n., r.t., 85%; b) Cbz-Asp(OtBu)-OH, HATU, HOAT, DIPEA, DMF, o.n., r.t., 89%; c) H_2, 10% Pd/C, THF/water 1:1, o.n., r.t., quant.; d) HATU, HOAT, DIPEA, 1.4 mM in DMF, o.n., r.t., 68%; e) TFA/TMSBr/thioanisol/EDT/phenol 70:14:10:5:1, 2h, r.t., 70%.

1.3 Daunomycin conjugates

1.3.1 Synthesis

C[DKPf3-RGD]-PEG-4-N_3 (**34**, **Scheme 3**) was prepared by pH-controlled coupling between the RGD ligand **15** and COOH-PEG-4-azide pre-activated as NHS ester (**33**, using EDC HCl and NHS). The pH was maintained around 7.3-7.6, with the addition of small amounts of NaOH 0.2 M, in order to prevent the hydrolysis of the NHS ester which can compete with the formation of the amide bond at pH > 7.6. Furthermore, in these conditions the guanidinium group of the arginine residue is protonated so that it does not compete with the primary benzylic amine of compound **15**.

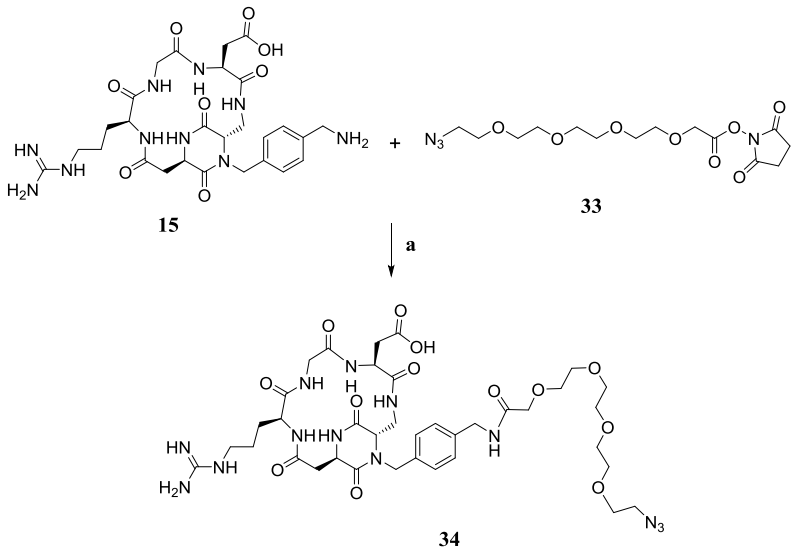

Scheme 3 Synthesis of intermediate *c*[DKPf3-RGD]-PEG-4-N_3 (**34**). a) PBS (pH 7.5), o.n., r.t., 40%.

Compound **16** was then synthesized as reported in **Scheme 4**. Rink amide resin (100-200 mesh, loading: 0.48 mmol/g, 144 µmol scale) was manually loaded with the Fmoc-propargylGly-OH. After a capping procedure to block the unreacted groups on the resin (acetic anhydride and DIPEA in DMF), Fmoc deprotection of the amino acid with 30% solution of piperidine in DMF (**35**, **Scheme 4**) was done. BisBoc-Aminooxyacetic acid was then manually coupled twice (Oxyma, DIC in DMF for 2 h) (**36**). Full cleavage of the peptide from the resin was done using TFA:TIS:water 90:2.5:2.5 (v/v/v) in the presence of 5 eq Boc-Aoa-OH. Dau was coupled to the aminooxyacetilated peptide **37**, dissolving the peptide in 0.2M NH_4OAc (10 mg/mL, pH 5), yielding intermediate **38**. After HPLC purification, **38** was linked to *c*[DKPf3-RGD]-PEG-4-N_3 **34** through CuAAC reaction, yielding final conjugate **16** in 56% yield.

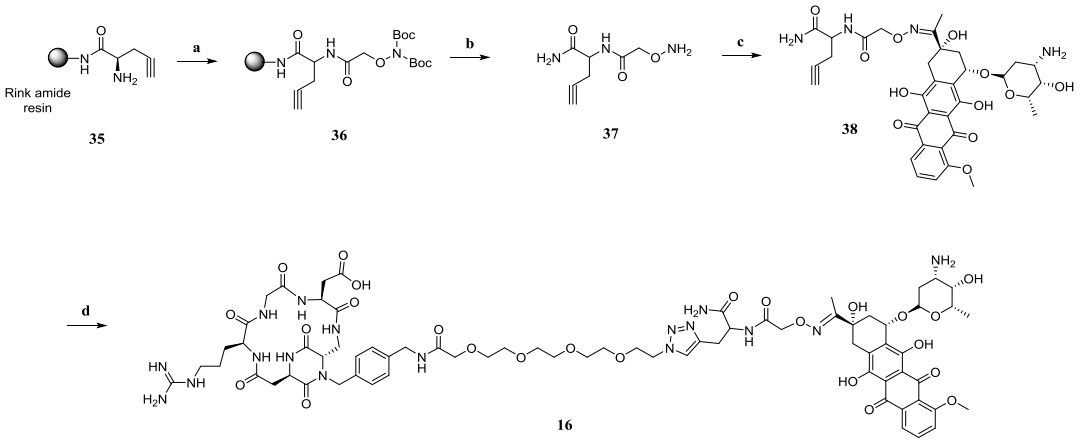

Scheme 4. Synthesis of conjugate *c*[DKPf3-RGD]-PEG-4-PropargylGly-Aoa-DAU (**16**). a) bisBoc-Aoa-OH 3 eq, oxyma 3 eq, DIC 3 eq, in DMF, 2h, r.t.; b) TFA:TIS:water 90:2.5:2.5 (v/v/v), 5eq Boc-Aoa-OH, 30%; c) 0.2M NH_4OAc (pH 5) at a peptide concentration of 10 mg/mL, Dau 30% excess, 64%; d) peptide **38** (1.3 eq), *c*[DKPf3-RGD]-PEG-4-N_3 (1 eq), sodium ascorbate, $CuSO_4$ $5H_2O$, *tert*-buthanol/H_2O 1:1, o.n., 56%.

Synthesis of compound **17** is reported in **Scheme 5**. The GFLG tetrapeptide was synthesized as C-terminal acid on a 2-chlorotrytil chloride resin (H-Gly-2CT Resin, 100-200 mesh, 0.87mmol/g, 0.015 mmol scale) by automated multiple solid-phase peptide synthesis (Fmoc strategy). BisBoc-Aminooxyacetic acid was coupled manually to the peptide using 3 eq. of the reagent, 3 eq. Oxyma and 3 eq. DIC for 2 h and the procedure was repeated twice (**40**, **Scheme 5**). Full cleavage of the peptide from the resin was done using TFA:TIS:water 90:2.5:2.5 in the presence of 5 eq Boc-Aoa-OH in order to avoid the formation of the acetone adduct with m/z = +40.[82] The peptide **41** was lyophilized from water:*tert*-butyl alcohol (1:3 v/v) and purified by preparative RP-HPLC (50-90 ACN in 45 min). The peptide was let to react with acetone in order to protect the Aoa moiety as *iso*propyliden group (**42**). *C*[DKPf3-RGD] **15** was then coupled to the C-terminus of the peptide using BOP and DIPEA in DMF, obtaining compound **43**. The *iso*propyliden group was then cleaved from the Aoa dissolving the peptide in 1M CH_3ONH_2 HCl containing NH_4OAc-buffer (0.2 M, pH 5) (20 eq at least). The reaction mixture was then directly purified by semi-preparative HPLC. Finally, Dau (30% excess) was coupled to the deprotected aminooxyacetylated peptide, dissolving the peptide in 0.2M NH_4OAc (10 mg/mL, pH 5), yielding conjugate **17** in 50% yield after HPLC purification.

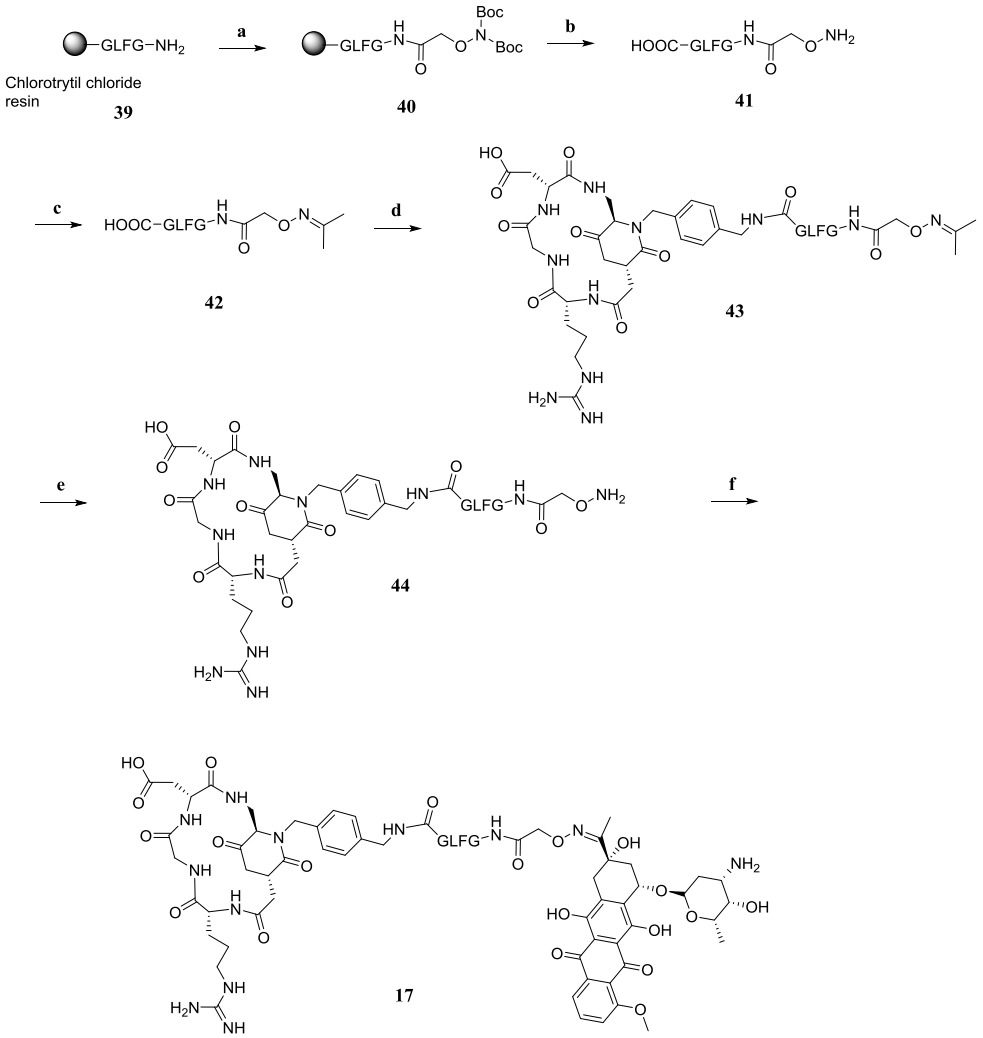

Scheme 5. Synthesis of conjugate *c*[DKPf3-RGD]-GLFG-Aoa-DAU **17**. a) bisBoc-Aoa-OH 3 eq, oxyma 3 eq, DIC 3 eq, in DMF, 2h, r.t.; b) TFA:TIS:water 90:2.5:2.5 (v/v/v), 5 eq Boc-Aoa-OH, 80%.; c) aceton, 2h, 92%; d) peptide 2 eq, *cyclo*[DKPf3-RGD]-CH_2NH_2 1 eq, BOP 1.8 eq, DIPEA 5 eq in DMF, 28%; e) 1M CH_3ONH_2 HCl in NH_4OAc-buffer (0.2 M, pH 5),88%; f) 0.2M NH_4OAc (pH 5) at a peptide concentration of 10 mg/mL, Dau 30% excess, 50%.

1.3.2 Early *in vitro* studies

Cytotoxicity and cellular uptake of the conjugates were analyzed at University of Cologne by PhD Student Lucia Feni, while binding affinity was assessed in University of Milan; these have to be considered only preliminary results as further biological analysis are still ongoing.

- **Binding affinity**

Conjugates (**16** and **17**, **Table 2**) containing the targeting moiety *c*[DKPf3-RGD] integrin ligand **15**, and controls (**9** and **15**, **Table 2**) were evaluated by Dr. Daniela Arosio (CNR-ISTM, Università degli Studi di Milano) for their binding affinity towards the isolated $\alpha_v\beta_3$ and $\alpha_v\beta_5$ integrin receptors. This test measured the ability of the conjugates to inhibit the binding of biotinylated vitronectin to the purified $\alpha_v\beta_3$ and $\alpha_v\beta_5$ receptors in a competitive binding assay. The immobilized integrin receptor ($\alpha_v\beta_3$ or $\alpha_v\beta_5$) was incubated with solutions of the conjugates (**16 and 17)** and controls **(9 and 15)** at different concentrations in presence of biotinylated vitronectin (1 $\mu g\ mL^{-1}$), then the bound vitronectin was measured. The half-maximal inhibitory concentrations (IC_{50}) are presented in **Table 2**.

Code	Conjugates and controls	IC_{50} [nM] $\alpha_v\beta_3$	IC_{50} [nM] $\alpha_v\beta_5$
9	*c*[DKP3-RGD]	4.5 ± 1.1	149 ± 25
15	*c*[DKPf3-RGD]	26.4 ± 3.7	>5000
16	*c*[DKPf3-RGD]-PEG_4-Aoa=Dau	14.0 ± 1.6	6300 ± 400
17	*c*[DKPf3-RGD]- GLFG-Aoa=Dau	5.8 ± 0.6	2100 ± 100

Table 2 Inhibition of biotinylated vitronectin binding to $\alpha_v\beta_3$ and $\alpha_v\beta_5$ receptors of conjugates and controls.

The two conjugates **16** and **17** retained a good binding affinity for the $\alpha_v\beta_3$ receptor with IC_{50} values in the nanomolar range. Furthermore, data reported in **Table 2** showed that the selectivity towards $\alpha_v\beta_3$ receptor is also retained for all the conjugates tested; in fact the IC_{50} values for the $\alpha_v\beta_5$ receptor are in the micromolar range.

- **MTT-based cytotoxicity assay**

Cytotoxicity was evaluated on U87 (human glioblastoma, $\alpha_v\beta_3$ +) and HT-29 (human colorectal adenocarcinoma, $\alpha_v\beta_3$ -) cell lines, through MTT-based assays by Lucia Feni, working under the supervision of professor Ines Neundorf (University of Cologne, Germany).
U87 ($\alpha_v\beta_3$ expressing cell line) and HT-29 ($\alpha_v\beta_3$ non expressing cell line) were treated with different concentrations of the conjugates for 72 hours with washout. Cells were washed after 6 hours of

incubation, the media was replaced and then the cells were incubated for other 66 hours. This procedure has been used intending to simulate the *in vivo* conditions where the administered prodrug is rapidly cleared from the tumor extracellular environment. In this way the conjugates degraded or unbound to the integrin receptors are removed from the medium, minimizing the effect of metabolites produced by extracellular cleavage of the linker. The cell viability was quantified by MTT (3-(4,5-dimethylthiazol-2-yl)-2,5-diphenyltetrazolium bromide) assay.

Cytotoxicity data are reported in **Figure 21**. The cytotoxicity of the congiugate which presents also a cell penetrating peptide (for CPP see paragraph 1.4.1) between our targeting moiety *c*[DKPf3-RGD] and Dau, (conjugate **19**, **Figure 20** synthesized by Lucia Feni) was also reported (graph **A**, **Figure 21**). The CPP used was the so called sC18 (previously developed by Neundorf's group[83]) and it was inserted with the aim to enhance the cellular uptake of the peptide.

All the three conjugates showed enhanced cytotoxicity towards U87 cells compared to HT-29 cells; this is much more evident for conjugate **19** (*c*[DKPf3-RGD]-PEG_4-sC18(Lys_{13}-Aoa=Dau) which is more effective in U87 cells compared to our conjugates which did not have sC18, **16** (graph **B**) and **17** (graph **C**). In conclusion, the targeting moiety is essential for the selectivity towards $\alpha_v\beta_3$ for all the conjugates tested, and the presence of a cell penetrating peptide is important to improve cytotoxicity, likely due to the increased propensity to enter cells.

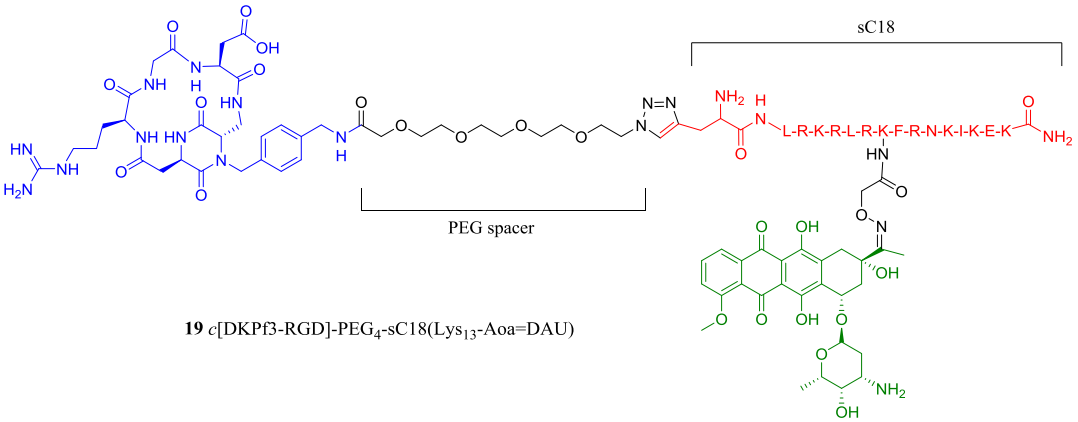

Figure 20: Conjugate **19** (*c*[DKPf3-RGD]-PEG_4-sC18(Lys_{13}-Aoa=Dau) synthesized by PhD student Lucia Feni, Neundorf's group, University of Cologne.

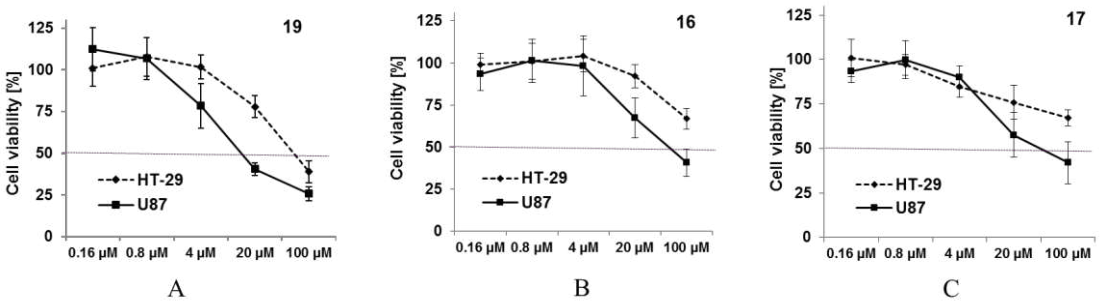

Figure 21 MTT-based cytotoxicity assay on U87 ($\alpha_v\beta_3$ +) and HT-29 ($\alpha_v\beta_3$ -) cells of the peptide-drug conjugates **19**, **16** and **17.** (15 min incubation with the peptides, then washout and measure after 72h).

- **Cellular uptake**

The amount of conjugate which is actually internalized by the cells was measured through cellular uptake studies. In the case of all our conjugates, the fluorescent properties of Dau were exploited. Data relative to conjugate **16** and **17**, together with conjugate **19**, are reported in the graph in **Figure 22**. After 30 min incubation of both U87 ($\alpha_v\beta_3$ +) and HT-29 ($\alpha_v\beta_5$ -) cells with the conjugates, the fluorescent intensity was measured. All the conjugates showed a significantly lower uptake for HT-29 cells, so once again the selectivity of our conjugates was confirmed. Notably, the presence of the cell penetrating peptide in conjugate **19**, allowed a much more important uptake.

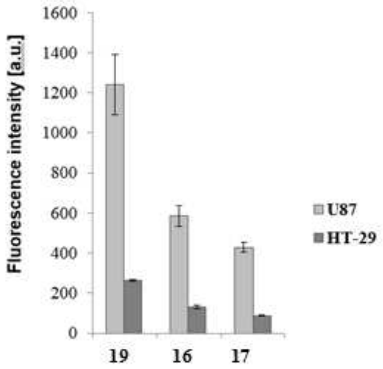

Figure 22 Cellular uptake for the conjugates **16**, **17** and **19**. Cellular uptake ratios (U87/HT-29): 4.7 for compound **19**, 4.5 for compound **16** and 4.9 for compound **17**.

1.4 Paclitaxel conjugates

1.4.1 Cell Penetrating Peptides (CPPs)

One major problem with drug candidates is their low membrane permeability which dramatically interfere with systemic drug distribution. This problem is related to the drug's hydrophilic nature, which is, on the other hand, necessary for drug administration. In most cases, good cell uptake is then reached raising the administrated drug's quantities, leading to dramatic side-effects on healthy tissues. This is much more true in the case of neurodegenerative diseases; drugs have to cross the blood-brain barrier to pass from vasculatures into the parenchyma of the nervous system which has exactly the opposite aim to prevent this passage. It is then obvious the necessity to improve the translocation process of drugs across the cell membrane.
Cell penetrating peptides (CPPs) are short peptidic sequences (typically no more than 30 residues) which can ubiquitously cross cell membranes in energy dependent/independent manners without showing toxicity and without apparent recognition of any receptors.[84]
In 1991, Joliot and co-workers demonstrated that a transcription factor of *Drosophilia melanogaster* (the peptidic homeodomain of Antennapedia), regulated neuronal morphogenesis after entering neurons.[85] Three years later, Derossi *et al*. identified the basic domain, corresponding to the third helix of the Antennapedia homeodomain, bearing the translocation properties; the 16-amino-acid peptide was named as penetratin (sequence RQIKIWFQNRRMKWKK).[86] In the same manner, the trans-activator of transcription (TAT, sequence RKKRRQRRR) protein of HIV-1 was demonstrated to be efficiently internalized by cells *in vitro*.[87]

- **Classification and uptake mechanisms**

Although the uptake mechanisms by which CPPs internalize is a not well known chapter of this story, it is possible to do some considerations; physical-chemical properties of CPPs, cell type and cell membrane constitution are driving force in choosing the uptake mechanism.[88] Cationic CPPs (as TAT and penetratin) show concentration-dependent uptake mechanisms and the formation of electrostatic interactions with the phosfolipid bilayer is the first step for cellular entry in most cases. Amphipathic CPPs need to assume a helical secondary structure to enter, exposing the hydrophobic face to the membrane and the hydrophilic face to the solvent.[88]
Anyway, nonendocytic or energy-independent and the endocytic pathways are the two most important cellular uptake mechanisms of CPP.[89]
Endocytosis is a process which naturally occurs in cells. It consists in the endocytic entry and the subsequent endosome escape to avoid lysosomally degradation.[89,90] Endocytosis can be mediated by Caveolae, Clathrin or it can happen through macropinocytosis (**Figure 23**).[91]
Notably, cells recycle the entire cell surface one to five times per hour trough internalization.[88,92] This continuous internalization should enable peptides, which can easily interact with cell membrane, to enter the cell through endocytic pathways.[88]
Direct translocation across the cell membrane foresees an energy and temperature-independent destabilization of the membrane. Inverted micelles formations and pore formation are only hypothesis to explain direct translocation mechanism.[89–91]

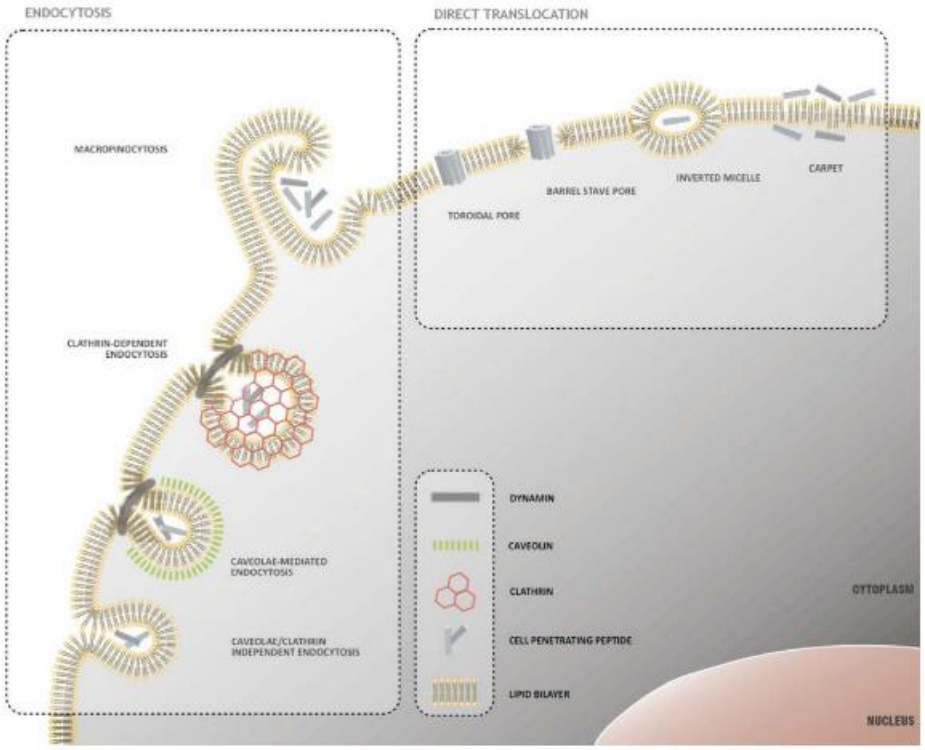

Figure 23. Mechanism of peptide uptake through cell membrane. Adapted from ref 92.

- **CPPs as delivery systems**

CPPs were used as vectors for siRNA[93], small molecules, proteins or other peptides[94], both in vitro[95] and in vivo[96]. More interesting for the aim of this thesis are CPPs as drug delivery systems.
The conjugation of drugs with CPPs can be a valuable way to overcome multi-drug resistance and toxicity in tumor therapy.[97] Improved activity has been detected when diverse chemotherapeutics, such as Taxol[98], Methotrexate[99], and Dox[100] where linked to CPPs. Some of these drug delivery systems are shown in **Table 3**.
In 2013, Duong and co-workers developed the drug delivery system based on synergic properties of DOX and PTX as drugs, a folate targeting moiety (folate receptors are overexpressed on the surface of different cancer cells) and the CPP TAT peptide.[101] Their system showed an improved efficacy with respect to the unfunctionalized single drug-loaded micelles (IC50 value of 0.172 μM D/0.043 μM P, with respect to the IC50 value of 3.873 μM for D-micelles and 0.790 μM for P-micelles). CPPs can also incorporate a functional motif and have cytostatic and cytotoxic effect.[102]

Anticancer agent	CPP	Results
Methotrexate	YTA2, YTA4	At 1 μM, the peptide–MTX conjugates were shown to overcome MTX resistance and kill the cells more efficiently than MTX alone.
Doxorubicin	TAT, Pen, MCa_{Abu}	Dox–CPPs are able to induce caspase-dependent apoptosis in human cancer cells at low dose.
	LMWP	LMWP–PR–Dox conjugate offers a great potential for intracellular delivery of therapeutic agents into tumor cells in achieving highly effective yet safe drug therapy.
	R8-PLD	R8-PLD addresses the problem of poor cell penetration by PLD to increase its therapeutic efficacy
	$(RW)_4$, Cyclic $[W(RW)_4]$	Cyclic [W $(RW)_4$]-Dox can be used as a potential prodrug for improving the cellular delivery and retention of Dox.
	CADY-1	Experimental animals treated with a CADY-1/Dox complex exhibited better tolerance and anti-tumor activity than animals treated with either liposomal Dox or the free form of Dox.
	R8	The conjugate of Dox with R8 effectively suppressed tumor proliferation without decreasing mouse weight after intravenous injection.
	TAT, penetrating	It was demonstrated that pen is as effective as TAT for the efficient delivery of Dox into cells. This vector based delivery can overcome the reduced Dox sensitivity observed in CHO, HUVEC and MDA-MB 231 cells over NG 108.15 and MCF7 cells.
Vincristine sulfate	R7	Folate and R7-modified PLGA–PEG NPs could be a potential vehicle for delivering chemotherapeutic agents such as VCR and breast cancer therapy.
Paclitaxel	TATp-Cys	Paclitaxel-loaded TATp-modified PEG–PE micelles were prepared. TATp-modified micelles demonstrated an increased interaction with cancer cells compared to non-modified micelles resulting in a significant increase of the in vitro cytotoxicity to different cancer cells.
Taxol	R8	Conjugation of R8 to Taxol via disulfide linkers can provide a variety of benefits including improved administration as a result of enhanced aqueous solubility, altered biodistribution, lengthened pharmacokinetics, and, most importantly, the ability to overcome MDR elicited by the drug alone

Table 3 . Examples of CPPs in anticancer drug delivery. Adapted from ref. 100

Drug targeting is also essential in order to minimize the effects of the drug on healty cells. Drug-carrier conjugates bearing small molecules, RGD peptides, antibodies etc. have been used to direct the drug on the membrane of cancer cells. However, the theoretical effectiveness of these conjugates was not demonstrated in practice as many factors need to be discussed further; the lack of understanding about the pharmacokinetic profile of the conjugate, the appropriate ligand and the uptake mechanism are some important aspects.[103] Hypothetically, if the delivery of the drug carrier conjugate is done through parenteral routes, the conjugate reaches the target via the systemic circulation. A possible mechanism of internalization can be as the one represented in **Figure 24**. The conjugate may undergo receptor mediated endocytosis, after targeting the receptor. The conjugate then pass to the early and the late endosome and finally to the lysosome. The receptors will be restored on the surface. The drop of the pH inside the lysosomes may affects the linkage between the drug and the peptide.[103]

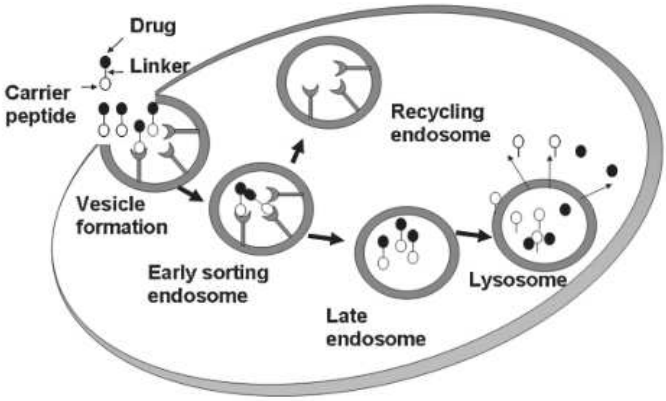

Figure 24. Hypotetical mechanism of internalization of a peptide-drug conjugate. Adapted from ref 106

- **CPP-drug conjugation strategies**

Different strategies can be used in order to link the drug to the CPP, depending on the chemical characteristics of both, drug and CPP. Of course, the choice of the right conjugation procedure is essential just because it can affect several aspects including the mechanism of entry in the cell, the route of administration of the construct or, banally, the availability of the drug inside the cells.[91,103] In the majority of the cases, a covalent linkage is used in the CPP-drug constructs both stable or cleavable linkages. In 2012, Wender *et al*. conjugated the CPP R8 (octaarginine) to the Taxol through a disulfide linkage which is cleaved in the reducing conditions of the cytosol, thus releasing there the free drug.[104] Oxime linkage was used by Lelle *et al*. to link the R8 with DOX.[105] In another work, sC18 was linked through amide bond to Cymantrene by Splith et al.[106]

- **Cationic antimicrobial peptides**

Cationic antimicrobial peptides (CAMPs) are short amphiphilic peptides (12 - 50 amino acids) bearing basic amino acids (arginine, lysine and histidine) in a big amount such that they are characterized by a net positive charge (+2 to +7) and with approximately 50% of hydrophobic amino acids. Although their relative small length, they are mostly found assuming tertiary structure as β-sheet, α-helices or loops. The mechanism of action foresees the disruption of the membrane bi-layer in a detergent-like manner, as a consequence of their accumulation on the membrane itself, folding in amphiphilic conformations when interacting with the negatively charged membrane phospholipids, leading to pore formation.[107] They were initially found to modulate innate host defence as they are mostly produced at site of inflammation or infections in all leaving species as immediate non-specific defence.[108] Their properties make them good candidates in therapeutic anctibacterial use[109], but some recent studies demonstrated their utility also in cancer biology.[110,111] Two biggest groups of antimicrobial peptides are present in humans: defensins and cathelicidins. Defensins contain six cysteine residues which are highly conserved although the variability in the sequences. Cathelicidins have a conserved N-terminal domain, known as the cathelin domain, and a C-terminal domain bearing the antimicrobial properties. In humans, the precursor protein has a mass of 18 kDa therefore it is named hCAP18.[107,110]

1.4.1.1 sC18 as CPP

In 1994, Tossi and co-workers[112] identified the primary antibacterial domain in the lipopolysaccharide binding protein CAP18. Highly cationic sequence in its C-terminal domain (named C18, ^{106}GLRKRLRKFRNKIKEKLKKI^{125}) was identified as responsible of CAP18's antimicrobial properties due to the tendency to adopt an amphipathic α-helical conformation. In fact, disruption of the helix possibly eliminates the antibacterial activity toward both Gram-negative and Gram-positive bacteria. Based on these considerations and taking into account the sequence analogy between Tat (^{48}GRKKRRQRRRPPQ^{60}) peptide and the C18 fragment, Neundorf *et al.* hypothesized that a shorter analogue of CAP18, residues 106-121, named sC18 (sequence: ^{106}GLRKRLRKFRNKIKEK^{121}) still maintained the CPPs' properties (same number of Arg and Lys residues as in Tat peptide).[83] They actually demonstrated, by flow cytometry analysis, that the new CPP sC18 and Tat had a comparable internalization efficiency. In addition, circular dichroism studies showed the tendency of sC18 to adopt α-helical structure which was in agreement with that reported for the parent C18.

In 2012, Hoyer *et al.*[113] demonstrated that dimeric version of sC18 enhanced cellular uptake in different cell lines, but also increased cytotoxicity in some cases. They also demonstrated the ability of the sC18 to carry cytostatic compounds such as Cymantrene and Chlorambucil into tumor cells, notably increasing their therapeutic potential.
It was further shown that a shortened version of sC18 (sC18*, ^{106}GLRKRLRKFRNK^{117}) also has cell penetrating capabilities.[114]

1.4.2 Synthesis

Synthesis of the PTX conjugate was planned in both solid and solution phase. Three main building blocks were considered:
-the targeting moiety with the PEG-4-N_3 spacer (*c*[DKPf3-RGD]-PEG-4-N_3)
-sC18 bearing the cysteine linked to Lys_{13} through β-alanine spacer (sC18 branched)
-PTX connected to the maleimide moiety through the self-immolative linker
The targeting moiety *c*[DKPf3-RGD]-PEG-4-N_3 **34** was synthesized as described in **Scheme 3**.

- **Synthesis of sC18 branched peptide (45)**

Synthesis of the CPPs sC18 was done using Solid phase peptide synthesis[115] (SPPS). In SPPS, the synthesis of peptides is carried out on a solid resin support, while unreacted reagents and by-products are simply removed *via* washing as the growing peptide chains remain attached to the resin. In this way, purification of peptide intermediates is redundant and the whole process can be carried out in one single reaction vessel. Furthermore coupling cycles are shorter than in traditional peptide synthesis. This simple procedure also allows for automatization, making possible, in a short time, parallel synthesis of different and long peptides. The *N*α-group of every amino acid and side chains are blocked by a protecting group to avoid unwanted side-reactions. The amino acid's carboxy group must be activated since it is not sufficiently electrophilic for coupling to proceed. Carbodiimides are often employed as activators but their use can lead to racemization.[116] Therefore the use of racemization suppressants, such as HOBt, or its non-explosive alternative Oxyma, which traps intermediates prone to racemization and forms the activated species is necessary.[117] Finally, the peptide is fully deprotected and cleaved off the resin support. Crude peptide sample must be purified to remove side-products lacking one or more amino acids considering that aminoacylation is not quantitative.[118]
Fmoc/*t*Bu strategy was adopted for the sC18 synthesis; α-amino groups were protected by the base-labile Fmoc group and side-chains were protected by *t*Bu or other acid-labile groups in order to ensure the complete orthogonality. The peptide sequence sC18 (^{106}GLRKRLRKFRNKIKEK^{121}) was synthesized on a Rink-amide resin (Fmoc-L-Lys(Boc)-Rink Amide, 0.015 mmol scale) by automated multiple solid-phase peptide synthesis (aSPPS) using a robot system.
The synthetic strategy is reported in **Scheme 6**. As previously mentioned, the peptide was synthesized on Rink Amide resin mainly by aSPPS starting from the C-terminal amino acid.
Lys_{13} was coupled manually as Fmoc-Lys(DDe)-OH, then the peptide was again elongated by automation. The N-terminal Gly^{106} was replaced by propargylGly as the targeting moiety *c*[DKPf3-RGD]-PEG-4-N_3 is then linked *via* the copper catalyzed alkyne-azide cycloaddition (CuAAC).

After selective cleavage of Dde protecting group on Lys_{13} using hydrazine in DMF, Fmoc-β-Ala and Fmoc-Cys(Trt)-OH were sequentially coupled manually to the resin (using a double coupling step, HATU, DIPEA and Oxyma, DIC). After Fmoc deprotection on Cys, peptide **45** was cleaved from the resin using a mixture of H_2O/TIS/TFA 2.5:2.5:95. Pure peptide **45** was obtained after HPLC purification in 63% yield.

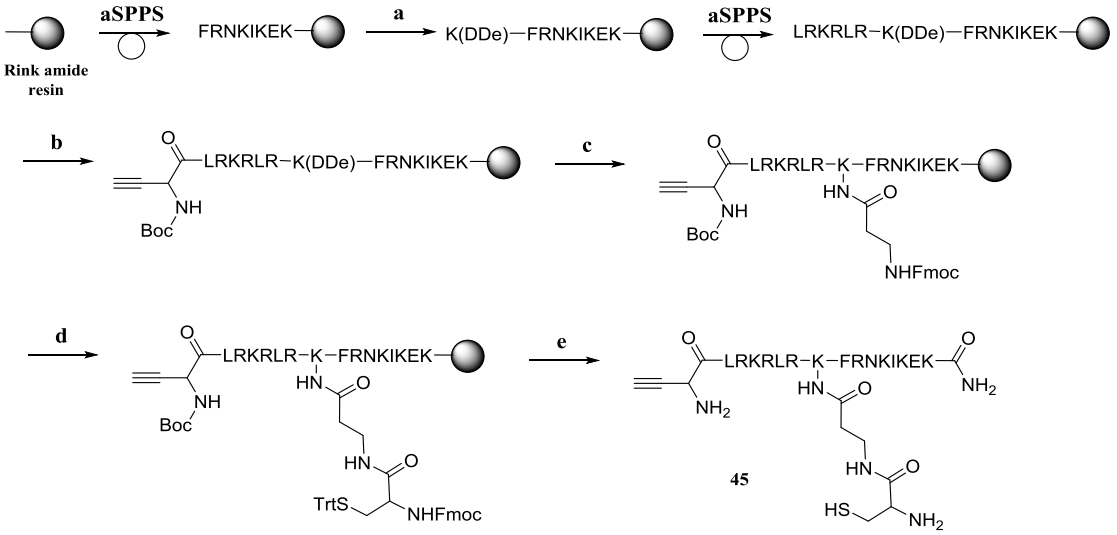

Scheme 6 Synthesis of the sC18 peptide (**45**). Reagents and conditions: a) Fmoc-Lys(Dde)-OH, Oxyma, DIC, DMF, 2 h, r.t.; b) 1) Fmoc-Pra-OH, Oxyma, DIC, DMF, 2 h, r.t., 2) 20% piperidine in DMF, 45 min, r.t., 3) Boc_2O, DIPEA in DCM; c) 1)3% hydrazine in DMF, 2) Fmoc-β-Ala-OH, Oxyma, DIC, DMF, 2 h, r.t.; d) 1) 20% piperidine in DMF, 45 min, r.t., 2) Fmoc-Cys(Trt)-OH, Oxyma, DIC, DMF, 2 h, r.t.; e) 1) 20% piperidine in DMF, 45 min, r.t., 2) H_2O/TIS/TFA 2.5:2.5:95. 3h, r.t., 63%.

- **Synthesis of maleimide-Val-Ala-PAB-diamine-PTX**

First of all Paclitaxel was activated at 2'-OH position with 4-nitrophenylchloroformate in presence of pyridine in DCM (**46**, **Scheme 7**).

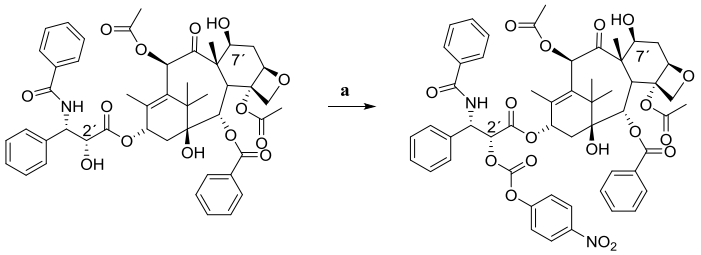

46

Scheme 7 Synthesis of 2'-(4-Nitrophenoxycarbonyl)paclitaxel (**46**). Reagents and conditions: a) p-nitrophenyl chloroformate, pyridine, THF, 0°C to r.t., 55%.

Synthesis of maleimide-Val-Ala-PAB-diamine-Ptx (**54**) is still ongoing and it was planned as described in **Scheme 8**. The lysosomally cleavable linker Val-Ala containing the *p*-aminobenzyl alcohol (PABA) self-immolative spacer was prepared following the procedure of Kratz and coworkers.[119] The synthesis was carried out in solution starting from commercial Fmoc-Val-OH (**47**) which was activated with NHS and DCC (1:1) in THF. The latter was then coupled to free alanine using $NaHCO_3$ as a base in a mixture water/THF/diethyl ether to obtain Fmoc-Val-Ala-OH (**48**) in 93% yield. *P*-aminobenzyl alcohol reacted with the dipeptide **48** in a mixture of DCM/MeOH 2:1, using EEDQ as coupling agent to avoid racemization, giving Fmoc-Val-Ala-PABOH **49** (78%). The hydroxy group of **49** was activated with *p*-nitrophenyl chloroformate in THF, using pyridine as HCl scavenger, to afford the activated linker Fmoc-Val-PAB-PNP **50** in 66% yield. Compound **50** was then let to react with N-Boc- N,N'-dimethylethilendiamine in THF, in presence of DIPEA, yielding Fmoc-Val-PAB-PNP-diamine **51** in 74% yield. Fmoc- deprotection of **51** was carried out in solution with piperidine in DMF, avoiding the isolation of the free amine. Indeed, after piperidine removal, the crude amine was treated with glutaric anhydride affording compound **52**. After activation of the carboxylic group in **52** with DIC and NHS, N-(2-aminoethyl)maleimide-TFA salt was coupled obtaining the bifunctional linker **53** (55%). The rest of the synthesis is still ongoing. We planned to link the activated PTX (2'-(4-Nitrophenoxycarbonyl)paclitaxel **46**) to the linker **53**, using DIPEA, HOAt in DMF, to afford the maleimide-Val-Ala-PAB-diamine-PTX **54**.

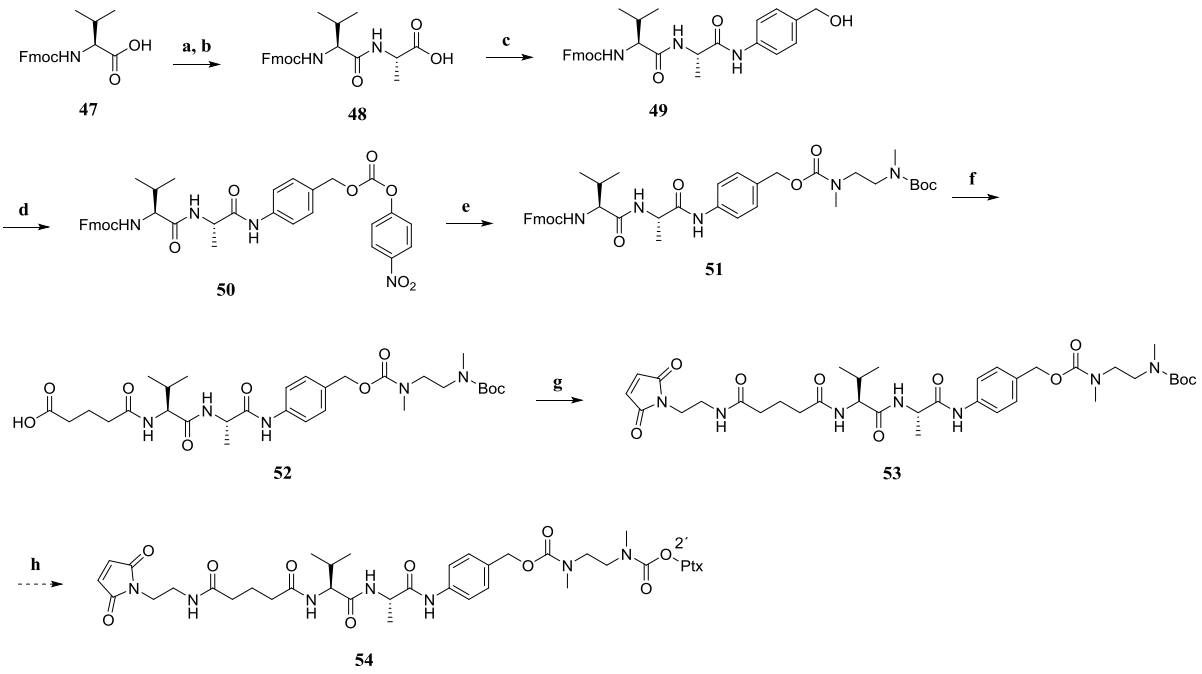

Scheme 8. Synthesis of maleimide-Val-Ala-PAB-diamine-Ptx (**54**). a) DCC, NHS, THF, 0°C to rt. overnight; b) Alanine, $NaHCO_3$, THF/diethyl ether/water 1:1:1, r.t., 4 days, 48% over two steps; c) p-aminobenzyl alcohol, EEDQ, DCM/MeOH 2:1, r.t. 48 h, 78%; d) p-nitrophenyl chloroformate, pyridine, THF, 0°C to r.t., 4h, 66%; e) N-Boc- N,N´-dimethylethilendiamine, DIPEA, THF, overnight, 74%; f) 1) piperidine DMF, 2h; 2) glutaric anhydride, DMAP, DIPEA, DMF, overnight, 89% over two steps; g) 1) DIC, NHS, DMF, on; 2) N-(2-aminoethyl)maleimide-TFA salt, DIPEA,, 55% over two steps; h) reaction ongoing, 1) TFA in DCM; 2) 2´-(4-nitrophenoxycarbonyl)PTX, DIPEA, HOAt, DMF, 24h.

As the last step of the previous synthetic pathway, the last two steps of the final conjugate's synthesis (**Scheme 9**) are ongoing. They consist in two click reactions; the thiol-maleimide click reaction and the CuAAC reaction with the *c*[DKPf3-RGD]-CH_2NH_2-PEG-4-N_3, yielding final conjugate **18**.

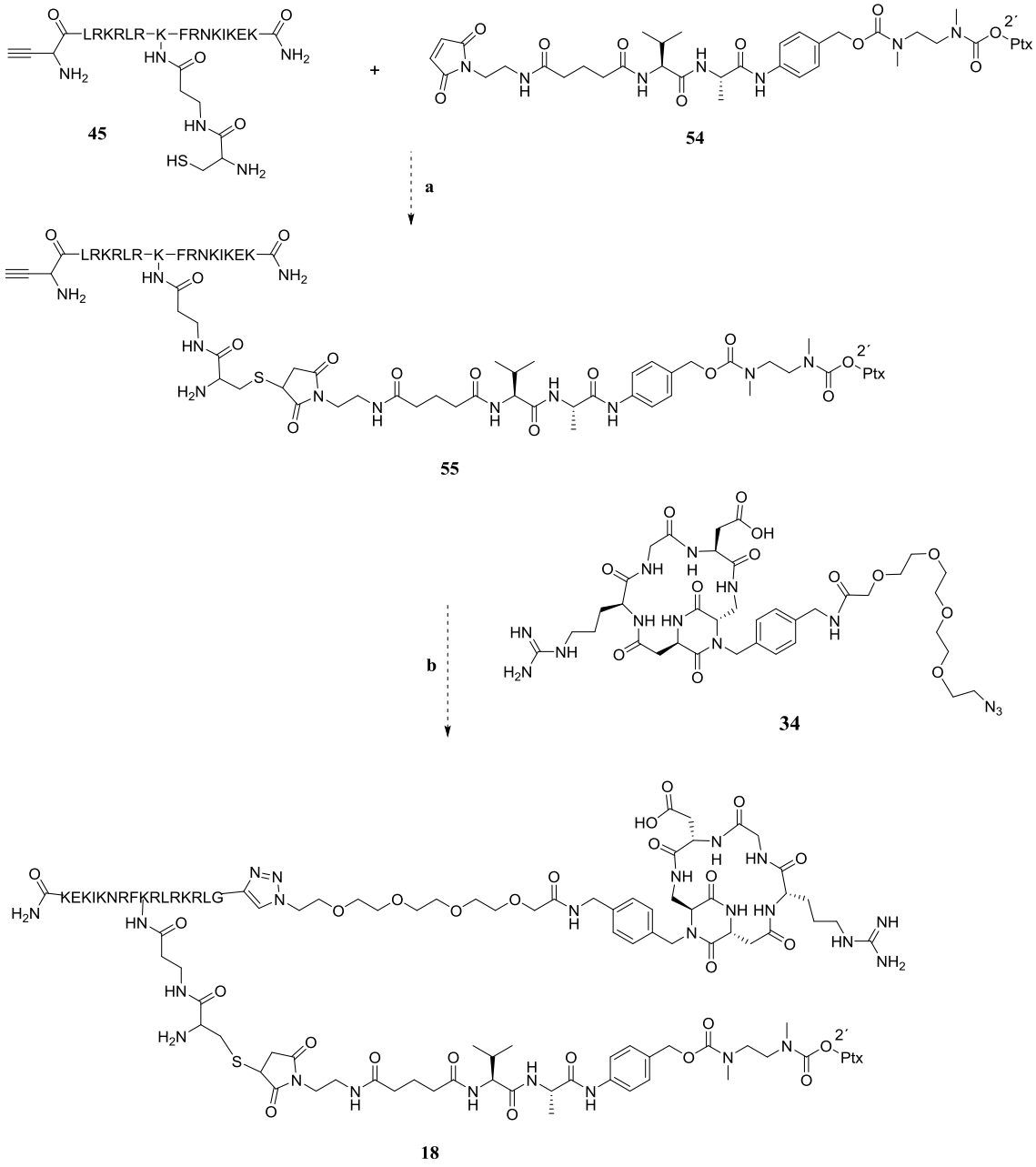

Scheme 9. Synthesis of the conjugate sC18-*c*[DKPf3-RGD]- Val-Ala-PAB-diamine-Ptx **18**. a) PBS (pH=7), ACN, r.t., 1h; b) Sodium ascorbate, $CuSO_4.5H_2O$, *tert*-buthanol/H_2O 1:1, o.n.

1.5 Conclusions and outlooks

With the aim of synthesizing small molecule drug conjugates bearing the potent integrin ligand *c*[DKPf3-RGD], previously developed by our group, two new Daunomicin conjugates (**16** and **17**) were synthesized and characterized. In addition, a conjugate bearing the CPP sC18 (**19**) was synthesized in collaboration with Neundorf's group (University of Cologne). In conjugate **16** the targeting moiety was linked to the drug (Dau) through a PEG-4 spacer *via* a dipeptide Propargyl-glycine-aminooxyacetic acid in order to insert an uncleavable linker. On the other hand, conjugate **17** show the protease cleavable linker GFLG linked to the Dau through oxyme linkage with aminooxyacetic acid, while the targeting moiety is linked through a simple amide bond. Preliminary biological studies were conducted both in University of Cologne and University of Milan. Conjugates **16** and **17** were tested *in vitro* to determine their ability to inhibit the binding of biotinylated vitronectin to the purified $\alpha_v\beta_3$ and $\alpha_v\beta_5$ receptors in a competitive binding assay. They retained a good binding affinity for the $\alpha_v\beta_3$ receptor with IC_{50} values in the nanomolar range and a selectivity towards $\alpha_v\beta_3$ receptor. The importance of their selectivity was also remarked by cytotoxic assays and cellular uptake. The presence of the sC18 in conjugate **19** demonstrated the great potential of the use of a CPP to increase uptake and thus, cytotoxicity. More in-depth biological analysis and also further analysis (for example serum stability) are currently ongoing.

Synthesis of an additional conjugate (**18**) bearing our integrin targeting moiety, a cell penetrating peptide and Paclitaxel as cytotoxic payload was planned. Cell penetrating properties of sC18 were exploited to improve the CPP-mediate internalization of the entire conjugate and in consequence enhance cytotoxicity. The presence of a self-immolative spacer (PABC-N,N'-di-methylethylenediamine) and a lysosomally cleavable dipeptide linker (Val-Ala), was chose in order to have Ptx releasing as free drug inside the cell. The synthesis of the three building blocks was almost complete, the last steps are missing. Once the conjugate will be ready, it will be tested for its ability to penetrate cell membrane (cellular uptake) and for its cytotoxicity.

2 New DKP-based peptidomimetic inhibitors of cadherin homophilic interactions

2.1 Cadherins

Cadherins are transmembrane proteins involved in diverse fundamental cellular processes including cell-cell adhesion, cell recognition and signalling. Cadherin binding is usually homophilic, so that adhesion via cadherins is an intercellular adhesion. Differently, integrins and proteoglycans are involved in cell–matrix as well as cell–cell interactions. However, a heterotypic interaction between E-cadherin and the integrin $\alpha_E\beta_7$ was reported in 1998[120]; the involvement of cadherins in cell–matrix interactions on artificial substrates, coated with the extracellular domain of cadherins was also demonstrated.[121,122]

- **Families**

Hundreds human cadherins have been identified and classified into three families: major cadherins (CDH), protocadherins (PCDH) expressed primarily in the nervous system, and cadherin-related proteins (CDHR). Epithelial cadherin (E-cadherin) is the progenitor member in cadherin family.[123,124] Its N-terminal domain (extracellular domain) was determined by NMR studies in 1995.[125] In the same year, the first crystal structure of the murine Neuronal cadherin (N-cadherin) domain was solved by Shapiro *et al.*[126] Since then, lots of cadherin structures were studied and listed.[123,124]

Another classification provides for the distinction of type I (classical) and type II cadherins linked to the actin cytoskeleton, on the bases of sequence homologies.[127]

- **Structure and mode of action**

Cadherins are transmembrane glycoproteins composed by five extracellular domains arranged in tandem and linked via calcium ions, and a cytoplasmic domain normally associated with some cytoplasmic proteins (**Figure 25**). The N- and C-termini of the cadherin protein chain are located outside and inside the cell, respectively. The N-terminal region, or ectodomain, consists of a variable number of highly conserved sequences which are repeated in the extracellular domain. Classical cadherins contain five extracellular domains that are commonly known as EC1- EC5. The conformational stability and the capacity to mediate cell-cell adhesion of the cadherin is ensured by the presence of Ca^{2+} ions located between neighboring extracellular domains. The presence of

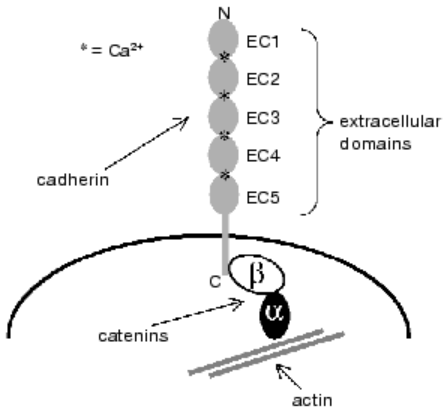

Figure 25: Cadherin structure. Adapted from ref 133.

Ca^{2+} is necessary for cadherin adhesive function and, it is no accident that their name is the contraction of 'calcium-dependent adherent protein'.[128,129]

The cytoplasmic domain of classical cadherins is normally associated with catenin and actin filaments. The cadherin–catenin complex is necessary for providing cell–cell adhesion.[130] This was also confirmed by the fact that recombination or deletion of specific portion in the cytoplasmic domain significantly affects the formation of cadherin-catenin complex and the proteosomal degradation of cadherin.[131] Already in 1988, Nagafuchi and Takeichi demonstrated that the cytoplasmic domain is essential for providing normal cell-cell adhesion.[132].

In the last years, different studies were conducted to elucidate the cadherin-mediated adhesion mechanism. Some studies on type I cadherins are in agreement with the formation of a "swap dimer". The N-terminal β-strand from the EC1 domain of each paired cadherin exchanges with that of the partner molecule; the six-residue-long N-terminal portion of the protein, usually referred to as the "adhesion arm" (DWVIPP in E- and N-human and mouse cadherins) is positioned in an "acceptor pocket" of the other cadherin, to form the trans homodimer (**Figure 26**).[133,134] The presence of a conserved Trp in position 2 on the adhesion arm, which is accommodated into the hydrophobic acceptor pocket, was established. In addition, some other conserved interactions were depicted, as reported in the **Figure 27**: a salt bridge between the N-terminal Asp1-NH_2 and carboxyl group of Glu89 as well as the hydrogen bond between Trp2 and the carbonyl group of Asp90.[133]

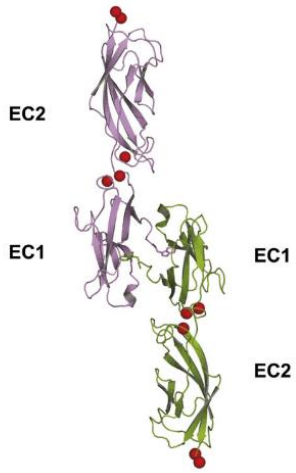

Figure 26 Swap dimer. Adapted from ref 136

Another interaction is established among the planar carboxyl group of Glu89 and the aliphatic side chain of Met92 from the acceptor pocket onto the pyrrole ring of the Trp2.[133]

This is consistent with that found in numerous other structures of adhesive type I and type II ectodomain fragments.[126,128,134]

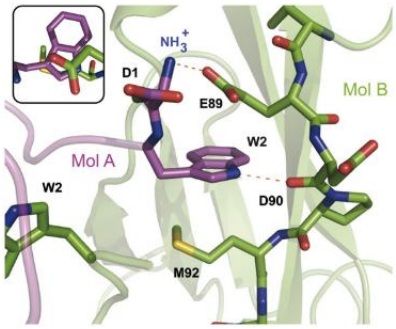

Figure 27 Interaction between the N-terminal part (bearing the Trp2) of the magenta cadherin and the hydrophobic acceptor pocket of the green cadherin forming the "swap dimer". Adapted from ref. 136.

The crystal structures of the complete ectodomains of N- and E-cadherin were studied and compared with the previously determined structure of C-cadherin.[128] The three crystals have in common the well-characterized trans strand swap adhesive interface between EC1 domains, and a

lateral *cis* interface in which a different EC1 domain interacts with the EC2 domain of a neighboring cadherin (**Figure 28**).[134]

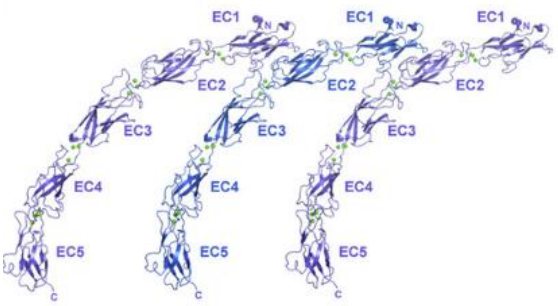

Figure 28 Structure formed by cis interactions between parallel ectodomain in N-cadherin. Adapted from ref 137

Proper amino acid mutations, in the human E-cadherin, were introduced at the *cis* interface level in order to determine their role in the adhesion mechanism; the mutations resulted in loss of ability to form cell-cell junctions; indeed, the combination with the trans interactions produces stable structures, but cis interactions are not on their own able to produce observable adhesive structures on an isolated cell surface.[134] So, the adhesive junction formation is the result of cooperativity between cis and trans interactions.[135]

Interestingly, domains EC1–EC5 have an extra residue near their N terminus, usually Pro, that inserts into the hydrophobic pocket of its domain, in order to do not strand swap. However, in isolated EC1, and in domains EC2–EC5, Trp2 inserts into the corresponding pocket in its own domain. In the type II cadherins, Trp4 is also highly conserved and it participates in swapping interactions.[136]

A model for the binding mechanism of type I cadherins was proposed by Parisini *et al.*[133] and it is shown in **Figure 29.** Cadherins are synthesized as an inactive forms in which the adhesion arm lacks of a free N terminus so the salt bridge with Glu89 is not formed. The adhesion arm can fit in the hydrophobic pocket of EC1 only after proteolytic activation. Intercalation of Trp2 is stabilized by a stacking interaction with Glu89 and Met92, and the formation of the salt bridge between Glu89 and the now free N-terminal amine. However, an equilibrium exists between the closed and the opened form in which the adhesion arm is dissociated from the body of EC1. The adherents junctions is formed when the open adhesion arm is stabilized by binding to an opposing cadherin, creating swap trans dimers through inter-molecular docking of Trp2 and salt bridge formation.[133]

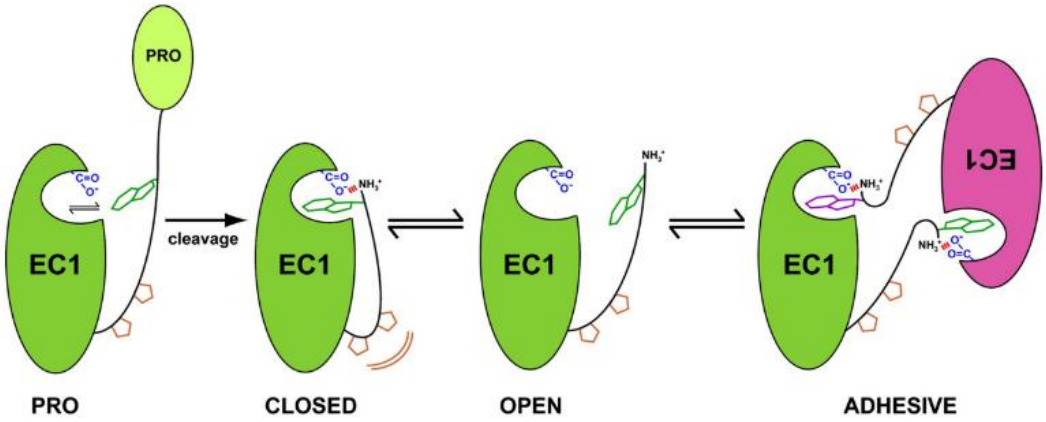

Figure 29 Proposed mechanism for the swap dimer formation. Adapted from ref 136

A very similar mechanism was found for type II cadherins; cadherin-11, cadherin-8 and MN-cadherin were studied from the crystallographic point of view.[137] The adhesive interaction is again confined to the EC1 domains. However, in type II cadherins, the side chains of Trp2 and Trp4 of the swapped strand, insert into a larger pocket in the hydrophobic core of the partner molecule. Notably, the structural features of type II and type I cadherins suggest that members of one family are not compatible as binding partners for members of the other family. In other words, binding specificities of type I cadherin are orthogonal to the ones of type II cadherin [137,138]

Anyway, the cadherin dimerization pathway, leading from the monomer to dimer formation, is highly dynamic as it involves different intermediate steps. Indeed, it has been showed that cadherins pass through an intermediate dimeric state known as "X-dimer"; it is kinetically important in the dimerization of classical cadherins by lowering the energy barrier of the adhesive mechanism.[139] The X-dimer of the P-cadherin was isolated and characterized and it was found that the monomeric P-cadherin dimerizes only after stabilization by Ca^{2+} between the EC1 and EC2 domains (**Figure 30**).[140]

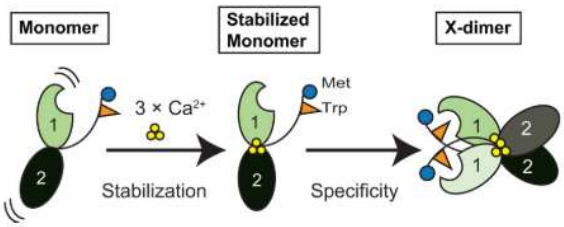

Figure 30 Mechanism of X-dimerization. Adapted from ref 143

- **Cadherins and cancer**

A great variety of studies have shown the existence of a connection between cancer progression and dysregulation of cadherins.[141] It has been demonstrated that neuronal and vascular endothelial cadherin (VE-cadherin) play a key role during blood vessel formation and that N- and osteoblast cadherin (OB-cadherin) promote cancer cell metastasis; in this sense, N-, VE- and OB-cadherin can be seen as target for anticancer therapy.[142] However, E-cadherin represents the most interesting subject in the involvement of the cadherin family in drug resistance, angiogenesis, cancer cell invasion, and metastasis and hence in cancer progression. The relationship between E-cadherin dysfunction and cancer progression has been identified in the fact that epithelial tumor cells often lose E-cadherin as they became metastatic.[141] Indeed, E-cadherin acts as a suppressor of invasion and metastasis potentially in the regulation of β-catenin signalling, in the inhibition of mitogenic signalling through growth factor receptors and in the possible determination of epithelial polarity.[143]

E-cadherin has been addressed as a tumor suppressor in various adenocarcinoma, such as lung, laryngeal, colorectal, gastric, prostate, and pancreatic cancer as reviewed by Birchemeier and Behrens in 1994;[144] one reason was that E-cadherin inhibits epithelial-mesenchymal transitions (EMT).[145]
However, more recent studies support the idea that E-cadherin is important for disease progression in some cases. The case of the ovarian cancer is particularly interesting; tumor proliferation is improved through E-cadherin by activation of the protein kinase (MEK/ERK) pathway in development of ovarian epithelial cancers as reported in 2012 by Dong *et al.*[146]
Anyway, cadherins and their regulators can become valuable potential therapeutic targets.

2.1.1 Peptidomimetic ligands to cadherins

The rational design of ligands targeting cadherin protein-protein interactions is still in its early days. Since Shapiro *et al.*[126] in 1995 highlighted the contribution of the HAV (His89-Ala80-Val81) and INP (Ile53-Asn54-Pro55) sequences to the cadherin-mediated adhesion mechanism, libraries of peptide and non-peptide molecules mimicking this sequence were developed in order to inhibit the dimerization process.[147,148] The HAV and INP motifs are part of the extracellular domain 1 (EC1), which was demonstrated to take part in the adhesion mechanism of type I cadherins. The importance of the residues flanking the HAV motif, in developing small peptides antagonists of N-cadherin, was also determined.[149] N-cadherin is a potential target for anticancer therapy also because cancer progression is often characterized by the 'cadherin switch' from epithelial E to mesenchymal N cadherins; the downregulation of E-cadherin and the over-expression of N-cadherin would lead to the transition from a benign to a malignant cancer phenotype.[150]
Peptide named ADH-1 (**Figure 31**) with the formula N-Ac-CHAVC-NH_2 was developed by *Adherex Technologies* Inc. as antagonist of N-Cadherin. It has been shown to inhibit angiogenesis but, up to now, it has been subjected to few clinical trials.[151] ADH-1 was demonstrated not to have an effect on normal vasculature; indeed its toxicity at the doses tested in animals[152] and humans[153] was low. Ovarian cancer might be successfully treated using ADH-1.[153] Clinical trials performed using ADH-1 in combination with melphalan have shown very promising results in the treatment of melanoma.[154]

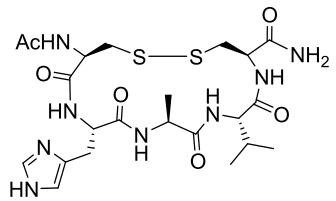

ADH-1

Figure 31 Structure of ADH-1 or Exherin

2.1.2 First generation DKP-based peptidomimetics

The first library of peptidomimetics based on the N-terminal "adhesion arm" (^{1}DWVI^{4}, Asp-Trp-Val-Ile) of N- and E- cadherin was reported in 2015.[155] The library comprises peptidomimetics with the general formula NH_3^+-Asp-scaffold-Ile-NHR bearing different conformationally constrained scaffolds and a benzyl moiety, in order to mimic the Trp2 pose of the native N-terminal sequence. These peptidomimetics were first designed using a docking protocol on a model of the EC1 fragment of N- and E- cadherin; the best candidates (**Figure 32**) were then selected considering their matching with the main binding interactions. All the three ligands form the salt bridge between the N-charged Asp1 of the N-terminal and the side chain carboxylate of Glu89 and insert the benzyl ring in the hydrophobic pocket of Trp2. Anyway, only structures **57** and **58** reproduce the backbone conformation of the native sequence. The ligands were synthesized and their ability to inhibit cadherin binding was tested on EOC cells (N-cadh-expressing EOC cell line SKOV3 and N-cadh-Fc chimeric protein).[155] Inhibition of N-cadh homophilic bynding by ligands **57** and **58** at 2 mM was
78% and 84%, respectively, and 50% and 65% at 1 mM concentration. At 2 mM concentration ADH-1 and **56** provided about 50% inhibition of N-cadh-Fc/cells interactions and appeared nearly ineffective at 1 mM concentration (**Figure 33**). Conversely, when tested on the E-cadh-expressing EOC cell line OAW42, at the concentration of 2 mM **56** and **58** gave about 50% inhibition of E-cadh-Fc binding to the cells while ADH-1 showed 30% inhibition, indicating a slightly better efficacy compared to ADH-1 in inhibiting also E-cadh homophilic interactions.[155]
In conclusion, compounds **57** and **58** were found to be effective in inhibiting N-cadh homophilic and, in slightly lower extent, also E-cadh homophilic adhesion.

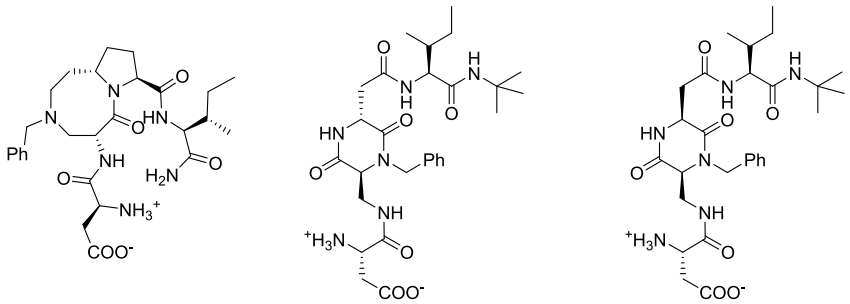

56 **57** **58**

Figure 32 Peptidomimetic ligands with the general formula NH_3^+-Asp-scaffold-Ile-NHR, **56**-**58**.

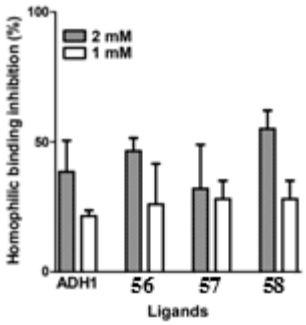

Figure 33 Inhibition of N-cadh binding by the peptidomimetic ligands **56**-**58** and the inhibition by ADH-1 as control. Adapted from ref 158.

From the chemical point of view, ligands **57** and **58** are particularly able to mimic the conformation of the native sequence DWVI through the presence of the diketopiperazine (DKP) scaffold which replaces the central dipeptide Trp2-Val3 unit of the DWVI sequence.[155]

In fact, DKPs represent privileged structures for drug discovery.[156] Reducing the susceptibility to metabolic amide bond cleavage and inducing conformational rigidity are the results of constraining the nitrogen atom of an α-amino amide into a DKP ring. As reported previously, they can be functionalized, from the chemical and stereochemical point. Notably, ligands **57** and **58** differ for the stereochemistry at the carbon stereocenter in the DKP ring.

The library of peptidomimetics discussed, represent the first generation of DKP-based peptidomimetics which are able to specifically bind to N-cadherin even in the μM range; in particular the ligand **58** is one of the best cadherin homophilic inhibitor reported to date.[155]

One year later, Nardone *et al.*[157] published the first crystal structure of human E-cadherin-(Val3)-EC1EC2 fragment (lacking of the first two amino acids Asp-Trp at the N terminus) co-crystalized with ligand **58**. The fragment was used instead of the native form, in order to obtain the hydrophobic pocket of Trp-2 intrinsically unoccupied and so more easily accessible to the ligand **58**.

Figure 34 shows the crystal structures of the E-cadh fragment without (A) and with (B) ligand **58**; the fragment is unable to form the swap dimer because of the lack of the Trp2 so it was found in the X-dimer conformation. The ligand binds across the two cadherins and it does not interact with the Trp2 pocket (as suggested by previously preliminary studies); in particular, the phenyl ring is inserted into a hydrophobic cavity formed by Ile4, Pro5, Ile7, and Val22 residues**.** This interaction was the evidence of an inhibitory mechanism in which the ligand binds across the weakly adhesive X-dimer conformation at the level of the two adhesion arms (**Figure 35**). In the free structure, some water molecules occupy the space which is then occupied by the ligand **58** in the ligated form, as shown by the electron density map in **Figure 36**.[157]

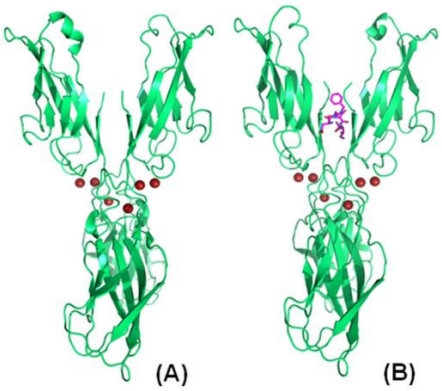

Figure 34 Crystal structure of E-cadherin-EC1EC2 fragment in its free form (**A**) and in the presence of the ligand **58** (**B**). Adapted from ref 160.

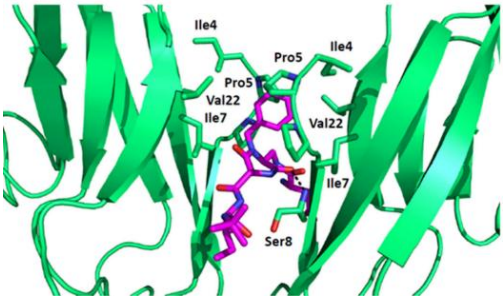

Figure 35 Binding interactions of the ligand **58** into the binding region between two fragment EC1EC2. Adapted from ref 160.

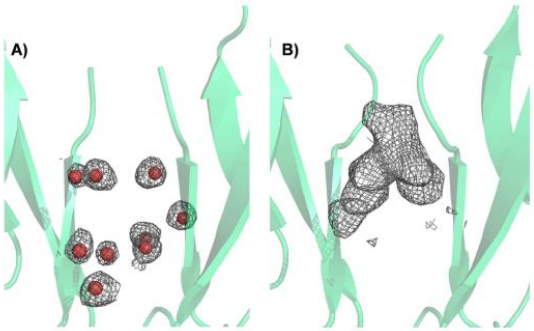

Figure 36 Electron density map in the binding region of the free structure (**A**) and in the presence of the ligand **58** (**B**). adapted from ref 160.

The binding of the ligand to the intermediate X-dimer is able to block the system at the weakly adhesive X-dimer conformation, thus avoiding the formation of the strand dimer.

2.2 Second generation DKP based peptidomimetics

As reported previously, the key interactions formed in the binding pocket during the homophilic adhesion are: (i) a salt bridge between the N-terminal Asp1-NH_2 and carboxyl group of Glu89, (ii) the hydrogen bond between Trp2 and the carbonyl group of Asp90 and (iii) the interaction of the key Trp2 with the hydrophobic pocket.[133]
Ligands **57** and **58** are able to, (i) form the salt bridge with the Glu89 and (iii) insert the benzyl ring in the hydrophobic pocket; but it is clear that they cannot form (ii) the hydrogen bond with the Asp90 because the benzyl group is not an HB (hydrogen bond)-donor.
Identical interactions were depicted for N-cadherin [155] by crystallographic methods as shown in **Figure 37**.

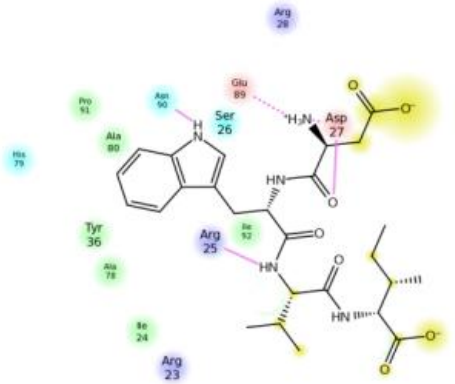

Figure 37 2D representation of the DWVI interactions into the N-cadherin binding site. Adapted from ref 158.

It seems, therefore, obvious the need to improve the ability of the ligand to bind the homophilic active site developing the second generation DKP-based peptidomimetics.

2.2.1 Aim of the project

The aim of our project is then to improve the first generation ligands by adding a HB-donor group. We decided to replace the benzyl group and insert an indolyl moiety on the DKP scaffold aiming to fulfill all the key interactions in the homophilic adhesion site. In these way the ligand is much more similar to the N-terminal sequence DWVI of the adhesion arm.
In order to develop the second generation DKP-based peptidomimetic inhibitors of cadherin homophilic interactions, docking studies were performed (Prof. Belvisi, Università degli Studi di Milano) to identify the best mimics containing the indolyl moiety on the DKP scaffolds. The results have shown that to obtain the optimization of the key interactions with E-cadherin the *trans*-DKP3 scaffold (**59**) needs a methyl-indolyl moiety, while the *cis*-DKP1 scaffold (**60**) needs the ethyl-indolyl moiety.

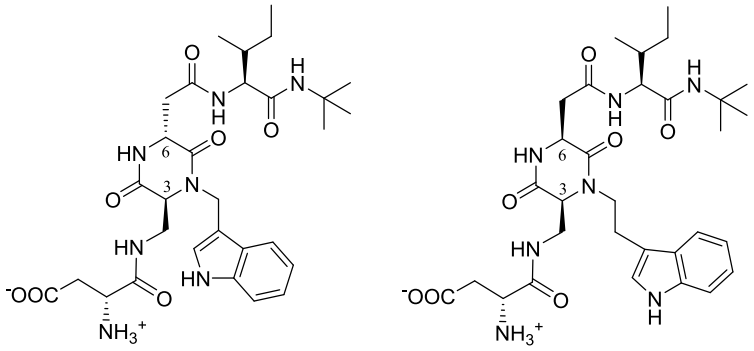

59 3S, 6R **60** 3S, 6S

Figure 38 Structures of the second generation DKP-based ligand as inhibitors of cadherin interactions: ligand with the DKP3 (3S, 6R) scaffold (**59**) and ligand with the DKP1 (3S, 6S) scaffold (**60**).

Furthermore, we planned to synthesize a cyclic ligand for cadherin homophylic interactions, as showed below (**Figure 39**).

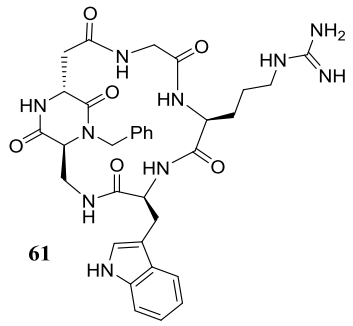

61

Figura 39 Structure of *c*(DKP3-Gly-Arg-Trp) (**61**)

We started with the synthesis of the ligand **59** bearing the DKP3-indolyl scaffold.

2.2.2 Synthesis of Asp-DKP3-indolyl-Ile (59)

- **Synthesis of the DKP3-indolyl scaffold**

The synthesis of the scaffold was planned in solution (**Scheme 10**) starting from (*S*)-serine **62** and (*R*)-aspartic acid **19**. (R)-aspartic acid β-allyl ester and (*R*)-*N*-(*tert*-butoxycarbonyl)aspartic acid β-allyl ester **20** were easily prepared according to literature procedure[158] as well as (*S*)-serine methyl ester **21**.[159] Indole-3-carboxaldehyde **63** was Mtr protected at the nitrogen using Mtr-Cl and DIPEA, yielding N-indole (Mtr)-3-carboxaldehyde **64** in reasonable yields (44%). The Mtr protecting group was chosen because of its orthogonality with the others protecting groups (Boc- and Allyl-). (*S*)-*N*-indolyl (Mtr) serine methyl ester **65** was prepared via reductive amination with N-indole (Mtr)-3-carboxaldehyde **64** using $NaBH(OAc)_3$ as reducing agent; acidic conditions, catalytic amount of AcOH, were necessary to accelerate the reaction and to obtain better yields (64%).
(*S*)-*N*-indolyl (Mtr) serine methyl ester **65** was then coupled with (*R*)-*N*-(*tert*-butoxycarbonyl) aspartic acid β-allyl ester **20**, using HATU, HOAt as coupling agents and DIPEA in DMF, to form the isopeptide **66** in good yield (around 80%). Notably, the yields were comparable with the ones of the coupling between the *N*-benzylserine methyl ester and the **20** as reported previously.[50]
After Boc-deprotection of **66** and cyclization to form the diketopiperazine scaffold DKP3 **67**, the introduction of the azide group was carried out through a Mitsunobu-type reaction. The azido derivative **68** was then converted into the NHBoc-compound **69** through one-pot Staudinger reduction-Boc protection. De-allylated compound **70** was obtained via Pd(0) catalyzed Tsuji-Trost reaction.

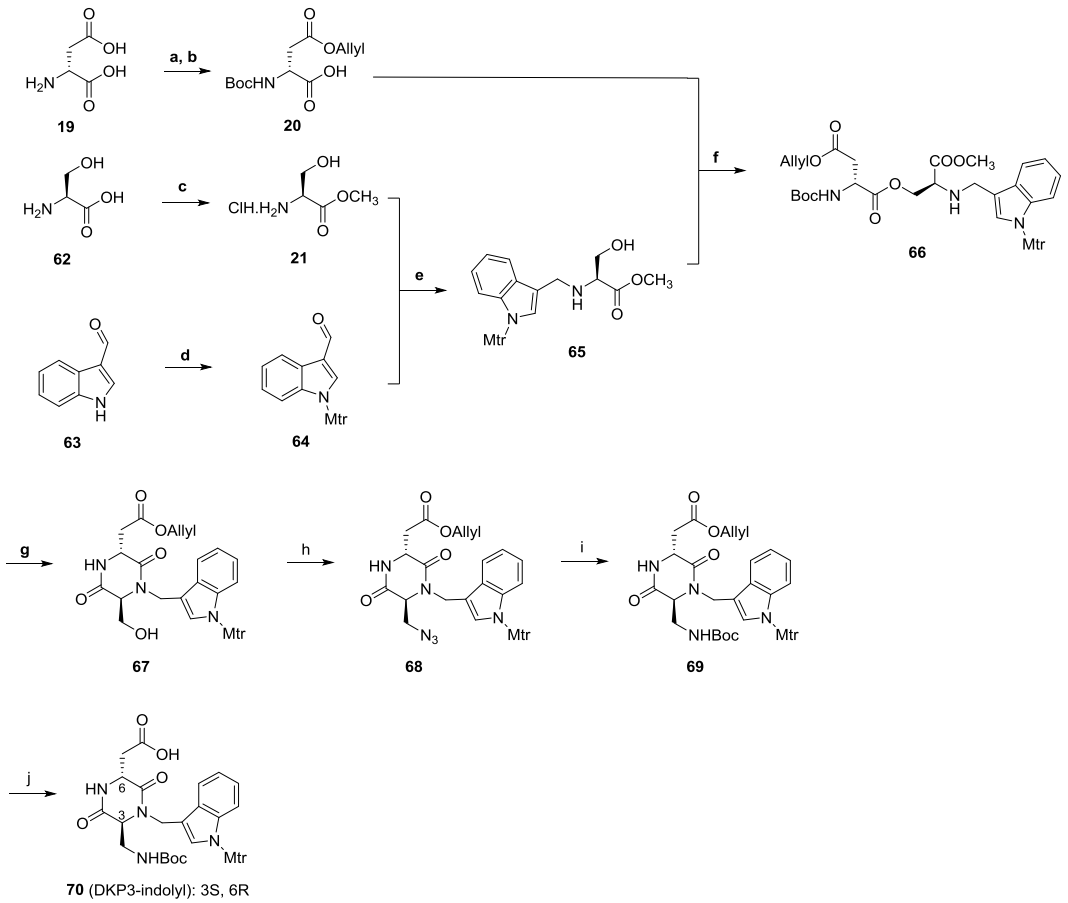

Scheme 10 Synthesis of DKP3-indolyl scaffold (**70**). Reagents and conditions: a) CH_3COCl, Allyl alcohol, 0-5°C; b) Boc_2O, TEA, H_2O/Dioxane 1:1 (v/v), r.t.; c) CH_3COCl, CH_3OH, reflux d) Mtr-Cl, DIPEA, dry THF, 0°C then r.t., under N_2,o.n., 44%; e) $NaBH(AcO)_3$, AcOH, dry THF, r.t., under N_2, 64%; f) HATU, HOAt, DIPEA, dry DMF, 0°C to r.t., under N_2, o.n., 80%; g) 1) TFA/DCM 1:2,0°C then r.t.; 2) DIPEA, iPrOH, r.t., 80%; h) PPh_3, DIAD, HN_3.tol, dry DCM/Tol 4/6, -20°C, under N_2, 5h, 88%; i) Me_3P in THF, Boc-ON, dry THF, -20°C to r.t., 70%; j) Pyrrolidine, PPh_3, $[Pd(PPh_3)_4]$, DCM, quant.

The synthesis of the peptidomimetic ligand of cadherin homophylic interactions (**Scheme 11**) was then continued on the scaffold **70**.

- **Synthesis of ligand Asp-DKP3-indolyl-Ile (59)**

Boc-Ile-CONHtBu **73** was prepared starting from L-Ile OH **71**; first NHBoc protection (**72**) and then amide formation with *tert*-butyl amine in presence of HOBt and EDC to form the active ester. After Boc deprotection to form the TFA salt (**74**), direct coupling with **70** was accomplished to afford **75** in good yield. The amino group of the DKP scaffold was first deprotected from the Boc-group and then coupled with Boc-Asp (OtBu)-OH using HATU, HOAT and DIPEA to afford the final linear peptide fully protected **76** in 67% yield.

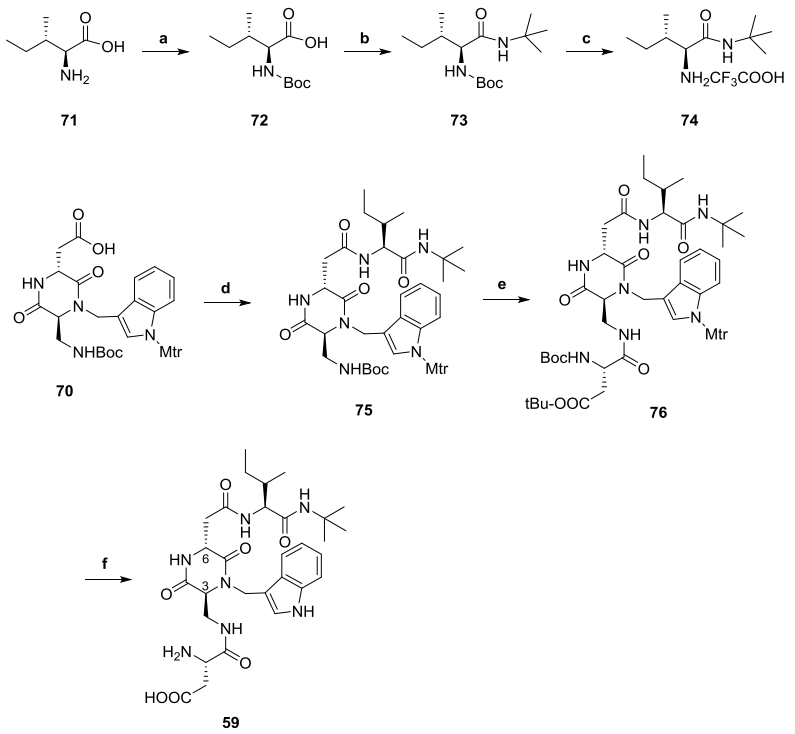

Scheme 11 Synthesis of Asp-DKP3-indolyl-Ile-NHtBu (**59**). Reagents and conditions: a) Boc_2O, TEA, H_2O/THF 1:1 (v/v), r.t., 95%; b) HOBt, EDC HCl, *tert* butylamine, DMF 0°C to r.t., 54%; c) TFA/DCM 1:2,0°C then r.t.; d) **73**, HATU, HOAt, DIPEA, dry DMF, 0°C to r.t., under N_2 o.n., 62% ; e) 1) TFA/DCM 1:2,0°C then r.t; 2) Boc-Asp(OtBu)-OH, HATU, HOAt, DIPEA, dry DMF, 0°C to r.t., under N_2, 67%; f) different conditions, see the text.

The deprotection of the ligand from the remaining protecting groups (Boc- and tBu- on the aspartic acid and Mtr- group on the NH-indolyl) was the most challenging step.

The final deprotection was carried out using first Reagent K[160] (82.5% TFA, 5% phenol, 5% H_2O, 5% thioanisole, 2.5% EDT) which is the cleavage cocktail used previously in our group for the final deprotection of the cyclic RGD-DKP integrin ligands containing essentially the same protecting groups (Boc-, tBu ester-, Mtr-).[51] We found that these conditions were not suited in our case for the final deprotection; in fact, degradation and in some cases loss of the entire methyl-indolyl group was detected with no presence of the fully deprotected ligand. We also tried to use the conditions reported in 1982[161] for deprotection of the Mtr group from Trp, Lys and the imidazole group of His (MSA/ EDT/thioanisole 85.5/4.5/10 v/v/v), but also in this case decomposition and traces of the presence of the ligand lacking in the Indolyl group was detected by mass spectrometry (results not shown). A possible explanation for this reaction outcome is that the methyl indolyl moiety, linked to the nitrogen of the DKP, is more susceptible to electrophilic substitution. Anyhow the problem is not related to the Mtr-deprotection from the Indolyl moiety, but it is related to the intrinsic structure of our ligand. To overcome this problem, it is clear that a change in the synthetic pathway and, more specifically, in the protecting group scheme would be necessary. However, this would introduce an even higher degree of complexity; to avoid this, we considered a different strategy to introduce the required cadherin binding epitope. This will be illustrated in the next paragraph.

2.2.3 Synthesis of cyclic ligands

In order to synthesize valuable ligands for cadherin homophylic interactions, we continued our investigations in this field. We decided to switch our attention towards cyclic ligands based on the DKP3 scaffold and containing amino acids bearing the correct functionalities to interact with the protein. Docking studies with human E-cadherin and molecular dynamics simulations were therefore set up and the *c*(DKP3-Gly-Arg-Trp) (**61**, **Figure 39**) resulted to be a very interesting ligand.

Cyclic peptides show a better biological profile compared to their linear homologues, due to their conformational rigidity. In addition, they show resistance to hydrolysis by peptidases due to the lack of both amino and carboxyl ends and crossing the cell membrane is enhanced with respect to the linear peptides. The role of cyclic peptides in clinic is important. Tyrocidine A and Gramicidine S in **Figure 40** (which showed antibacterial activity), are only examples to confirm this.[162]

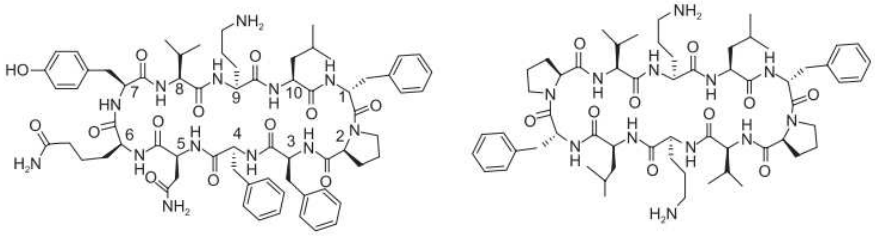

Figure 40 Structure of tyrocidine A (left) and Gramicidine S (right).

The synthesis of the *c*(Gly-DKP3-Trp-Arg) was planned in solution. First the scaffold COOH-DKP3-NHBoc **82** was synthesized as previously reported by our group.[52] **Scheme 12** shows the synthetic pathway for the DKP3 scaffold.

A serine ligation strategy was selected.[81] Starting from either (S)-Ser and (R)-Asp, (S)-*N*-benzylserine methyl ester **77** and (R)-*N*-(*tert*-butoxycarbonyl)aspartic acid β-allyl ester **20** were easily prepared according to literature procedure.[158,159] Direct coupling between **20** and **77** was chosen (in order to avoid the introduction of further protecting groups) and the generation of the isopeptide **78** was achieved in high yield (67%), instead of the expected dipeptide **78***.[81] After boc-deprotection of **78** and cyclization to obtain **79**, the introduction of the azide group was carried out through a Mitsunobu-type reaction (75%). The azido derivative **80** was converted into the NHBoc-compound **81** through one-pot Staudinger reduction-Boc protection (68%). De-allylation (via a Pd(0) catalyzed Tsuji-Trost reaction) followed to afford the final product **82** in almost quantitative yield.

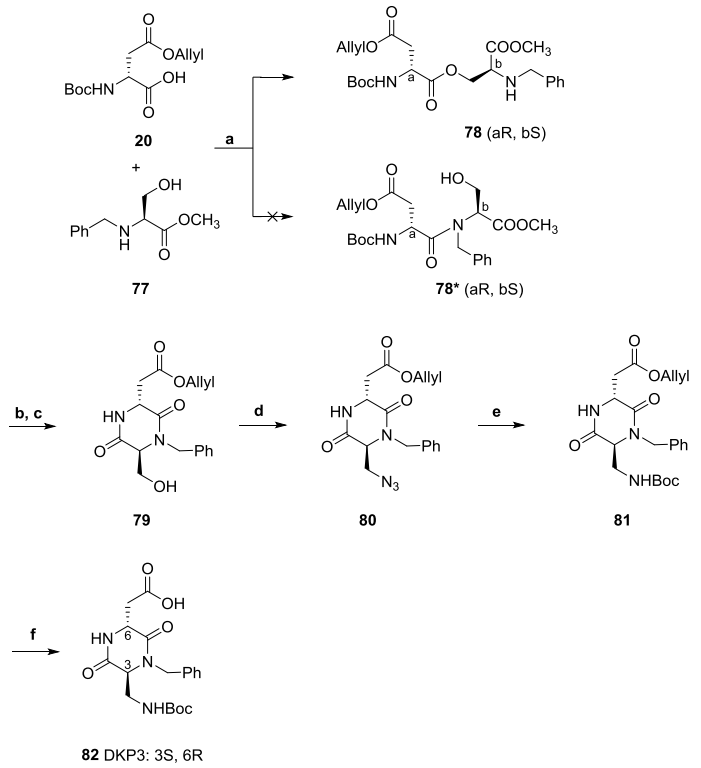

Scheme 12 Synthesis of the scaffold DKP3 (**82**). Reagents and conditions: a) EDC·HCl, DMAP, DCM, r.t., o.n., 67%; b) TFA/DCM 1:2 (v/v), 0°C to r.t.; c) DIPEA, iPrOH, r.t., o.n., 80%; d) HN_3, DIAD, PPh_3, DCM/toluene 4:6 (v/v), 6h, -20°C, 75%; e) Me_3P, BocON, THF, -20°C to r.t., 68%; f) pyrrolidine, PPh3, $[Pd(PPh_3)_4]$, DCM, 0°C to r.t., quant.

The mechanism of the isopeptide formation was deeply studied by means of NMR in our research group (**Scheme 13**).[81] NMR spectra confirmed the mechanism via *O*,*N*-acyl transfer.[163] Selective *O*-acylation of the unprotected β-hydroxyl group of *N*-benzylserine methyl ester is preferred over the formation of the tertiary amide. In addition the resulting ester bond is stable in solution to *O*,*N*-acyl transfer which occurs spontaneously upon Boc- deprotection with simultaneous formation of the diketopiperazine ring.

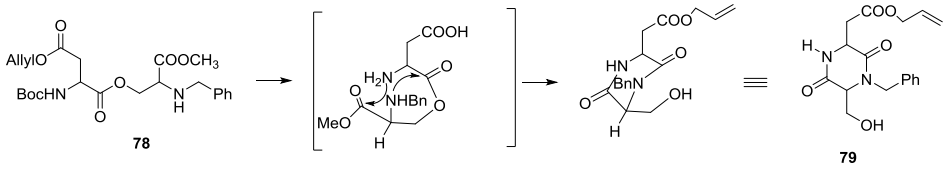

Scheme 13 DKP formation mechanism from the isopeptide

The conversion of the hydroxyl group to the azide group (compound **79** into **80**) was achieved through the Mitsunobu reaction (**Scheme 14**). The reaction is critical since the activated hydroxyl functionality could undergo β-elimination before reacting with the nucleophile hydrazoic acid. The

reaction was monitored and the temperature was kept around -20°C in order to minimize the formation of the β-elimination product (**83**).

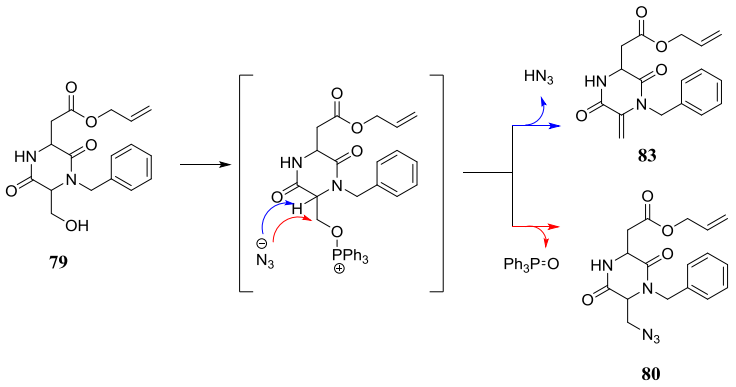

Scheme 14 Mitsunobu-type reaction mechanism on the DKP scaffold

The conversion of **80** into **81**, involved a one-pot Staudinger reduction-Boc protection. The azide reacts with the phosphine to generate phosphazide intermediate which then loses N_2 forming an iminophosphorane. In this one-pot Staudinger-Boc protection, the iminophosphorane reacts directly with 2-(tert-butoxycarbonyloxyimino)-2-phenylacetonitrile (Boc-ON) affording the desired Boc-protected amine in very good yield. Notably, in a classical Staudinger reaction, the hydrolysis of this last intermediate leads to the amine and the very stable phosphine oxide. The mechanism is reported in **Scheme 15**.

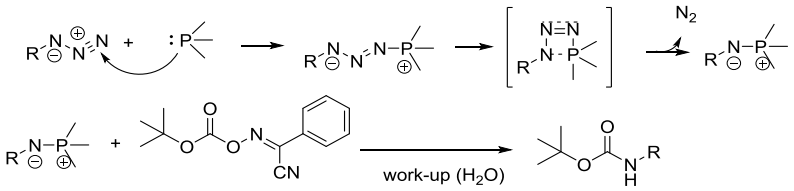

Scheme 15 One-pot Staudinger-Boc protection reaction on the azide

Deallylation on **81** was performed in the presence of a catalytic amount of *Palladium tetrakis(triphenylphosphine)* ([$Pd(PPh_3)_4$]), and pyrrolidine (which is necessary as allyl scavenger) as nucleophile (catalytic cycle in **Scheme 16**). Such methodology is particularly interesting for peptide synthesis because of the compatible deprotection conditions in the presence of labile *t*Bu and Boc groups.[164] The final amino acid derivative (**82**) was obtained in good yields (80-90%).

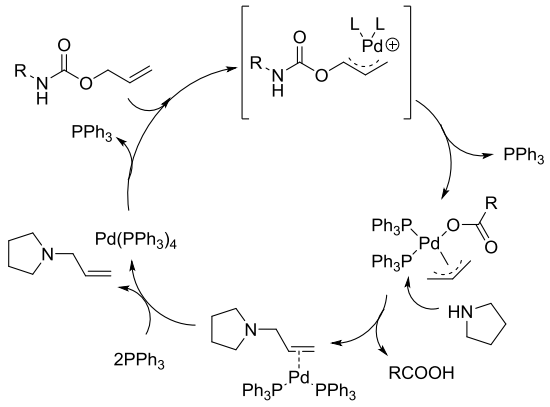

Scheme 16 Deallylation mechanism

Once we synthesized the DKP3 scaffold **82**, we continued the synthesis of the cyclic ligand in solution. The synthetic pathway is depicted in **Scheme 17**. Compound **84** was synthesized in good yield (80%), starting from **82** and Gly-OBn HCl, using HATU and HOAt as coupling agents and DIPEA as a base. After Boc deprotection, Fmoc-Trp(Boc)-OH was coupled using the same coupling conditions as the previous step, obtaining compound **85**. The tryptophan was chosen Fmoc- and Boc- protected in order to fulfill the orthogonality with the OBn-protecting group on the Glycine. Fmoc- deprotection to set the tryptophan's amino group free was achieved in quantitative yield, treating the peptide with piperidine in DMF. Coupling with Cbz-Arg(Mtr)-OH was done directly on the crude Fmoc- deprotected compound and **86** was obtained in good yield (70%). Once the linear peptidomimetics Cbz-Arg(Mtr)-Trp(Boc)-DKP3-Gly-OBn (**86**) was obtained, it was deprotected from the Cbz and Bn groups through hydrogenolysis. The linear deprotected derivative (**87**) was subjected to macrolactamization. The protected cyclic peptide **88** was obtained in a fairly good yield (60%). A final side-chain deprotection afforded the desired compound (**61**) which was purified by preparative HPLC (30% yield).

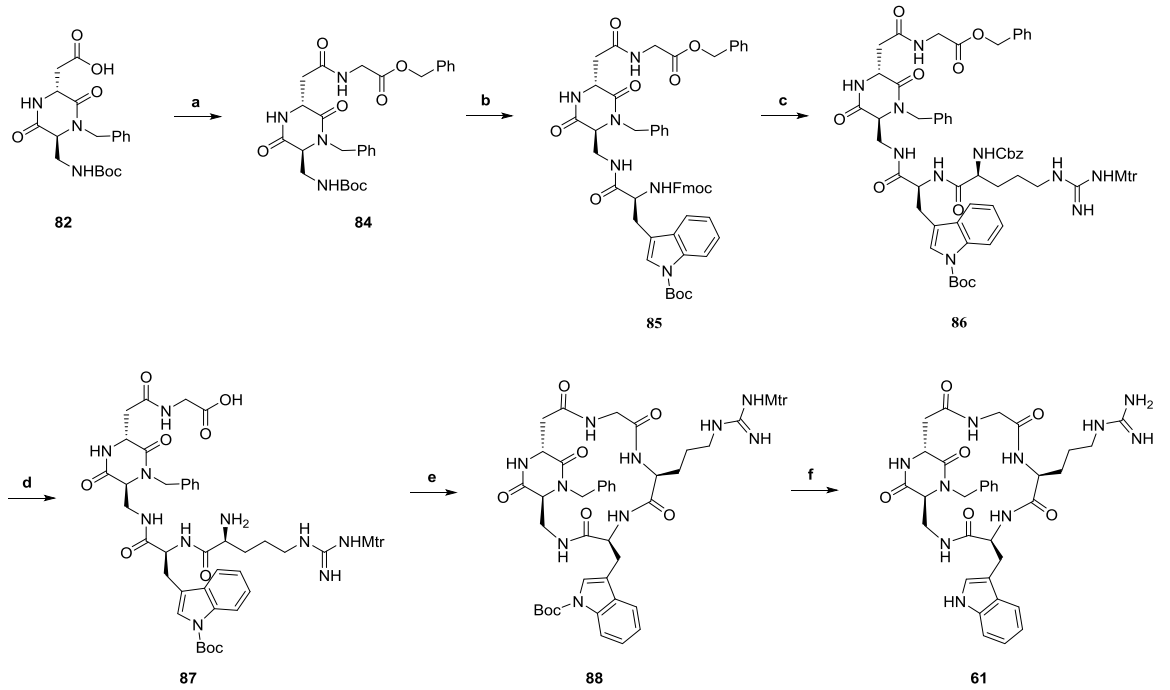

Scheme 17 Synthetic pathway for *c*(Gly-DKP3-Trp-Arg) (**61**). Reagents and conditions: a) Gly-OBn HCl, HATU, HOAt, DIPEA, dry DMF, 0°C to r.t., under N_2, 93%; b) 1) TFA/DCM 1:2 (v/v), 0°C then r.t. 2) Fmoc-Trp(Boc)-OH, HATU, HOAt, DIPEA, dry DMF, 0°C to r.t., under N_2, 60%; c) 1) piperidine in dry DMF, 2h, under N_2; 2) Cbz-Arg(Mtr)-OH, HATU, HOAt, DIPEA, dry DMF, 0°C to r.t., under N_2, 72%; d) H_2, Pd/C, THF/water 1:1, r.t., o.n., quant.; e) HATU, HOAt, DIPEA, DMF, 0°C to r.t., under N_2, 60%; f) TFA/Thioanisole/EDT/anisole 90/5/3/2, 2h, 30%.

2.3 Conclusions and outlooks

A second generation of linear peptidomimetic inhibitors of cadherin homophilic interactions (**76**) was developed, bearing the newly synthesized DKP3-indolyl scaffolds **70**. Unfortunately, problems during the final deprotections of **76** were faced, so the final linear peptide fully deprotected (**59**) was not detected. A new synthetic pathway, likely involving the use of a different protecting group strategy, needs to be developed although this would involve a cumbersome work to define the complete orthogonality among the different groups.

In alternative, a new cyclic peptidomimetic ligand **61** was synthesized. In this case the indolyl moiety was inserted as amino acid tryptophan in the ligand together with Arginine, Glycine and the DKP3 scaffold. Compound **61** will be tested for its ability to inhibit calcium dependent cadherin binding using N- or E-cadh-expressing cell lines.

PART II

1. Design of cyclic CPP-DKP scaffolds for drug delivery

1.1 Cyclic peptides as therapeutic agents

Chemists have been attracted by cyclic molecules for a long time, especially after the discovery of Gramicidin S (**Figure 41**) in 1944 by Gause and Brazhnikova. Gramicidin S was used to treat septic gunshot wounds during the Second World War, as it showed antiseptics activity.[165] Since then, cyclic peptides have gained significant therapeutic potential and many have been used as therapeutic agents (e.g. octreotide, calcitonin, cyclosporine A, etc.)[166] also in consideration of their increased resistance to proteases with respect to linear peptides. Cyclosporin A (**Figure 42**) is an orally bioavailable peptide drug due to its high membrane permeability; it was approved in 1983 as an immunosuppressive therapeutic drug in patients undergoing transplants.[167] Romidepsin (**Figure 43**) is a potent antitumor drug which induces apoptosis in malignant cells.[168]

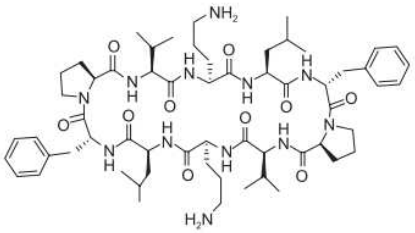

Figure 41 Gramicidin S

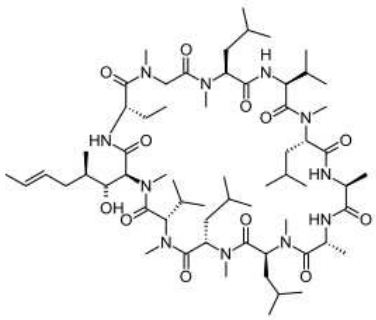

Figure 42 Cyclosporin A

Cyclization of certain sequences of membrane-active peptides enhances their antimicrobial activity. The restriction of the available conformations is crucial for ensuring a better activity. In fact, cyclic peptides can adopt an amphipathic arrangement and, in this way, they are able to perturb the membrane by forming pores. Such conformations are more seldom met in linear peptides, in which entropy reduces the formation of structures with amphipathic-like character.[169]

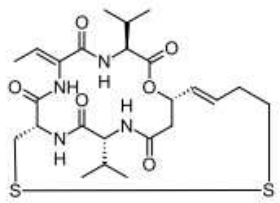

Figure 43 Romidepsin

1.1.1 Peptide's macrocyclization

Cyclic peptides, especially larger ones, are notoriously difficult to synthesize. The ground-state E geometry is important; because of this geometry, small and medium-sized ring are unable to assume the ring like conformation which is essential for obtaining cyclization. Of course this is not the case of larger cycle, which in turn have the problem to avoid intermolecular reactivity.
Peptide cyclization can be achieved in different ways: head-to-tail (N-terminus to C-terminus), head-to-side chain, side chain-to-tail or side-chain-to-side-chain as represented schematically in **Figure 44**.[170]

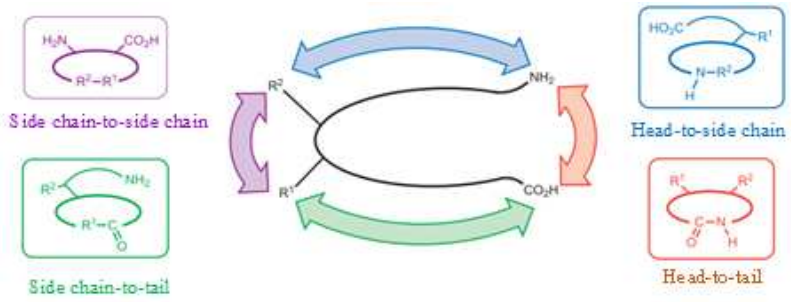

Figure 44 Schematic representation of different ways for peptides cyclization. Adapted from ref 174

Macrocyclization gives the best yields if a high dilution strategy is used; for this reason, solid-supported macrocyclizations can be very effective.[171] Several efforts have been done for directing macrocyclization over the past years: conformational pre-organization[172], formation of internal hydrogen bonds or β-sheet structures[173], introduction of pseudo-proline[174], metal-ion assisted cyclizations[175], *etc.* are only some ways used to improve macrocyclization.

1.2 Cyclic cell penetrating peptides

As discussed in **Part I**, cell penetrating peptides are considered promising devices for medical development. Peptide cyclization was demonstrated to be an effective strategy for enhancing cellular uptake rates and promoting endosomal escape thus enhancing cytoplasmic distribtion.[176–179]
In 2011 Lättig-Tünnemann *et al.* demonstrated that the transduction entrance efficiency (which corresponds to a non-endocytic mode of entry cells) of arginine-rich peptides is enhanced when guanidinium groups are forced into maximally distant positions simply by peptide cyclization. The higher structural rigidity of the arginine-rich peptides leads to higher uptake rate with respect to the flexible linear counterpart.[177]
In the majority of the literature's cases, peptide cyclization is achieved *via* the chemoselective copper-catalyzed azide-alkyne cycloaddition (CuAAC).[180,181] In particular, triazole-bridged cyclic

peptides were synthesized and characterized, in the laboratories of Professor Neundorf's group (University of Cologne) where I spent a six-month research period.[114,182]

For example, the synthesis and biological evaluation of a CPP based on human calcitonin (hCT) was reported by Neundorf's group. Side-chain cyclization was achieved via CuAAC reaction (**Figure 45**).

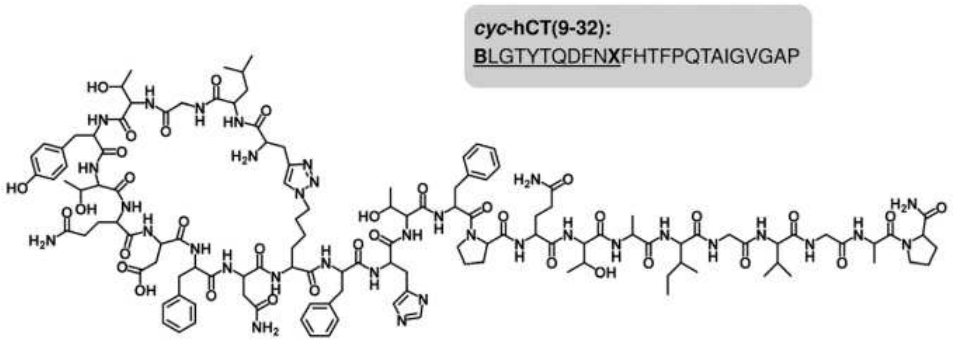

Figure 45 Cyclic hCT(9-32). Adapted from reference 186

N

o cytotoxic effects and efficient intracellular uptake were determined for the peptide in **Figure 45**. Moreover, preliminary studies using this novel peptide as drug transporter for daunorubicin were performed.

On the other hand, a fragment of the cell penetrating peptide sC18 ([106]GLRKRLRKFRNK[117] namely sC18*) was cyclized via CuAAC reaction, with different ring size (obtaining cyclic molecules **89**, **90**, **91**, **Figure 46**).[114] Substitution of glycine and lysine by propargylglycine and ε-azidolysine respectively, allowed for selective side chain cyclization via "click chemistry". The three cyclic peptides differ essentially for the number of arginine residues which are incorporated into the cyclic moiety, with the aim of studying how the amount and position of guanidinium groups affect the peptide membrane activity. Their proteolytic stability was tested and they showed to be much more stable than the linear peptides. Furthermore, the cyclic peptide did not show any cytotoxicity when incubated with different human cell lines such as human breast adenocarcinoma cells (MCF-7), colon adenocarcinoma cells (HCT-15), cervical carcinoma cells (HeLa), and embryonic kidney cells (HEK-293). Interaction studies using artificial membrane systems were conducted and all the cyclic peptides readily translocated through the membrane; among the three cyclic peptides, cyclic **91** (**Figure 46**) showed the highest membrane translocation activity.[114]

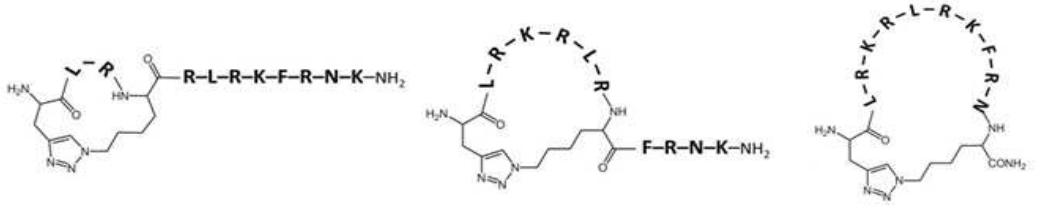

89 **90** **91**

Figure 46 sC18 cyclic peptides containing one (**89**), three (**90**) or four (**91**) arginine residues in the cyclic moiety.

1.3 Aim of the project

Encouraged by these results, in collaboration with Lucia Feni (PhD student in Professor Neundorf's group, Institute of Biochemistry, University of Cologne), we planned to replace the triazole bridge of compound **91** with a more spatially oriented and rigid scaffold such as the bifunctional diketopiperazines (DKP) showed in the previous chapter, thus developing new cyclic sC18* peptides which correspond to cyclic peptide **91**. The *cis*- (DKP1) and *trans*- (DKP3) diketopiperazine rigid scaffolds were used for the synthesis of compound **92** and **93**, (**Figure 47**) respectively.

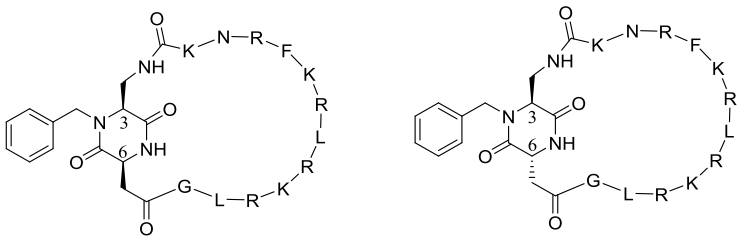

Figure 47 sC18-cyclic peptides with the *cis*-DKP scaffold (structure **92**) and the *trans*-DKP scaffold (structure **93**).

1.3.1 Synthesis of *c*(sC18*-DKP)

First of all, scaffolds DKP1 and DKP3 were synthesized as reported in **Scheme 18**. Compounds **80** and **97** were synthesized as previously reported in **Part I** (Paragraph 2.2.3, **Scheme 12**), starting from L-Ser and L-Asp for **97** (**Scheme 18**) and starting from L-Ser and D-Asp for compound **80** (**Scheme 18**). We decided to avoid the use of a protecting group on the DKP scaffold keeping the azido group on the DKP scaffold and to reducing it to amino group directly on resin.
Compounds **98** and **99**, were synthesized treating compounds **97** and **80** with a catalytic amount of $Pd[P(Ph_3)]_4$ in presence of *N*-methylaniline to remove the allyl ester and to obtain the desired azido acids.

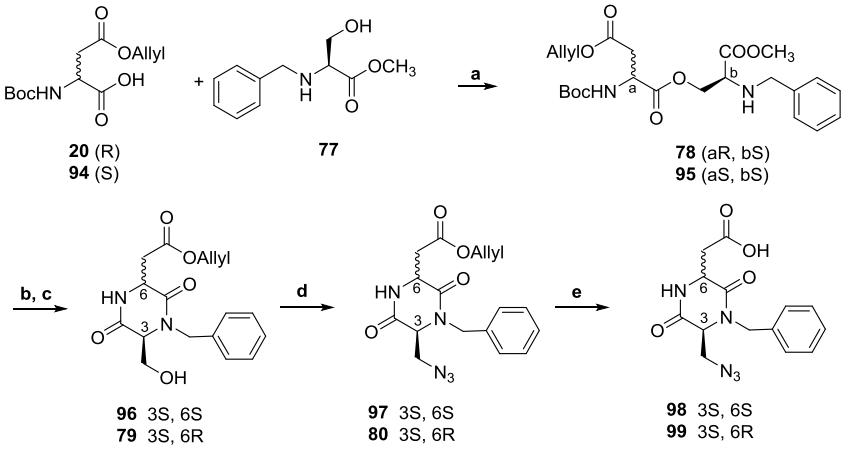

Scheme 18 Synthesis of the DKP1 and DKP3 scaffolds. Reagents and conditions: a) EDC·HCl, DMAP, DCM, 67%; b) TFA/DCM 1:2 (v/v), 0°C to r.t.; c) DIPEA, *i*PrOH, o.n., r.t., 80%; d) HN_3, DIAD, PPh_3, DCM/toluene 1:2 (v/v), 6h, 75% (58% for **96**); e) $Pd[P(Ph_3)]_4$, *N*-methylaniline, dry DCM, under N_2, 60%.

With the azido acids **98** and **99** in our hands, the synthesis of the sC18-DKP linear peptides was performed on solid phase through automated SPPS.
Different strategies were adopted for the synthesis of the cyclic compounds, as shown in the retrosynthetic **Scheme 19**.
The two synthetic pathways differ essentially for the site of cyclization. In pathway A the amino group of the DKP scaffold is involved in the formation of the peptide bond with the C-terminal carboxyl group, while in pathway B cyclization was achieved through the formation of peptide bond between two amino acids in the $sC18^*$ sequence (as showed in **Scheme 19**). In fact, we planned to exploit the tendency of the *cis*-DKP1 scaffold to keep the two branched ends in the same direction, like forming a β-sheet,[13] trying to achieve a higher level of preorganization in the final structure.

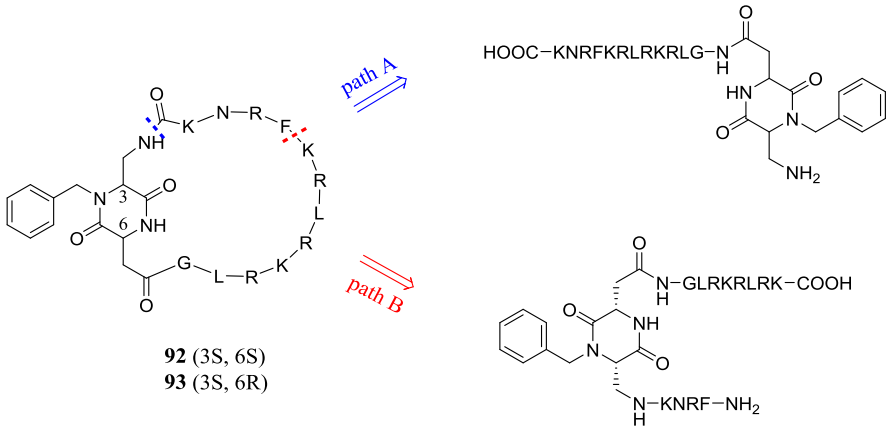

Scheme 19 Retrosynthetic pathways for the synthesis of the cyclic [sC18*-DKP] compounds **92** or **93**

Synthetic pathway A (for both cycle **92** and **93**) is reported in **Scheme 20**. sC18* peptide was synthesized as C-terminal acid on a Fmoc-Lys(Boc)-OH, preloaded 2-chlorotrytil chloride resin, by automated multiple solid-phase peptide synthesis (Fmoc strategy). Compounds **98** and **99**, DKP1 and DKP3 respectively, were coupled manually to the peptide using Oxyma and DIC as coupling agents (**101**, **Scheme 20**). Reduction of the azido group on the DKP scaffolds (**102**) was achieved using a 2M solution of DL-dithiothreitol (DTT) in DCM and in presence of DIPEA in almost quantitative yields. Full cleavage of the peptide from the resin was done using weak acidic conditions (acetic acid) in order to obtain the peptide fully protected at the amino acid side chains (**103**). In this way only the C-term and the N-term are free to react, forming a peptide bond. The cyclization step was done using PyBOP, HOBt as coupling agents and DIPEA in DMF. Final deprotection was achieved with TFA in the presence of scavengers such as phenol, water, thioanisole, EDT. The peptides were then purified on HPLC, yielding the cyclic compounds **92** and **93**.

The cyclization step was most challenging; overall yields were quite low for both cyclic peptides (the best result was 16% yield). However, considering the length of the peptide, we considered such yields acceptable. In some cases the presence of epimers was detected by LC-MS (data not shown).

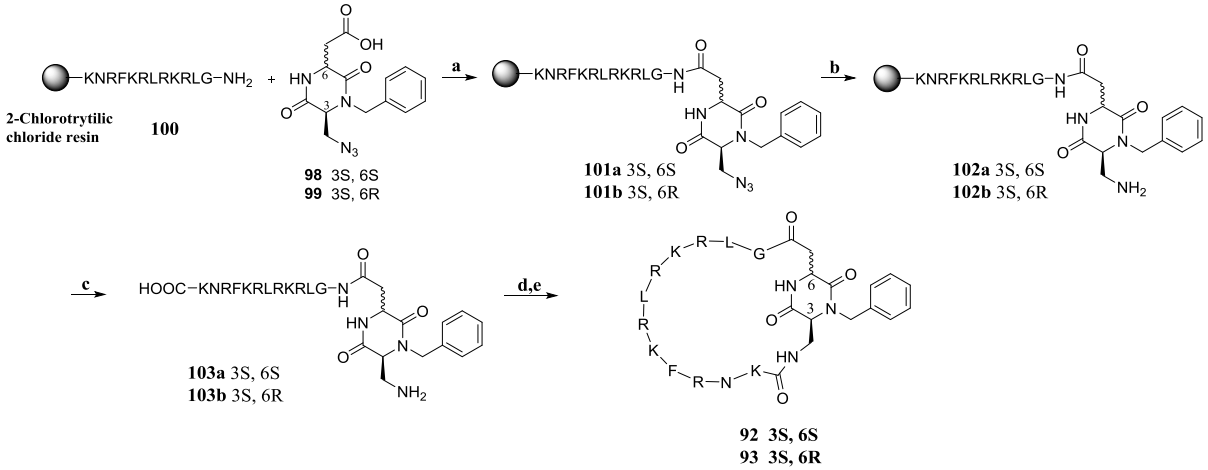

Scheme 20 Synthesis of the two sC18-cyclic peptides with the *cis*-DKP scaffold (**92**) and the *trans*-DKP scaffold (**93**). Reagents and conditions: a) Oxyma, DIC, o.n.; b) DTT (2M), DIPEA (1M), DCM, 2h; c) acetic acid/ TFE/ DCM 1:1:8; d) [0.65mM] peptide concentration, PyBOP (5eq), HOBt (5eq), DIPEA (6eq), dry DMF, 24h, r.t.; e) full deprotection with TFA/phenol/water/thioanisole/EDT 82,5:5:5:5:2,5.

Trying to obtain better yields, we decided to synthesize cyclic peptide **92** (containing the *cis*-DKP1 scaffold) as proposed in **pathway B** (**Scheme 21**). The sC18* sequence was synthesized again on solid phase but anchoring the peptide to the resin through Lys^{113} (instead of the N-terminal Lys^{117} as in pathway A). After coupling the DKP1 scaffold, the peptide was elongated by manual coupling of the remaining amino acids, obtaining the linear peptide **108**. The latter was cyclized using the same condition of pathway A. Yields around 7 % were obtained, probably due to the formation of truncated sequences during the elongation step after DKP coupling.

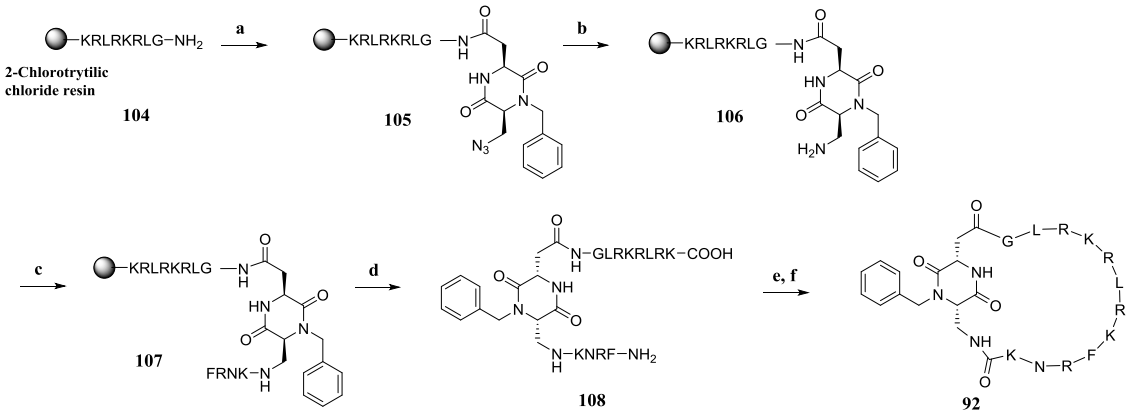

Scheme 21 Synthetic strategy relative to **pathway B**. Reagents and conditions: a) HATU, DIPEA, 2h; b) DTT (2M), DIPEA (1M), DCM, 2h; c) elongation with Lys, Asn, Arg and Phe; d) acetic acid/ TFE/ DCM 1:1:8; e) [0.65mM] peptide concentration, PyBOP (5eq), HOBt (5eq), DIPEA (6eq), dry DMF, 24h, r.t.; f) full deprotection with TFA/phenol/water/thioanisole/EDT 82,5:5:5:5:2,5.

1.3.2 Synthesis of *c*-sC18*(reversed sequence)-DKP

In addition, a linear sC18* with C-term and N-term exchanged (sequence: ^{117}KNRFKRLRKRLG^{106}) was also synthesized and its cyclized version with *cis*-DKP1 (**109**) was developed.

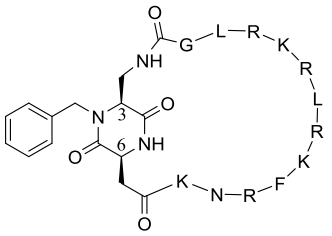

109

Figure 48 *c*(rev-sC18*-DKP1) compound **109**

The synthesis of the cyclic version of a reversed sC18*-DKP1 peptide was done as reported in **Scheme 22**. In this way, the cyclization occurs on the glycine residue which can not undergo epimerization.

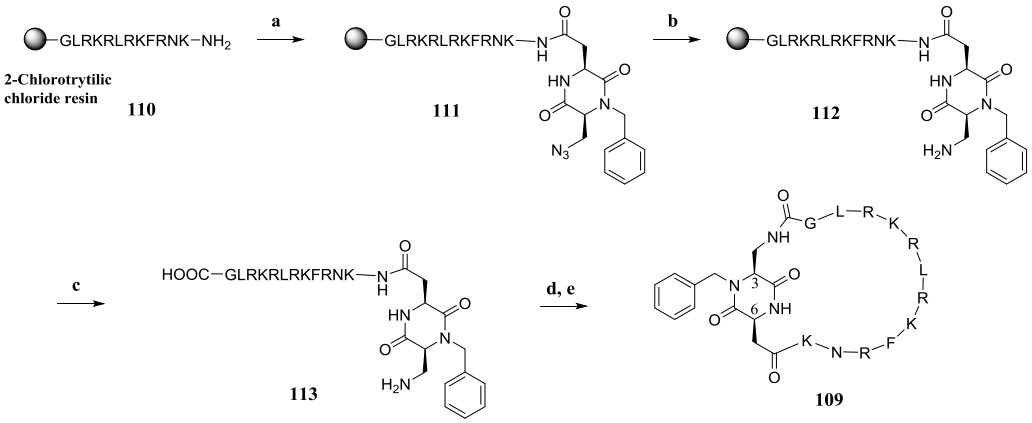

Scheme 22 Synthesis of *c*(rev-sC18*-DKP1) **109**. Reagents and conditions: a) Oxyma, DIC, o.n.; b) DTT (2M), DIPEA (1M), DCM, 2h; c) acetic acid/ TFE/ DCM 1:1:8; d) [0.65mM] peptide concentration, PyBOP (5eq), HOBt (5eq), DIPEA (6eq), dry DMF, 24h, rt; e) full deprotection with TFA/phenol/water/thioanisole/EDT 82,5:5:5:5:2,5.

The peptide was synthesized on a H-Gly-OH preloaded 2-chlorotrytil chloride resin by automated multiple solid-phase peptide synthesis (Fmoc strategy) using a robot system. The synthetic strategy is the same as in path a (**Scheme 20**) and in this case yields were around 3-6 %.

1.3.3 Synthesis of linear sC18*-DKP

Linear peptides corresponding to the cyclic **91** and **92** were also synthesized in order to study their behaviour and compare it with the cyclic versions. Their synthesis is reported in **Scheme 23**.

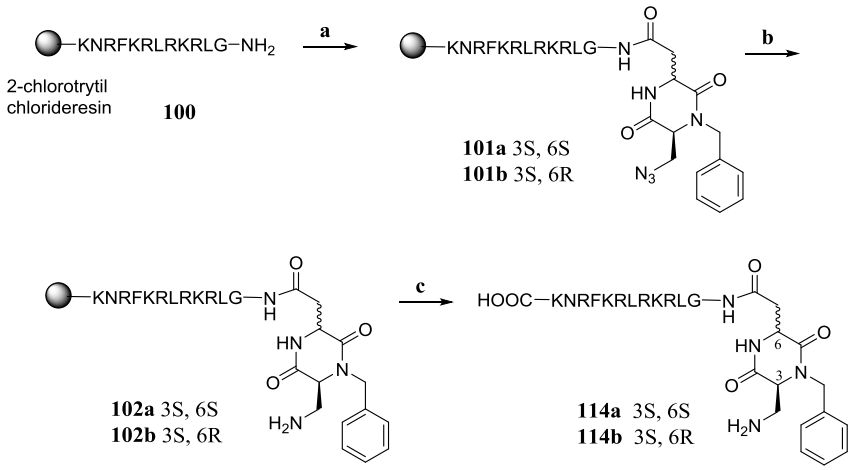

Scheme 23 Synthetic strategy for linear peptides (**114a** and **114b**). Reagents and conditions: a) Oxyma, DIC, o.n.; b) DTT (2M), DIPEA (1M), DCM, 2h; c) full cleavage with TFA:TIS:water 9.5:2.5:2.5 for 3h at rt (60% for **114a** and 48% for **114b**).

Linear peptides sC18*-DKP **102a** and **102b** were treated with a mixture of TFA:TIS:water in order to obtain both cleavage from the resin and deprotection of all the amino acids' side chains. Peptides **114a** and **114b** were purified on preparative HPLC, obtaining final peptides (60% yield for **114a** and 48% for **114b**) with purities >95%.

1.4 Structural investigations on cyclic (92 and 93) and linear (114a, b) peptides

- Circular Dichroism studies

Cyclic peptides **92** and **93** were studied with CD spectroscopy to evaluate their secondary structure. The CD spectrum is generated from the sum of contributes of each amide moiety present in the peptide; in fact, the chromophores of the amides, aligned in different ways, result in the fact that each structural element has characteristic CD spectra (**Figure 49**). For example, α-helical peptides have negative bands at 222 nm and 208 nm and a positive band at 193 nm. Peptides with antiparallel β-sheets have negative bands at 218 nm and positive bands at 195 nm, while disordered proteins have very low ellipticity above 210 nm and negative bands near 195 nm.[183]

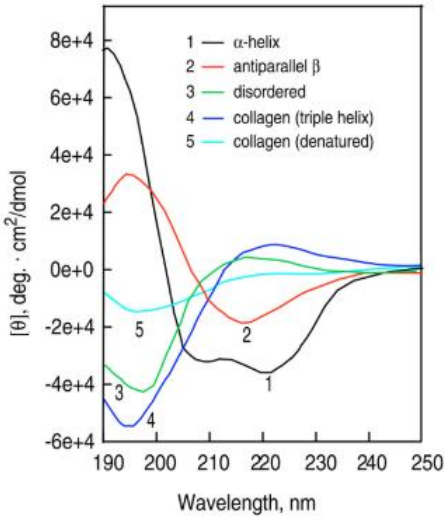

Figure 49 CD spectra of representative secondary structures. In particular, **1** (black) α-helical, **2** (red) antiparallel β-sheet and **3** (cyan) disordered conformations. Adapted from ref 187

In **Figure 50**, CD spectra of the cyclic peptides **92** and **93** in phosphate buffer and in presence of trifluoroethanol, are reported. Trifluoroethanol (TFE) is a cosolvent which has been widely used in the field of structural biology as membrane mimetic agent.[184] Compounds **92** (*c*DKP1) and **93** (*c*DKP3) in PBS buffer seem to adopt disordered structures, whereas in the presence of TFE, the peptides seem to be more structured with two minima around 203 nm and 222 for peptide **92** and two less intense minima around 210 and 222 for peptide **93**; anyway their behavior does not fit with any canonical secondary structure.

CD spectra of the linear versions, **114a** and **114b**, are also reported in **Figure 50**; the two linear versions assume disordered structures in phosphate buffer, while they seem to reorganize in α-helical structures in presence of TFE as usual for sC18 linear peptides. As a consequence, the DKP scaffolds did not perturb the properties of linear sC18 in phosphate buffer.

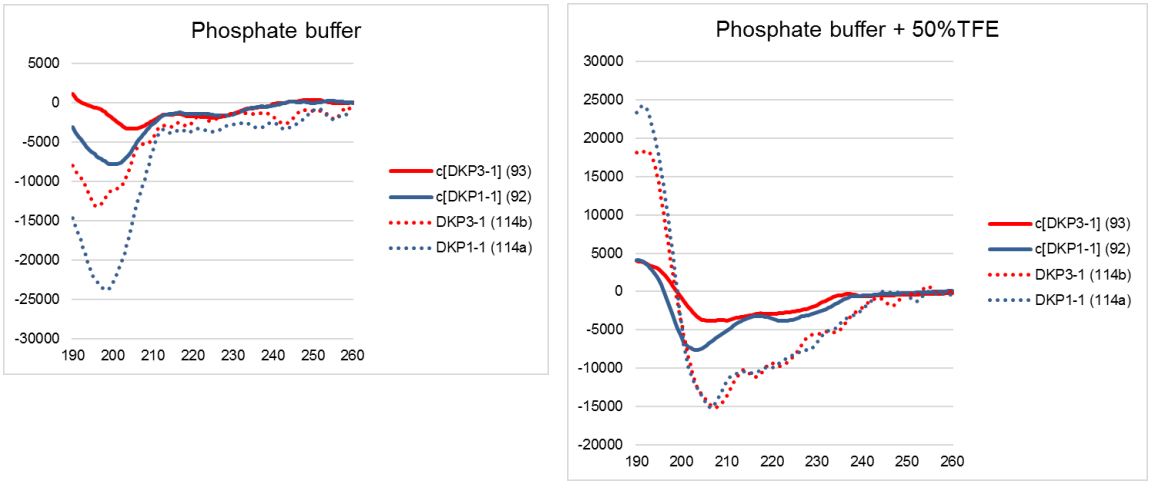

Figure 50 CD spectra of cyclic **92** (blue line) and **93** (red line) and linear **114a** (dashed blue line) and **114b** (dashed red line) in PBS buffer and in presence of 50% TFE.

- **NMR studies**

In collaboration with Dr. Díaz (Organic Chemistry, University Cologne), the three dimensional structures of both linear and cyclic derivatives of DKP1-sC18 peptide were investigated by NMR spectroscopy.
The conformational preferences of the peptides in solution and also in membrane mimetic medium (i.e. SDS micelles, SDS= sodium dodecyl sulfate) were studied in order to explore details about the translocation's mechanism of CPPs inside the cells, using a simple model system.
The linear peptides **114a** and **114b** were analyzed in solution. After assignment of the NMR signals and using the array of internuclear distances derived from the NOESY spectra, the conclusion was that both peptides exhibit a random coil structure in solution, as not identifiable secondary structure was found, no matter the temperature we used to acquire the spectra (i.e. 283 K or 298 K).
On the other hand, both peptides were found to assume α-helix structures in presence of SDS micelles (**Figure 51**). This result is not surprising since it is known that the structure of the native CAP18 peptide switches from random coil to helix upon addition of TFE. The presence of DKP1 in the sequence does not seem to play a role since any special interaction between DKP1 and any other residue of the peptide sequence (i.e. participation in hydrogen bonds to stabilize the helix) was detected. The position of the residue (first residue, N-terminus) seems to preclude such possibility and it is not involved in helix stabilization.

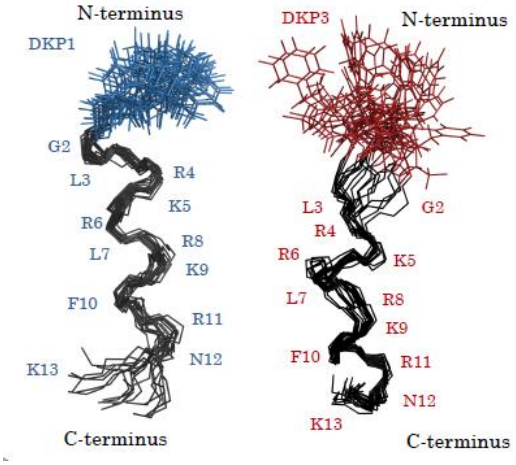

Figure 51: Overlapping of the 20 energy-favored structures of peptide **114a** (left) and **114b** (right) in the presence of SDS micelles. The backbones of these linear peptides show an α-helical structure.

For what concerns the cyclic peptide DKP1-sC18 **92**, NMR spectra at 298 K were acquired and an ensemble of structures using experimental NOE restraints (internuclear distances) were calculated, obtaining the ten lowest energy structures for peptide **92** (**Figure 52**).

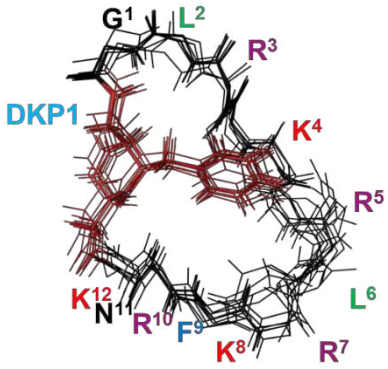

Figure 52: Ensemble of the 10 lowest energy structures of cyclic peptide **92**. For the sake of clarity only backbone traces are shown (black) and the linker DKP1 (red) at 298K.

Cyclic peptide **92** does not show signs of secondary structure in solution at 298 K. On the other hand, spectra acquired at 283 K, in particular NOESY spectra, showed a relatively large number of NH-NH cross peaks, suggesting that temperature influences the equilibrium between different conformations of the peptide and supporting the existence of structural families/clusters. Anyway, the temperature coefficients do not support this assumption and they seem to indicate absolute absence of hydrogen bonds. Further investigations are ongoing (molecular dynamics) in order to explore the possible compatibility with the experimental data and whether they could be explained, with the experimental NMR restraints deduced from the spectra (i.e. NOE cross peaks and the corresponding internuclear distances).
The NMR analysis of both cyclic peptides **92** and **93** in presence of SDS micelles are still ongoing.

1.5 Conclusions and outlooks

New cyclic sC18* peptides, bearing *cis*- (DKP1) and *trans*- (DKP3) diketopiperazine rigid scaffolds, were synthesized (compound **92** and **93**, **Figure 47**). Different retrosynthetic approaches were used for their synthesis trying to enhance the cyclization yields; unfortunately, no big differences were found in yields of this last step. Linear counterparts (**114a** and **114b**) of the cyclic compounds were also synthesized in order to study their characteristics and supposed different behavior towards membrane mimetic media.

Structural investigation on cyclic compounds **92** and **93** was done through circular dichroism studies and in addition, the three dimensional structures of both linear and cyclic derivatives of DKP1-sC18 peptide was investigated by NMR spectroscopy in collaboration with the University of Cologne.

Structures of cyclic compounds, both in absence and in presence of TFE, seemed not to fit with any canonical secondary structure (CD spectra). Linear peptides **114a** and **114b** were analyzed in solution, by mean of NMR, and both peptides exhibit a random coil structure in solution. On the other hand, both linear peptides were found to assume α-helix structures in presence of SDS micelles.

Further investigations in this field are ongoing for the cyclic compounds **92** and **93**. We are currently planning to develop labeled and drug-conjugate with cyclic compounds in order to study their biological activity and the possibility to use them as drug delivery systems.

Experimental part

General Remarks and Procedures

Materials and methods

All manipulations requiring anhydrous conditions were carried out in flame dried glassware, with magnetic stirring and under a nitrogen atmosphere. All commercially available reagents were used as received. Anhydrous solvents were purchased from commercial sources and withdrawn from the container by syringe, under a slight positive pressure of nitrogen. The reactions were monitored by TLC using silica gel 60 F_{254} pre-coated glass plates (0.25 mm thickness). Visualization was accomplished by irradiation with a UV lamp and/or stining with a potassium permanganate alkaline solution, ninhydrin or ceric ammonium molibdate solution. Flash column chromatography was performed according to the method of Still and co-workers[185] using Chromagel 60 ACC (40-63 μm) silica gel. Proton NMR spectra were recorded on a spectrometer operating at 400.16 MHz. Proton chemical shift are reported in ppm (δ) with the solvent reference relative to TMS employed as the internal standard. The following abbreviations are used to describe spin multiplicity s = singlet, d = doublet, t = triplet, q = quartet, m = multiplet, bs = broad signal, dd = doublet of doublet, ddd = doublet of doublet of doublet, ddt = doublet of doublet of triplet. Carbon NMR spectra were recordered on a spectrometer operating at 100.63 MHz, with complete proton decoupling. Carbon chemical shift are reported in ppm (. δ) relative to the TMS with the respective solvent resonance as the internal standard. ESI-MS spectra were recordered on the ion trap spectrometer Finnigan LCQ Advantage.

RP-HPLC purification and analysis (University of Milan)

The HPLC purifications were performed using a Dionex Ultimate 3000 instrument equipped with a Dionex RS Variable Wavelenght Detector (column: Atlantis® Prep T3 OBD™ 5 μm 19 × 100 mm). The crude reaction mixture was dissolved in water and the solution was filtered (polypropylene, 0.45 μm, 13 mm ɵ, PK/100) and injected in the HPLC, affording purified products. Purity analysis for each compound was carried out on a Dionex Ultimate 3000 instrument equipped with a Dionex RS Variable Wavelenght Detector (column: Atlantis® Prep T3 OBD™ 5 μm 19 × 100 mm). 1 mg of purified product was dissolved in 1 mL of H_2O and was injected using the same gradient used in the purification step. The analysis of the integrals and the relative percentage of purity was performed with the software Cromeleon 6.80 SR11 Build 3161.

RP-HPLC purification and analysis (University of Cologne)

Purity determination by analytical HPLC and qualitative analysis by HPLC-ESI-MS

In order to determine peptides identity and final purity, the samples were analysed by HPLC-ESI-MS (LC-MS) for qualitative analysis and by RP-HPLC for purity determination. The flowrate used was 0.6 mL/min, detection took place at 220 nm. Samples were diluted 1:1 in H_2O/ACN/additive

(90:10:0.1, v/v/v). The chromatography was performed on a linear gradient ranging from 10% - 60% B in A (A: 0.1% additive in H_2O, B: 0.1% additive in ACN) over 15 min, or 10% - 50% B in A over 25 min. Purity of a sample was determined by calculating the ratio of the product peak area to the total peptide peak area in the UV-chromatogram. For qualitative analysis, FA was used as an additive. For purity determination, TFA was used instead, as it results in a more constant background in the UV-chromatogram.

Peptide purification by preparative RP-HPLC: the crude peptide mixture was dissolved in H_2O/ACN/TFA (90:10:0.1, v/v/v) and centrifuged at 14,000 X g for 5 min. The supernatant was transferred into a glass reservoir for sample injection. The chromatography was performed on a linear gradient of B in A (A: 0.1% TFA in H_2O, B: 0.08% TFA in ACN) which varied depending on the composition of the crude peptide mixture. The flowrate used was 6 mL/min on the full-preparative column for samples containing more than 6 mg of peptide, or 1.5 mL/min on the semi-preparative column for samples containing 6 mg of peptide or less. Peptides were detected at 220 nm and 250 nm and peptide containing fractions were collected accordingly. Afterwards, ACN was removed from the fractions by an evaporation and concentration system and then used in a 1:1 dilution with H_2O/ACN/FA (90:10:0.1, v/v/v) or H_2O/ACN/TFA (90:10:0.1, v/v/v) for qualitative analysis or purity determination by HPLC-ESI-MS, respectively. Fractions containing pure samples of the desired peptide were combined and freeze-dried.

General procedures for solution phase synthesis

GP1. GENERAL PROCEDURE 1 FOR Boc DEPROTECTION REACTIONS:

To a solution of the *N*-Boc-protected amino acid or peptide in CH_2Cl_2 (0.13 M) was added half a volume of TFA. The reaction mixture was stirred for 2h at r.t. and then concentrated at reduced pressure. The excess of TFA was azeotropically removed from the residue with toluene. Diethyl ether was added and the resulting suspension was evaporated under reduced pressure to afford the corresponding TFA salt.

GP2. GENERAL PROCEDURE 2 FOR COUPLING REACTIONS:

To a solution of the *N*-protected amino acid in DMF, under nitrogen atmosphere and at 0°C, HATU (1.3 eq), HOAt (1.3 eq) and DIPEA (4 eq) were added successively. After 30 min, a solution of the *N*-deprotected TFA salt of the peptide in DMF was added and the reaction mixture was stirred at 0°C for 1h and at r.t. overnight. The mixture was afterwards diluted with EtOAc and consecutively washed with 1M $KHSO_4$ (2x), acqueous $NaHCO_3$ (2x) and brine (2x), and dried over Na_2SO_4. Volatiles were evaporated under reduced pressure to afford the crude product.

GP3. GENERAL PROCEDURE 3 FOR Cbz AND OBn HYDROGENOLYTIC CLEAVAGE:

Protected compound (1 eq.) was dissolved in a mixture of THF/H_2O (1:1) and Pd/C 10% (0.1 eq.) was added. The reaction mixtures were subjected to three vacuum/hydrogen cycles and then left stirring overnight at room temperature under 1 bar of hydrogen. The mixture was filtered through Celite, and the cake was washed thoroughly with THF/H_2O (1:1). The filtrate was concentrated and dried to give the crude product as white solid (100%).

GP4. GENERAL PROCEDURE 4 FOR MACROLACTAMIZATION:

HATU (4 eq.), HOAt (4 eq.) and DIPEA (6 eq.) were added successively to a 1.4 Mm solution of deprotected linear compound (1 eq.) in DMF, under a nitrogen atmosphere and at 0°C. After stirring the reaction mixture at 0°C for 1 h, it was allowed to reach room temperature and stirred overnight. DMF was then removed under reduced pressure. The mixture was afterwards diluted with EtOAc and consecutively washed with 1M $KHSO_4$ (2x), acqueous $NaHCO_3$ (2x) and brine (2x) and dried over Na_2SO_4. Volatiles were evaporated under reduced pressure to afford the crude product.

GP5. GENERAL PROCEDURE 5 FOR Mtr AND OtBu ESTER REMOVAL:

Protected macrolactam was treated for 2h with TFA, in the presence of ion scavengers: thioanisole (5%), EDT (3%), anisole (2%). After TFA removal under reduced pressure, the residue was dissolved in a 1:1 mixture of diisopropyl ether/water. Phases were separated, and the aqueous layer

was washed several times with diisopropyl ether. The aqueous phase was concentrated under reduced pressure to give the crude product, which was purified by HPLC.

GP6. GENERAL PROCEDURE FOR Fmoc DEPROTECTION REACTIONS:

A 0.01 M solution of the *N*-Fmoc-protected compound (1 eq) in DMF was cooled to 0 °C under nitrogen atmosphere. Piperidine (5 eq) was added and the reaction was stirred at room temperature for 2 h. The mixture was diluted with EtOAc (20x volume of DMF) and washed twice with a saturated aqueous solution of $NaHCO_3$. The organic phase was dried over Na_2SO_4 and concentrated at rotavapor. CH_2Cl_2 was added to the residue and evaporated to afford a yellow solid. The crude was left under vacuum for 2 h and then used as starting material for the subsequent step.

Preparation of hydrazoic acid

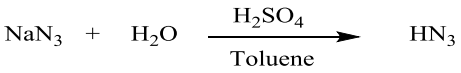

In a three-necked flask, NaN_3 (3 g) was dissolved in H_2O (3 mL). Once completely dissolved, toluene (20 mL) was added and the reaction mixture was cooled to 0°C under vigorous stirring. Concentrated H_2SO_4 (1.2 mL) was added extremely slowly, so that the solution temperature did not exceed 10°C. the reaction was stirred for 1 h at 0°C and then filtered on cotton wool. The residue was washed twice with toluene. The toluene solution was titrated by diluting 1 ml in distilled water (50 mL), and addition of NaOH (0.1 M) with phenolphthalein as indicator.

General procedures for SPPS

All Nα-Fmoc protected amino acids were obtained from Iris Biotech (Marktredwitz, Germany), resins additionally from Merckmillipore (Darmstadt, Germany). Chemicals and one-use articles were produced by Alfa Aesar (Karlsruhe, Germany), Applichem (Darmstadt, Germany), Merck (Darmstadt, Germany), Roth (Karlsruhe, Germany), Sigma Aldrich (Taufkirchen, Germany), Sarstedt (Numbrecht, Germany) and Fischer Scientific (Pittsburgh, USA).
Standard *N*α-Fmoc protected amino acids were side-chain protected as follows: Trt (cysteine, histidine, asparagine, glutamine), O*t*Bu (aspartate, glutamate), Boc (lysine) and Pbf (arginine).

Automated solid phase peptide synthesis (SPPS)

Full length peptides or parts of them were synthesized by a SPPS robot (Syro II peptide synthesizer, MultiSynTech , Witten, Germany).following the protocol given beneath. The required amino acid solutions and reagents were prepared manually. All amino acids were dissolved in DMF except for Phe, for which NMP was used.
A Fmoc strategy was selected and the following resin were used: Fmoc-Rink amide resin (200 mesh, loading: 0.48 mmol/g, Iris Biotech), H-L-Lys(Boc)-2CT (200-400 mesh, loading: 0.74mmol/g, Iris Biotech), 2-Chlorotrityl chloride Resin (100-200 mesh, 1.6 mmol/g, Iris Biotech). The resin was swollen for 10 min in 800 µL DMF and the solvent was then removed. For the first Fmoc-group cleavage, 400 µL 40% piperidine in DMF were added to the resin (3 min reaction time), followed by removal of solvent and subsequent addition of 200 µL DMF and 200 µL 40% piperidine in DMF (10 min reaction time). The resin was then washed 4 times with each 600 µL of DMF. Subsequent Fmoc deprotections were performed by incubating the resin in 400 µL of 40% piperidine in DMF for 3 min, removal of the solvent, addition of 200 µL DMF and 200 µL 40% piperidine in DMF and letting the reaction take place for 10 min. Lastly, the resin was washed 4 times each with 800 µL of DMF.
Amino acids were coupled by adding 300 µL of the respective *N*α-Fmoc-protected amino acid solution (corresponding to 8 eq.) to the resin, as well as 50 µL of 2.4 M Oxyma in DMF and 50 µL of 2.4 M DIC in DMF. The resin was incubated for 40 min with the reaction mixture, washed with 800 µL of DMF and the coupling step was repeated once again in order to increase the reaction yield. The Fmoc-group of the newly attached amino acid was then cleaved, and the next amino acids coupled in the same manner by the robot until the desired sequence was synthesized. Finally, the resin was washed manually 5x with DMF, DCM, MeOH, and Et_2O, respectively, and dried in a vacuum concentrator for 10 min.

GP7 GENERAL PROCEDURE FOR MANUAL RESIN LOADING

The first *C*-terminal amino acid was coupled manually to the resin. For this, the resin was first swollen in DMF for at least 15 min while shaking at r.t., followed by removal of the solution. 5 eq. of the Fmoc-protected amino acid to be coupled and 5 eq. of Oxyma were dissolved separately in 200 µL DMF each and then mixed together. 5 eq. of DIC were added to the solution which was then loaded onto the resin. The reaction was performed o.n. (r.t., shaking). The next day, the resin

was washed 5x with DMF, DCM, MeOH, and Et_2O, respectively, and dried in a vacuum concentrator for 10 min. If the loading was not sufficient, it was repeated.

- **Determination of resin loading**

The amount of loaded resin can be quantified by cleaving the Fmoc-group of the previously attached amino acid. The quantitative analysis is done by quantitative detection at 300 nm of the dibenzofulvene formed. For this, a defined amount of loaded resin was treated with 500 µL of 30% piperidine in DMF and shaken for 30 min at RT in order to cleave the Fmoc-group. After centrifugation, 250 µL of the supernatant were transferred into a new micro tube and mixed with 1.5 mL of 30% piperidine in DMF. This solution was diluted 1:10 with 30% piperidine in DMF and its absorption at 300 nm measured in a quartz cuvette. The resin loading L_{300} in mmol/g was calculated as follows.

$$L_{300} = \frac{E_{300}}{\varepsilon \cdot l} \cdot \frac{2 \cdot V}{m_{resin}}$$

L_{300} [mmol/g]: absorption at 300 nm; ε [$M^{-1}cm^{-1}$]: molar attenuation coefficient of dibenzofulvene (= 7800 M-1 cm-1); l [cm]: light path length; m_{resin} [g]: mass of loaded resin; V[mL]: 1.75 mL.

- **Resin capping**

In order to prevent unreacted groups on the resin from coupling with amino acids during the ongoing peptide synthesis, these groups were blocked by acetylation. The resin was then swollen in 1 mL DCM for 15 min and the solvent was removed. 400 µL DCM, 50 µL DIPEA and 50 µL acetic anhydride were added to the resin. After 15 min of shaking at RT, the solvent was removed; the resin was washed 5x with DCM, MeOH, and Et_2O, respectively. Finally, the resin was dried for 10 min in a vacuum concentrator.

GP8. GENERAL PROCEDURE 8 FOR KAISER TEST:

Kaiser test is used to detect free amino groups and thus to verify the completion of a coupling or deprotection reaction. A few resin beads were transferred into a 1.5 mL micro tube and treated with one drop of solution I (1.0 g Ninhydrin in 20 mL EtOH), solution II (80 g phenol in 20 mL EtOH), and solution III (0.4 mL aqueous KCN-solution (1 mM) in 20 mL pyridine), respectively. The mixture was incubated at 95 °C for 5 min in a thermomixer. The test was defined positive if the solution turned blue, indicating free amino groups. A yellow solution indicated a negative result with no free amino groups. A mixture without resin and a mixture with ethanolamine were used as negative and positive controls, respectively.

GP9. GENERAL PROCEDURE 9 FOR MANUAL AMINO ACID COUPLING:

In some cases, amino acids were coupled manually to ensure the maximum coupling yield. For this, the resin was first swollen in DMF for at least 15 min while shaking, followed by removal of the

solution. The Fmoc-group of the *N*-terminal amino acid was removed by treating the resin with 500 µL 30% piperidine in DMF for 20 min (r.t., shaking). Afterwards, the resin was washed 5x with DMF and incubated again for 20 min in 500 µL 30% piperidine in DMF (r.t., shaking), followed by five washing steps with DMF. Next, 5 eq. of the Fmoc-protected amino acid to be coupled and 5 eq. of Oxyma were dissolved separately in 200 µL DMF each and then mixed together. 5 eq. of DIC were added to the solution which was then loaded onto the resin. After 2 h, the resin was washed 5x with DMF and the coupling step was repeated once again. Finally, the resin was washed 5x with DMF, DCM, MeOH, and Et_2O and dried in a vacuum concentrator for 10 min. If the Kaiser test returned a positive result, the procedure was repeated once again under more vigorous conditions by replacing Oxyma and DIC with the stronger reagent HATU and DIPEA. 2 eq. of the Fmoc-protected amino acid to be coupled and 2 eq. of HATU were dissolved separately in 150 µL DMF each, mixed together and loaded onto the swollen resin. Then, 2 eq. of DIPEA were directly added to the reaction mixture and set aside for 2 h (r.t., shaking). The resin was then washed and dried.

GP10. GENERAL PROCEDURE 10 FOR Fmoc DEPROTECTION

After swelling the resin in DMF for 10 min, two deprotection steps were carried out treating the resin with 30% piperidine in DMF (2x20 min). The resin was then washed with DMF and the vial was empty.

GP11. GENERAL PROCEDURE 11 FOR SAMPLE CLEAVAGE

To verify the success of the coupling reactions and to analyse the resulting product, a sample cleavage was performed for every peptide and critical synthesis step.
Few beeds of dry resin were transferred into a micro tube and the peptides cleaved off the resin by incubating the resin for 3 h (r.t., shaking) with 100 µL of a mixture of H2O/TIS/TFA (2.5:2.5:95, v/v/v). To precipitate the peptides, 1 mL ice-cold Et_2O was added to the reaction and the mixture was stored for a minimum of 1 h or o/n at -20 °C. The peptides were washed five times by centrifugation at 10,000 x g and 4 °C for 5 min. After every centrifugation step, the supernatant was removed, and the precipitate resuspended in 1 mL ice-cold Et_2O. After drying the precipitate in a vacuum concentrator for 15 min, it was dissolved in 100 µL H_2O/*t*BuOH (2:1, v/v). After a final centrifugation step at 13,300 x g for 5 min, the supernatant was diluted 1:1 in H_2O/ACN/FA (90:10:0.1, v/v/v) for qualitative analysis by HPLC-ESI-MS (LC-MS).

GP12. GENERAL PROCEDURE 12 FOR FULL CLEAVAGE

The dry resin was incubated for 3 h (r.t., shaking) with 1 mL of a mixture of H_2O/TIS/TFA (2.5:2.5:95, v/v/v). To precipitate the peptides, the reaction mixture was added to 10 mL of ice-cold Et_2O and stored at -20 °C for a minimum of 1 h or o/n. The peptides were then washed five times by centrifugation at 5000 x g and 4 °C for 5 min. After every centrifugation step, the supernatant was removed, and the precipitate resuspended in 10 mL ice-cold Et_2O. After drying the precipitate in a vacuum concentrator for 15 min, it was dissolved in H_2O/*t*BuOH (composition between 2:1 v/v

and 1:2 v/v, depending on the nature of the peptide). The peptide solution was diluted 1:1 in H_2O/ACN/FA (90:10:0.1, v/v/v) for qualitative analysis by HPLC-ESI-MS (LC-MS). Finally, the peptides were freeze-dried.

GP13. GENERAL PROCEDURE 13 FOR DKPs' COUPLING

The resin was swollen in DMF for at least 15 min while shaking, followed by removal of the solution. Next, 3 eq. of the **97** or **98** were weighted and 3 eq. of Oxyma were dissolved separately in 200 µL DMF each and then mixed together. 3 eq. of DIC were added to the solution which was then loaded onto the resin. After 2 h, the resin was washed 5x with DMF and the coupling step was repeated once again. Finally, the resin was washed 5x with DMF, DCM, MeOH, and Et_2O and dried in a vacuum concentrator for 10 min. If the Kaiser test returned a positive result, the procedure was repeated once again under more vigorous conditions by replacing Oxyma and DIC with (the stronger reagent) HATU and DIPEA. 2 eq. of the Fmoc-protected amino acid to be coupled and 2 eq. of HATU were dissolved separately in 150 µL DMF each, mixed together and loaded onto the swollen resin. Then, 2 eq. of DIPEA were directly added to the reaction mixture and set aside for 2 h (r.t., shaking). The resin was then washed and dried.

GP14. GENERAL PROCEDURE 14 FOR AZIDE REDUCTION ON RESIN

The resin was then treated with DTT (2M) in 500µL of DCM. Then DIPEA (1M, 87µL) was added. The reaction was left shaking at room temperature for 2h. Then the solvent was sucked away and the resin was washed. washed 5x with DMF, DCM, MeOH, and Et_2O and dried in a vacuum concentrator for 10 min.

GP15. GENERAL PROCEDURE 15 FOR CLEAVAGE FROM THE RESIN

The resin was treated with a solution of DCM:TFE:Acetic acid 8:1:1 for 2 h at r.t. to cleave the peptide from the resin without touching the protecting group on the side chains. The solution was put in a vial and the resin was washed two times more with the same solution DCM:TFE:Acetic acid 8:1:1 v/v/v. The solvent was evaporated under reduced pressure and the crude was subjected directly to the next step.

GP16. GENERAL PROCEDURE 16 FOR FULL DEPROTECTION OF THE PEPTIDE

The crude was treated with TFA/phenol/water/Thioanisole/EDT 82,5:5:5:5:2,5 v/v/v/v/v (1ml in tot). The reaction was kept under stirring at r.t. for 3h. Then the mixture was put in a vial containing 10 ml of cold Et_2O in order to precipitate the peptide. The mixture was centrifuged and washed five times with cold Et_2O. The crude was then dissolved in H2O:ACN 90:10 v/v + 0.1% TFA and purified on semipreparative RP-HPLC.

Synthesis of integrin ligand-based conjugates

All the intermediates **19**-**28** (**Scheme 1**), **29**-**32** (**Scheme 2**) required for the synthesis of *c*[DKPf3-RGD]-CH_2NH_2 **15** were synthesized according to literature procedure and their analytical data were in agreement with those already published.[51,52]

14-Azido-3,6,9,12-tetraoxatetradecanoic acid -NHS ester (33)

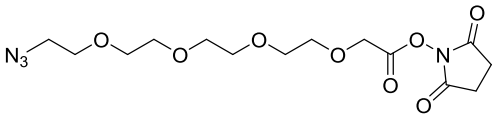

Chemical Formula: $C_{14}H_{22}N_4O_8$
Molecular Weight: 374,35

100 µL (0.5 mmol, 1 eq.) of a 0.5 M solution of 14-azido-3,6,9,12-tetraoxatetradecanoic acid (0.5 M in *tert*-butyl methyl ether) were diluted in 100 µL of dry DCM under argon and cooled to 0°C. EDC HCl (12,5 mg, 0.065 mmol, 1.3 eq.) and NHS (7.5 mg, 0.065 mmol, 1.3 eq.) were sequentially added to the solution and the reaction mixture was stirred overnight at r.t. The mixture was diluted in 10 mL of DCM and the organic phase was washed with water (3 × 3 mL), dried over $MgSO_4$, filtrated and concentrated under reduced pressure to give the product as a transparent oil (18.2 mg, 97% yield). The crude product was used in next step without further modifications.
Rf= 0.35 (DCM/MeOH 95:5); ^{1}H NMR (400 MHz, $CDCl_3$): δ 4.52 (s, 2H), 3.81–3.79 (m, 2H), 3.68-3.65 (m, 12H), 3.39 (t, *J* = 5.0 Hz, 2H), 2.85 (s, 4H).

C[DKPf3-RGD]-PEG-4-N_3 (34)

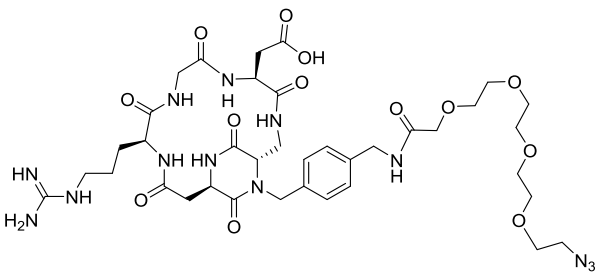

Chemical Formula: $C_{37}H_{55}N_{13}O_{13}$
Molecular Weight: 889,93

To a solution of compound **33** (8 mg, 21 µmol, 2 eq.) in 400 µL of ACN was added *c*[DKPf3-RGD]-CH_2NH_2 (**15**) (9 mg, 11 µmol, 1 eq.) dissolved in 600 µL of PBS pH 7. The pH was adjusted to 7.4 with a solution of NaOH 0.2 M and the reaction was stirred overnight at room temperature. The mixture was filtered into a 3 mL vial, centrifuged and purified by preparative HPLC (gradient: from 90% (H_2O + 0.1% TFA)/10% ACN) to 55% (H_2O + 0.1 % TFA)/45% ACN in 16 mins, t_R product = 8.8 min). The collected fraction was concentrated under reduced pressure and freeze-dried from 1:1 water/ACN to afford the product as a white solid (5.3 mg, 40% yield).

^{1}H NMR (400 MHz, D_2O) δ 7.36 (dd, *J* = 15.6, 8.4 Hz, 4H), 5.13 (d, *J* = 15.5 Hz, 1H), 4.91 (m, 1H), 4.63 – 4.59 (m, 1H), 4.50 (s, 3H), 4.32 – 4.17 (m, 3H), 4.15 (s, 2H), 4.12 (d, *J* = 4.1 Hz, 1H), 3.99 (dd, *J* = 14.8, 4.6 Hz, 1H), 3.83 (d, *J* = 17.2 Hz, 1H), 3.77 (m, 2H), 3.75 – 3.70 (m, 3H), 3.69 – 3.58 (m, 10H), 3.47 – 3.42 (m, 2H), 3.27 (m, 3H), 3.09 (dd, *J* = 15.1, 3.8 Hz, 1H), 2.69 (dd, *J* = 15.1, 11.6 Hz, 1H), 2.05 – 2.01 (m, 1H), 1.88 – 1.83 (m, 1H), 1.74 – 1.63 (m, 2H); MS (ESI+): *m/z* calculated for $[C_{37}H_{56}N_{13}O_{13}]^+$= 889.93 $[M + H]^+$, found: 890.50.

Dipeptide PropargylGly-Aoa (37)

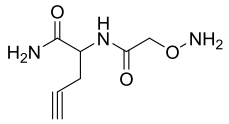

Chemical Formula: $C_7H_{11}N_3O_3$
Molecular Weight: 185,18

Dipeptide **37** was synthesized on solid phase using Fmoc-Rink amide resin (100-200 mesh, loading: 0.48mmol/g, 144µmol scale). Rink amide resin was deprotected from Fmoc group (**GP10**). Fmoc-PropargylGly-OH was manually coupled to the resin (**GP7**). After Fmoc-deprotection (**GP10**), $(Boc)_2$Aoa-OH was coupled to the resin (**GP9**). The dipeptide was finally cleaved from the resin (**GP12**). The solid was solubilized in water:tBuOH 1:3 (v/v) and lyophilized. The crude was then purified on preparative RP-HPLC (10-60 ACN in 45 min). The desired product was obtained as a white foam (7.8 mg, 30%). MS (ESI+): *m/z* calculated for $[C_7H_{12}N_3O_3]^+$= 185.18 $[M + H]^+$, found: 186.09.

PropargylGly-Aoa=Dau (38)

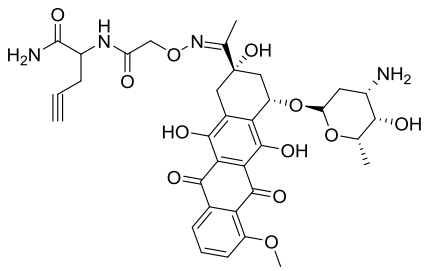

Chemical Formula: $C_{34}H_{38}N_4O_{12}$
Molecular Weight: 694,69

The dipeptide propargylglycine-Aoa **37** (7.8 mg) was dissolved in 0.2M NH_4OAc at a peptide concentration of 10 mg/mL. Then Dau was added in 30% excess (26 mg). The reaction mixture was stirred at r.t. for 12h. The reaction was check in LC-MS and the mixture was injected directly in HPLC and purified (20-70 ACN in 45 min). The final product **38** was obtained as a red solid (18,6 mg, 64%). MS (ESI+): *m/z* calculated for $[C_{34}H_{39}N_4O_{12}]^+$= 695.69 $[M + H]^+$, found: 696.07.(SPK8)

c[DKPf3-RGD]-PEG-4-PropargylGly-Aoa-Dau (16)

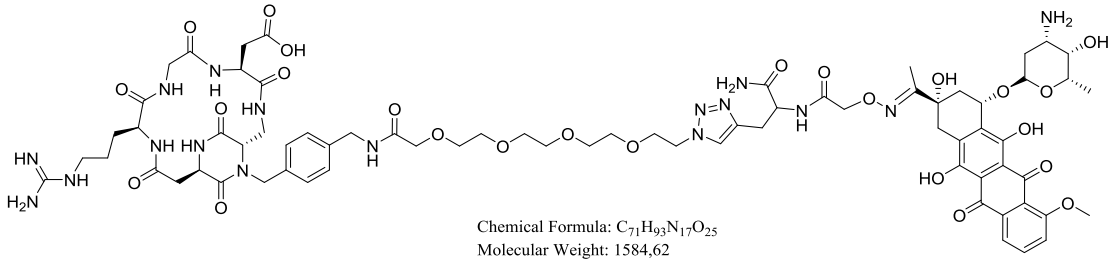

Chemical Formula: $C_{71}H_{93}N_{17}O_{25}$
Molecular Weight: 1584,62

Compound **38** (1.3 eq, 2.74 mg, 3.95 mmol) was weighted in a schlenk tube and dissolved in tBuOH:water 1:1 (v/v) at 10 mM concentration under argon atmosphere. Compound **34** (1 eq, 2.7 mg, 3.04 mmol) was added. $CuSO_4$ *$5H_2O$ (0.5 eq, 0.38mg, 1.52mmol) and sodium ascorbate (0.6 eq, 0.35 mg, 1.8 mmol) were added to the reaction, as solutions in water. The reaction was left under stirring for 2h. The reaction mixture was then injected directly in HPLC and purified (20-70 ACN in 45 min). 2.7 mg (56%) of the final conjugate were obtained. MS (ESI+): *m/z* calculated for $[C_{71}H_{94}N_{17}O_{25}]^+$= 1584.62 $[M + H]^+$, found: 1585.99.

Peptide Aoa-GFLG-COOH (41)

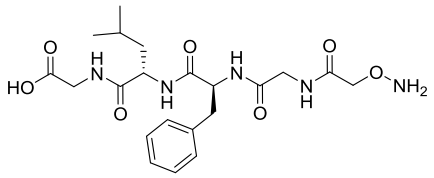

Chemical Formula: $C_{21}H_{31}N_5O_7$
Molecular Weight: 465,51

Pentapeptide **41** was synthesized on solid phase using 2-chlorotrytil chloride resin preloaded with Gly (H-Gly-2CT Resin, 100-200 mesh, 0.87mmol/g, 130 mmol scale) by automated multiple solid-phase peptide synthesis. $(Boc)_2$Aoa-OH was manually coupled to the resin (**GP9**). The peptide was finally cleaved from the resin in the presence of Boc-Aoa (5 eq) (**GP12**). The solid was solubilized in water:tBuOH 1:3 (v/v) and lyophilized. The crude was then purified on preparative RP-HPLC (50-90 ACN in 45 min). the desired product was obtained as a white foam (49 mg, 80%). MS (ESI+): *m/z* calculated for $[C_{21}H_{32}N_5O_7]^+$= 465.51 $[M + H]^+$, found: 466.26.

Peptide >=Aoa-GFLG-COOH (42)

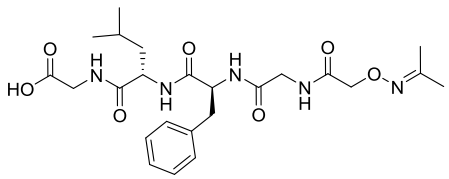

Chemical Formula: $C_{24}H_{35}N_5O_7$
Molecular Weight: 505,57

The aminooxyacetylated peptide **41** (30 mg, 64 µmol) was dissolved in aceton (1.8 mL) and let react for 30 min. Aceton was then evaporated until dryness to obtain white crystals (30 mg, 92%). Peptide **42** was used in the next step without purification. MS (ESI+): *m/z* calculated for $[C_{24}H_{36}N_5O_7]^+$= 505.57 $[M + H]^+$, found: 505.99.

>=Aoa-GFLG-PEG-4-*c*[DKPf3-RGD] (43)

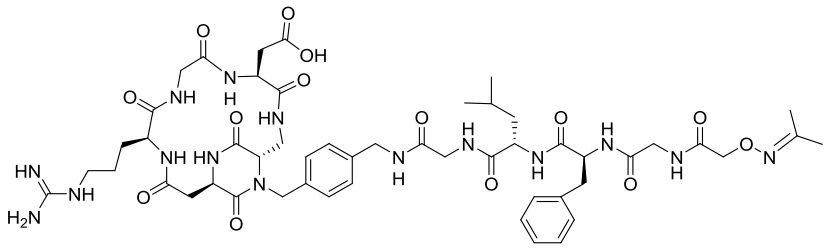

Chemical Formula: $C_{51}H_{71}N_{15}O_{14}$
Molecular Weight: 1118,22

Peptide **42** (12.68 µmol, 6.4 mg, 2 eq) and BOP (11.41 µmol, 5.05 mg, 1.8 eq) were dissolved in DMF. DIPEA (34.2 µmol, 6µL, 5.4 eq) was added and the linker was pre-activated for 20 min. Compound **15** (6.34 µmol, 4 mg, 1 eq) was dissolved in DMF and it was added to the mixture of the activated linker. The reaction was left under stirring for 3h. The reaction mixture was then directly purified by HPLC and purified (20-70 ACN in 30 min) and the product (2 mg) was obtained in 28% yield. MS (ESI+): *m/z* calculated for $[C_{51}H_{72}N_{15}O_{14}]^+$= 1118.22 $[M + H]^+$, found: 1117.94.

Aoa-GFLG-PEG-4-*c*[DKPf3-RGD] (44)

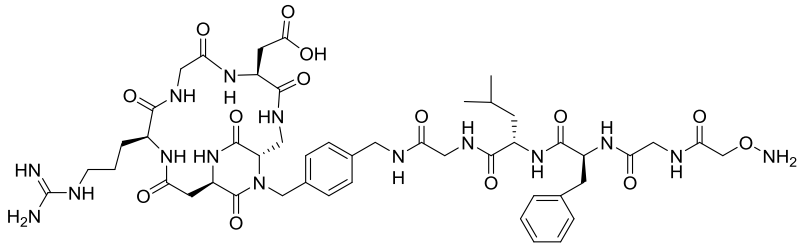

Chemical Formula: $C_{48}H_{67}N_{15}O_{14}$
Molecular Weight: 1078,16

Peptide **43** (1.79 µmol, 2 mg, 1 eq) was dissolved in 1M CH_3ONH_2 HCl containing NH_4OAc-buffer (0.2 M, pH 5) (20 eq). The reaction mixture was then directly purified by semi-preparative HPLC and the fraction containing the product was lyofilized (1.7 mg, 88%). MS (ESI+): *m/z* calculated for $[C_{51}H_{72}N_{15}O_{14}]^+$= 1078.16 $[M + H]^+$, found: 1077.92.

-Dau-Aoa-GFLG-PEG-4-*c*[DKPf3-RGD] (17)

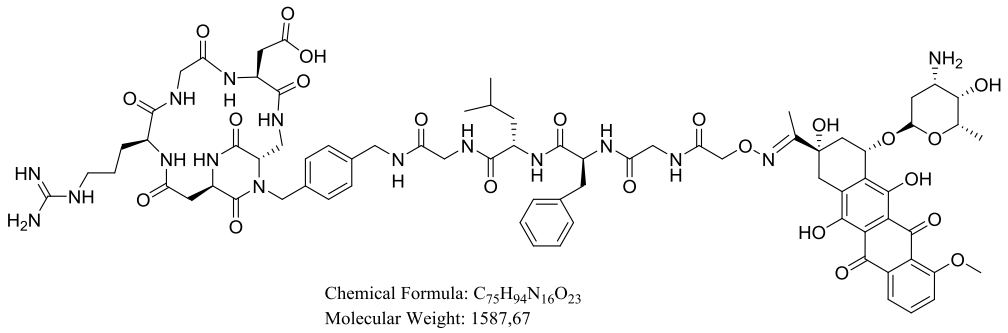

Chemical Formula: $C_{75}H_{94}N_{16}O_{23}$
Molecular Weight: 1587,67

The deprotected aminooxyacetylated peptide (2.7 mg, 2.5 μmol) **44** was dissolved in 0.2M NH_4OAc (pH 5) at a peptide concentration of 10 mg/mL. Dau (1.7 mg) was added in 30% excess; the reaction mixture was stirred for 24h at r.t. The mixture was directly purified by HPLC (20-70 ACN in 30 min), yielding the conjugate **17** (2.4 mg, 50%). MS (ESI+): *m/z* calculated for $[C_{75}H_{95}N_{16}O_{23}]^+ = 1587.67$ $[M + H]^+$, found: 1588.16.

sC18 branched peptide for Ptx conjugate (45)

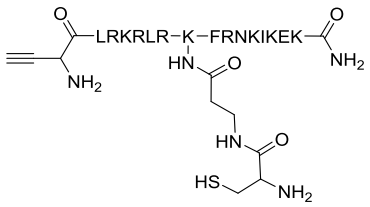

Chemical Formula: $C_{101}H_{181}N_{37}O_{21}S$
Molecular Weight: 2281,86

Peptide **45** was synthesized on solid phase using Fmo-Rink amide resin (200 mesh, loading: 0.48 mmol/g, 0.015 mmol scale) by automated multiple solid-phase peptide synthesis. Once the first part of the peptide ^{114}FRNKIKEK^{121} was ready, Fmoc-L-Lys(DDe)-OH was manually coupled (**GP9**). The peptide was then subjected to elongation on the roborter for the remaining amino acids ^{105}LRKRLR^{112}. The last amino acid, Fmoc-Pra-OH (propargylglycine), was manually coupled (**GP9**). After its Fmoc deprotection (**GP10**), Boc protection was accomplished (10 eq Boc_2O, 1 eq DIPEA in DCM, 2h, shaking, r.t.). Resin was washed with 5xDMF, 5xDCM, 5xMeOH, 5x Et_2O. Dde group on the Lys_{13} was cleaved treating the resin with 1 mL 3% (v/v) hydrazine in DMF and shaked for ten minutes at r.t.. The cleavage was repeated ten times. Resin was washed with 5xDMF, 5xDCM, 5xMeOH, 5xEt_2O. Fmoc-βAla-OH was manually coupled (**GP9**). After Fmoc deprotection of βAla (**GP10**), Fmoc-L-Cys(Trt)-OH was coupled (**GP9**). Fmoc deprotection of Cys (**GP10**) followed. The peptide was finally cleaved from the resin (**GP12**).
The solid was solubilized in water and lyophilized. The crude was then purified on preparative RP-HPLC (20-70 ACN in 45 min). Peptide **45** was obtained as a white foam (21.5 mg, 63%, purity >95%). HRMS (ESI+): *m/z* calculated for $[C_{101}H_{182}N_{37}O_{21}S]^+ = 2281.4032$ $[M + H]^+$, found: 2281.4097.

2'-(4-Nitrophenoxycarbonyl) paclitaxel (46)

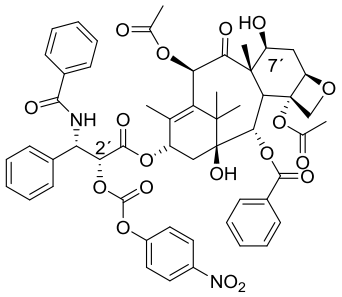

Chemical Formula: $C_{54}H_{54}N_2O_{18}$
Molecular Weight: 1019,02

Paclitaxel (100 mg, 0.12 mmol, 1 eq) was dissolved in dry DCM (1 mL) under a nitrogen atmosphere. Pyridine (28 µL, 0.351 mmol, 3 eq) was added dropwise and the mixture was cooled to -20°C. A solution of 4-nitrophenylchloroformate (36 mg, 0.175 mmol, 1.5 eq) in dry. DCM (1 mL) was then added under a nitrogen atmosphere. The mixture was warmed to 0°C and stirred until no unreacted paclitaxel was observable by TLC (approximately 4h; eluent:4:6 hexane/AcOEt). The mixture was then diluted with AcOEt (100 mL) and washed with a 1M aqueous solution of $KHSO_4$ (10 mL) and brine (10 mL). The organic phase was dried over Na_2SO_4 and concentrated. The crude residue was purified by flash column chromatography (Hexane/EtOAc 3:7) to afford 2'-(4-nitrophenoxycarbonyl)paclitaxel (**46**) as a white foam (68 mg, 55%yield).

Rf=0.26 (4:6 hexane/AcOEt); ^{1}H NMR (400 MHz, CD_2Cl_2) δ = 8.25 (d, *J*=9.1, 2H), 8.16 (d, *J*=7.3, 2H), 7.76 (d, *J*=7.3, 2H), 7.63 (m, 1H), 7.57 - 7.51 (m, 3H), 7.57 – 7.39 (m, 10H), 7.36 (d, *J*=9.1, 2H), 6.94 (d, *J*=9.3, 1H), 6.31 (m, 1H), 6.27 (s, 1H), 6.08 (dd, *J*=9.3, 2.6, 1H), 5.67 (d, *J*=7.1, 1H), 5.55 (d, *J*=2.8, 1H), 4.98 (d, *J*=8.2, 1H), 4.42 (m, 1H), 4.31 (d, *J*=8.4, 1H), 4.17 (d, *J*=8.4, 1H), 3.81 (d, *J*=7.0, 1H), 2.53 (m, 1H), 2.48 (s, 3H), 2.43 (m, 1H), 2.24 (dd, J=15.5, 8.9 Hz, 1H), 2.20 (s, 3H), 1.94 (s, 1H), 1.91 (d, *J*=5.3, 2H), 1.82 (m, 1H), 1.70 (s, 1H), 1.64 (s, 3H), 1.24 (s, 3H), 1.13 (s, 3H). ^{13}C NMR (101 MHz, CD_2Cl_2): d=204.1, 171.7, 170.4, 167.9, 167.5, 167.2, 155.4, 152.2, 146.2, 142.7, 136.8, 134.1, 134.0, 133.5, 132.5, 130.6, 129.8, 129.6, 129.1, 127.5, 127.1, 125.8, 122.1, 84.7, 81.4, 79.5, 78.4, 76.7, 75.9, 75.5, 73.0, 72.5, 58.8, 53.2, 46.1, 43.6, 36.1, 36.0, 27.0, 23.1, 22.4, 21.0, 15.0, 9.8 ppm.

Fmoc-Val-Ala-OH (48)

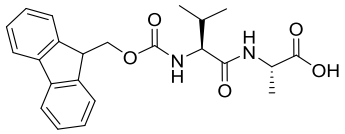

Chemical Formula: $C_{23}H_{26}N_2O_5$
Molecular Weight: 410,47

Commercially available Fmoc-(L)-Val-OH (5.0 g, 14.9 mmol, 1 eq) was dissolved in THF and NHS (1.7 g, 14.9 mmol, 1 eq) was added as a solution in THF. DCC (3.0 g, 14.9 mmol, 1 eq) was added at 0°C. the mixture was allowed to reach room temperature and stirred for 16 hours. Then, the solid DCU byproduct was removed by filtration and washed with THF. The filtrate was dried under reduced pressure, and the resulting glassy solid was used without further purification.
The glassy solid obtained was then solubilized in DME (dimethoxyethane, 40 ml) and added to a solution of H-Ala-OH (1.4 g, 15.6 mmol, 1.05 eq) and saturated $NaHCO_3$ in water (40 ml). THF (22 ml) was added to aid solubility and the mixture was stirred at room temperature for 3 days. Acqueous citric acid (15%, 100 mL) was added, and the mixture was extracted twice with 10% iso-

propanol/EtOAc. The organic layer was washed twice with water and then the solvents were evaporated to afford a white solid. The white solid was dried in vacuo and then triturated and sonicated with ether. The product (**48**) was collected by filtration, and it was obtained as white solid. (5.7 g, 93%).

^{1}H NMR (400 MHz, DMSO-d_6) δ = 12.50 (bs, 1H), 8.20 (d, J=6.9, 1H), 7.89 (d, J=7.5, 2H), 7.75 (t, J=6.5, 2H), 7.44-7.31 (m, 5H), 4.40-4.10 (m, 4H), 3.90 (t, J=7.1, 1H), 2.06-1.85 (m, 1H), 1.27 (d, J=7.3, 3H), 0.97-0.75 (m, 6H). ^{13}C-NMR (100 MHz, DMSO-d_6) δ = 173.96, 170.95, 156.06, 143.90, 143.79, 140.69, 127.63, 127.04, 125.39, 120.08, 65.67, 59.77, 47.47, 46.67, 30.50, 19.12, 18.20, 17.10.

Fmoc-Val-Ala-PAB-OH (49)

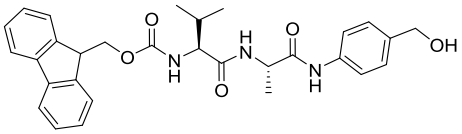

Chemical Formula: $C_{30}H_{33}N_3O_5$
Molecular Weight: 515,61

Under nitrogen atmosphere a suspension of dipeptide **48** (913 mg, 2.2 mmol, 1 eq), 4-aminobenzyl alcohol (328 mg, 2.66 mmol, 1.2 eq) and EEDQ (823 mg, 3.33 mmol, 1.5 eq) in DCM was treated with MeOH until a clear solution was obtained. The mixture was stirred for 3 days in the dark at r.t. A precipitated was formed. After filtration, the precipitated was washed with diethyl ether and sonicated. The procedure was repeated twice and the solid was dried in high vacuo (898 mg, 78%).

R_f = 0,13 (EtOAc/Hexane 6:4); ^{1}H NMR (400 MHz, DMSO-d_6) δ = 9.91 (s, 1H), 8.15 (d, J=7.0, 1H), 7.89 (d, J=7.5, 2H), 7.74 (t, J=6.9, 1H), 7.53 (d, J=7.2, 2H), 7.44-7.39 (m, 3H), 7.32 (t, J=7.4, 3H), 7.23 (d, J=8.3, 2H), 5.09 (t, J=5.6, 1H), 4.43 (d, J=5.5, 3H), 4.20-4.30 (m, 3H), 3.91 (t, J=7.9, 1H), 2.02-1.97 (m, 1H), 1.31 (d, J=7.0, 3H), 0.90-0.85 (m, 6H). ^{13}C-NMR (100 MHz, DMSO-d_6) δ = 170.97, 170.86, 156.13, 143.86, 143.77, 140.69, 140.67, 137.53, 137.41, 127.62, 127.04, 126.88, 125.34, 120.08, 118.85, 65.68, 62.56, 59.98, 48.95, 46.66, 30.36, 19.16, 18.22, 18.11.

Fmoc-Val-Ala-PAB-PNP (50)

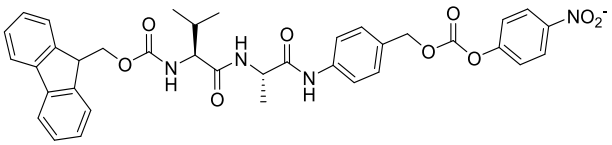

Chemical Formula: $C_{37}H_{36}N_4O_9$
Molecular Weight: 680,71

Compound **49** (680 mg, 1.32 mmol, 1 eq) was dissolved in dry THF under nitrogen atmosphere. Pyridine (266 µL, 3.3 mmol, 2.5 eq) was added and the solution was cooled at 0°C. 4-Nitrophenylchloroformate (400 mg, 1.98 mmol, 1.5 eq) was added and the stirred reaction became milky. The mixture was allowed to reach r.t. and stirred for 3 h. The reaction was then diluted with EtOAc (200 mL) and washed with 1M $KHSO_4$ (2 x 50 mL) and brine (1 x 50 mL). The organic

phase was dried over Na_2SO_4 and concentrated. The crude residue was purified by flash chromatography (charged as solid load, gradient: Hexane/EtOAc 4/6) to afford the product (**50**) as a white solid (594 mg, 66%).

R_f = 0,5 (EtOAc/Hexane 6:4); ^{1}H NMR (400 MHz, DMSO-d_6) δ = 10.07 (s, 1H), 8.31 (d, J=9.0, 2H), 8.19 (d, J=6.8, 1H), 7.89 (d, J=7.5, 2H), 7.74 (t, J=7.2, 2H), 7.64 (d, J=8.4, 2H), 7.57 (d, J=9.0, 2H), 7.42-7.40 (m, 4H), 7.32 (t, J=7.3, 2H), 5.24 (s, 2H), 4.48-4.37 (m, 1H), 4.35-4.16 (m, 3H), 3.95-3.89 (m, 1H), 2.02-1.97 (m, 1H), 1.31 (d, J=7.0, 3H), 0.90-0.85 (m, 6H). ^{13}C-NMR (100 MHz, DMSO-d_6) δ = 171.22, 171.04, 156.13, 155.28, 151.93, 145.17, 143.86, 140.69, 139.42, 129.46, 129.28, 127.62, 127.04, 126.17, 125.38, 122.59, 1120.07, 119.03, 70.23, 65.67, 59.94, 49.05, 46.66, 30.37, 19.15, 18.24, 17.99.

Fmoc-Val-Ala-PAB-PNP-(N-Boc)-dimethylethylendiamine (51)

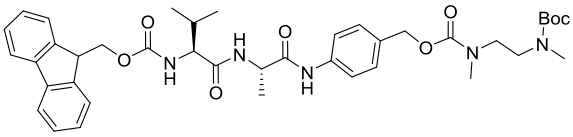

Chemical Formula: $C_{40}H_{51}N_5O_8$
Molecular Weight: 729,88

Fmoc-Val-Ala-PAB-PNP (**50**) (594 mg, 0.87 mmol, 1 eq) was dissolved in dry THF under nitrogen atmosphere. A solution of the Boc N-N-dimethylethilendiamine (328 mg, 1.74 mmol, 2 eq) and DIPEA (380 µL, 2.18 mmol, 2.5 eq) in dry THF was added at 0°C. the mixture was stirred overnight at r.t. The solvent was removed by rotary evaporation. EtOAc was then added and the solution was washed with 1M aqueous $KHSO_4$ (2x) and a saturate aqueous solution of $NaHCO_3$ (2x). the organic phase was dried over Na_2SO_4 and concentrated. The crude residue was purified by flash chromatography (Hexane:EtOAc 3:7) to afford the product (475 mg, 74%).

R_f = 0,36 (EtOAc/Hexane 7:3); ^{1}H NMR (400 MHz, CD_3OD) δ = 7.78 (d, J=7.5, 2H), 7.64 (m, 2H), 7.57 (m, 2H), 7.38 (t, J=7.4, 2H), 7.31-7.28 (m, 4H), 5.04 (s, 2H), 4.50 (q, J=7.0, 1H), 4.40-4.36 (m, 2H), 4.21 (t, J=6.7 1H),3.95 (d, J=6.8), 3.41-3.35 (m, 4H), 2.93 (s,rotamers A+B, 3H), 2.84 (s, rotamr A, 3H), 2.73 (s, rotamer B, 3H), 2.12-2.04 (m, 1H), 1.43 (m, 3H) 1.41 (s, 9H), 0.98-0.94 (m, 6H). ^{13}C-NMR (100 MHz, CD_3OD) δ = 174.10, 172.94, 158.85, 145.33, 145.17, 142.60, 139.67, 139.54, 133.63, 130.00, 129.66, 128.78, 128.18, 126.20, 121.17, 120.93, 68.24, 67.99, 62.26, 51.02, 48.45, 48.00, 47.65, 31.86, 28.69, 19.69, 18.66, 17.99.

Glutaric anhydride-Val-Ala-PAB-PNP-(N-Boc)-dimethyl ethylendiamine (52)

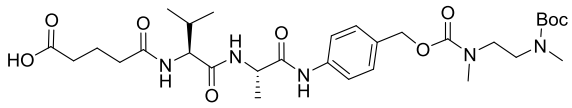

Chemical Formula: $C_{30}H_{47}N_5O_9$
Molecular Weight: 621,73

The N-Fmoc protected peptide (**51**) (470 mg, 0.644 mmol, 1 eq) was dissolved in dry DMF (0.1M) under nitrogen atmosphere. Piperidine (318 µL, 3.22 mmol, 5 eq) was added and the reaction was stirred for 2h at r.t. the mixture was then diluted with EtOAc (20x DMF volume) and washed twice with saturated $NaHCO_3$; the organic phase was dried over anhydrous Na_2SO_4 and concentrated under reduced pressure. A yellowish solid was obtained after adding DCM and evaporating. The crude free amine so obtained was dissolved in dry DMF (8 mL) and cooled to 0°C under N_2. Glutaric anhydride (184 mg, 1.61 mmol, 2.5 eq), DMAP (20 mg, 0.161 mmol, 0.25 eq) and DIPEA (420 µL, 2.41 mmol, 3.75 eq) were added. The mixture was allowed to reach r.t. and stirred overnight. The reaction was then diluted with EtOAc and washed with $KHSO_4$ and brine. The organic phase was dried and concentrated. The crude was then purified by flash chromatography on silica gel (from 100% DCM to DCM/MeOH 9:1+0.1% acetic acid), affording the final compound (**52**) in 89% yield.

R_f = 0,32 (DCM/MeOH 95:5+0.1% acetic acid); ^{1}H NMR (400 MHz, CD_3OD) δ = 7.59 (s, 2H), 7.33-7.31 (m, 2H), 5.05 (s, 2H), 4.51-4.45 (m, 1H), 4.18 (d, J=7.1, 1H), 3.42-3.31 (m, 4H), 2.94 (s, rotamers A+B, 3H), 2.85 (s, rotamer A, 3H), 2.75 (s, rotamer B, 3H), 2.37-2.31 (m, 4H), 2.14-2.05 (m, 1H), 1.94-1.87 (m, 2H) 1.42 (s, 12H), 1.06-0.89 (m, 6H). ^{13}C-NMR (100 MHz, CD_3OD) δ = 177.46, 175.85, 173.70, 173.03, 158.04, 157.97, 139.70, 139.56, 133.83, 133.65, 130.00, 129.68, 121.16, 81.20, 80.90, 68.26, 67.97, 60.39, 51.08, 47.96, 47.66, 35.8, 35.58, 35.29, 35.18, 34.63, 34.5, 31.73, 28.69, 22.35, 19.71, 18.72, 17.95.

Maleimide-Glutaric anhydride-Val-Ala-PAB-PNP-(N-Boc)-dimethyl ethylendiamine (53)

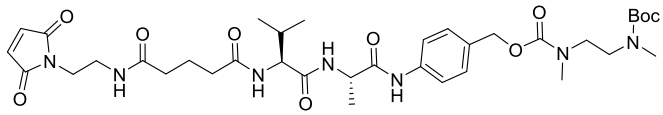

Chemical Formula: $C_{36}H_{53}N_7O_{10}$
Molecular Weight: 743,86

Compound **52** (50 mg, 0.080 mmol, 1 eq) was dissolved in dry DCM/DMF 1mL:200µL. DIC (18.5µL, 1.12 mmol, 1.5 eq), NHS (13 mg, 0.112 mmol, 1.4 eq) were added and the reaction was stirred o.n. A solution of N-(2-aminoethyl)maleimide-TFA salt in dry DMF (500 µL) and DIPEA (38 µL, 0.40 mmol, 5 eq) was added to the previous solution. The reaction was stirred for 2h. After the removal of DMF, the reaction mixture was purified by flash column chromatography (DCM/MeOH from 97:3 to 9:1) affording compound **1.27** in moderate yield (33 mg, 55%).

R_f = 0,45 (DCM/MeOH 9:1); ^{1}H NMR (400 MHz, CD_3OD) δ = 7.59 (m, 2H), 7.32 (m, 2H), 6.79 (s, 2H), 5.49 (s, 1H), 4.48 (q, *J*=6.9, 1H), 4.21–4.19 (m, 1H), 3.66–3.57 (m, 3H), 3.42 – 3.33 (m, 6H), 2.94 (s, rotamers A+B, 3H), 2.85 (s, rotamer A, 3H), 2.75 (s, rotamer B, 3H), 2.32 – 2.27 (m,

3H), 2.16–2.11 (m, 3H), 1.91–1.82 (m, 2H), 1.45–1.42 (m, 12H), 0.99 (t, *J*=7.4, 6H).^{13}C NMR (100 MHz, CD_3OD) δ = 179.81, 177.48, 175.80, 175.02, 173.71, 173.01, 172.61, 139.66, 139.56, 133.83, 133.67, 130.00, 129.68, 121.16, 81.20, 80.90, 68.20, 67.93, 60.38, 51.08, 47.96, 47.66, 38.90, 38.45, 38.11, 35.76, 35.29, 35.18, 34.63, 34.50, 31.76, 28.69, 22.86, 19.73, 18.68, 18.02. MS (ESI+): *m/z* calculated for $[C_{36}H_{54}N_7O_{10}]^+$= 744.86 $[M + H]^+$, found: 745.09.

Synthesis of peptidomimetics inhibitors of Cadherins

All the intermediates **71**, **72** and **73** required for the synthesis of peptidomimetic **59** were synthesized according to literature procedure and their analytical data were in agreement with those already published.[155]
COOH-DKP3-NHBoc (**82**) was synthesized as previously reported by our group and the its analytical data, together with those of its intermediates (**77**-**81**), were in in agreement with data already published.[52]

N-indole (Mtr)-3-carboxaldehyde (64)

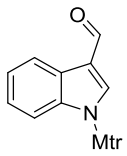

Chemical Formula: $C_{19}H_{19}NO_4S$
Molecular Weight: 357,42

To a solution of indole-3-carbaldehyde (1 g, 7 mmol, 1 eq) in dry THF (30 mL), DIPEA (3.6 mL, 20.7 mmol, 3 eq) and 4-methoxy-2,3,6-trimethylbenzenesulfonyl chloride (Mtr-Cl, 1.72 g, 7 mmol, 1 eq) were added at 0°C. The mixture was stirred for 1h at 0°C, then at room temperature for 48h. The crude was purified by flash chromatography on silica gel eluting EtOAc:Hexane 4:6 v/v to afford the product as a brown foam (540 mg, 44%).

R_f = 0,8 (EtOAc/Hexane 7:3); ^{1}H-NMR(400 MHz, $CDCl_3$) δ = 10.11 (s, 1H), 8.29 (d, 1H), 8.26 (s, 1H), 7.33 (m, 1H), 7,27 (m, 2H), 6.68 (s, 1H), 3.88 (s, 3H), 2.75 (s, 3H), 2.35 (s, 3H), 2.07 (s, 3H); ^{13}C-NMR (100 MHz, $CDCl_3$) δ 185.37, 161.13, 140.63, 140.21, 136.62, 135.31, 126.43, 126.29, 125.94, 125.87, 124.58, 122.55, 120.45, 112.66, 112.33, 55.69, 24.28, 17.36, 11.98. MS (ESI) *m/z* calcd for $[C_{19}H_{19}NO_4SNa]^+$: 380.09; found: 380.16 $[M+Na]^+$.

(*S*)-*N*-indolyl (Mtr) serine methyl ester (65)

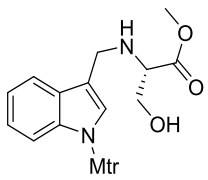

Chemical Formula: $C_{23}H_{28}N_2O_6S$
Molecular Weight: 460,55

To a solution of indole-3-carbaldehyde-Mtr protected (**63**) (1.39 g, 3.89 mmol, 1 eq) in dry THF (54 mL),L-Ser-OMe (605 mg, 3,89 mmol, 1 eq), $NaBH(OAc)_3$ (1.15 g, 5.45 mmol, 1.4 eq) and acetic acid (213 µL, 3.89 mmol, 1 eq) were added. The mixture was stirred for 18h at r.t. and then it

was diluted with EtOAc (80 mL) and washed with a saturated solution of $NaHCO_3$. Organic phases were reunited, dried over Na_2SO_4 anhydrous, filtered and evaporated under reduced pressure. The crude was purified by flash chromatography on silica gel eluting EtOAc:Hexane 1:1 to afford the product as a yellow oil (1.15 g, 64%).

R_f = 0,1 (EtOAc/Hexane 1:1); ^{1}H NMR (400 MHz, $CDCl_3$) δ = 7.67 (d, J=6.5, 1H), 7.55 (s, 1H), 7.35 (d, J=7.1, 1H), 7.25 – 7.19 (m, 2H), 6.66 (s, 1H), 4.12 (d, J=7.5, 1H), 3.95 (d, J=13.5, 1H), 3.88 (s, 3H), 3.86 – 3.84 (m, 1H), 3.77 (s, 3H), 3.70 – 3.66 (m 1H), 3.68 (dd, J=10.9, 6.2, 2H), 3.53 (dd, J=6.0, 4.5, 1H), 2.96 (s, 1H), 2.74 (s, 3H), 2.36 (s, 3H), 2.08 (s, 3H); ^{13}C-NMR (100 MHz, $CDCl_3$) δ = 172.76, 160.53, 140.20, 140.08, 135.28, 129.31, 127.87, 125.81, 124.49, 122.66, 119.66, 116.79, 112.71, 112.41, 62.28, 61.73, 60.38, 55.60, 52.35, 42.82, 24.27, 17.39, 11.95.

MS (ESI) *m/z* calcd for $[C_{23}H_{28}N_2O_6SNa]^+$: 483.16; found: 483.16 $[M+Na]^+$.

Isopeptide (66)

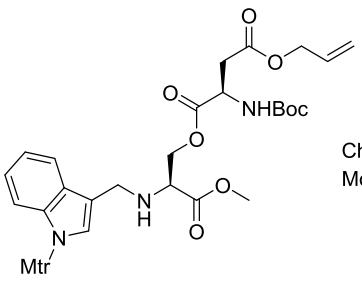

Chemical Formula: $C_{35}H_{45}N_3O_{11}S$
Molecular Weight: 715,82

(*S*)-*N*-indolyl (Mtr) serine methyl ester **65** (1.15 g, 2.50 mmol, 1 eq) was coupled with (R)-*N*-(*tert*-butoxycarbonyl) aspartic acid β-allyl ester **20** (0.888 g, 3.25 mmol, 1.3 eq.) according to general procedure **GP2**. The residue was purified by flash chromatography on silica gel eluting (Hex/EtOAc 6:4) to afford the desired products as a white foam in 80% yield.

R_f = 0,7 (EtOAc/Hexane 6:4); ^{1}H NMR (400 MHz, $CDCl_3$) δ = 7.69 (d, *J*=7.0, 1H),7.52 (s, 1H), 7.33 (d, *J*=7.4, 1H), 7.22-7.15 (m, 2H), 6.64 (s, 1H), 5.87 (ddt, *J*=16.3, 10.9, 5.6, 1H), 5.50 (d, *J*=7.8, 1H), 5.25 (dd, *J*=28.8, 13.8, 2H), 4.58 (d, *J*=5.5, 1H), 4.54 (t, *J*=6.1, 2H), 4.47 (dd, *J*=11.0, 4.4, 1H), 4.35 (dd, *J*=10.9, 4.5, 1H), 4.05 (d, *J*=13.4, 1H), 3.89 (d, *J*=13.8, 1H),3.85 (s,3H), 3.74 (s,3H), 3.60 (t, *J*=4.1, 1H), 2.97 (d, *J*=16.7, 1H), 2.84 (dd, *J*=16.9, 4.5, 1H), 2.72 (s, 3H), 2.34 (s, 3H), 2.06 (s, 3H), 1.43 (s, 9H). ^{13}C-NMR (100 MHz, $CDCl_3$) δ = 172.24, 170.60, 170.46, 160.45, 155.25, 140.12, 140.00, 135.29, 131.69, 129.45, 127,96, 125.71, 124.51, 124.33, 122.47, 120.01, 118.54, 117.59, 112.55, 112.39, 80.10, 65.85, 65.63, 58.97, 55.57, 52.24, 49.94, 42.88, 36.71, 28.26, 24.24, 17.37, 11.93. MS (ESI) *m/z* calcd for $[C_{35}H_{45}N_3O_{11}SNa]^+$: 738.82; found: 738.23 $[M+Na]^+$.

OH-DKP3-Indolyl-COOAllyl (67)

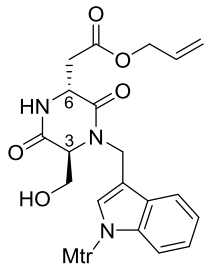

Chemical Formula: $C_{29}H_{33}N_3O_8S$
Molecular Weight: 583,66

Compound **66** (486 mg, 0.694 mmol, 1 eq) was deprotected according to the general procedure **GP1**. The TFA salt was then solved in isopropanol (10 mL) and DIPEA (480 µL, 2.78 mmol, 4 eq) was added at r.t., monitoring the formation of the DKP by TLC (EtOAc). The crude was then concentrated under reduced pressure and purified by flash chromatography on silica gel eluting hexane:EtOAc (from 1:9 to 100% EtOAc). The product was recovered as a white foam (80%).

R_f = 0,3 (EtOAc); ^{1}H NMR (400 MHz, $CDCl_3$) δ = 7.74 (s, 1H), 7.65 – 7.63 (m, 1H), 7.49 (s, 1H), 7.35 – 7.31 (m, 1H), 7.26 – 7.23 (m, 2H), 6.71 (s, 1H), 5.97 – 5.87 (ddd, *J* = 16.2, 11.0, 5.8 Hz, 1H), 5.55 (d, *J* = 15.2 Hz, 1H), 5.38 – 5.25 (m, 2H), 4.76 – 4.73 (dd, *J* = 7.7, 3.8 Hz, 1H), 4.68 – 4.58 (m, 2H), 4.33 (d, *J* = 15.2 Hz, 1H), 4.13 – 4.01 (m, 2H), 3.94 (s, 1H), 3.93 (s, 3H), 3.31 (dd, *J* = 17.4, 3.8 Hz, 1H), 2.90 (dd, *J* = 17.4, 8.0 Hz, 1H), 2.77 (s, 3H), 2.40 (s, 3H), 2.13 (s, 3H). ^{13}C-NMR (100 MHz, $CDCl_3$) δ = 170.73, 168.29, 166.56, 160.56, 140.04, 140.05, 135.08, 131.59, 128.81, 127.64,126.23, 125.88, 124.73, 122.93, 119.83, 118.72, 113.60, 112.52, 112.45, 65.80, 61.37, 61.13, 55.60, 51.21, 38.30, 37.12, 24.20, 17.36, 11.96. MS (ESI) *m/z* calcd for $[C_{29}H_{33}N_3O_8SNa]^+$: 606.20; found: 606.68 $[M+Na]^+$.

N_3-DKP3-Indolyl-COOAllyl (68)

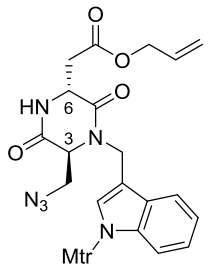

Chemical Formula: $C_{29}H_{32}N_6O_7S$
Molecular Weight: 608,67

Compound **67** (790 mg, 1.35 mmol, 1 eq) was solved in dry DCM: dry Toluene 1:2, under nitrogen atmosphere. The solution was cooled at -20°C and PPh_3 (460 mg, 1.75 mmol, 1.3 eq) was added. HN_3 (1.35 M in toluene, 8.7 mmol, 6.5 mL, 6.5 eq,) and DIAD (372 µL, 1.89 mmol, 1.4 eq) were sequentially added dropwise under these conditions. The reaction was stirred at -20°C for 5h. the

mixture was purified and charged directly on silica gel column chromatography eluting hexane/EtOAc 3:7. The desired product was obtained as white foam (88%).

R_f = 0,46 (EtOAc/Hexane 8:2); ^{1}H NMR (400 MHz, $CDCl_3$) δ = 7.63 (s, 1H), 7.54-7.51 (m, 1H), 7.28-7.26 (m, 1H), 7.21-7.19 (m, 2H), 6.68 (s, 1H), 6,64 (s, 1H), 5.93-5.84 (m, 1H), 5.44 (d, J = 15.2, 1H), 5.35-5.25 (m, 2H), 4.62-4.53 (m, 3H), 4.26 (d, J = 15.2, 1H), 3.97 (t, 1H), 3.91 (dd, J = 12.7-3.2, 1H), 3.86 (s, 3H), 3.77 (dd, J = 12.7-3.2, 1H), 3.35 (dd, J = 17.5-3.1, 1H), 2.76 (dd, J = 20.2-10.6, 1H), 2.70 (s, 3H), 2.32 (s, 3H), 2.06 (s, 3H). ^{13}C-NMR (100 MHz, $CDCl_3$) δ = 171.12, 166.34, 166.09, 161.12, 140.60, 140.52, 135.63, 131.87, 128.98, 128.01, 126.65, 126.43, 125.45, 123.56, 120.08, 119.63, 113.67, 113.18, 112.95, 66.45, 58.69, 56.08, 52.15, 51.59, 39.05, 37.88, 24.71, 17.83, 12.44. MS (ESI) *m/z* calcd for $[C_{29}H_{33}N_6O_7SNa]^+$: 609.67; found: 609.82 $[M+H]^+$

NHBoc-DKP3-Indolyl-COOAllyl (69)

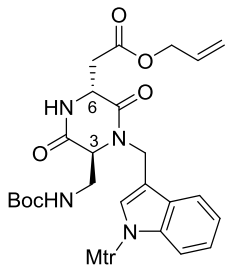

Chemical Formula: $C_{34}H_{42}N_4O_9S$
Molecular Weight: 682,79

Compound **68** (365 mg, 0.6 mmol, 1 eq) was dissolved in dry THF (11 mL) under nitrogen atmosphere and the solution was cooled at -20°C. Me_3P (1.2 mL, 1.2 mmol, 2 eq) and Boc-ON (295 mg, 1.2 mmol, 2 eq) were sequentially added under these conditions. The mixture was allowed to reach room temperature and it was stirred for 5h. After dilution with DCM the reaction mixture was sequentially washed with distilled water (3 x 30 mL) and brine (2 x 30 mL). The organic phase was then dried over Na_2SO_4 anhydrous and volatiles were removed under reduced pressure; then under vacuum. The crude was purified by flash chromatography on silica gel eluting hexane:EtOAc (from 4:6). The product was recovered as a yellowish foam (70%).

R_f = 0,6 (EtOAc/Hexane 8:2); ^{1}H NMR (400 MHz, $CDCl_3$) δ = 7.67 (s, 1H), 7.55-7.53 (m, 1H), 7.28-7.27 (m, 1H), 7.20-7.17 (m, 2H), 6.73 (s, 1H), 6,62 (s, 1H), 5.92-5.82 (m, 1H), 5.64 (d, J = 15.2, 1H), 5.33-5.24 (m, 2H), 5.01 (s, 1H), 4.62 (m, 2H), 4.46 (d, J = 7.9, 1H), 4.29 (d,J = 15.1, 1H), 3.88 (s, 1H), 3.85 (s, 3H), 3.81-3.78 (m, 1H), 3.56 (d, J =11.7, 1H), 3.37 (dd, J =17.5-2.1, 1H), 2.69 (m, 4H), 2.32 (s, 3H), 2.05 (s, 3H), 1.46 (s, 9H). ^{13}C-NMR (100 MHz, $CDCl_3$) δ = 171.02, 166.93, 164.70, 160.70, 147.91, 140.23, 140.21, 135.30, 131.52, 128.97, 127.83, 126.82, 126.04, 124.90, 123.09, 119.93, 119.29, 113.58, 112.78, 112.58, 66.15, 58.75, 55.74, 51.18, 40.97, 38.21, 38.19, 28.48, 24.39, 17.51, 12.12. MS (ESI) *m/z* calcd for $[C_{34}H_{43}N_8O_9S]^+$: 683.79; found: 684.11 $[M+H]^+$.

NHBoc-DKP3-Indolyl-COOH (70)

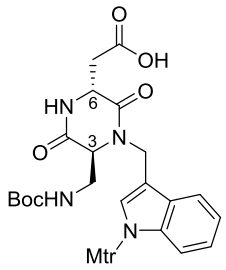

Chemical Formula: $C_{31}H_{38}N_4O_9S$
Molecular Weight: 642,72

Compound **69** (438 mg, 0.641 mmol, 1 eq) was dissolved in dry DCM (13 mL) and it was cooled to 0°C. Pyrrolidine (101 µL, 1.22 mmol, 1.9 eq), Ph_3P (67 mg, 0.256 mmol, 0.4 eq) and $[Pd(Ph_3P)_4]$ (52 mg, 0.045 mmol, 0.07 eq) were sequentially added at 0°C. The reaction mixture was stirred under these conditions. After 1h, the mixture was diluted with EtOAc and acidified with a 1M $KHSO_4$; the phases were separated and the aqueous phase was extracted twice with EtOAc. Organic layers were reunited, dried over Na_2SO_4 anhydrous and volatiles were removed under reduced pressure, then under vacuum. The crude was taken up with DCM and filtered over a small pad of celite. The product (402 mg, quantitative) was used without further purification.

NHBoc-DKP3-Indolyl-Ile-NH*t*Bu (75)

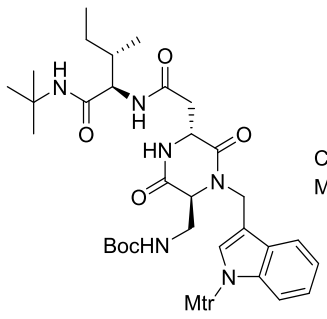

Chemical Formula: $C_{41}H_{58}N_6O_9S$
Molecular Weight: 811,01

Compound **73** (65 mg, 0.229 mmol, 1 eq) was deprotected according the general procedure **GP1**. The corresponding TFA salt (**74**) was then coupled with **70** (147 mg, 0.229 mmol, 1 eq) according to general procedure **GP2**. The residue was purified by flash chromatography on silica gel (DCM/MeOH 97:3) to afford the desired product (**75**) as a yellowish foam (115 mg, 62%).

R_f = 0,2 (DCM/MeOH 95:5); ^{1}H-NMR (400 MHz, $CDCl_3$) δ = 7.69 (s, 1H), 7.59 – 7.42 (m, 2H), 7.24 (s, 1H), 7.19 – 7.08 (m, 2H), 7.06 (br s, 1H), 6.62 (s, 1H), 6.28 (br s, 1H), 5.71 (br s, 1H), 5.60 (d, J=15.2, 1H), 4.49 (d, J=6.4, 1H), 4.29 (d, J=15.2, 1H), 4.17 (t, J=8.1, 1H), 3.81 (m, 5H), 3.49 (m, 1H), 3.23 (d, J=14.4, 1H), 2.68 (s, 4H), 2.37 (s, 1H), 2.31 (s, 3H), 2.03 (s, 3H), 1.73 (s, 1H), 1.42 (s, 10H), 1.28 (s, 9H), 1.10 (m, 1H), 0.96 – 0.70 (m, 6H).^{13}C-NMR (100 MHz, $CDCl_3$) δ =

170.63, 170.18, 167.30, 165.73, 160.66, 156.39, 140.22, 140.14, 135.23, 129.04, 127.86, 126.79, 125.99, 124.79, 123.12, 119.90, 113.65, 112.66, 112.56, 58.82, 58.41, 55.71, 51.66, 40.80, 38.75, 38.28, 37.69, 28.73, 28.50, 25.30, 24.34, 17.51, 15.37, 12.10, 11.24. MS (ESI) *m/z* calcd for $[C_{41}H_{59}N6O_9S]^+$: 812.01; found: 812.93 $[M+Na]^+$.

Boc-Asp(O*t*Bu)-DKP3-Indolyl-Ile-NH*t*Bu (76)

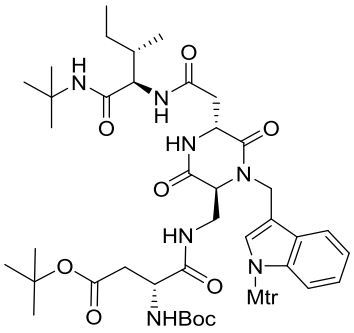

Chemical Formula: $C_{49}H_{71}N_7O_{12}S$
Molecular Weight: 982,20

Compound **75** (35 mg, 0.043 mmol, 1 eq) was deprotected according the general procedure **GP1**. The corresponding TFA salt was then coupled with Boc-L-Asp(O*t*Bu)-OH (109 mg, 0.337 mmol, 3 eq) according to general procedure **GP2**. The residue was purified by flash chromatography on silica gel (DCM:MeOH 95:5) to afford the desired product (**76**) as white foam (29 mg, 67%).

R_f = 0,5 (DCM/MeOH 9:1); ^{1}H NMR (400 MHz, $CDCl_3$) δ = 7.71 (s, 1H), 7.53-7.51 (m, 1H), 7.28-7.26 (m, 1H, overlapping with solvent signal), 7.21-7.17 (m, 2H), 7.05 (br s, 1H), 6.63 (s, 1H), 6.52 (br. s, 1H), 5.77 (br s, 1H), 5.63-5.59 (m, 2H), 4.56 (d, J = 5.6, 1H), 4.42 (s, 1H), 4.31 (d, J = 15.2, 1H), 4.14 (s, 1H), 4.03-4.01 (m, 1H), 3.89 (s, 1H), 3.85 (s, 3H), 3.60 (d, J = 12.0, 1H), 3.18 (d, J = 15.8, 1H), 2.88-2.90 (m, 1H), 2.69 (s, 3H), 2.62-2.56 (m, 2H), 2.32 (s, 3H),2.06 (s, 3H), 1.51-.48 (m, 1H), 1.44 (s, 9H), 1.42 (s, 9H), 1.28 (s, 9H), 1.16-1.11 (m, 2H), 0.92-0.88 (m, 6H). ^{13}C-NMR (100 MHz, $CDCl_3$) δ = 172.16, 170.76, 170.18, 168.25, 165.52, 160.69, 150.79, 147.28, 140.18, 136.36, 129.03, 127.18, 126.04, 124.84, 123.15, 119.85, 113.60, 112.76, 112.59, 58.33, 58.21, 55.75, 38.00, 28.80, 28.44, 28.22, 25.37, 24.40, 23.07, 17.55, 15.43, 12.15, 11.49, 10.44. MS (ESI) *m/z* calcd for $[C_{49}H_{71}N_7O_{12}SNa]^+$: 1004.49; found: 1004.72 $[M+Na]^+$.

NHBoc-DKP3-Gly(OBn) (84)

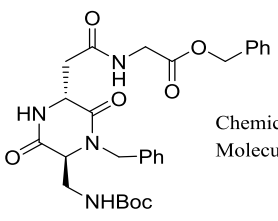

Chemical Formula: $C_{28}H_{34}N_4O_7$
Molecular Weight: 538,60

NHBoc-DKP3-COOH (**82**) (460 mg, 1.17 mmol, 1 eq) was coupled with Gly-OBn HCl (177 mg, 1.41 mmol, 1.2 eq) according to general procedure **GP2**. The residue was purified by flash chromatography on silica gel (DCM/MeOH from 93:7 to 90:10) to afford the desired product as a white foam (580 mg, 93%).

R_f = 0,58 (DCM/MeOH 9:1); ^{1}H NMR (400 MHz, acetone-d_6) δ = 7.81 (t, J=5.4, 1H), 7.43-7.26 (m, 10H), 6.53 (bs 1H), 5.42 (d, J=15.3), 5.18 (s, 2H), 4.52 (m, 1H), 4.11-4.01 (m, 3H), 3.84-3.81 (m, 2H), 3.53-3.50 (m, 1H), 3.18 (dd, J=15.7, 3.5, 1H), 2.69 (dd, J=15.7, 8.8, 1H), 1.42 (s, 9H). ^{13}C-NMR (100 MHz, acetone-d_6) δ = 171.58, 170.46, 167.58, 167.02, 156.90, 137.79, 137.02, 129.48, 129.31, 129.06, 128.95, 128.88, 128.29, 67.13, 60.80, 52.09, 47.78, 41.81, 41.38, 38.50, 28.63. MS (ESI) *m/z* calcd for $[C_{28}H_{34}N_4O_7Na]^+$: 561.6; found: 560.98 $[M+Na]^+$.

Fmoc-Trp(Boc)-DKP3-Gly(OBn) (85)

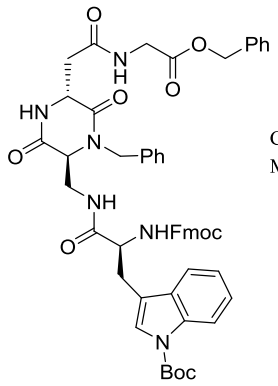

Chemical Formula: $C_{54}H_{54}N_6O_{10}$
Molecular Weight: 947,06

Compound **84** (80 mg, 0.148 mmol, 1 eq) was deprotected according the general procedure **GP1**. The corresponding TFA salt was then coupled with Fmoc-Trp(Boc)-OH (93 mg, 0.177 mmol, 1.2 eq) according to general procedure **GP2**. The residue was purified by flash chromatography on silica gel (DCM:MeOH from 97:3 to 9:1) to afford the desired product as white foam (83 mg, 60%).

R_f = 0,6 (DCM/MeOH 9:1); ^{1}H NMR (400 MHz, acetone-d_6) δ = 8.20 (m, 1H), 8.12 (d, J=7.7, 1H), 7.86 (s, 1H), 7.68-7.70 (m, 5H), 7.55 (t, J=8.31, 2H), 7.39-7.18 (m, 17H), 5.47 (d, J=15.3, 1H), 5.05 (s, 2H), 4.76-4.70 (m, 2H), 4.30-4.24 (m, 1H), 4.20 (d, J=15.3, 1H), 4.13-4.08 (m, 2H), 3.99-3.98 (m, 4H), 3.81-3.79 (m, 1H), 3.42-3.26 (m, 1H), 3.20-3.14 (m, 2H), 2.82 (dd, J=16.0, 7.4, 1H), 2.72 (s, 3H), 1.57 (s, 9H). ^{13}C-NMR (100 MHz, acetone-d_6) δ = 173.61, 171.36, 170.43, 167.73, 167.19, 157.14, 150.18, 144.83, 141.86, 137.41, 136.78, 136.22, 134.80, 134.69, 131.39, 131.19, 131.07, 129.39, 129.18, 128.88, 128.83, 128.34, 128.20, 127.83, 126.20, 126.08, 125.09, 124.97, 123.24, 120.61, 120.07, 115.80, 67.42, 67.06, 60.18, 55.87, 52.00, 47.73, 47.61, 41.74, 40.10, 38.27, 28.34, 28.19. MS (ESI) *m/z* calcd for $[C_{54}H_{54}N_6O_{10}Na]^+$: 970.06; found: 969.66 $[M+Na]^+$.

Cbz-Arg(Mtr)-Trp(Boc)-DKP3-Gly(OBn) (86)

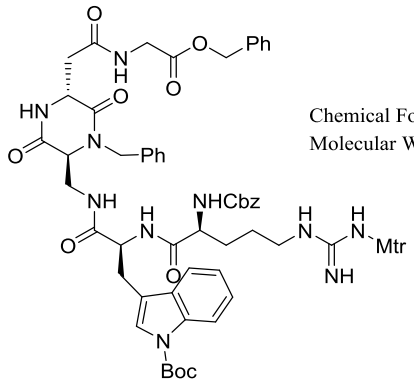

Chemical Formula: $C_{63}H_{74}N_{10}O_{14}S$
Molecular Weight: 1227,40

The N-Fmoc protected peptide **85** (83 mg, 0.0876 mmol, 1 eq) was diluted in dry DMF (876 µL) under nitrogen atmosphere and treated with piperidine (43 µL, 0.438, 5 eq). The mixture was stirred for 2 h. After dilution with EtOAc, the mixture was washed twice with saturated $NaHCO_3$; the organic phase was dried over Na_2SO_4 and concentrated. The product was obtained as a yellowish solid and it was used in the next step without purifications. The N-Fmoc deprotected peptide (83 mg, 0.0876 mmol, 1 eq) was then coupled with Cbz-Arg(Mtr)-OH (65 mg, 0.105 mmol, 1.2 eq) according to general procedure **GP2**. The residue was purified by flash chromatography on silica gel (DCM:MeOH from 95:5 to 9:1) to afford the desired product as white foam (78 mg, 72%).

R_f = 0,5 (DCM/MeOH 9:1); ^{1}H NMR (400 MHz, acetone-d_6) δ = 8.09 (d, J=8.0, 1H), 7.89 (m, 2H), 7.80 (t, J=5.6, 1H), 7.67 (s, 1H), 7.61 (d, J=7.7, 1H), 7.56 (s, 1H), 7.45 – 7.09 (m, 17H), 6.66 (s, 1H), 6.53 (br s, 3H), 5.61 (s, 1H), 5.38 (d, J=15.3, 1H), 5.10 (s, 2H), 5.02 (dd, J=34.2, 12.5, 2H), 4.81 (m, 1H), 4.64 (m, 1H), 4.28 (m, 1H), 4.11 (d, J=15.4, 1H), 4.02 (m, 2H), 3.97 – 3.85 (m, 3H), 3.80 (m, 5H), 3.24 (m, 3H), 3.12 (m, 3H), 2.74 (dd, J=15.9, 7.8, 1H), 2.68 (s, 3H), 2.63 (s, 3H), 2.08 (s, 3H), 1.89 – 1.74 (m, 1H), 1.72 – 1.57 (m, 11H), 1.56 – 1.47 (m, 2H). ^{13}C-NMR (100 MHz, acetone-d_6) δ =. 173.27, 171.67, 170.52, 167.57, 167.31, 158.96, 157.61, 157.11, 150.30, 139.16, 137.96, 137.37, 137.13, 136.92, 136.25, 135.68, 131.33, 129.50, 129.29, 129.19, 128.93, 128.69, 128.63, 128.35, 125.21, 125.08, 124.88, 123.29, 120.03, 117.03, 115.84, 112.51, 67.19, 66.98, 60.21, 55.87, 55.83, 55.31, 54.32, 51.96, 47.70, 43.77, 41.83, 40.18, 38.13, 28.30, 27.88, 26.08, 24.32, 18.73, 13.22. MS (ESI) *m/z* calcd for $[C_{63}H_{74}N_{10}O_{14}SNa]^+$: 1250.40; found: 1248.99 $[M+Na]^+$.

NH_2-Arg(Mtr)-Trp(Boc)-DKP3-Gly-COOH (87)

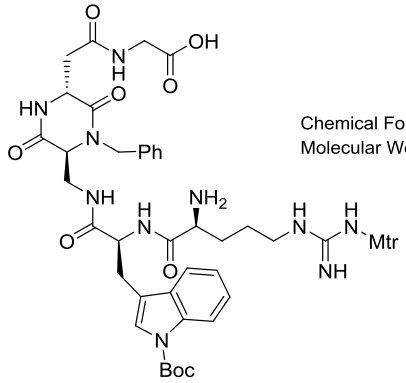

A solution of compound **86** (78 mg, 0.0635 mmol, 1 eq) in THF/H_2O 1:1 v/v (23 mL) was treated with 10% Pd/C (15 mg, 0.0138 mmol, 0.2 eq), and the flask was purged three times with vacuum/H_2. The mixture was stirred at r.t. overnight under H_2 atmosphere, then filtered through a pad of celite and the celite cake was washed thoroughly with THF/H_2O1:1 (v/v). the solvents were removed under vacuum to give the crude product **87** as a yellowish solid (75 mg, quantitative), which was used without further purification.

***C*[Arg(Mtr)-Trp(Boc)-DKP3-Gly] (88)**

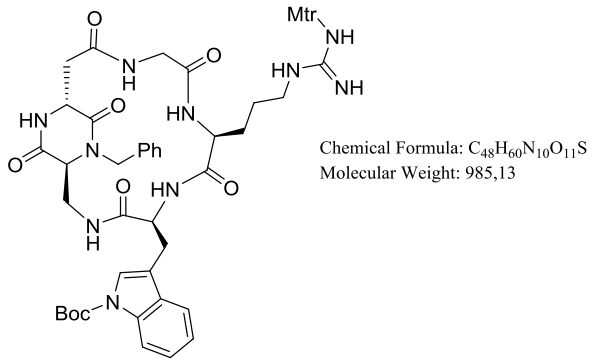

Compound **87** (75 mg, 0.0739 mmol, 1 eq) was cyclized in the presence of HATU (126 mg, 0.332, 4.5 eq), HOAt (45 mg, 0.332, 4.4 eq) and DIPEA (77 µL, 0.443 mmol, 6 eq) under the conditions described in **GP4**. The crude was purified by flash chromatography on silica gel (DCM:MeOH from 95:5) to afford the desired product as white foam (40 mg, 60%).

R_f = 0,3 (DCM/MeOH 9:1); ^{1}H NMR (400 MHz, acetone-d_6) δ = 8.10 (d, J=8.2, 1H), 8.01 (s, 1H), 7.88 (d, J=6.4, 1H), 7.80 (br s, 1H), 7.54 (s, 1H), 7.51 (d, J=7.8, 1H), 7.41 – 7.26 (m, 6H), 7.25 – 7.12 (m, 2H), 6.68 (s, 1H), 6.43 (br s, 1H), 6.33 (br s, 1H), 5.49 (d, J=14.8, 1H), 5.21 (d, J=11.2, 1H), 4.88 - 4.86 (m, 1H), 4.59 – 4.45 (m, 1H), 4.44 – 4.36 (m, 1H), 4.27 (d, J=14.9, 1H), 4.19 (dd, J=13.3, 6.9, 1H), 3.97 (s, 1H), 3.83 (s, 3H), 3.66 – 3.49 (m, 2H), 3.33 – 3.31 (m, 1H), 3.21 – 3.02

(m, 4H), 2.70 (s, 3H), 2.65 (s, 3H), 2.11 (s, 3H), 2.03 – 1.92 (m, 2H), 1.92 – 1.75 (m, 1H), 1.64 (s, 9H), 1.56 (d, J=6.6, 2H), 1.44 (d, J=6.5, 2H). ^{13}C-NMR (100 MHz, acetone-d_6) δ =. 174.39, 174.04, 173.50, 172.84, 168.31, 167.32, 158.88, 157.56, 150.26, 139.13, 137.04, 136.92, 136.33, 136.15, 130.99, 129.83, 129.03, 128.86, 125.48, 125.32, 124.79, 123.14, 119.98, 116.80, 116.05, 112.50, 67.69, 61.36, 56.01, 55.87, 55.76, 54.01, 51.45, 49.21, 47.62, 45.43, 41.33, 39.63, 35.79, 28.29, 27.63, 27.28, 25.38, 24.28, 19.44, 18.68, 17.59, 17.15, 12.12. MS (ESI) *m/z* calcd for $[C_{48}H_{60}N_{10}O_{11}SNa]^+$: 1008.13; found: 1008.33 $[M+Na]^+$.

C[Arg-Trp-DKP3-Gly] (61)

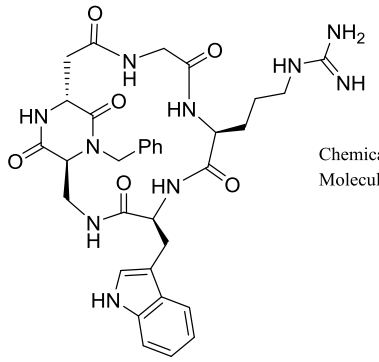

Chemical Formula: $C_{33}H_{40}N_{10}O_6$
Molecular Weight: 672,75

Compound **88** (5 mg, 0.0052 mmol) was treated with TFA (150 µL), in the presence of ion scavengers thioanisole (8 µL), ethanedithiol (5 µL) and anisole (3 µL). The mixture was stirret at r.t. for 2h. All volatiles were then evaporated and the crude was dissolved in a mixture of water and diisopropyl ether 1:1 (5 mL). The aqueous phase was washed several times with diisopropyl ether and then concentrated under reduced pressure to give the crude compound. It was purified by semipreparative-HPLC [gradient: 90% H_2O + 0.1% TFA/ 10% CH_3CN + 0.1% TFA to 30% H_2O + 0.1% TFA/ 70% CH_3CN + 0.1% TFA] in 12 min; flow: 5 mL/min, t_R (product) = 4 min c.a. to afford the desired product **61** as white foam (1 mg, 30%). MS (ESI) *m/z* calcd for $[C_{33}H_{41}N_{10}O_6]^+$:673.75; found:673.22 $[M+H]^+$.

Synthesis of cyclic CPP-DKP scaffold for drug delivery

DKP1 and DKP3 scaffolds, **97** and **80** respectively, were synthesized according to previously reported procedures and their analytical data were in agreement with those already published.[52]

N_3-DKP1-COOH (98) and N_3-DKP3-COOH (99)

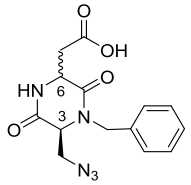

Chemical Formula: $C_{14}H_{15}N_5O_4$
Molecular Weight: 317,31

98 3S, 6S
99 3S, 6R

Allyl-protected peptide (**97** or **80**) (230 mg, 0.644 mmol, 1 eq) was dissolved in dry DCM (6 mL) under a nitrogen atmosphere, and the mixture was cooled to 0°C. [$Pd(PPh_3)_4$] (223 mg, 0.193, 0.3 eq) and freshly distilled N-methylaniline (84 µL, 0.773 mmol, 1.2 eq) were added successively. The mixture was then allowed to reach r.t. After 1h of stirring, the mixture was diluted with EtOAc (40 mL) and extracted with acqueous $NaHCO_3$ (4 x 20 mL). The combined acqueous phase were acidified to pH 2 by adding $KHSO_4$ (1 M solution) and then extracted with DCM (4 x 20 mL). The resulting organic phase was dried over Na_2SO_4 and the solvent was evaporated to afford the desired as a slightly yellow solid (121 mg, 60%) which was used without further purification. Rf= 0.2 (DCM/MeOH 9:1);

sC18*-DKP-NH_2 103a and 103b

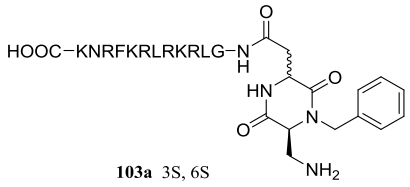

103a 3S, 6S
103b 3S, 6R

sC18* (^{106}GLRKRLRKFRNK^{117}) was synthesized on a 2-chlorotrytil chloride resin (H-L-Lys(Boc)-2CT, loading: 0.74mmol/g, 0.015 mmol scale) by automated multiple solid-phase peptide synthesis (Fmoc strategy) using a robot system. **98** or **99** were coupled to the peptide according to **GP13**. The azido group was reduced following **GP14**. Then cleavage from the resin was done according to **GP15**.

Cyclic(sC18*-DKP1) (92) and *c*(sC18*-DKP3) (93)

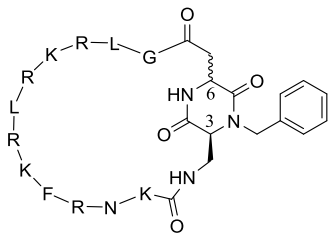

Chemical Formula: $C_{83}H_{139}N_{31}O_{16}$
Molecular Weight: 1827,23

92 3S, 6S
93 3S, 6R

10 mg (5.42mmol, 1 eq) of the full protected linear peptide **103a, b** were dissolved in 8,3 ml (0.65mM) of dry DMF, under nitrogen atmosphere. PyBOP (14.1mg, 27.1µmol, 5eq), HOBt (3.7mg, 27.1µmol, 5eq) and DIPEA (5.66 µL, 35.5µmol, 6eq) were added under these conditions. The reaction was left under stirring at 4°C for 48h. The mixture was then diluted with EtOAc and extracted with brine and saturated $NaHCO_3$. The organic phase was then dryied at reduced pressure and directly subjected to full cleavage according to **GP16**. The crude was then purified on semipreparative RP-HPLC (10-60 ACN in 45 min, tR = 24 min). The peptide was freeze-dried from water obtaining a white solid (1.6 mg, 16%). LC/MS: *m/z* calculated for $[C_{83}H_{140}N_{31}O_{16}]^{+}$= 1828.23, found fragmentation patterns: $[M+2]^{2+}$ = 914.6, $[M+3]^{3+}$ = 610.8, $[M+4]^{4+}$ = 457.9, $[M+5]^{5+}$ = 366.6.

Linear sC18*-DKP1 (108)

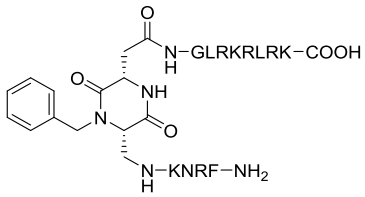

The sequence ^{106}GLRKRLRK^{113} was synthesized on a 2-chlorotrytil chloride resin (H-L-Lys(Boc)-2CT, loading: 0.74mmol/g, 0.015 mmol scale) by automated multiple solid-phase peptide synthesis (Fmoc strategy) using a robot system. **98** was coupled to the peptide according to **GP13**. The azido group was reduced following **GP14**. Fmoc-L-Lys(Boc)-OH was manually coupled following **GP9**. Fmoc deprotection was then accomplished (**GP10**). The resin was subjected to automated elongation for the remaining amino acids. Then the peptide was cleaved from the resin (**GP15**). The solvent was evaporated under reduced pression. 28 mg of linear peptide **108** were obtained.

Linear sC18*(reversed sequence)-DKP1 (113)

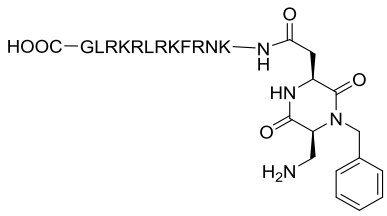

sC18 reversed sequence (^{117}KNRFKRLRKRLG^{106}) was synthesized on a 2-chlorotrytil chloride resin (H-Gly-2CT, loading: 0.87 mmol/g, 0.015 mmol scale) by automated multiple SPPS (Fmoc strategy) using a robot system. DKP-1 (**98**) was coupled (**GP13**). The resin was treated according to **GP14**. Then cleavage from the resin (**GP15**). 27 mg of linear peptide were obtained.

c-sC18*(reversed sequence)-DKP1 (109)

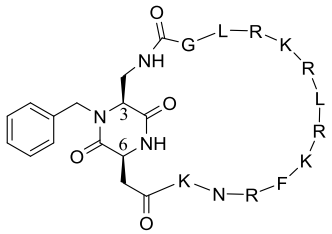

Chemical Formula: $C_{83}H_{139}N_{31}O_{16}$
Molecular Weight: 1827,23

7 mg (5.42mmol, 1 eq) of the full protected linear peptide **113** were dissolved in 5,8 ml (0.65mM) of dry DCM:dry DMF 9:1 v/v, under nitrogen atmosphere. PyBOP (9.8 mg, 18.9 µmol, 5eq), HOBt (2.5 mg, 18.9 µmol, 5eq) and DIPEA (3.9 µL, 22.7 µmol, 6 eq) were added under these conditions. The reaction was left under stirring at r.t. for 6 days. The mixture was then diluted with EtOAc and extracted with brine and saturated $NaHCO_3$. The organic phase was then dryied under vacuum and the subjected to full deprotection. The peptide was fully deprotected according to **GP16**. The crude was purified on semipreparative RP-HPLC (10-60 ACN in 45 min, tR = 22 min). The peptide was freeze-dried from water obtaining a white solid (0.3 mg, 3%). LC/MS: *m/z* calculated for $[C_{83}H_{140}N_{31}O_{16}]^+$= 1828.23, found fragmentation patterns: $[M+2]^{2+}$ = 914.6, $[M+3]^{3+}$ = 610.8, $[M+4]^{4+}$ = 457.9, $[M+5]^{5+}$ = 366.6.

Linear sC18*-DKP1 (114a) and linear sC18*-DKP3 (114b)

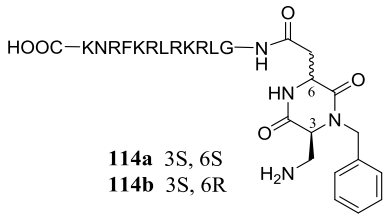

114a 3S, 6S
114b 3S, 6R

Chemical Formula: $C_{83}H_{141}N_{31}O_{17}$
Molecular Weight: 1845,24

The sC18* (^{106}GLRKRLRKFRNK^{117}) was synthesized on a 2-chlorotrytil chloride resin (H-L-Lys(Boc)-2CT, loading: 0.74mmol/g, 0.015 mmol scale) by automated multiple solid-phase peptide synthesis (Fmoc strategy) using a robot system. **98** or **99** were coupled to the peptide according to **GP13**. The azido group was reduced following **GP14**. Then cleavage from the resin was done according to **GP16**.

The peptides were freeze-dried from water obtaining a white solid (60% yield for **114a** and 48% yield for **114b**). LC/MS: *m/z* calculated for $[C_{83}H_{142}N_{31}O_{16}]^{+}$= 1846.24, found fragmentation patterns: $[M+2]^{2+}$ = 923.6, $[M+3]^{3+}$ = 616.1, $[M+4]^{4+}$ = 462.3, $[M+5]^{5+}$ = 370.0.

HPLC traces of the Final Products

HPLC trace of *c*[DKPf3-RGD]-PropargylGly-Aoa=Dau (**16**), purity: 96%

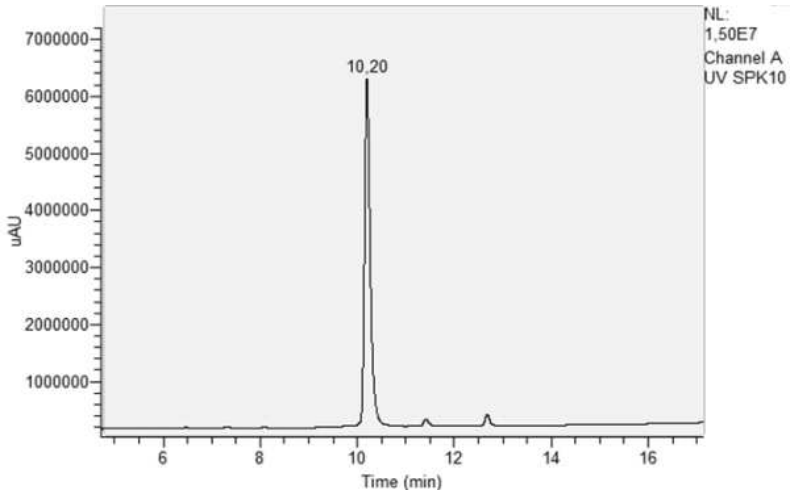

HPLC trace of *c*[DKPf3-RGD]-GLFG-Aoa=Dau (**17**), purity: 98%

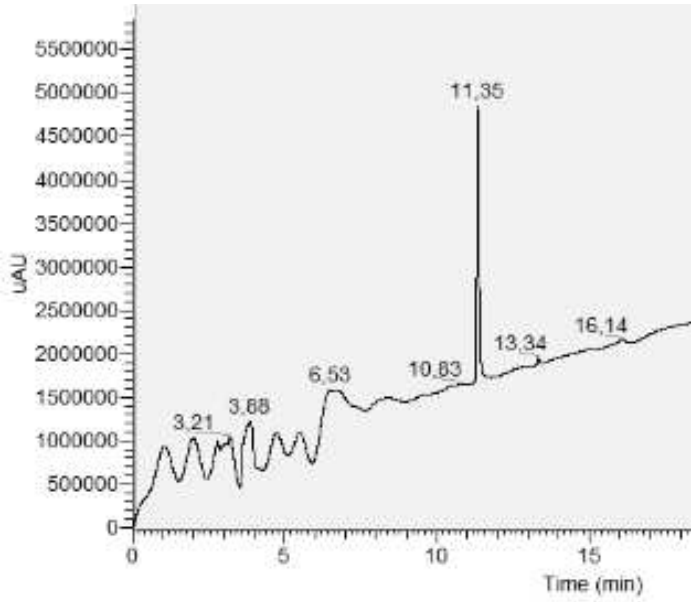

HPLC traces of linear sC18*-DKP **114a**. Purity: > 98%

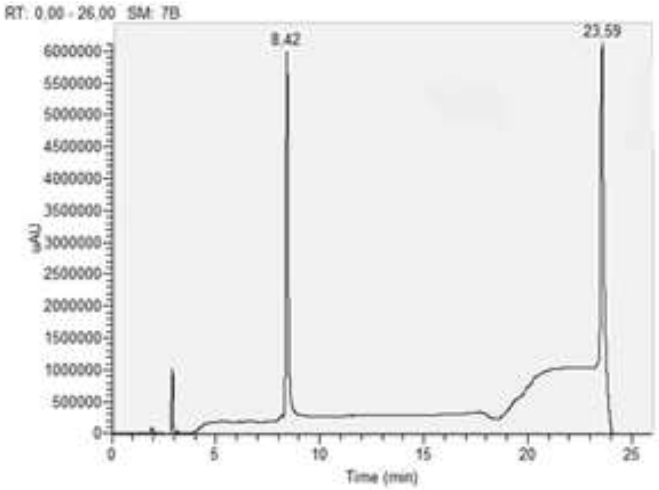

HPLC traces of linear sC18*-DKP **114b**. Purity: > 98%

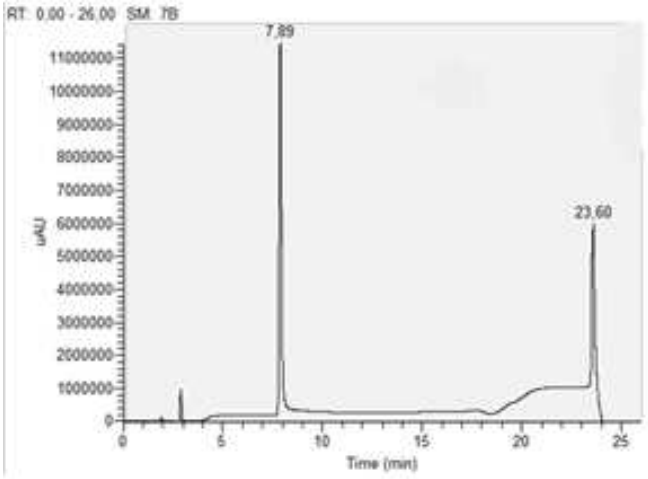

Appendix of NMR spectra

2’-(4-Nitrophenoxycarbonyl) paclitaxel (46)

^{1}H-NMR (400 MHz, CD_2Cl_2)

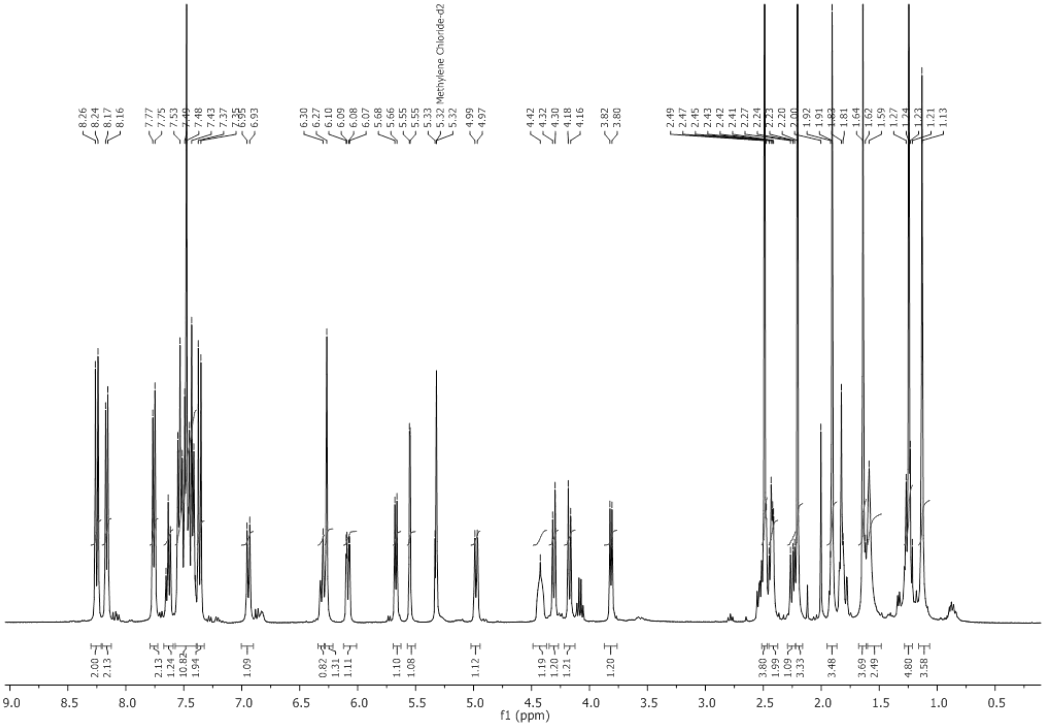

^{13}C-NMR (101 MHz, CD_2Cl_2)

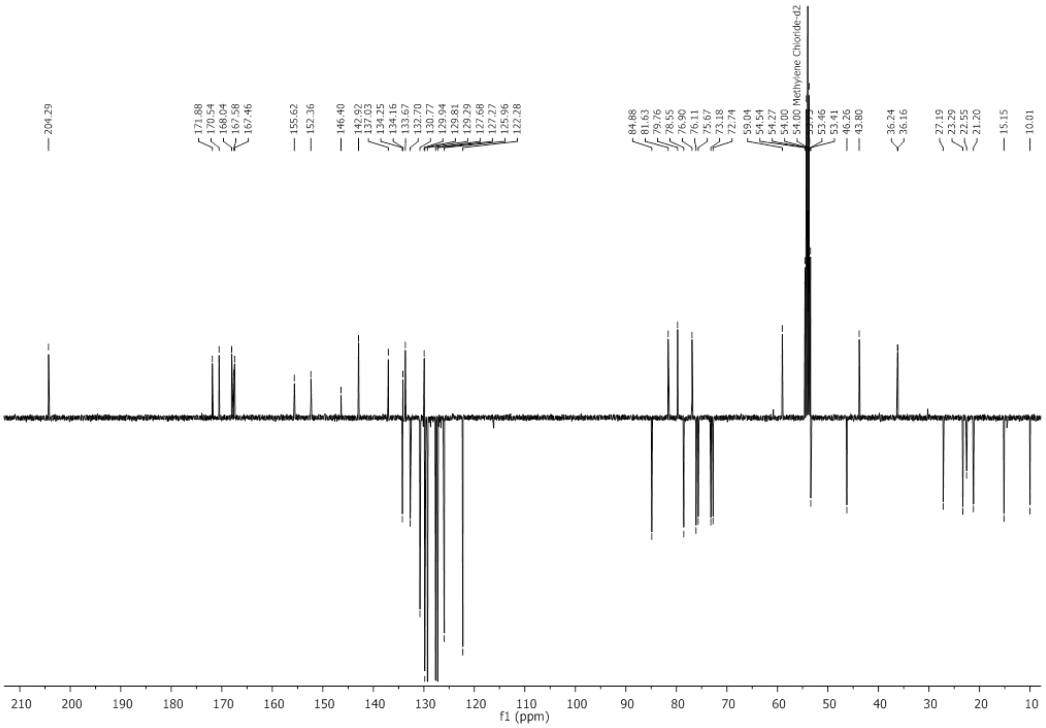

Glutaric anhydride-Val-Ala-PAB-PNP-dimethyl ethylendiamine (52)

^{1}H-NMR (400 MHz, CD_3OD)

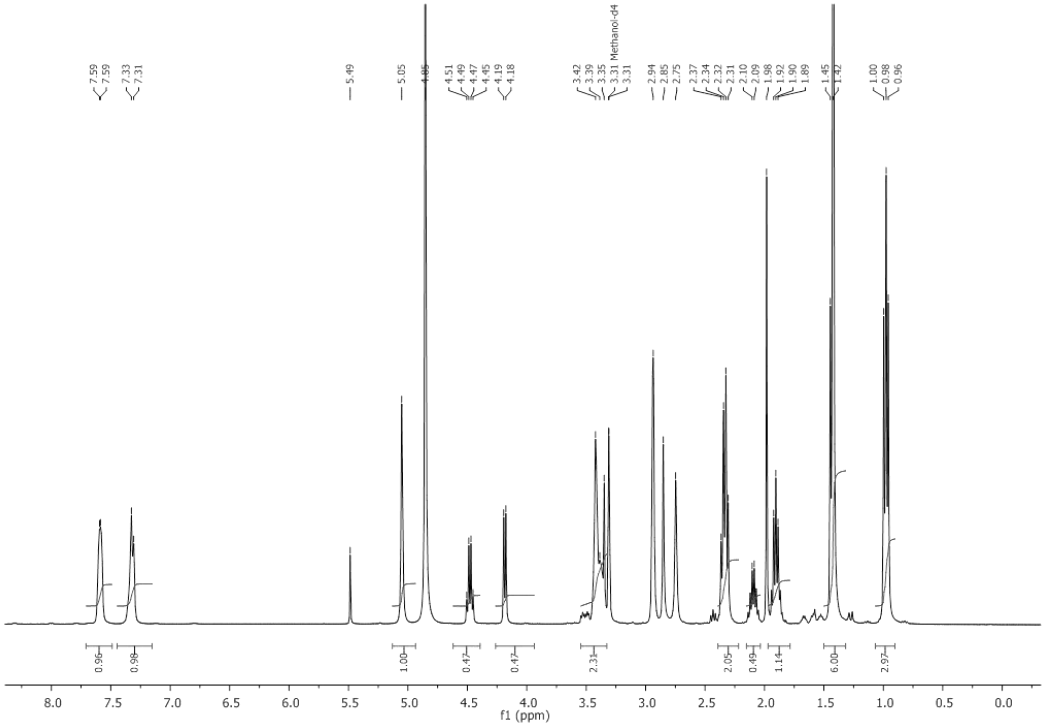

^{13}C-NMR (101 MHz, CD_3OD)

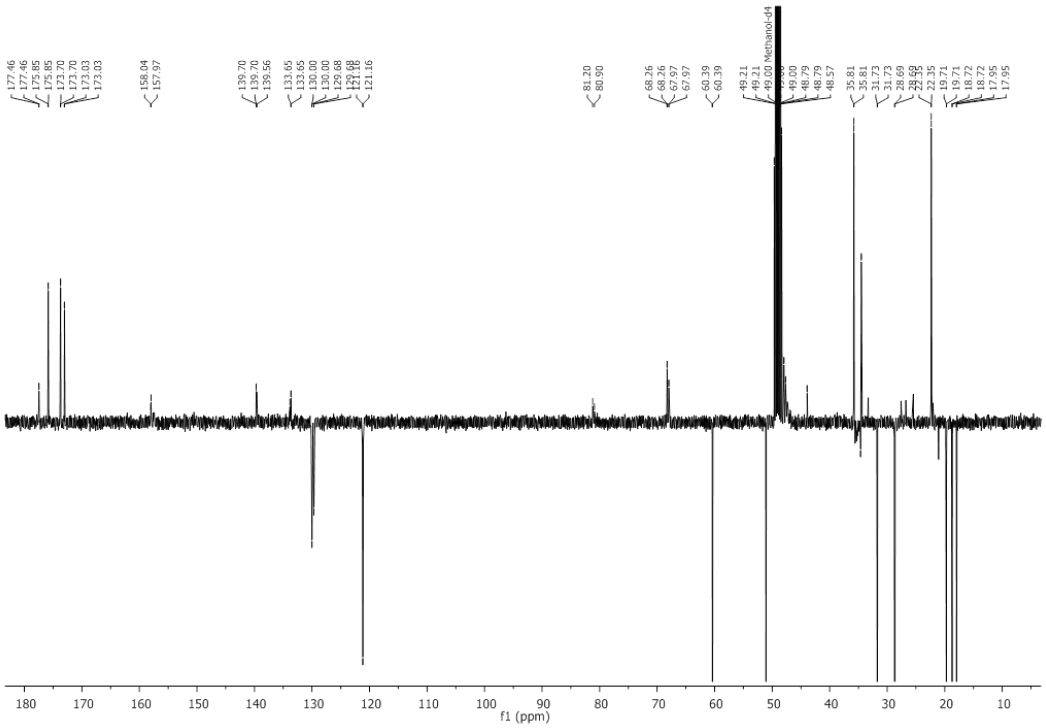

Maleimide-Glutaric anhydride-Val-Ala-PAB-PNP-dimethyl ethylendiamine (53)

^{1}H-NMR (400 MHz, CD_3OD)

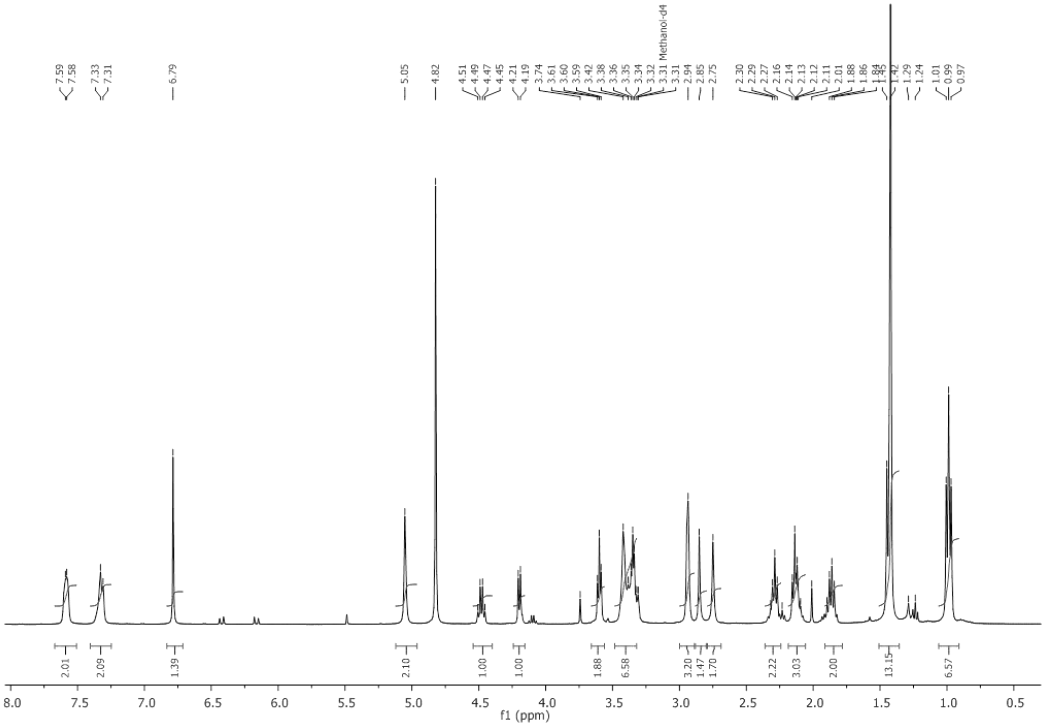

^{13}C-NMR (101 MHz, CD_3OD)

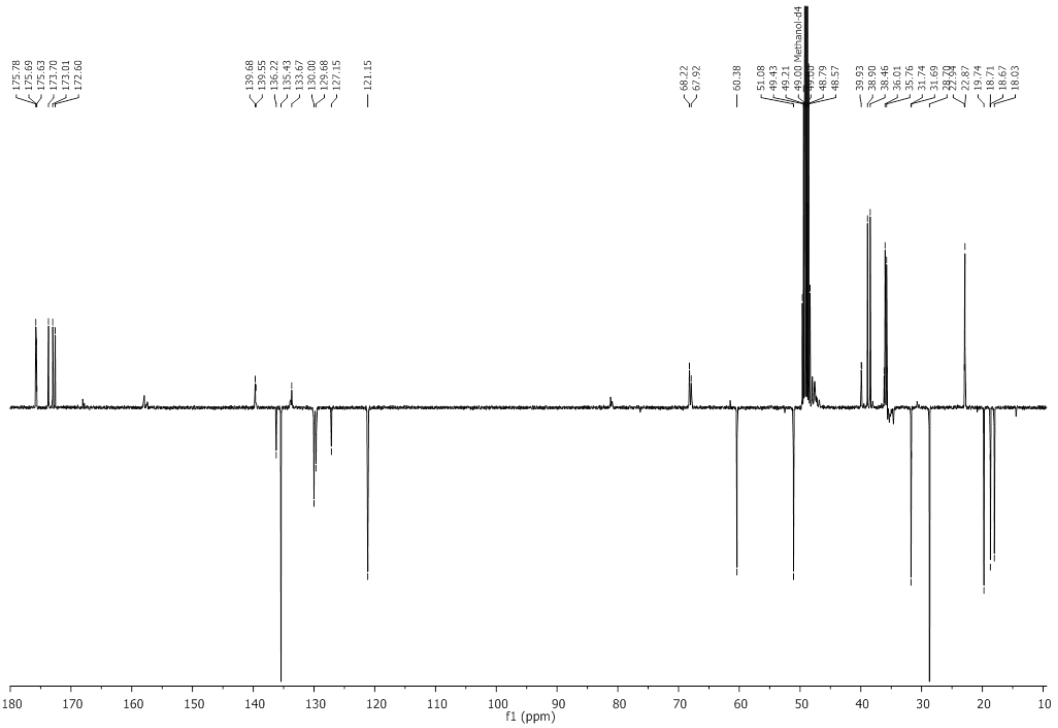

N-indole (Mtr)-3-carboxaldehyde (64)

^{1}H-NMR (400 MHz, $CDCl_3$)

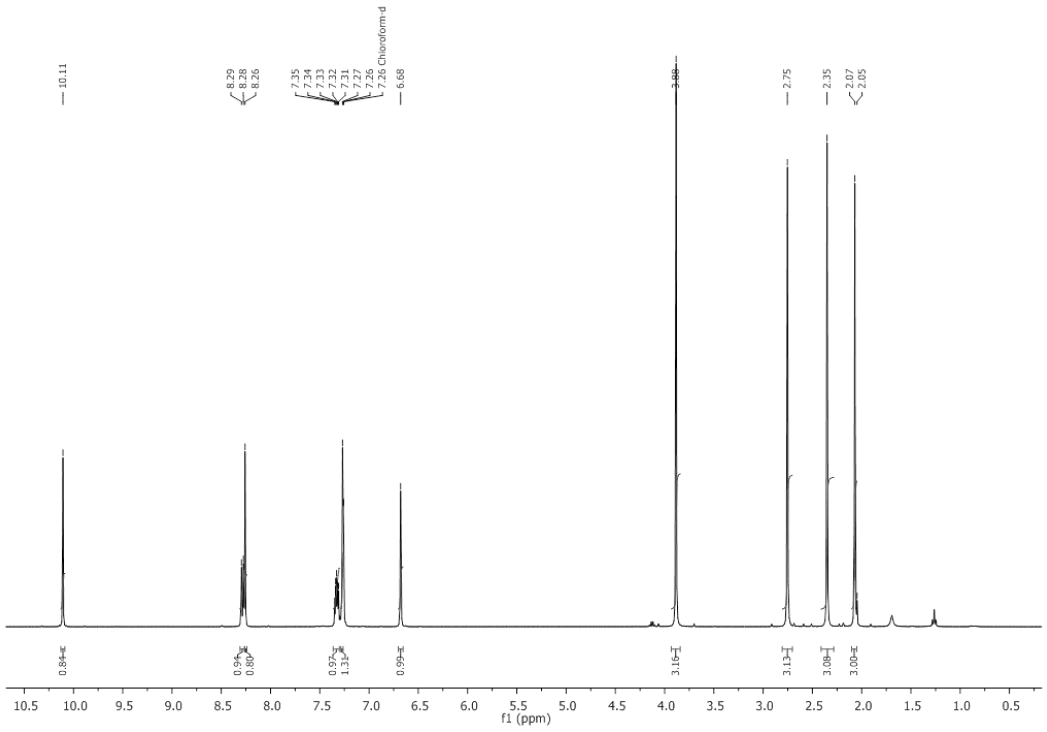

^{13}C-NMR (101 MHz, $CDCl_3$)

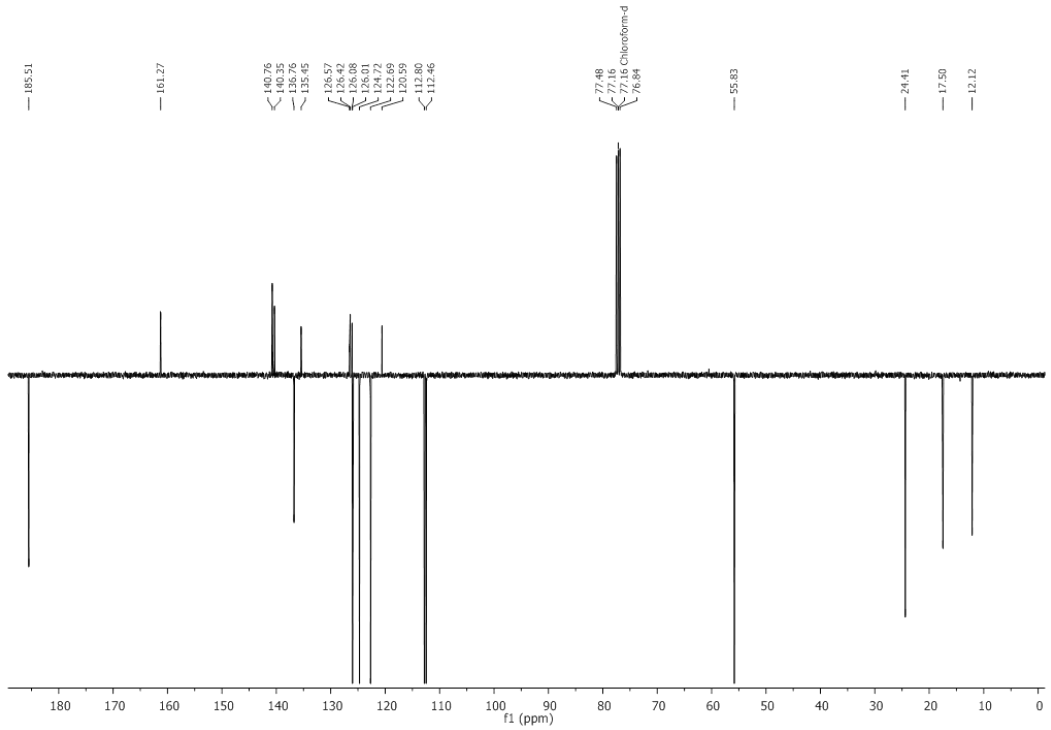

(*S*)-*N*-indolyl (Mtr) serine methyl ester (65)

^{1}H-NMR (400 MHz, $CDCl_3$)

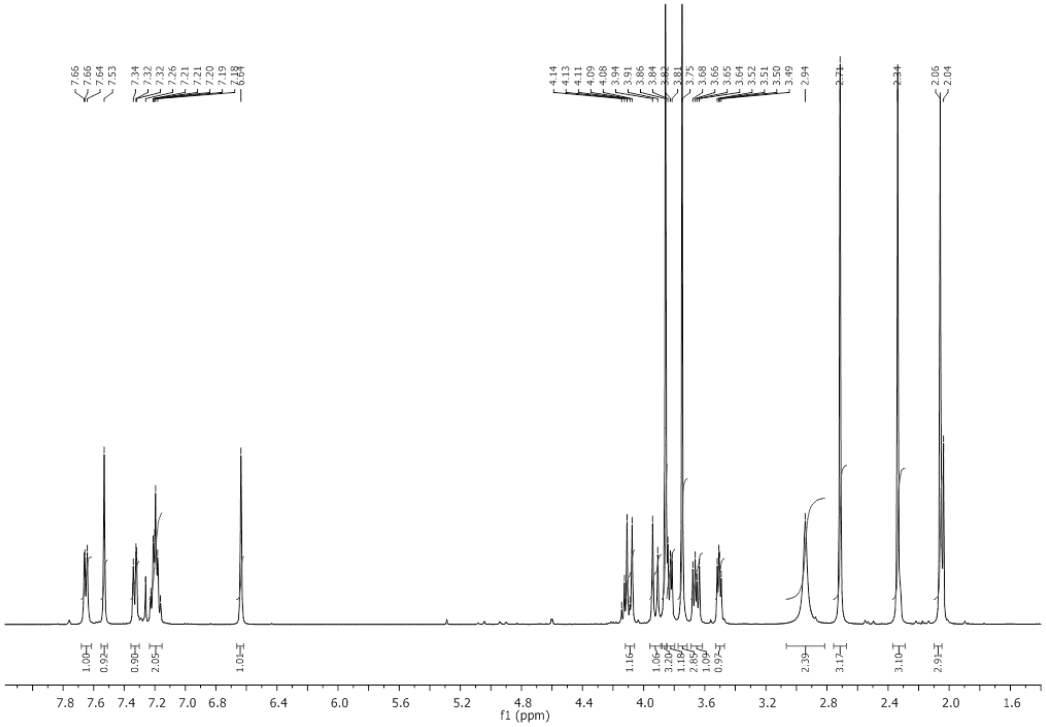

^{13}C-NMR (101 MHz, $CDCl_3$)

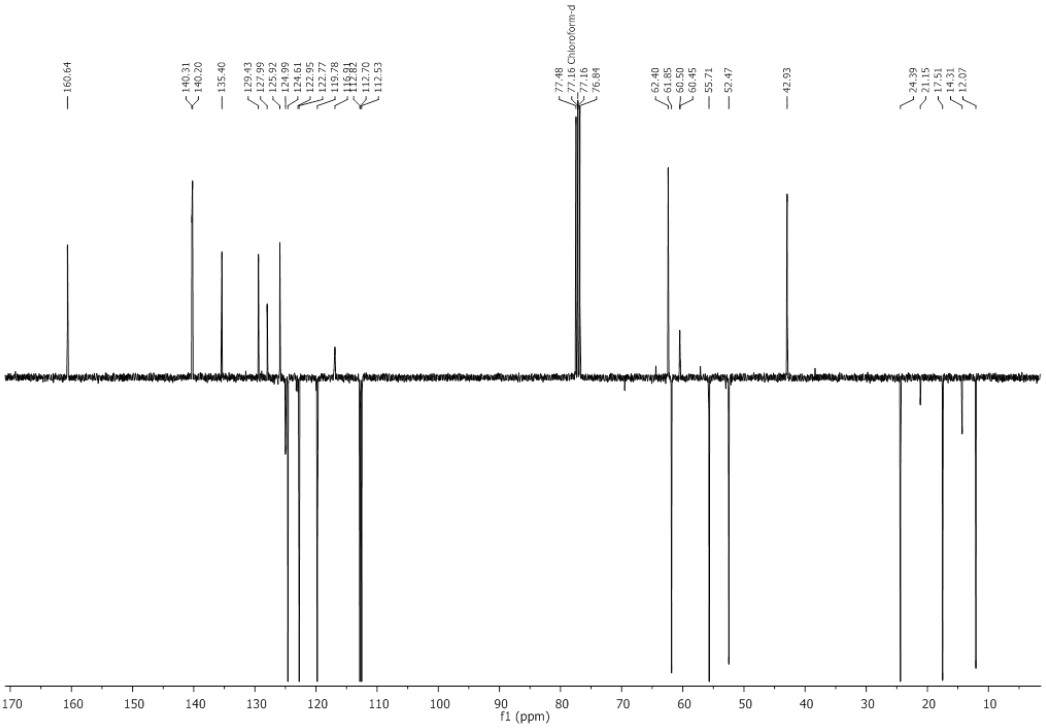

Isopeptide (66)

^{1}H-NMR (400 MHz, $CDCl_3$)

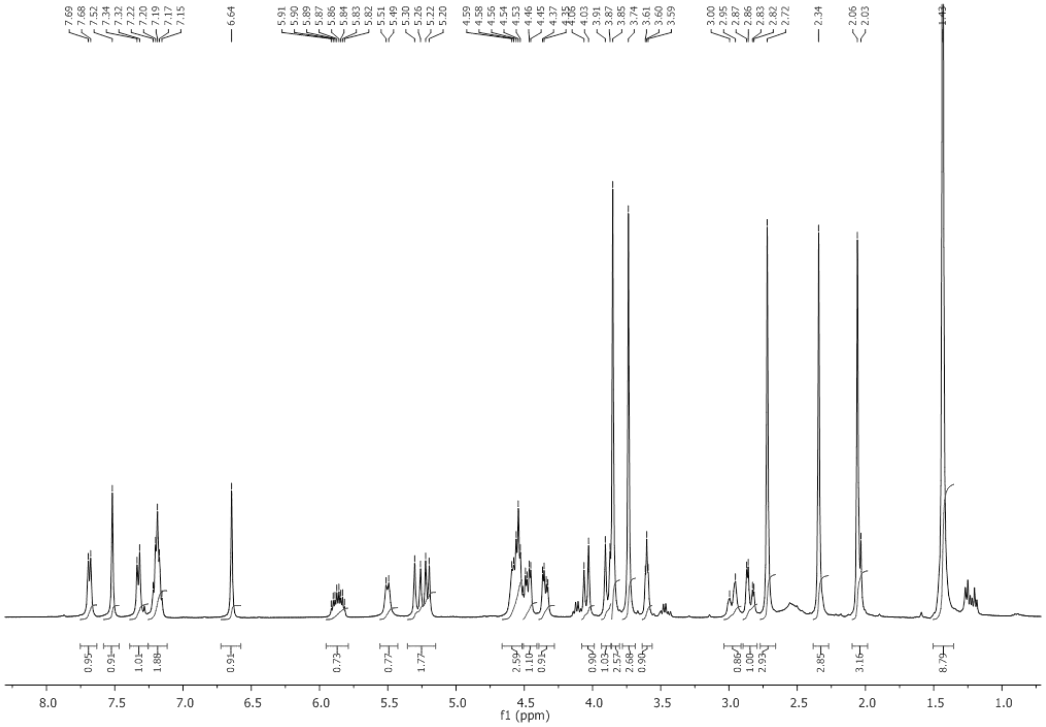

^{13}C-NMR (101 MHz, $CDCl_3$)

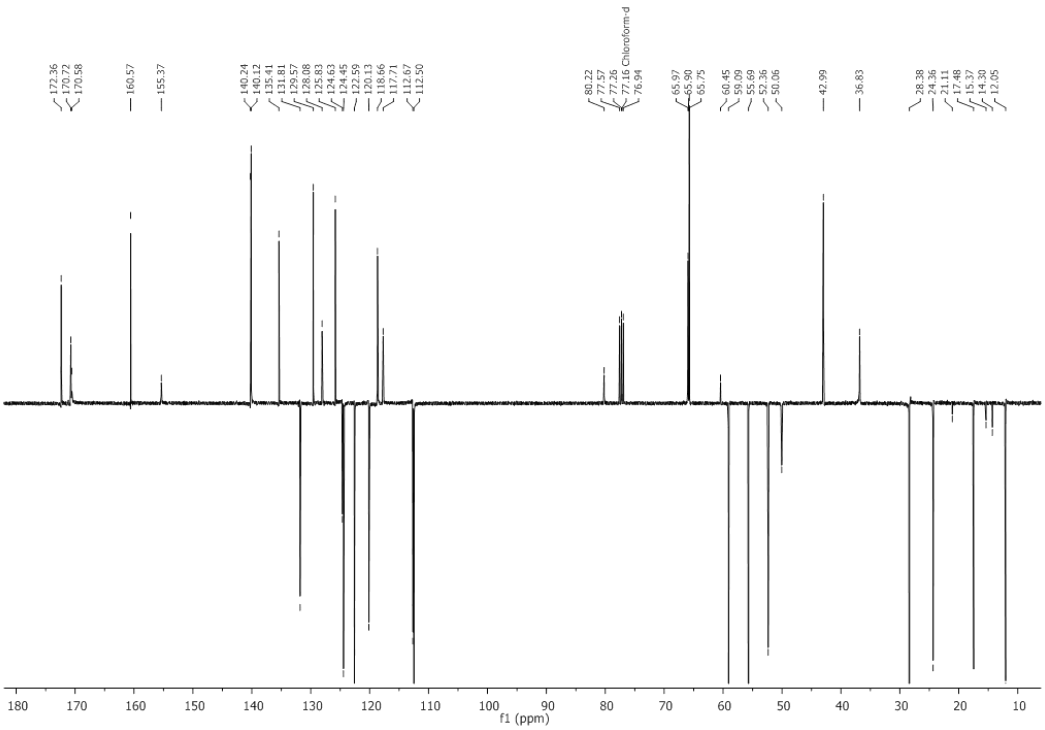

OH-DKP3-indolyl-COOAllyl (67)

^{1}H-NMR (400 MHz, $CDCl_3$)

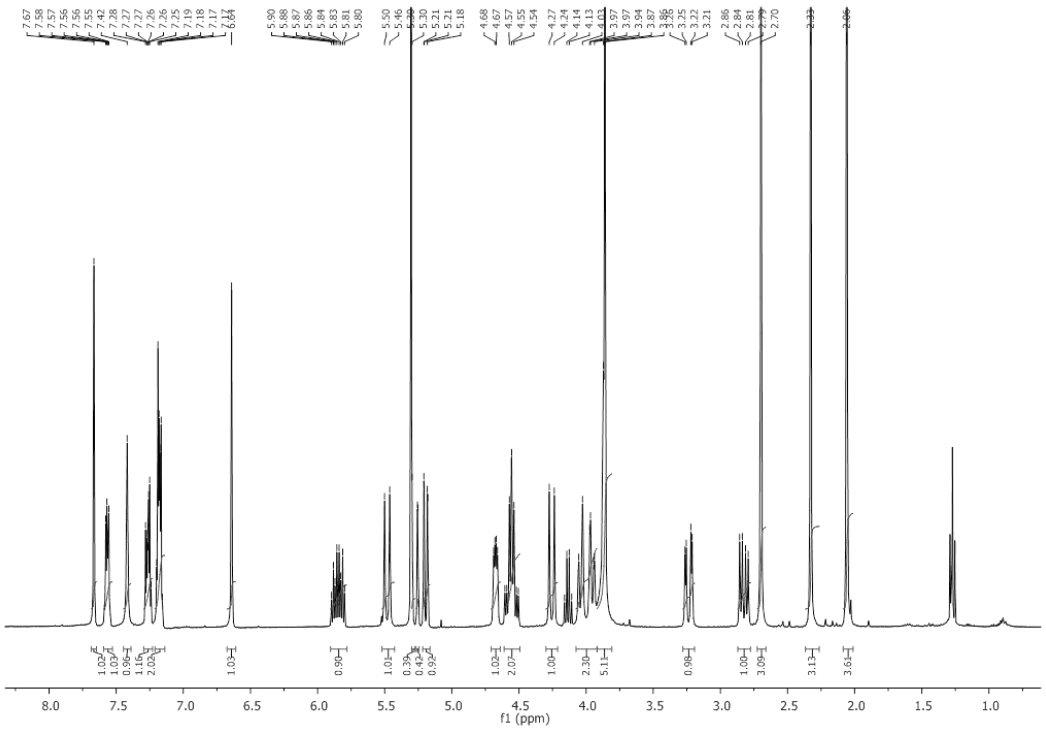

^{13}C-NMR (101 MHz, $CDCl_3$)

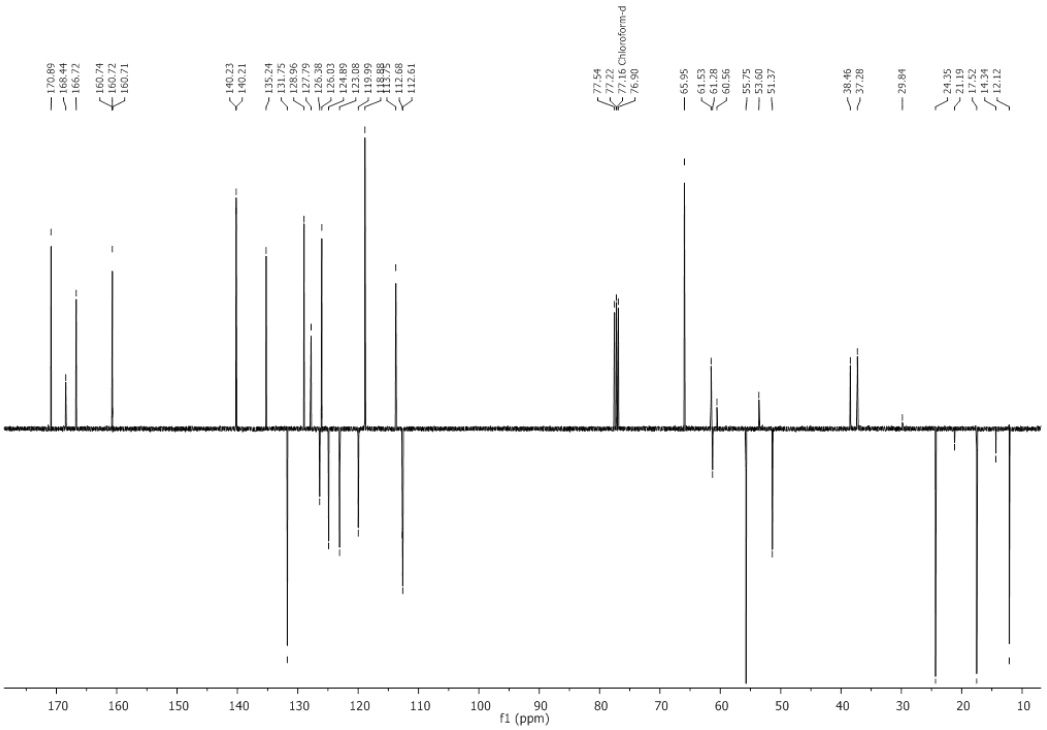

N_3-DKP3-indolyl-COOAllyl (68)

^{1}H-NMR (400 MHz, $CDCl_3$)

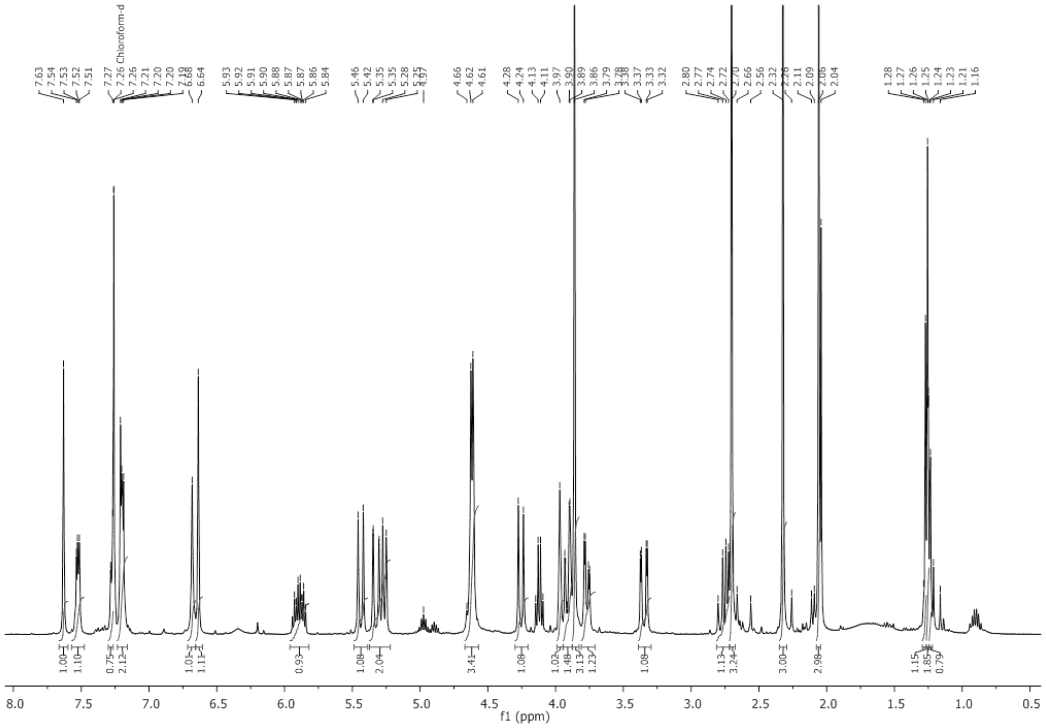

^{13}C-NMR (101 MHz, $CDCl_3$)

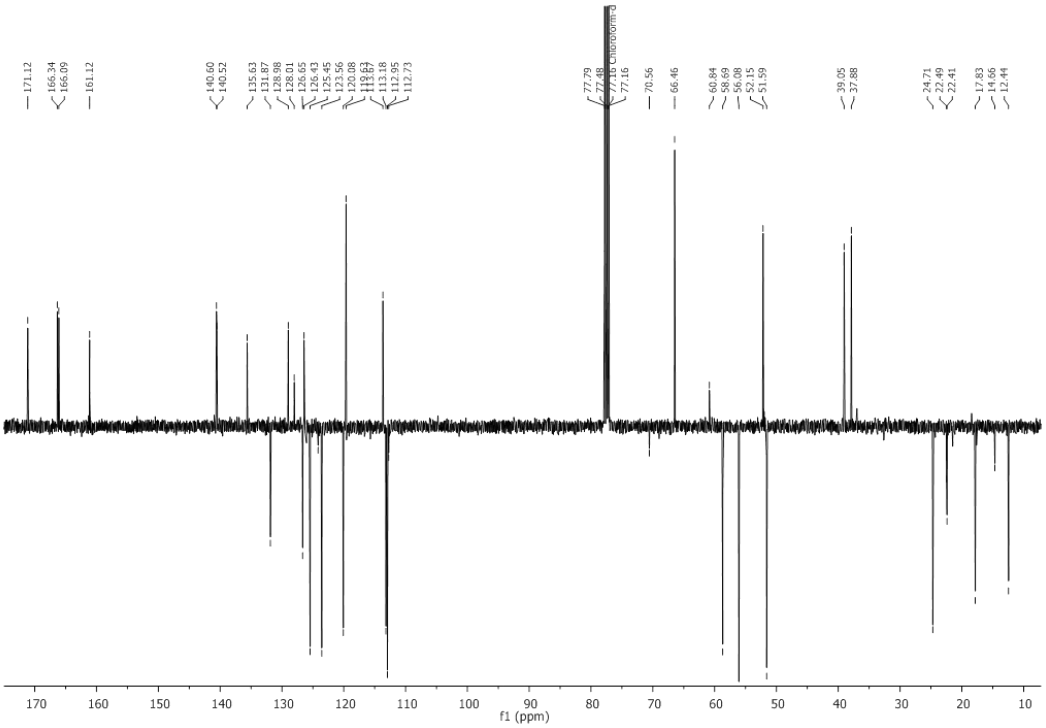

NHBoc-DKP3-indolyl-COOAllyl (69)

^{1}H-NMR (400 MHz, $CDCl_3$)

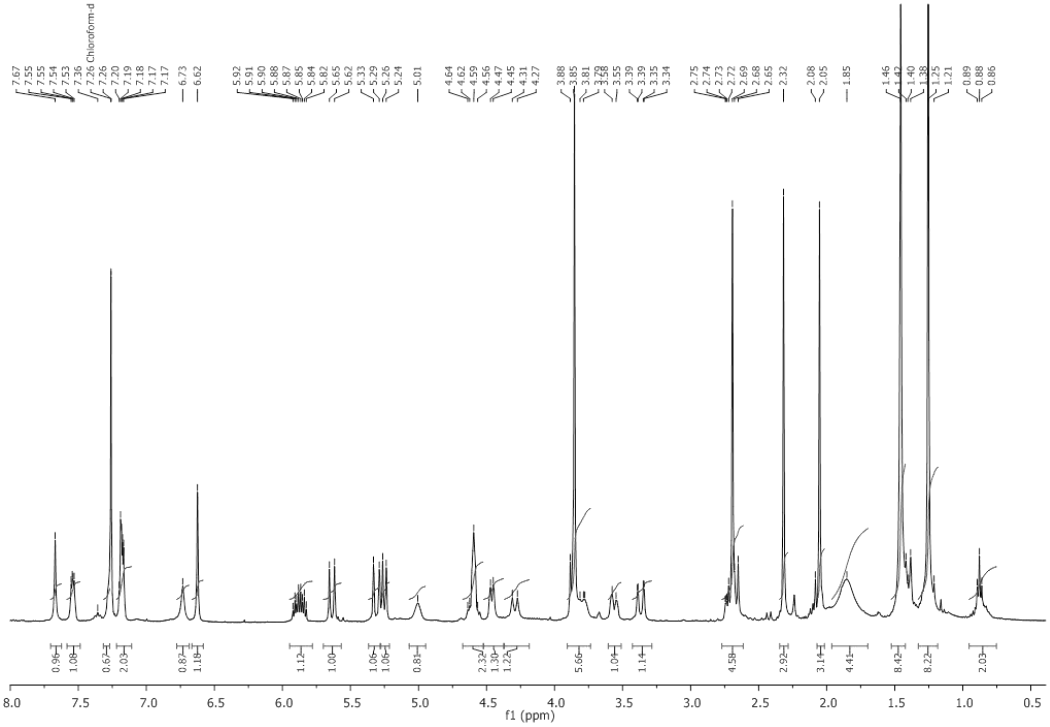

^{13}C-NMR (101 MHz, $CDCl_3$)

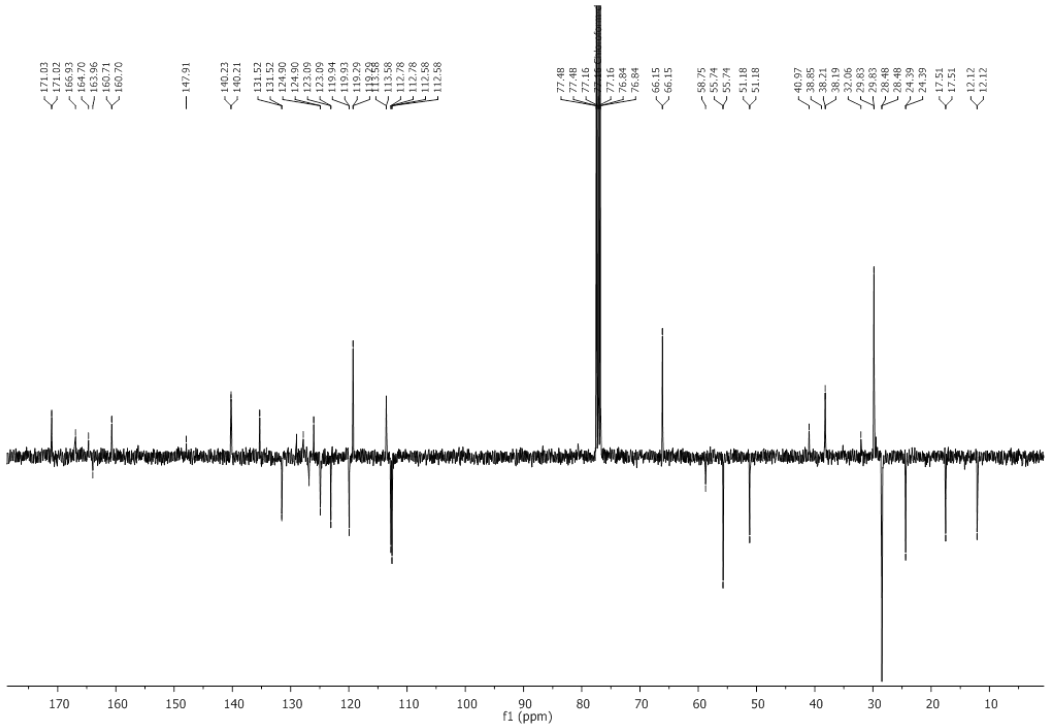

NHBoc-DKP3-indolyl-Ile-NH*t*Bu (75)

^{1}H-NMR (400 MHz, $CDCl_3$)

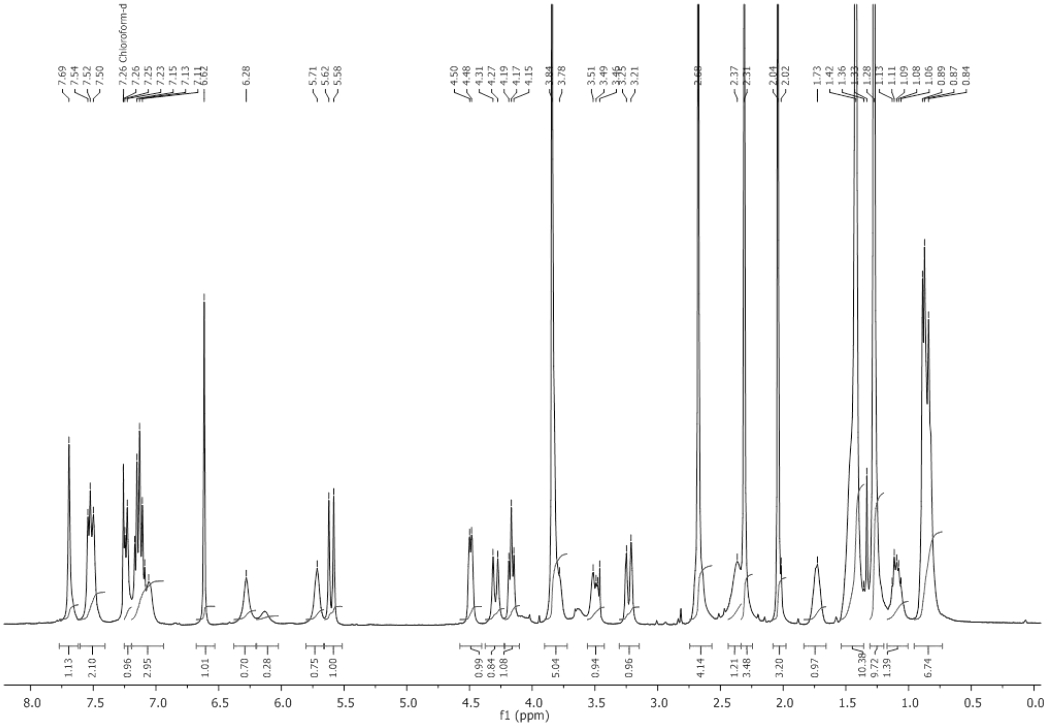

^{13}C-NMR (101 MHz, $CDCl_3$)

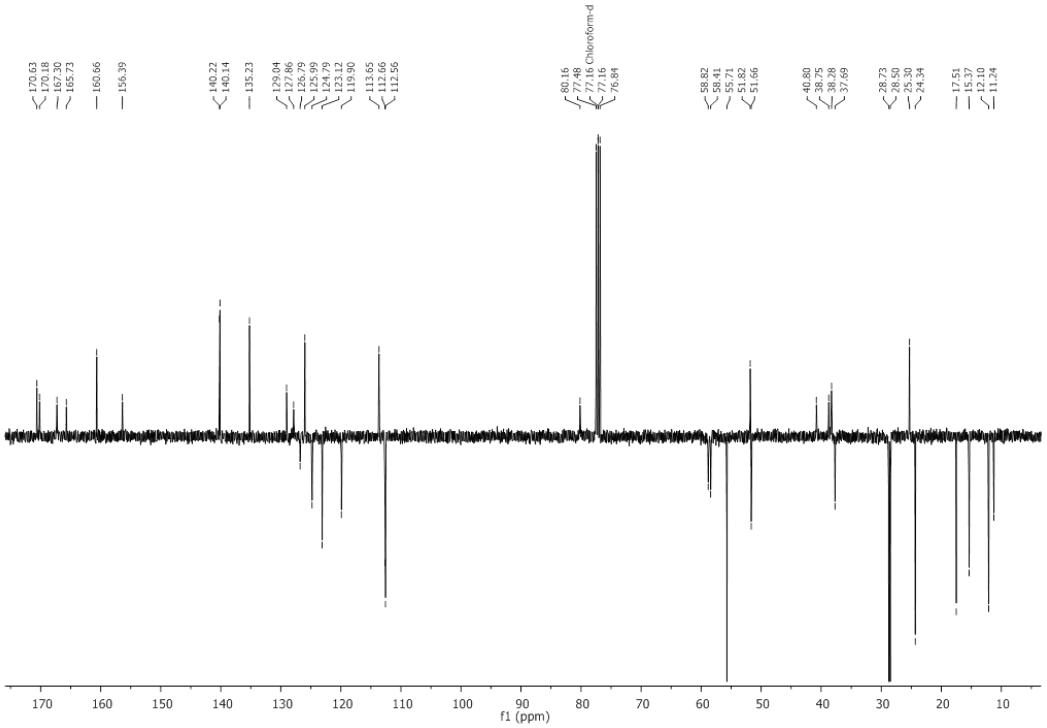

O*t*Bu-Asp(NHBoc)-DKP3-indolyl-Ile-NH*t*Bu (76)

^{1}H-NMR (400 MHz, $CDCl_3$)

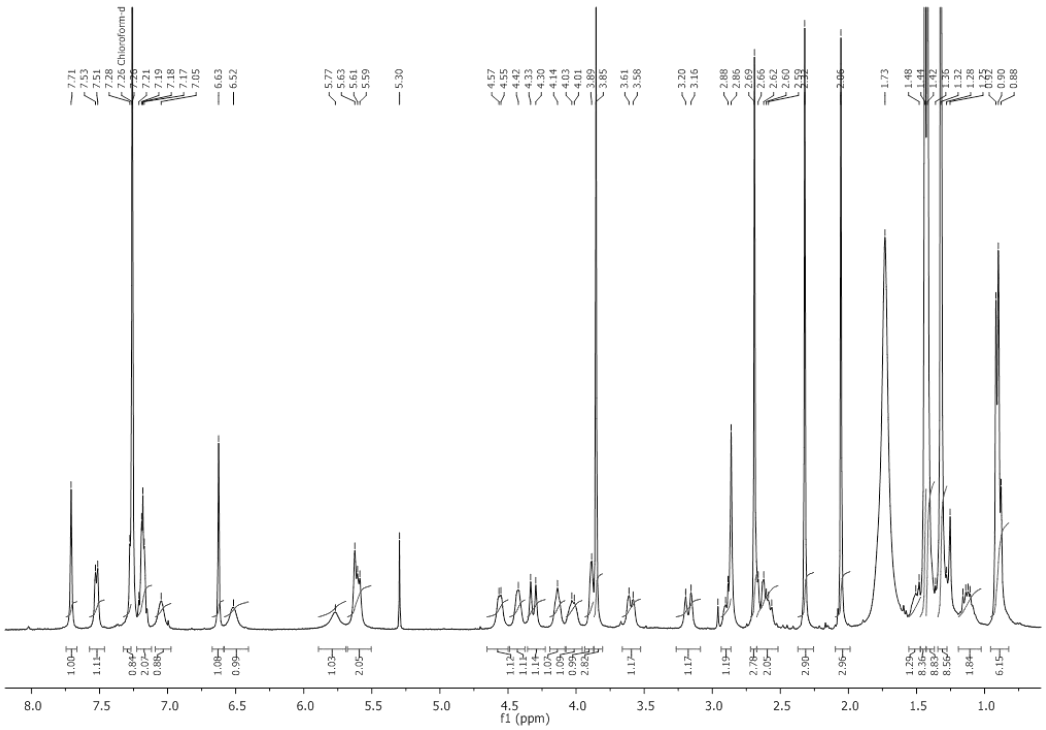

^{13}C-NMR (101 MHz, $CDCl_3$)

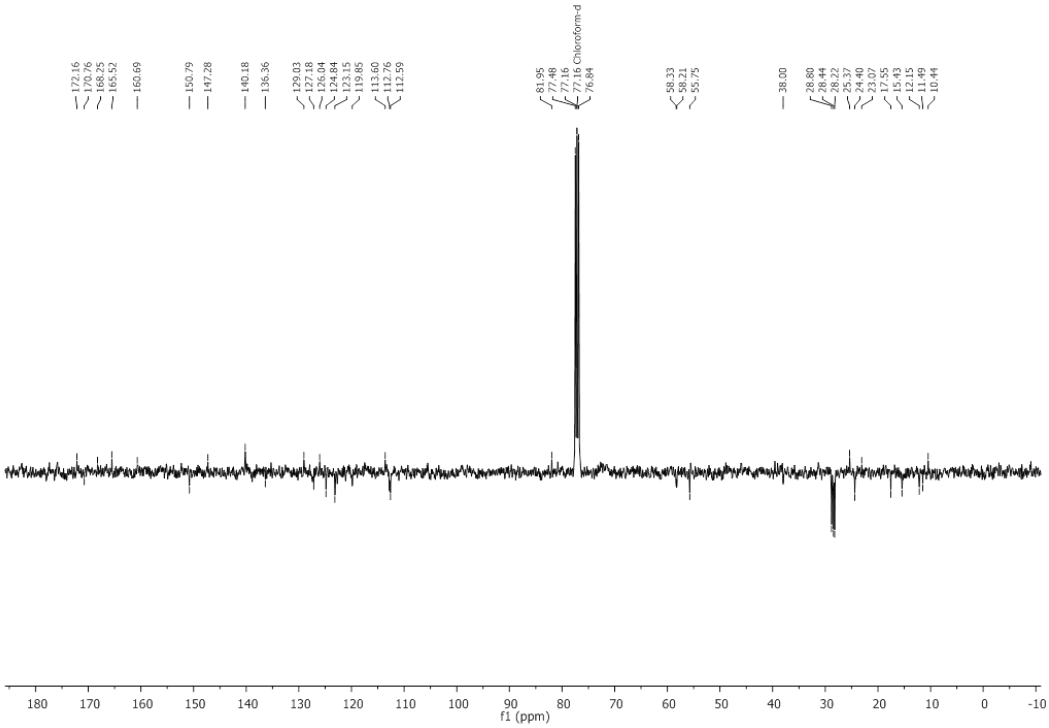

NHBoc-DKP3-Gly(OBn) (84)

^{1}H-NMR (40 MHz, Acetone-d^{6})

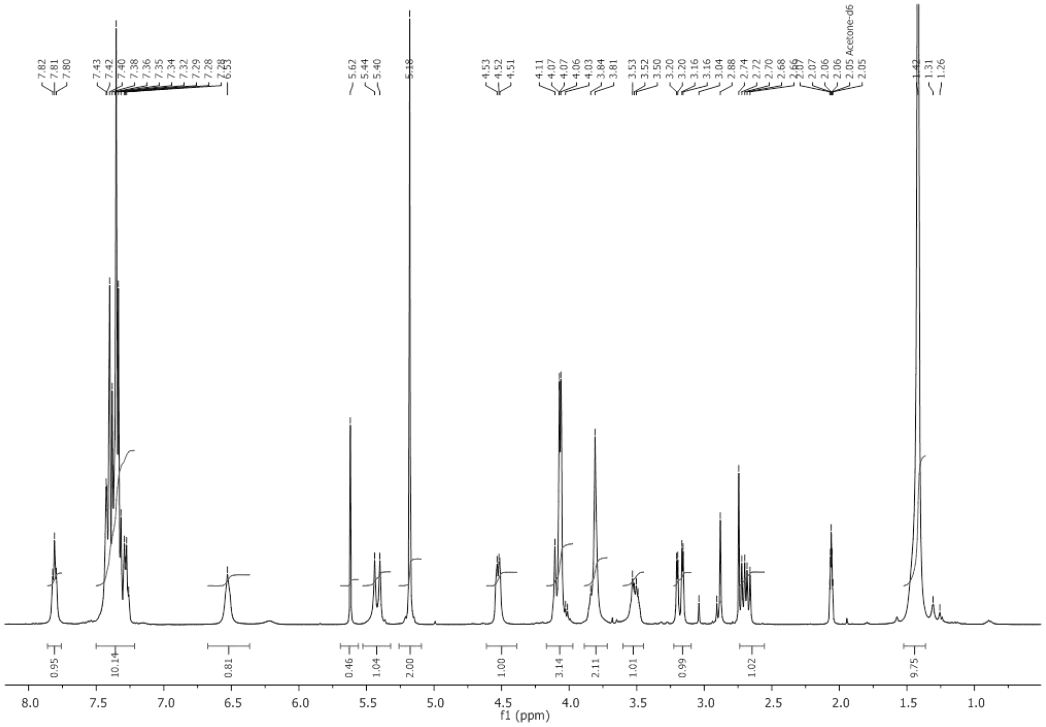

^{13}C-NMR (101 MHz, Acetone-d^{6})

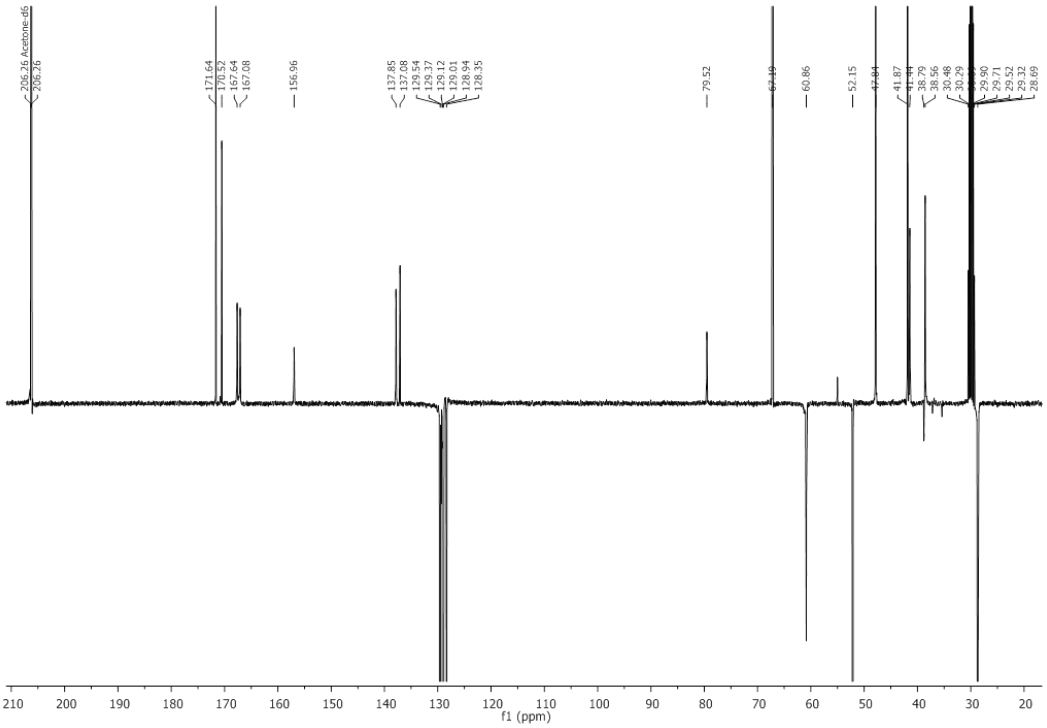

Fmoc-Trp(Boc)-DKP3-Gly(OBn) (85)

^{1}H-NMR (40 MHz, Acetone-d^{6})

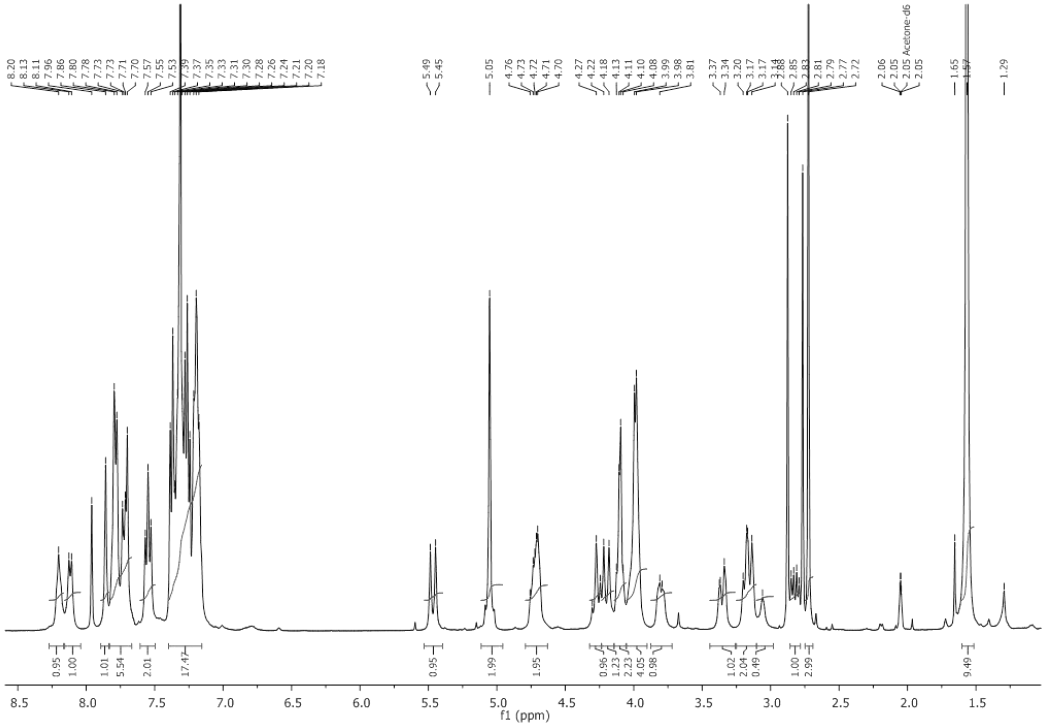

^{13}C-NMR (101 MHz, Acetone-d^{6})

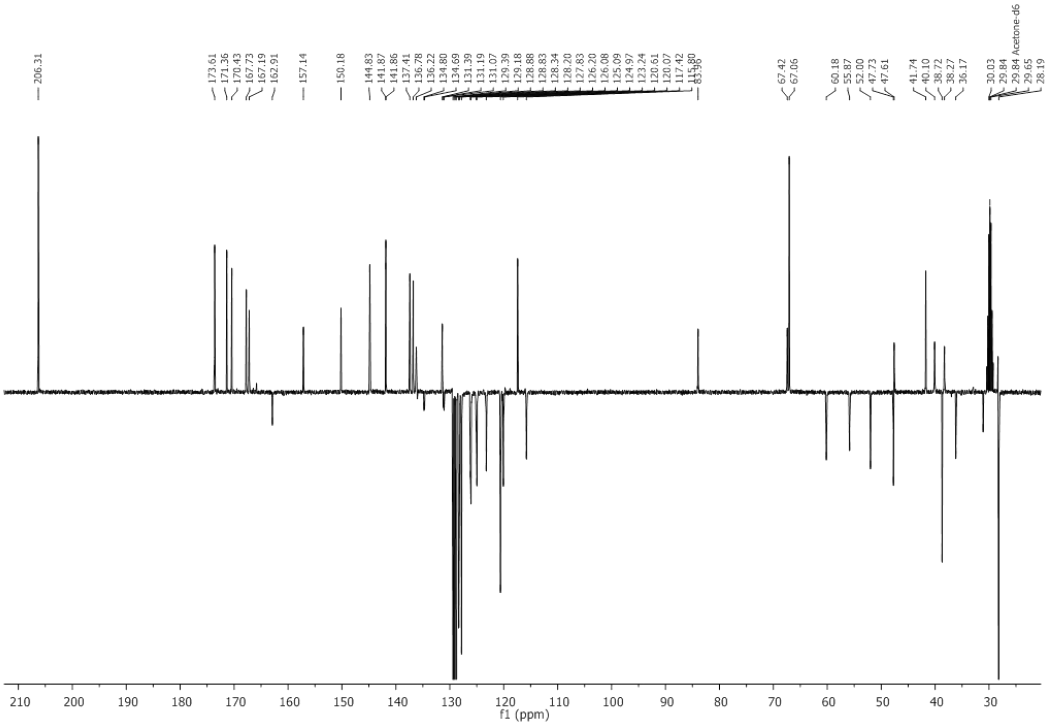

Cbz-Arg(Mtr)-Trp(Boc)-DKP3-Gly(OBn) (86)

^{1}H-NMR (40 MHz, Acetone-d^{6})

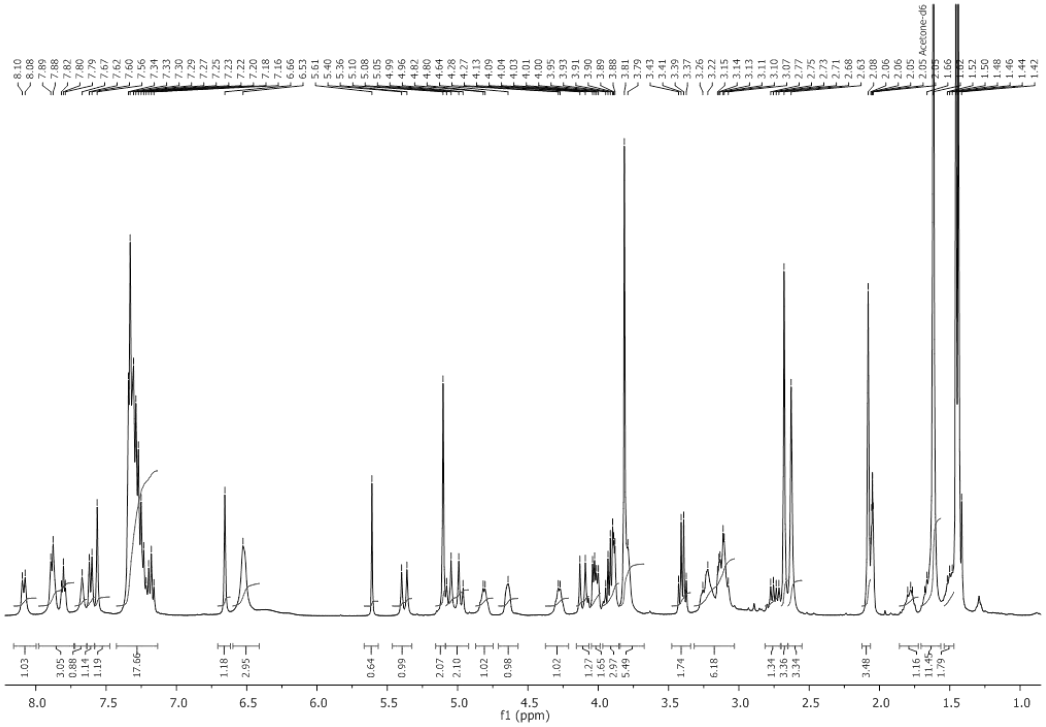

^{13}C-NMR (101 MHz, Acetone-d^{6})

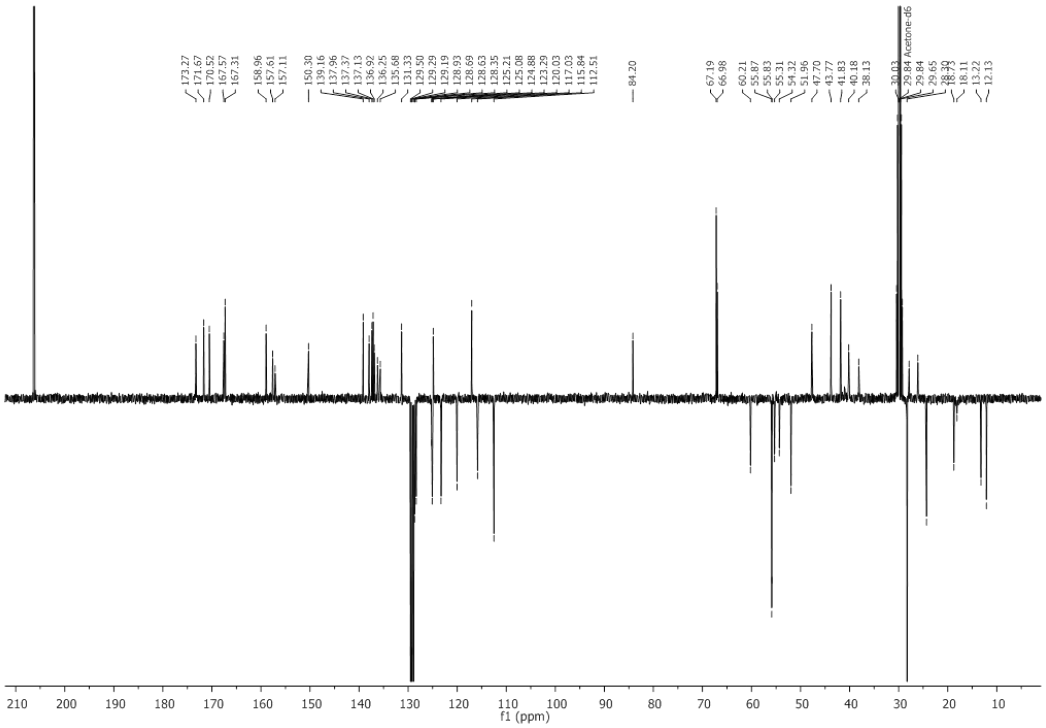

C[Arg(Mtr)-Trp(Boc)-DKP3-Gly] (88)

^{1}H-NMR (40 MHz, Acetone-d^{6})

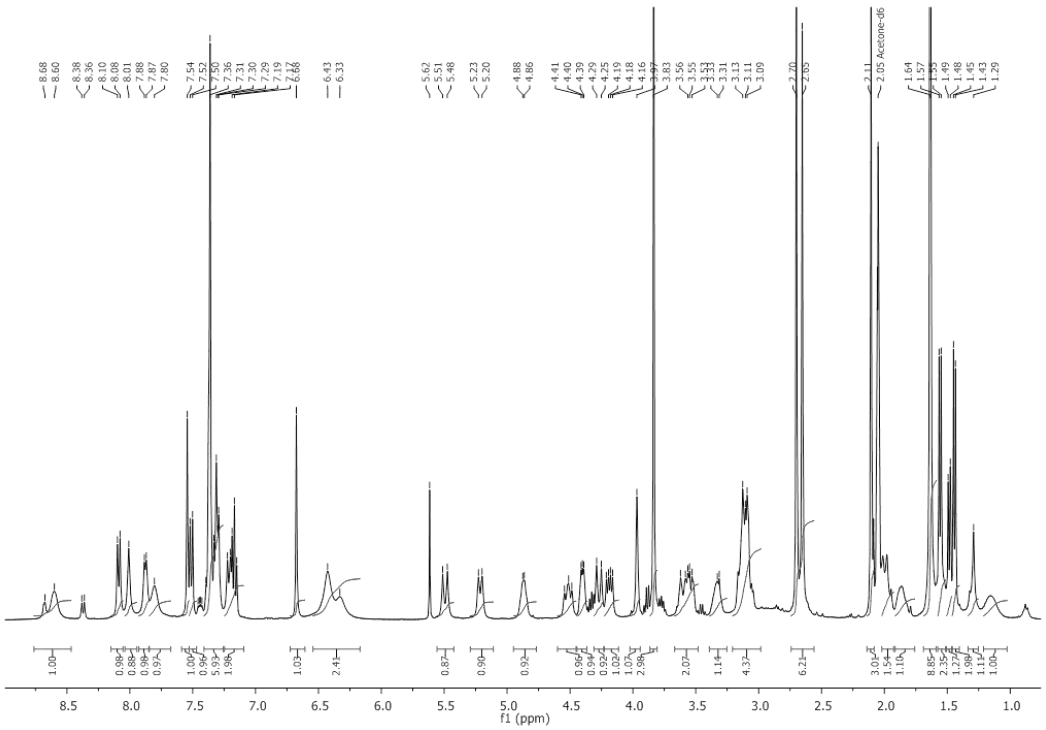

^{13}C-NMR (101 MHz, Acetone-d^{6})

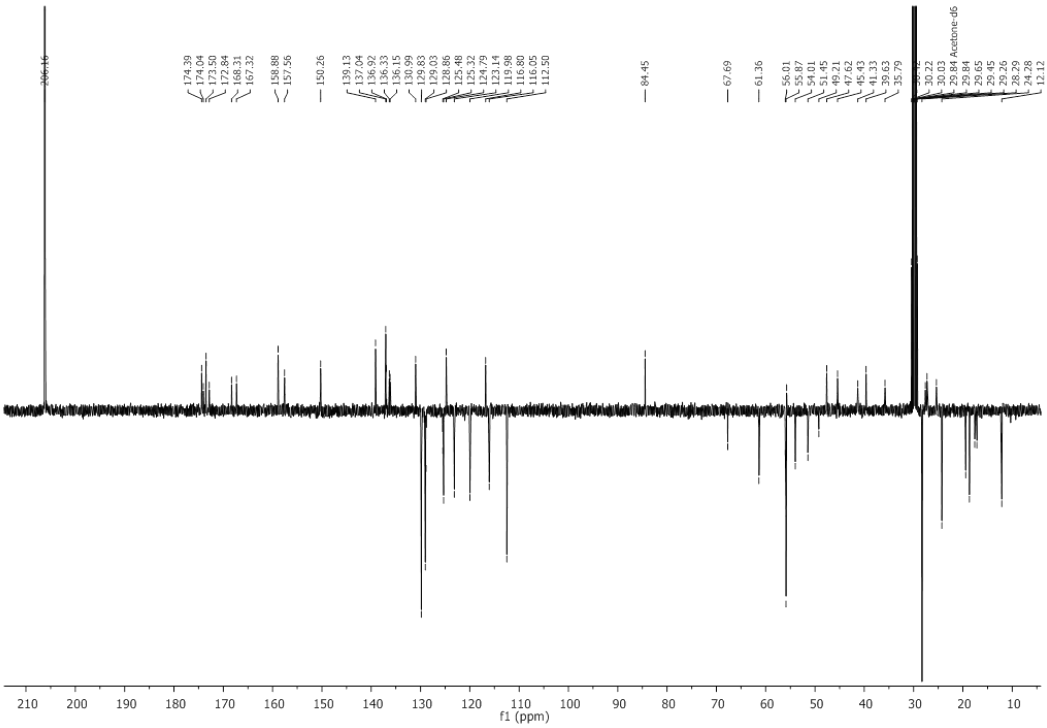

References

(1) Teichmann, S. A. Principles of Protein-Protein Interactions. *Bioinformatics* **2002**, *18* (SUPPL. 2), 13–20.

(2) De Las Rivas, J.; Fontanillo, C. Protein-Protein Interactions Essentials: Key Concepts to Building and Analyzing Interactome Networks. *PLoS Comput. Biol.* **2010**, *6* (6), 1–8.

(3) Marcotte, E. M.; Pellegrini, M.; Ng, H. L.; Rice, D. W.; Yeates, T. O.; Eisenberg, D. Detecting Protein Function and Protein-Protein Interactions from Genome Sequences. *Science* **1999**, *285* (5428), 751–753.

(4) Phizicky, E. M.; Fields, S. Protein-Protein Interactions: Methods for Detection and Analysis. *Microbiol. Rev.* **1995**, *59* (1), 94–123.

(5) Cummings, C. G.; Hamilton, A. D. Disrupting Protein–protein Interactions with Non-Peptidic, Small Molecule α-Helix Mimetics. *Curr. Opin. Chem. Biol.* **2010**, *14* (3), 341–346.

(6) Davis, J. M.; Tsou, L. K.; Hamilton, A. D. Synthetic Non-Peptide Mimetics of α-Helices. *Chem. Soc. Rev.* **2007**, *36* (2), 326–334.

(7) Ivanov, A. A.; Khuri, F. R.; Fu, H. Targeting Protein-Protein Interactions as an Anticancer Strategy. *Trends Pharmacol. Sci.* **2013**, *34* (7), 393–400.

(8) Whitby, L. R.; Boger, D. L. Comprehensive Peptidomimetic Libraries Targeting Protein-Protein Interactions. *Acc. Chem. Res.* **2012**, *45* (10), 1698–1709.

(9) Kozakov, D.; Hall, D. R.; Chuang, G.-Y.; Cencic, R.; Brenke, R.; Grove, L. E.; Beglov, D.; Pelletier, J.; Whitty, A.; Vajda, S. Structural Conservation of Druggable Hot Spots in Protein-Protein Interfaces. *Proc. Natl. Acad. Sci.* **2011**, *108* (33), 13528–13533.

(10) Wells, J. A.; McClendon, C. L. Reaching for High-Hanging Fruit in Drug Discovery at Protein-Protein Interfaces. *Nature* **2007**, *450* (7172), 1001–1009.

(11) Arkin, M. R.; Tang, Y.; Wells, J. A. Small-Molecule Inhibitors of Protein-Protein Interactions: Progressing toward the Reality. *Chem. Biol.* **2014**, *21* (9), 1102–1114.

(12) Pelay-Gimeno, M.; Glas, A.; Koch, O.; Grossmann, T. N. Structure-Based Design of Inhibitors of Protein-Protein Interactions: Mimicking Peptide Binding Epitopes. *Angew. Chemie - Int. Ed.* **2015**, *54* (31), 8896–8927.

(13) Vahdati, L.; Fanelli, R.; Bernadat, G.; Correia, I.; Lequin, O.; Ongeri, S.; Piarulli, U. Synthesis and Conformational Studies of a Stable Peptidomimetic B-Hairpin Based on a Bifunctional Diketopiperazine Turn Inducer. *New J. Chem* **2015**, *39*, 3250.

(14) Harris, T. J. C.; Tepass, U. Adherens Junctions: From Molecules to Morphogenesis. *Nat. Rev. Mol. Cell Biol.* **2010**, *11* (7), 502–514.

(15) Yang, X.; Hou, D.; Jiang, W.; Zhang, C. Intercellular Protein-Protein Interactions at Synapses. *Protein Cell* **2014**, *5* (6), 420–444.

(16) Hynes, R. O. Integrins: A Family of Cell Surface Receptors. *Cell* **1987**, *48* (4), 549–554.

(17) Das, V.; Kalyan, G.; Hazra, S.; Pal, M. Understanding the Role of Structural Integrity and Differential Expression of Integrin Profiling to Identify Potential Therapeutic Targets in Breast Cancer. *J. Cell. Physiol.* **2018**, *233* (1), 168–185.

(18) Hynes, R. O. Integrins: Bidirectional, Allosteric Signaling Machines. *Cell* **2002**, *110* (6), 673–687.

(19) Raab-Westphal, S.; Marshall, J. F.; Goodman, S. L. Integrins as Therapeutic Targets: Successes and Cancers. *Cancers (Basel).* **2017**, *9* (9), 1–28.

(20) Cox, D.; Brennan, M.; Moran, N. Integrins as Therapeutic Targets: Lessons and Opportunities. *Nat. Rev. Drug Discov.* **2010**, *9* (10), 804–820.

(21) Calderwood, D. a. NIH Public Access. **2014**, *14* (8), 503–517.

(22) Thinn, A. M. M.; Wang, Z.; Zhu, J. The Membrane-Distal Regions of Integrin α Cytoplasmic Domains Contribute Differently to Integrin inside-out Activation. *Sci. Rep.* **2018**, *8* (1), 1–17.

(23) Durrant, T. N.; Van Den Bosch, M. T.; Hers, I. Integrin AIIbβ3outside-in Signaling. *Blood* **2017**, *130* (14), 1607–1619.

(24) Moser, M.; Legate, K. R.; Zent, R.; Fässler, R. The Tail of Integrins, Talin, and Kindlins. *Science* **2009**, *324* (5929), 895–899.

(25) Humphries, J. D.; Byron, A.; Humphries, M. J. Integrin Ligands at a Glance. *J. Cell Sci.* **2006**, *119* (Pt 19), 3901–3903.

(26) Desgrosellier, J. S.; Cheresh, D. Integrins in Cancer: Biological Implications and Therapeutic Opportunities. *Nat. Rev. Cancer* **2010**, *10* (1), 9–22.

(27) Guo, W.; Giancotti, F. G. Integrin Signalling during Tumour Progression. *Nature Reviews Molecular Cell Biology*. Nature Publishing Group October 1, 2004, pp 816–826.

(28) Cao, Z.; Suo, X.; Chu, Y.; Xu, Z.; Bao, Y.; Miao, C.; Deng, W.; Mao, K.; Gao, J.; Xu, Z.; et al. Peptides Derived from the Integrin β Cytoplasmic Tails Inhibit Angiogenesis. *Cell Commun. Signal.* **2018**, *16* (1), 38.
(29) Pierschbacher, M. D.; Ruoslahti, E. Cell Attachment Activity of Fibronectin Can Be Duplicated by Small Synthetic Fragments of the Molecule. *Nature* **1984**, *309* (5963), 30–33.
(30) Aumalley, M.; Gurrath, M.; Muller Gerhard; Calvetd, J.; Kessler, H.; Tim, R. Arg-Gly-Asp Constrained within Cyclic Pentapeptides. Strong and Selective Inhibitors of Adhesion To Vitronectin and Laminin Fragment P1. *FEBS Lett.* **1991**, *291* (1), 50–54.
(31) Dechantsreiter, M. A.; Planker, E.; Mathä, B.; Lohof, E.; Hölzemann, G.; Jonczyk, A.; Goodman, S. L.; Kessler, H. N-Methylated Cyclic RGD Peptides as Highly Active and Selective AVβ3 Integrin Antagonists. *J. Med. Chem.* **1999**, *42* (16), 3033–3040.
(32) Mas-Moruno, C.; Rechenmacher, F.; Kessler, H. Cilengitide: The First Anti-Angiogenic Small Molecule Drug Candidate. Design, Synthesis and Clinical Evaluation. *Anticancer. Agents Med. Chem.* **2010**, *10* (10), 753–768.
(33) Stupp, R.; Hegi, M. E.; Gorlia, T.; Erridge, S. C.; Perry, J.; Hong, Y. K.; Aldape, K. D.; Lhermitte, B.; Pietsch, T.; Grujicic, D.; et al. Cilengitide Combined with Standard Treatment for Patients with Newly Diagnosed Glioblastoma with Methylated MGMT Promoter (CENTRIC EORTC 26071-22072 Study): A Multicentre, Randomised, Open-Label, Phase 3 Trial. *Lancet. Oncol.* **2014**, *15* (10), 1100–1108.
(34) Nabors, L. B.; Fink, K. L.; Mikkelsen, T.; Grujicic, D.; Tarnawski, R.; Nam, D. H.; Mazurkiewicz, M.; Salacz, M.; Ashby, L.; Zagonel, V.; et al. Two Cilengitide Regimens in Combination with Standard Treatment for Patients with Newly Diagnosed Glioblastoma and Unmethylated MGMT Gene Promoter: Results of the Open-Label, Controlled, Randomized Phase II CORE Study. *Neuro. Oncol.* **2015**, *17* (5), 708–717.
(35) Tucci, M.; Stucci, S.; Felici, C.; Cafforio, P.; Resta, L.; Rossi, R.; Silvestris, F. Cilengitide Restrains the Osteoclast-like Bone Resorbing Activity of Myeloma Plasma Cells. *Br. J. Haematol.* **2016**, *173* (1), 59–69.
(36) Alva, A.; Slovin, S.; Daignault, S.; Carducci, M.; Dipaola, R.; Pienta, K.; Agus, D.; Cooney, K.; Chen, A.; Smith, D. C.; et al. Phase II Study of Cilengitide (EMD 121974, NSC 707544) in Patients with Non-Metastatic Castration Resistant Prostate Cancer, NCI-6735. A Study by the DOD/PCF Prostate Cancer Clinical Trials Consortium. *Invest. New Drugs* **2012**, *30* (2), 749–757.
(37) Xiong, J. P.; Stehle, T.; Zhang, R.; Joachimiak, A.; Frech, M.; Goodman, S. L.; Arnaout, M. A. Crystal Structure of the Extracellular Segment of Integrin αVβ3 in Complex with an Arg-Gly-Asp Ligand. *Science (80-.).* **2002**, *296* (5565), 151–155.
(38) Manzoni, L.; Belvisi, L.; Arosio, D.; Civera, M.; Pilkington-Miksa, M.; Potenza, D.; Caprini, A.; Araldi, E. M. V.; Monferini, E.; Mancino, M.; et al. Cyclic RGD-Containing Functionalized Azabicycloalkane Peptides as Potent Integrin Antagonists for Tumor Targeting. *ChemMedChem* **2009**, *4* (4), 615–632.
(39) Van Well, R. M.; Marinelli, L.; Altona, C.; Erkelens, K.; Siegal, G.; Van Raaij, M.; Llamas-Saiz, A. L.; Kessler, H.; Novellino, E.; Lavecchia, A.; et al. Conformational Analysis of Furanoid E-Sugar Amino Acid Containing Cyclic Peptides by NMR Spectroscopy, Molecular Dynamics Simulation, and X-Ray Crystallography: Evidence for a Novel Turn Structure. *J. Am. Chem. Soc.* **2003**, *125* (36), 10822–10829.
(40) Urman, S.; Gaus, K.; Yang, Y.; Strijowski, U.; Sewald, N.; De Pol, S.; Reiser, O. The Constrained Amino Acid B-Acc Confers Potency and Selectivity to Integrin Ligands. *Angew. Chemie - Int. Ed.* **2007**, *46* (21), 3976–3978.
(41) Zanardi, F.; Burreddu, P.; Rassu, G.; Auzzas, L.; Battistini, L.; Curti, C.; Sartori, A.; Nicastro, G.; Menchi, G.; Cini, N.; et al. Discovery of Subnanomolar Arginine-Glycine-Aspartate-Based Avb3/Avb5 Integrin Binders Embedding 4-Aminoproline Residues. *J. Med. Chem.* **2008**, *51* (6), 1771–1782.
(42) Sernissi, L.; Trabocchi, A.; Scarpi, D.; Bianchini, F.; Occhiato, E. G. Cyclic RGD Peptidomimetics Containing 4- and 5-Amino-Cyclopropane Pipecolic Acid (CPA) Templates as Dual AVβ3 and A5β1 Integrin Ligands. *Bioorg. Med. Chem.* **2016**, *24* (4), 703–711.
(43) Hodivala-Dilke, K. M.; Mchugh, K. P.; Tsakiris, D. A.; Rayburn, H.; Crowley, D.; Ullman-Cullere, M. B3-Integrin-Deficient Mice Are a Model for Glanzmann Thromboasthenia Showing Placental Defects and Reduce Survival. *J. Clin Investig.* **1999**, *103* (2), 229–238.
(44) Alghisi, G. C.; Ponsonnet, L.; Rüegg, C. The Integrin Antagonist Cilengitide Activates AVβ3, Disrupts VE-Cadherin Localization at Cell Junctions and Enhances Permeability in Endothelial Cells. *PLoS One* **2009**, *4* (2).
(45) Reynolds, A. R.; Hart, I. R.; Watson, A. R.; Welti, J. C.; Silva, R. G.; Robinson, S. D.; Da Violante, G.; Gourlaouen, M.; Salih, M.; Jones, M. C.; et al. Stimulation of Tumor Growth and Angiogenesis by Low Concentrations of RGD-Mimetic Integrin Inhibitors. *Nat. Med.* **2009**, *15* (4), 392–400.
(46) Cheng, K.; Kothapalli, S.-R.; Liu, H.; Koh, A. L.; Jokerst, J. V.; Jiang, H.; Yang, M.; Li, J.; Levi, J.; Wu, J. C.; et al. Construction and Validation of Nano Gold Tripods for Molecular Imaging of Living Subjects. *J. Am. Chem. Soc.* **2014**, *136* (9), 3560–3571.

(47) Lanzardo, S.; Conti, L.; Brioschi, C.; Bartolomeo, M. P.; Arosio, D.; Belvisi, L.; Manzoni, L.; Maiocchi, A.; Maisano, F.; Forni, G. A New Optical Imaging Probe Targeting AVβ3 Integrin in Glioblastoma Xenografts. *Contrast Media Mol. Imaging* **2011**, *6* (6), 449–458.
(48) Dal Corso, A.; Caruso, M.; Belvisi, L.; Arosio, D.; Piarulli, U.; Albanese, C.; Gasparri, F.; Marsiglio, A.; Sola, F.; Troiani, S.; et al. Synthesis and Biological Evaluation of RGD Peptidomimetic-Paclitaxel Conjugates Bearing Lysosomally Cleavable Linkers. *Chem. - A Eur. J.* **2015**, *21* (18), 6921–6929.
(49) Crisp, J. L.; Savariar, E. N.; Glasgow, H. L.; Ellies, L. G.; Whitney, M. A.; Tsien, R. Y. Dual Targeting of Integrin v 3 and Matrix Metalloproteinase-2 for Optical Imaging of Tumors and Chemotherapeutic Delivery. *Mol. Cancer Ther.* **2014**, *13* (6), 1514–1525.
(50) Ressurreição, A. S. M.; Bordessa, A.; Civera, M.; Belvisi, L.; Gennari, C.; Piarulli, U. Synthesis and Conformational Studies of Peptidomimetics Containing a New Bifunctional Diketopiperazine Scaffold Acting as a β-Hairpin Inducer. *J. Org. Chem.* **2008**, *73* (2), 652–660.
(51) Ressurreição, A. S. M.; Vidu, A.; Civera, M.; Belvisi, L.; Potenza, D.; Manzoni, L.; Ongeri, S.; Gennari, C.; Piarulli, U. Cyclic RGD-Peptidomimetics Containing Bifunctional Diketopiperazine Scaffolds as New Potent Integrin Ligands. *Chem. - A Eur. J.* **2009**, *15* (45), 12184–12188.
(52) Marchini, M.; Mingozzi, M.; Colombo, R.; Guzzetti, I.; Belvisi, L.; Vasile, F.; Potenza, D.; Piarulli, U.; Arosio, D.; Gennari, C. Cyclic RGD Peptidomimetics Containing Bifunctional Diketopiperazine Scaffolds as New Potent Integrin Ligands. *Chem. - A Eur. J.* **2012**, *18* (20), 6195–6207.
(53) Guzzetti, I.; Civera, M.; Vasile, F.; Araldi, E. M.; Belvisi, L.; Gennari, C.; Potenza, D.; Fanelli, R.; Piarulli, U. Determination of the Binding Epitope of RGD-Peptidomimetics to Avβ3 and AIIbβ3 Integrin-Rich Intact Cells by NMR and Computational Studies. *Org. Biomol. Chem.* **2013**, *11* (23), 3886.
(54) Fanelli, R.; Schembri, L.; Piarulli, U.; Pinoli, M.; Rasini, E.; Paolillo, M.; Galiazzo, M. C.; Cosentino, M.; Marino, F. Effects of a Novel Cyclic RGD Peptidomimetic on Cell Proliferation, Migration and Angiogenic Activity in Human Endothelial Cells. *Vasc. Cell* **2014**, *6* (1).
(55) Panzeri, S.; Zanella, S.; Arosio, D.; Vahdati, L.; Dal Corso, A.; Pignataro, L.; Paolillo, M.; Schinelli, S.; Belvisi, L.; Gennari, C.; et al. Cyclic IsoDGR and RGD Peptidomimetics Containing Bifunctional Diketopiperazine Scaffolds Are Integrin Antagonists. *Chem. - A Eur. J.* **2015**, *21* (16), 6265–6271.
(56) Colombo, R.; Mingozzi, M.; Belvisi, L.; Arosio, D.; Piarulli, U.; Carenini, N.; Perego, P.; Zaffaroni, N.; De Cesare, M.; Castiglioni, V.; et al. Synthesis and Biological Evaluation (in Vitro and in Vivo) of Cyclic Arginine–Glycine–Aspartate (RGD) Peptidomimetic–Paclitaxel Conjugates Targeting Integrin $\alpha_V\beta_3$. *J. Med. Chem.* **2012**, *55* (23), 10460–10474.
(57) Pina, A.; Dal Corso, A.; Caruso, M.; Belvisi, L.; Arosio, D.; Zanella, S.; Gasparri, F.; Albanese, C.; Cucchi, U.; Fraietta, I.; et al. Targeting Integrin AVβ3with Theranostic RGD-Camptothecin Conjugates Bearing a Disulfide Linker: Biological Evaluation Reveals a Complex Scenario. *ChemistrySelect* **2017**, *2* (17), 4759–4766.
(58) López Rivas, P.; Ranđelović, I.; Raposo Moreira Dias, A.; Pina, A.; Arosio, D.; Tóvári, J.; Mező, G.; Dal Corso, A.; Pignataro, L.; Gennari, C. Synthesis and Biological Evaluation of Paclitaxel Conjugates Involving Linkers Cleavable by Lysosomal Enzymes and AVβ3-Integrin Ligands for Tumor Targeting. *European J. Org. Chem.* **2018**, *2018* (23), 2902–2909.
(59) Alberto Dal Corso, Luca Pignataro, L. B. and C. G. Avβ3 Integrin-Targeted Peptide/Peptidomimetic-Drug Conjugates: In-Depth Analysis of the Linker Technology. *Curr. Top. Med. Chem.* **2016**, *16*, 314–329.
(60) Krall, N.; Scheuermann, J.; Neri, D. Small Targeted Cytotoxics: Current State and Promises from DNA-Encoded Chemical Libraries. *Angew. Chemie - Int. Ed.* **2013**, *52* (5), 1384–1402.
(61) Katsamakas, S.; Chatzisideri, T.; Thysiadis, S.; Sarli, V. RGD-Mediated Delivery of Small-Molecule Drugs. *Future Med. Chem.* **2017**, *9* (6), 579–604.
(62) Arosio, D.; Casagrande, C. Advancement in Integrin Facilitated Drug Delivery. *Adv. Drug Deliv. Rev.* **2016**, *97*, 111–143.
(63) Marelli, U. K.; Rechenmacher, F.; Sobahi, T. R. A.; Mas-Moruno, C.; Kessler, H. Tumor Targeting via Integrin Ligands. *Front. Oncol.* **2013**, *3*, 222.
(64) Temming, K.; Schiffelers, R. M.; Molema, G.; Kok, R. J. RGD-Based Strategies for Selective Delivery of Therapeutics and Imaging Agents to the Tumour Vasculature. *Drug Resistance Updates*. Churchill Livingstone December 2005, pp 381–402.
(65) Chen, K.; Chen, X. Integrin Targeted Delivery of Chemotherapeutics. *Theranostics* **2011**, *1*, 189–200.
(66) Gaertner, F. C.; Kessler, H.; Wester, H.-J.; Schwaiger, M.; Beer, A. J. Radiolabelled RGD Peptides for Imaging and Therapy. *Eur. J. Nucl. Med. Mol. Imaging* **2012**, *39* (S1), 126–138.
(67) Zanella, S.; Angerani, S.; Pina, A.; López Rivas, P.; Giannini, C.; Panzeri, S.; Arosio, D.; Caruso, M.; Gasparri, F.; Fraietta, I.; et al. Tumor Targeting with an IsoDGR–Drug Conjugate. *Chem. - A Eur. J.* **2017**, *23* (33), 7910–7914.
(68) Raposo Moreira Dias, A.; Pina, A.; Dal Corso, A.; Arosio, D.; Belvisi, L.; Pignataro, L.; Caruso, M.;

Gennari, C. Multivalency Increases the Binding Strength of RGD Peptidomimetic-Paclitaxel Conjugates to Integrin AVβ3. *Chem. - A Eur. J.* **2017**, *23* (58), 14410–14415.
(69) Bernabeu, E.; Cagel, M.; Lagomarsino, E.; Moretton, M.; Chiappetta, D. A. Paclitaxel: What Has Been Done and the Challenges Remain Ahead. *Int. J. Pharm.* **2017**, *526* (1–2), 474–495.
(70) Ryppa, C.; Mann-Steinberg, H.; Fichtner, I.; Weber, H.; Satchi-Fainaro, R.; Biniossek, M. L.; Kratz, F. In Vitro and in Vivo Evaluation of Doxorubicin Conjugates with the Divalent Peptide E-[c(RGDfK)2] That Targets Integrin α Vβ3. *Bioconjug. Chem.* **2008**, *19* (7), 1414–1422.
(71) Lee, M. H.; Kim, J. Y.; Han, J. H.; Bhuniya, S.; Sessler, J. L.; Kang, C.; Kim, J. S. Direct Fluorescence Monitoring of the Delivery and Cellular Uptake of a Cancer-Targeted RGD Peptide-Appended Naphthalimide Theragnostic Prodrug. **2012**.
(72) Burkhart, D. J.; Kalet, B. T.; Coleman, M. P.; Post, G. C.; Koch, T. H. Doxorubicin-Formaldehyde Conjugates Targeting A v B 3 Integrin. *Mol Cancer Ther* **2004**, *3* (12), 1593–1604.
(73) Wilhelm, M.; Mukherjee, A.; Bouvier, B.; Zakrzewska, K.; Hynes, J. T.; Lavery, R. Multistep Drug Intercalation: Molecular Dynamics and Free Energy Studies of the Binding of Daunomycin to DNA. *J. Am. Chem. Soc.* **2012**, *134* (20), 8588–8596.
(74) Minotti, G.; Sarvazyan, N. The Anthracyclines: When Good Things Go Bad. *Cardiovasc. Toxicol.* **2007**, *7* (2), 53–55.
(75) Minotti, G.; Cavaliere, A. F.; Mordente, A.; Rossi, M.; Schiavello, R.; Zamparelli, R.; Possati, G. Secondary Alcohol Metabolites Mediate Iron Delocalization in Cytosolic Fractions of Myocardial Biopsies Exposed to Anticancer Anthracyclines. Novel Linkage between Anthracycline Metabolism and Iron-Induced Cardiotoxicity. *J. Clin. Invest.* **1995**, *95* (4), 1595–1605.
(76) Duncan, R.; Kopecková-Rejmanová, P.; Strohalm, J.; Hume, I.; Cable, H. C.; Pohl, J.; Lloyd, J. B.; Kopecek, J. Anticancer Agents Coupled to N-(2-Hydroxypropyl)Methacrylamide Copolymers. I. Evaluation of Daunomycin and Puromycin Conjugates in Vitro. *Br. J. Cancer* **1987**, *55* (2), 165–174.
(77) Embleton, M. J.; Szekerke, M.; Hudecz, F.; Clegg, J. A.; Baldwin, R. W.; Kajtar, J. Synthesis, Conformation, Biodistribution and in Vitro Cytotoxicity of Daunomycin-Branched Polypeptide Conjugates. *Bioconjug. Chem.* **1992**, *3* (1), 49–57.
(78) Mezo, G.; Manea, M.; Szabí, I.; Vincze, B.; Kovács, M. New Derivatives of GnRH as Potential Anticancer Therapeutic Agents. *Curr. Med. Chem.* **2008**, *15* (23), 2366–2379.
(79) Orbán, E.; Mezo, G.; Schlage, P.; Csík, G.; Kulić, Ž.; Ansorge, P.; Fellinger, E.; Möller, H. M.; Manea, M. In Vitro Degradation and Antitumor Activity of Oxime Bond-Linked Daunorubicin-GnRH-III Bioconjugates and DNA-Binding Properties of Daunorubicin-Amino Acid Metabolites. *Amino Acids* **2011**, *41* (2), 469–483.
(80) Tripodi, A. A. P.; Tóth, S.; Enyedi, K. N.; Schlosser, G.; Szakács, G.; Mező, G. Development of Novel Cyclic NGR Peptide–daunomycin Conjugates with Dual Targeting Property. *Beilstein J. Org. Chem.* **2018**, *14*, 911–918.
(81) Marchini, M.; Mingozzi, M.; Colombo, R.; Gennari, C.; Durini, M.; Piarulli, U. Selective O-Acylation of Unprotected N-Benzylserine Methyl Ester and O,N-Acyl Transfer in the Formation of Cyclo[Asp-Ser] Diketopiperazines. *Tetrahedron* **2010**, *66* (49), 9528–9531.
(82) Mezö, G.; Szabó, I.; Kertész, I.; Hegedüs, R.; Orbán, E.; Leurs, U.; Bösze, S.; Halmos, G.; Manea, M. Efficient Synthesis of an (Aminooxy) Acetylated-Somatostatin Derivative Using (Aminooxy)Acetic Acid as a "carbonyl Capture" Reagent. *J. Pept. Sci.* **2011**, *17* (1), 39–46.
(83) Neundorf, I.; Rennert, R.; Hoyer, J.; Schramm, F.; Löbner, K.; Kitanovic, I.; Wölfl, S. Fusion of a Short HA2-Derived Peptide Sequence to Cell-Penetrating Peptides Improves Cytosolic Uptake, but Enhances Cytotoxic Activity. *Pharmaceuticals* **2009**, *2* (2), 49–65.
(84) Guidotti, G.; Brambilla, L.; Rossi, D. Cell-Penetrating Peptides: From Basic Research to Clinics. *Trends Pharmacol. Sci.* **2017**, *38* (4), 406–424.
(85) Joliot, A.; Pernelle, C.; Deagostini-Bazin, H.; Prochiantz, A. Antennapedia Homeobox Peptide Regulates Neural Morphogenesis. *Proc. Natl. Acad. Sci.* **1991**, *88* (5), 1864–1868.
(86) Derossi, D.; Joliot, A. H.; Chassaing, G.; Prochiantz, A. The Third Helix of the Antennapedia Homeodomain Translocates through Biological Membranes. *J. Biol. Chem.* **1994**, *269* (14), 10444–10450.
(87) Green, M.; Loewenstein, P. M. Autonomous Functional Domains of Chemically Synthesized Human Immunodeficiency Virus Tat Trans-Activator Protein. *Cell* **1988**, *55* (6), 1179–1188.
(88) Milletti, F. Cell-Penetrating Peptides: Classes, Origin, and Current Landscape. *Drug Discov. Today* **2012**, *17* (15–16), 850–860.
(89) Trabulo, S.; Cardoso, A. L.; Mano, M.; de Lima, M. C. P. Cell-Penetrating Peptides-Mechanisms of Cellular Uptake and Generation of Delivery Systems. *Pharmaceuticals* **2010**, *3* (4), 961–993.
(90) Bechara, C.; Sagan, S. Cell-Penetrating Peptides: 20 Years Later, Where Do We Stand? *FEBS Lett.* **2013**, *587*, 1693–1702.

(91) Care, A.; Editors, P. L. B. *Peptides and Biomaterials and Their Biomedical Applications*.
(92) Steinman, R. M.; Mellman, I. S.; Muller, W. A.; Cohn, Z. A. Endocytosis and the Recycling of Plasma Membrane. *J. Cell Biol.* **1983**, *96* (1), 1–27.
(93) Eguchi, A.; Dowdy, S. F. SiRNA Delivery Using Peptide Transduction Domains. *Trends Pharmacol. Sci.* **2009**, *30* (7), 341–345.
(94) Mäe, M.; Langel, Ü. Cell-Penetrating Peptides as Vectors for Peptide, Protein and Oligonucleotide Delivery. *Curr. Opin. Pharmacol.* **2006**, *6* (5), 509–514.
(95) Vives, E. Present and Future of Cell-Penetrating Peptide Mediated Delivery Systems: BIs the Trojan Horse Too Wild to Go Only to Troy? **2005**, No. 109, 77–85.
(96) Järver, P.; Mäger, I.; Langel, Ü. In Vivo Biodistribution and Efficacy of Peptide Mediated Delivery. *Trends Pharmacol. Sci.* **2010**, *31* (11), 528–535.
(97) Farkhani, S. M.; Valizadeh, A.; Karami, H.; Mohammadi, S.; Sohrabi, N.; Badrzadeh, F. Cell Penetrating Peptides: Efficient Vectors for Delivery of Nanoparticles, Nanocarriers, Therapeutic and Diagnostic Molecules. *Peptides* **2014**, *57*, 78–94.
(98) Dubikovskaya, E. A.; Thorne, S. H.; Pillow, T. H.; Contag, C. H.; Wender, P. A. Overcoming Multidrug Resistance of Small-Molecule Therapeutics through Conjugation with Releasable Octaarginine Transporters. *Proc. Natl. Acad. Sci. U. S. A.* **2008**, *105* (34), 12128–12133.
(99) Lindgren, M.; Rosenthal-Aizman, K.; Saar, K.; Eiríksdóttir, E.; Jiang, Y.; Sassian, M.; Östlund, P.; Hällbrink, M.; Langel, Ü. Overcoming Methotrexate Resistance in Breast Cancer Tumour Cells by the Use of a New Cell-Penetrating Peptide. *Biochem. Pharmacol.* **2006**, *71* (4), 416–425.
(100) Aroui, S.; Brahim, S.; De Waard, M.; Bréard, J.; Kenani, A. Efficient Induction of Apoptosis by Doxorubicin Coupled to Cell-Penetrating Peptides Compared to Unconjugated Doxorubicin in the Human Breast Cancer Cell Line MDA-MB 231. *Cancer Lett.* **2009**, *285* (1), 28–38.
(101) Duong, H. H. P.; Yung, L. Y. L. Synergistic Co-Delivery of Doxorubicin and Paclitaxel Using Multi-Functional Micelles for Cancer Treatment. *Int. J. Pharm.* **2013**, *454* (1), 486–495.
(102) Taylor, B. N.; Mehta, R. R.; Yamada, T.; Lekmine, F.; Christov, K.; Chakrabarty, A. M.; Green, A.; Bratescu, L.; Shilkaitis, A.; Beattie, C. W.; et al. Noncationic Peptides Obtained From Azurin Preferentially Enter Cancer Cells. *Cancer Res.* **2009**, *69* (2), 537–546.
(103) Majumdar, S.; Siahaan, T. J. Peptide-Mediated Targeted Drug Delivery. *Med. Res. Rev.* **2012**, *32* (3), 637–658.
(104) Wender, P. A.; Galliher, W. C.; Bhat, N. M.; Pillow, T. H.; Bieber, M. M.; Teng, N. N. H. Taxol-Oligoarginine Conjugates Overcome Drug Resistance in-Vitro in Human Ovarian Carcinoma. *Gynecol. Oncol.* **2012**, *126* (1), 118–123.
(105) Lelle, M.; Frick, S. U.; Steinbrink, K.; Peneva, K. Novel Cleavable Cell-Penetrating Peptide-Drug Conjugates: Synthesis and Characterization. *J. Pept. Sci.* **2014**, *20* (5), 323–333.
(106) Splith, K.; Neundorf, I.; Hu, W.; N'Dongo, H. W. P.; Vasylyeva, V.; Merz, K.; Schatzschneider, U. Influence of the Metal Complex-to-Peptide Linker on the Synthesis and Properties of Bioactive CpMn(CO)3 Peptide Conjugates. *Dalt. Trans.* **2010**, *39* (10), 2536.
(107) Lai, Y.; Gallo, R. L. AMPed up Immunity: How Antimicrobial Peptides Have Multiple Roles in Immune Defense. *Trends Immunol.* **2009**, *30* (3), 131–141.
(108) Hancock, R. E. W.; Diamond, G. The Role of Cationic Antimicrobial Peptides in Innate Host Defences. *Trends Microbiol.* **2000**, *8* (9), 402–410.
(109) Marr, A. K.; Gooderham, W. J.; Hancock, R. E. Antibacterial Peptides for Therapeutic Use: Obstacles and Realistic Outlook. *Curr. Opin. Pharmacol.* **2006**, *6* (5), 468–472.
(110) Pinheiro Da Silva, F.; MacHado, M. C. C. Antimicrobial Peptides: Clinical Relevance and Therapeutic Implications. *Peptides* **2012**, *36* (2), 308–314.
(111) Patel, S.; Akhtar, N. Antimicrobial Peptides (AMPs): The Quintessential 'Offense and Defense' Molecules Are More than Antimicrobials. *Biomed. Pharmacother.* **2017**, *95*, 1276–1283.
(112) Tossi, A.; Scocchi, M.; Skerlavajb, B.; Gennarobq, R. *Identification and Characterization of a Primary Antibacterial Domain in CAP1 8, a Lipopolysaccharide Binding Protein from Rabbit Leukocytes*; 1994; Vol. 339.
(113) Hoyer, J.; Schatzschneider, U.; Schulz-Siegmund, M.; Neundorf, I. Dimerization of a Cell-Penetrating Peptide Leads to Enhanced Cellular Uptake and Drug Delivery. *Beilstein J. Org. Chem.* **2012**, *8*, 1788–1797.
(114) Horn, M.; Reichart, F.; Natividad-Tietz, S.; Diaz, D.; Neundorf, I. Tuning the Properties of a Novel Short Cell-Penetrating Peptide by Intramolecular Cyclization with a Triazole Bridge. *Chem. Commun.* **2016**, *52* (11), 2261–2264.
(115) Merrifield, R. B. Solid Phase Synthesis (Nobel Lecture). *Angew. Chemie Int. Ed. English* **1985**, *24* (10), 799–810.

(116) El-Faham, A.; Albericio, F. Peptide-Coupling Reagents. In *Amino Acids, Peptides and Proteins in Organic Chemistry*; Wiley-VCH Verlag GmbH & Co. KGaA: Weinheim, Germany, 2011; Vol. 3, pp 407–444.
(117) Subirós-Funosas, R.; Prohens, R.; Barbas, R.; El-Faham, A.; Albericio, F. Oxyma: An Efficient Additive for Peptide Synthesis to Replace the Benzotriazole-Based HOBt and HOAt with a Lower Risk of Explosion. *Chem. - A Eur. J.* **2009**, *15* (37), 9394–9403.
(118) Mäde, V.; Els-Heindl, S.; Beck-Sickinger, A. G. Automated Solid-Phase Peptide Synthesis to Obtain Therapeutic Peptides. *Beilstein J. Org. Chem.* **2014**, *10*, 1197–1212.
(119) Hochdörffer, K.; Abu Ajaj, K.; Schäfer-Obodozie, C.; Kratz, F. Development of Novel Bisphosphonate Prodrugs of Doxorubicin for Targeting Bone Metastases That Are Cleaved PH Dependently or by Cathepsin B: Synthesis, Cleavage Properties, and Binding Properties to Hydroxyapatite as Well as Bone Matrix. *J. Med. Chem.* **2012**, *55* (17), 7502–7515.
(120) Higgins, J. M. G.; Mandlebrot, D. A.; Shaw, S. K.; Russell, G. J.; Murphy, E. A.; Chen, Y. T.; Nelson, W. J.; Parker, C. M.; Brenner, M. B. Direct and Regulated Interaction of Integrin α(E)B7with E-Cadherin. *J. Cell Biol.* **1998**, *140* (1), 197–210.
(121) Brieher, W. M.; Yap, A. S.; Gumbiner, B. M. Lateral Dimerization Is Required for the Homophilic Binding Activity of C-Cadherin. *J. Cell Biol.* **1996**, *135* (2), 487–496.
(122) Vleminckx, K.; Kemler, R. Cadherins and Tissue Formation: Integrating Adhesion and Signaling. *BioEssays* **1999**, *21* (3), 211–220.
(123) Hulpiau, P.; van Roy, F. Molecular Evolution of the Cadherin Superfamily. *Int. J. Biochem. Cell Biol.* **2009**, *41* (2), 349–369.
(124) Gul, I. S.; Hulpiau, P.; Saeys, Y.; van Roy, F. Evolution and Diversity of Cadherins and Catenins. *Exp. Cell Res.* **2017**, *358* (1), 3–9.
(125) Overduin, M.; Harvey, T. S.; Bagby, S.; Tong, K. L.; Yau, P.; Takeichi, M.; Ikura, M. 3-Dimensional Solution Structure and Calcium Interaction of the Epithelial Cadherin Domain Responsible for Selective Cell-Adhesion. *Protein Eng.* **1995**, *8* (5196), 42.
(126) Shapiro, L.; Fannon, A. M.; Kwong, P. D.; Thompson, A.; Lehmann, M. S.; Gerhard, G.; Als-Nielsen, J.; Als-Nielsen, J.; Colman, D. R.; Hendrickson, W. A. Structural Basis of Cell-Cell Adhesion by Cadherins. *Nature* **1995**, *374* (6520), 327–337.
(127) Pokutta, S.; Weis, W. I. Structure and Mechanism of Cadherins and Catenins in Cell-Cell Contacts. *Annu. Rev. Cell Dev. Biol.* **2007**, *23* (1), 237–261.
(128) Boggon, T. J.; Murray, J.; Chappuis-Flament, S.; Wong, E.; Gumbiner, B. M.; Shapiro, L. C Cadherin Ectodomain Structure and Implications for Cell Adhesion Mechanisms. *Science (80-.).* **2002**, *296* (5571), 1308–1313.
(129) Patel, S. D.; Chen, C. P.; Bahna, F.; Honig, B.; Shapiro, L. Cadherin-Mediated Cell-Cell Adhesion: Sticking Together as a Family. *Curr. Opin. Struct. Biol.* **2003**, *13* (6), 690–698.
(130) D. B. Ivanov, M. P. Philippova, and V. A. T. Full-Text. *Biochemistry* **2001**, *66* (10), 1174–1186.
(131) Chen, Y. T.; Stewart, D. B.; Nelson, W. J. Coupling Assembly of the E-Cadherin/β-Catenin Complex to Efficient Endoplasmic Reticulum Exit and Basal-Lateral Membrane Targeting of E-Cadherin in Polarized MDCK Cells. *J. Cell Biol.* **1999**, *144* (4), 687–699.
(132) Nagafuchi, A.; Takeichi, M. Cell Binding Function of E-Cadherin Is Regulated by the Cytoplasmic Domain. *EMBO J.* **1988**, *7* (12), 3679–3684.
(133) Parisini, E.; Higgins, J. M. G.; Liu, J. huan; Brenner, M. B.; Wang, J. huai. The Crystal Structure of Human E-Cadherin Domains 1 and 2, and Comparison with Other Cadherins in the Context of Adhesion Mechanism. *J. Mol. Biol.* **2007**, *373* (2), 401–411.
(134) Harrison, O. J.; Jin, X.; Hong, S.; Bahna, F.; Ahlsen, G.; Brasch, J.; Wu, Y.; Vendome, J.; Felsovalyi, K.; Hampton, C. M.; et al. The Extracellular Architecture of Adherens Junctions Revealed by Crystal Structures of Type i Cadherins. *Structure* **2011**, *19* (2), 244–256.
(135) Zhang, Y.; Sivasankar, S.; Nelson, W. J.; Chu, S. Resolving Cadherin Interactions and Binding Cooperativity at the Single-Molecule Level. *Proc. Natl. Acad. Sci.* **2009**, *106* (1), 109–114.
(136) Posy, S.; Shapiro, L.; Honig, B. Sequence and Structural Determinants of Strand Swapping in Cadherin Domains: Do All Cadherins Bind Through the Same Adhesive Interface? **2008**.
(137) Patel, S. D.; Ciatto, C.; Chen, C. P.; Bahna, F.; Rajebhosale, M.; Arkus, N.; Schieren, I.; Jessell, T. M.; Honig, B.; Price, S. R.; et al. Type II Cadherin Ectodomain Structures: Implications for Classical Cadherin Specificity. *Cell* **2006**, *124* (6), 1255–1268.
(138) Miloushev, V. Z.; Bahna, F.; Ciatto, C.; Ahlsen, G.; Honig, B.; Shapiro, L.; Palmer, A. G. Dynamic Properties of a Type II Cadherin Adhesive Domain: Implications for the Mechanism of Strand-Swapping of Classical Cadherins. *Structure* **2008**, *16* (8), 1195–1205.
(139) Harrison, O. J.; Bahna, F.; Katsamba, P. S.; Jin, X.; Brasch, J.; Vendome, J.; Ahlsen, G.; Carroll, K. J.; Price, S. R.; Honig, B.; et al. Two-Step Adhesive Binding by Classical Cadherins. *Nat. Struct. Mol. Biol.*

2010, *17* (3), 348–357.
(140) Kudo, S.; Caaveiro, J. M. M.; Goda, S.; Nagatoishi, S.; Ishii, K.; Matsuura, T.; Sudou, Y.; Kodama, T.; Hamakubo, T.; Tsumoto, K. Article Pubs.Acs.Org/Biochemistry Identification and Characterization of the X-Dimer of Human P-Cadherin: Implications for Homophilic Cell Adhesion. *Biochemistry* **2014**, *53*, 51.
(141) Berx, G.; van Roy, F. Involvement of Members of the Cadherin Superfamily in Cancer. *Cold Spring Harbor perspectives in biology*. 2009.
(142) Blaschuk, O. W.; Devemy, E. Cadherins as Novel Targets for Anti-Cancer Therapy. *Eur. J. Pharmacol.* **2009**, *625* (1–3), 195–198.
(143) Jeanes, A.; Gottardi, C. J.; Yap, A. S. Cadherins and Cancer: How Does Cadherin Dysfunction Promote Tumor Progression? *Oncogene* **2008**, *27*, 6920–6929.
(144) Birchmeier, W.; Behrens, J. Cadherin Expression in Carcinomas: Role in the Formation of Cell Junctions and the Prevention of Invasiveness. *BBA - Rev. Cancer* **1994**, *1198* (1), 11–26.
(145) Thiery, J. P. Epithelial–mesenchymal Transitions in Tumour Progression. *Nat. Rev. Cancer* **2002**, *2* (6), 442–454.
(146) Dong, L.-L.; Liu, L.; Ma, C.-H.; Li, J.; Du, C.; XU, S.; Han, L.-H.; Li, L.; Wang, X.-W. E-Cadherin Promotes Proliferation of Human Ovarian Cancer Cells in Vitro via Activating MEK/ERK Pathway. *Acta Pharmacol. Sin.* **2012**, *33* (6), 817–822.
(147) Williams, G.; Williams, E. J.; Doherty, P. Dimeric Versions of Two Short N-Cadherin Binding Motifs (HAVDI and INPISG) Function as N-Cadherin Agonists. *J. Biol. Chem.* **2002**, *277* (6), 4361–4367.
(148) Burden-Gulley, S. M.; Gates, T. J.; Craig, S. E. L.; Lou, S. F.; Oblander, S. A.; Howell, S.; Gupta, M.; Brady-Kalnay, S. M. Novel Peptide Mimetic Small Molecules of the HAV Motif in N-Cadherin Inhibit N-Cadherin-Mediated Neurite Outgrowth and Cell Adhesion. *Peptides* **2009**, *30* (12), 2380–2387.
(149) Williams, E.; Williams, G.; Gour, B. J.; Blaschuk, O. W.; Doherty, P. A Novel Family of Cyclic Peptide Antagonists Suggests That N-Cadherin Specificity Is Determined by Amino Acids That Flank the HAV Motif. *J. Biol. Chem.* **2000**, *275* (6), 4007–4012.
(150) Cavallaro, U.; Schaffhauser, B.; Christofori, G. Cadherins and the Tumour Progression: Is It All in a Switch? *Cancer Lett.* **2002**, *176* (2), 123–128.
(151) Blaschuk, O. W. N-Cadherin Antagonists as Oncology Therapeutics. *Philos. Trans. R. Soc. B Biol. Sci.* **2015**, *370* (1661), 20140039.
(152) Augustine, C. K.; Yoshimoto, Y.; Gupta, M.; Zipfel, P. A.; Selim, M. A.; Febbo, P.; Pendergast, A. M.; Peters, W. P.; Tyler, D. S. Targeting N-Cadherin Enhances Antitumor Activity of Cytotoxic Therapies in Melanoma Treatment. *Cancer Res.* **2008**, *68* (10), 3777–3784.
(153) Perotti, A.; Sessa, C.; Mancuso, A.; Noberasco, C.; Cresta, S.; Locatelli, A.; Carcangiu, M. L.; Passera, K.; Braghetti, A.; Scaramuzza, D.; et al. Clinical and Pharmacological Phase I Evaluation of Exherin^{TM} (ADH-1), a Selective Anti-N-Cadherin Peptide in Patients with N-Cadherin-Expressing Solid Tumours. *Ann. Oncol.* **2009**, *20* (4), 741–745.
(154) Beasley, G. M.; McMahon, N.; Sanders, G.; Augustine, C. K.; Selim, M. A.; Peterson, B.; Norris, R.; Peters, W. P.; Ross, M. I.; Tyler, D. S. A Phase 1 Study of Systemic ADH-1 in Combination with Melphalan via Isolated Limb Infusion in Patients with Locally Advanced in-Transit Malignant Melanoma. *Cancer* **2009**, *115* (20), 4766–4774.
(155) Doro, F.; Colombo, C.; Alberti, C.; Arosio, D.; Belvisi, L.; Casagrande, C.; Fanelli, R.; Manzoni, L.; Parisini, E.; Piarulli, U.; et al. Computational Design of Novel Peptidomimetic Inhibitors of Cadherin Homophilic Interactions. *Org. Biomol. Chem.* **2015**, *13* (9), 2570–2573.
(156) Borthwick, A. D. 2,5-Diketopiperazines: Synthesis, Reactions, Medicinal Chemistry, and Bioactive Natural Products. *Chem. Rev.* **2012**, *112* (7), 3641–3716.
(157) Nardone, V.; Lucarelli, A. P.; Dalle Vedove, A.; Fanelli, R.; Tomassetti, A.; Belvisi, L.; Civera, M.; Parisini, E. Crystal Structure of Human E-Cadherin-EC1EC2 in Complex with a Peptidomimetic Competitive Inhibitor of Cadherin Homophilic Interaction. *J. Med. Chem.* **2016**, *59* (10), 5089–5094.
(158) Webster, K. L.; Maude, A. B.; O'Donnell, M. E.; Mehrotra, A. P.; Gani, D. Design and Preparation of Serine–threonine Protein Phosphatase Inhibitors Based upon the Nodularin and Microcystin Toxin Structures. Part 3†. *J. Chem. Soc. Perkin Trans. 1* **2001**, *0* (14), 1673–1695.
(159) Thompson, C. M.; Frick, J. A.; Green, D. L. C. Synthesis, Configuration, and Chemical Shift Correlations of Chiral l,3,2-Oxazaphospholidin-2-Ones Derived from 1-Serine. *J. Org. Chem.* **1990**, *55* (1), 111–116.
(160) King, D. S.; Fields, C. G.; Fields, G. B. A Cleavage Method Which Minimizes Side Reactions Following Fmoc Solid Phase Peptide Synthesis. *Int. J. Pept. Protein Res.* **1990**, *36* (3), 255–266.
(161) Wakimasu M., Kitada C., F. M. 4-Methoxy-2,3,6-Trimethylbenzensulfonyl (Mtr): A New Amino and Imidazole Protecting Group in Peptide Synthesis. *Chem. Pharm. Bull* **1982**, *30* (8), 2766–2779.
(162) Joo, S. H. Cyclic Peptides as Therapeutic Agents and Biochemical Tools. *Biomol. Ther.* **2012**, *20* (1), 19–26.

(163) Coin, I. The Depsipeptide Method for Solid-Phase Synthesis of Difficult Peptides. *J. Pept. Sci.* **2010**, *16* (5), 223–230.
(164) David, C.; Bischoff, L.; Meudal, H.; Mothé, A.; De Mota, N.; DaNascimento, S.; Llorens-Cortes, C.; Fournié-Zaluski, M. C.; Roques, B. P. Investigation of Subsite Preferences in Aminopeptidase A (EC 3.4.11.7) Led to the Design of the First Highly Potent and Selective Inhibitors of This Enzyme. *J. Med. Chem.* **1999**, *42* (25), 5197–5211.
(165) Gause, G. F.; Brazhnikova, M. G. Gramicidin S and Its Use in the Treatment of Infected Wounds. *Nature* **1944**, *154* (3918), 703–703.
(166) Sewald, N.; Jakubke, H.-D. *Peptides : Chemistry and Biology*; Wiley-VCH, 2002; Vol. 3.
(167) Abdalla, M. A.; Mcgaw, L. J. Natural Cyclic Peptides as an Attractive Modality for Therapeutics: A Mini Review. *Molecules* **2018**.
(168) Li, K. W.; Wu, J.; Xing, W.; Simon, J. A. *Total Synthesis of the Antitumor Depsipeptide FR-901,228*; UTC, 1966; Vol. 49.
(169) Cirac, A. D.; Moiset, G.; Mika, J. T.; Koçer, A.; Salvador, P.; Poolman, B.; Marrink, S. J.; Sengupta, D. The Molecular Basis for Antimicrobial Activity of Pore-Forming Cyclic Peptides. *Biophys. J.* **2011**, *100* (10), 2422–2431.
(170) White, C. J.; Yudin, A. K. Contemporary Strategies for Peptide Macrocyclization. *Nat. Chem.* **2011**, *3* (7), 509–524.
(171) Alcaro, M. C.; Sabatino, G.; Uziel, J.; Chelli, M.; Ginanneschi, M.; Rovero, P.; Papini, A. M. On-Resin Head-to-Tail Cyclization of Cyclotetrapeptides: Optimization of Crucial Parameters. *J. Pept. Sci.* **2004**, *10* (4), 218–228.
(172) Blankenstein, J.; Zhu, J. Conformation-Directed Macrocyclization Reactions. *European J. Org. Chem.* **2005**, No. 10, 1949–1964.
(173) Daidone, I.; Neuweiler, H.; Doose, S.; Sauer, M.; Smith, J. C. Hydrogen-Bond Driven Loop-Closure Kinetics in Unfolded Polypeptide Chains. *PLoS Comput. Biol.* **2010**, *6* (1), e1000645.
(174) Pascal Dumy, *; Michael Keller; Declan E. Ryan; Barbara Rohwedder; Torsten Wöhr, and; Mutter, M. Pseudo-Prolines as a Molecular Hinge: Reversible Induction of Cis Amide Bonds into Peptide Backbones. **1997**.
(175) Zhang, L.; Tam, J. P. Metal Ion-Assisted Peptide Cyclization. *Tetrahedron Lett.* **1997**, *38* (25), 4375–4378.
(176) Cascales, L.; Henriques, S. T.; Kerr, M. C.; Huang, Y.-H.; Sweet, M. J.; Daly, N. L.; Craik, D. J. Identification and Characterization of a New Family of Cell-Penetrating Peptides: Cyclic Cell-Penetrating Peptides. *J. Biol. Chem.* **2011**, *286* (42), 36932–36943.
(177) Lättig-Tünnemann, G.; Prinz, M.; Hoffmann, D.; Behlke, J.; Palm-Apergi, C.; Morano, I.; Herce, H. D.; Cardoso, M. C. Backbone Rigidity and Static Presentation of Guanidinium Groups Increases Cellular Uptake of Arginine-Rich Cell-Penetrating Peptides. *Nat. Commun.* **2011**, *2* (1).
(178) Mandal, D.; Nasrolahi Shirazi, A.; Parang, K. Cell-Penetrating Homochiral Cyclic Peptides as Nuclear-Targeting Molecular Transporters. *Angew. Chemie* **2011**, *123* (41), 9807–9811.
(179) Traboulsi, H.; Larkin, H.; Bonin, M. A.; Volkov, L.; Lavoie, C. L.; Marsault, É. Macrocyclic Cell Penetrating Peptides: A Study of Structure-Penetration Properties. *Bioconjug. Chem.* **2015**, *26* (3), 405–411.
(180) Hong, V.; Presolski, S. I.; Ma, C.; Finn, M. â. G. Analysis and Optimization of Copper-Catalyzed Azide-Alkyne Cycloaddition for Bioconjugation. *Angew. Chem. Int. Ed.* **2009**, *48* (52), 9879–9883.
(181) Turner, R. A.; Oliver, A. G.; Lokey, R. S. Click Chemistry as a Macrocyclization Tool in the Solid-Phase Synthesis of Small Cyclic Peptides. *Org. Lett.* **2007**, *9* (24), 5011–5014.
(182) Reichart, F.; Horn, M.; Neundorf, I. Cyclization of a Cell-Penetrating Peptide via Click-Chemistry Increases Proteolytic Resistance and Improves Drug Delivery. *J. Pept. Sci.* **2016**, No. March, 421–426.
(183) Greenfield, N. J. Using Circular Dichroism Spectra to Estimate Protein Secondary Structure. *Nat. Protoc.* **2006**, *1* (6), 2876–2890.
(184) Chen, C.; Brock, R.; Luh, F.; Chou, P. J.; Larrick, J. W.; Huang, R. F.; Huang, T. huang. The Solution Structure of the Active Domain of CAP18 - a Lipopolysaccharide Binding Protein from Rabbit Leukocytes. *FEBS Lett.* **1995**, *370* (1–2), 46–52.
(185) Still, W. C.; Kahn, M.; Mitra, A. Rapid Chromatographic Technique for Preparative Separations with Moderate Resolution. *J. Org. Chem.* **1978**, *43* (14), 2923–2925.